INDUSTRIAL AND ENGINEERING CHEMISTRY

ANALYTICAL EDITION

VOLUME 18, NUMBER 6 | ISSUED JUNE 22, 1946 | CONSECUTIVE NUMBER 12

We acknowledge with thanks the action of J. T. Baker Chemical Co. in releasing the front cover of this issue for editorial purposes.

36,600 copies of this issue printed.

Published by the American Chemical Society at Easton, Pa. Editorial Headquarters: 1155 16th Street, N. W., Washington 6, D. C.; telephone, Republic 5301; cable, Jiechem (Washington). New York Editorial Branch: 60 East 42nd Street, New York 17, N. Y.; telephone, Murray Hill 2-4662. Chicago Editorial Branch: Room 819, 25 East Jackson Blvd., Chicago 4, Ill.; telephone, Wabash 7376. Business Office: American Chemical Society, 1155 16th Street, N. W., Washington 6, D. C. Advertising Office: 332 West 42nd Street, New York 18, N. Y.; telephone, Bryant 9-4430.

Entered as second-class matter at the Post Office at Easton, Pa., under the Act of March 3, 1879, as 24 times a year—Industrial Edition monthly on the 1st, Analytical Edition monthly on the 15th. Acceptance for mailing at special rate of postage provided for in Section 1103, Act of October 3, 1917, authorized July 13, 1918.

Remittances and orders for subscriptions and for single copies, notices of changes of address and new professional connections, and claims for missing numbers should be sent to the American Chemical Society, 1155 16th Street, N. W., Washington 6, D. C. Changes of address for the Industrial Edition must be received on or before the 18th of the preceding month and for the Analytical Edition not later than the 30th of the preceding month. Claims for missing numbers will not be allowed (1) if received more than 60 days from date of issue (owing to delivery hazards, no claims can be honored from subscribers in Continental Europe, Asia, or the Pacific Islands other than Hawaii), (2) if loss was due to failure of notice of change of address to be received before the dates specified in the preceding sentence, or (3) if the reason for claim is "missing from files".

Annual subscriptions—Industrial Edition and Analytical Edition sold only as a unit, members $3.00, nonmembers $4.00. Postage to countries not in the Pan-American Union $2.25; Canadian postage $0.75. Single copies—current issues, Industrial Edition $0.75, Analytical Edition $0.50, back numbers, Industrial Edition $0.80, Analytical Edition prices on request; special rates to members.

The American Chemical Society also publishes *Chemical and Engineering News*, *Chemical Abstracts*, and *Journal of the American Chemical Society*. Rates on request.

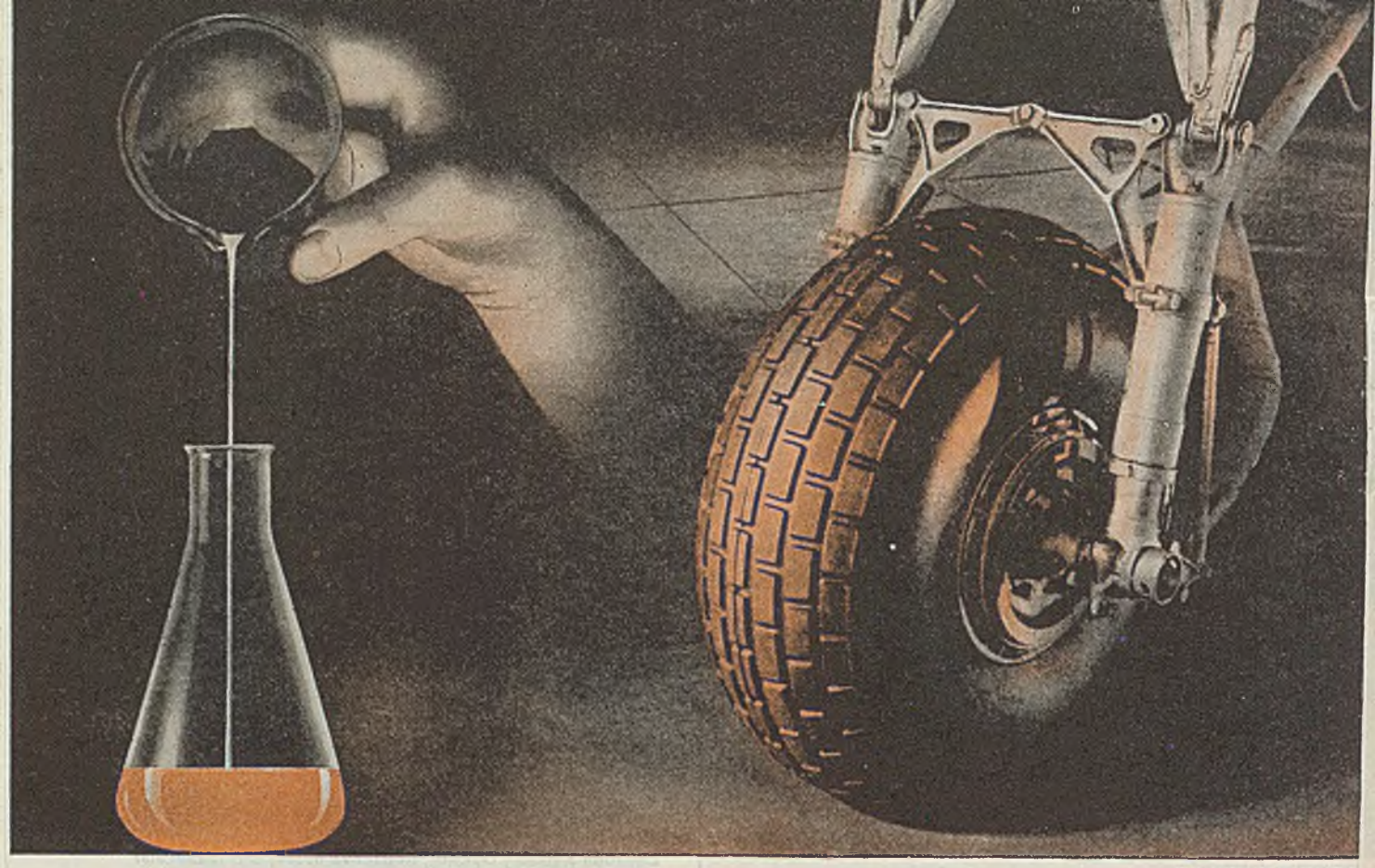

Photo of U. S. Rubber Com
Courtesy, Eastern Air Lin

RESEARCH . . .

GAVE REBIRTH TO THE RUBBER INDUSTRY

Synthetic rubber and the promise of additional natural rubber play a dual role in the oncoming, around-the-clock operation of rubber factories.

And in this speed-up peace program, the chemist has a real ally in Baker's Analyzed C.P. Chemicals and Acids, *low in sulphur derivatives.* For the amount of sulphur present in vulcanized rubber or in various compounding agents is one of many important tests.

There are several Baker's Analyzed C. P. Reagents that have extremely low indexes of sulphur impurities—C. P. Barium Chloride, Potassium Chlorate, Bromine, Mineral Acids and Eschka's Mixture. Moreover, this low sulphur content is plainly set forth on the label—*an actual analysis of the lot.* This is vitally important to chemists when methods must quickly yield an accurate, dependable evaluation.

The fact that you know the limits of vital impurities in your laboratory reagents, and know them in advance to the decimal, is important in controlling the quality of any product.

We urge you to ask your favorite chemical distributor for quotations on Baker's Analyzed C.P. Chemicals and Acids. Regardless of where you may be located there is a Baker distributor ready and eager to serve you promptly.

J. T. Baker Chemical Co., *Executive Offices and Plant:* Phillipsburg, N. J. *Branch Offices:* New York, Philadelphia, Boston and Chicago.

Purity defined — not to "maximum limits"—but to *the decimal* by actual lot analysis. That's the story of the Baker's Analyzed label.

"Baker's Analyzed"

C. P. CHEMICALS AND ACIDS

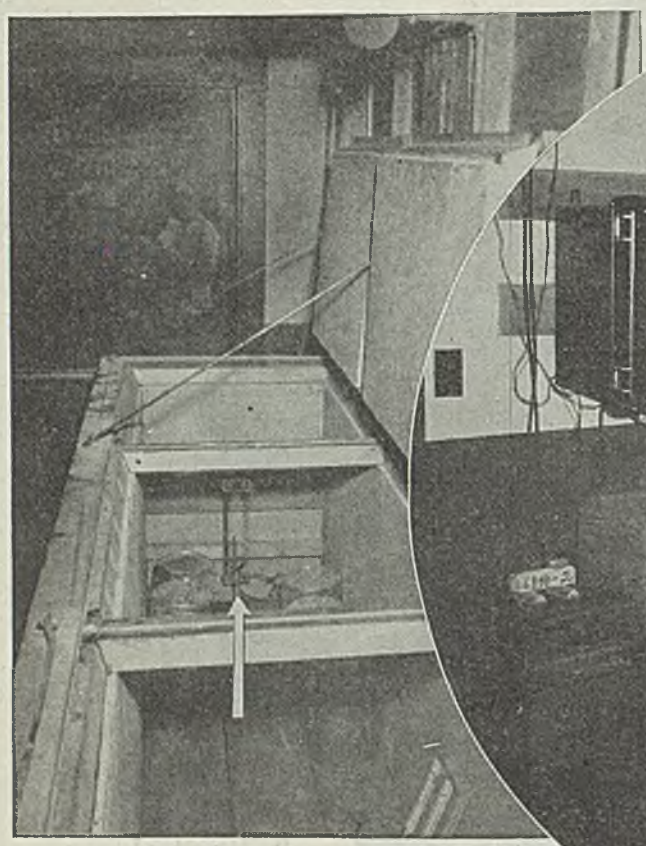

Test box for maintaining constant humidity at 100° F., used principally to study the action by the reactive aggregates and various portland cements. Note thermocouple, which reports temperature to Micromax in circle.

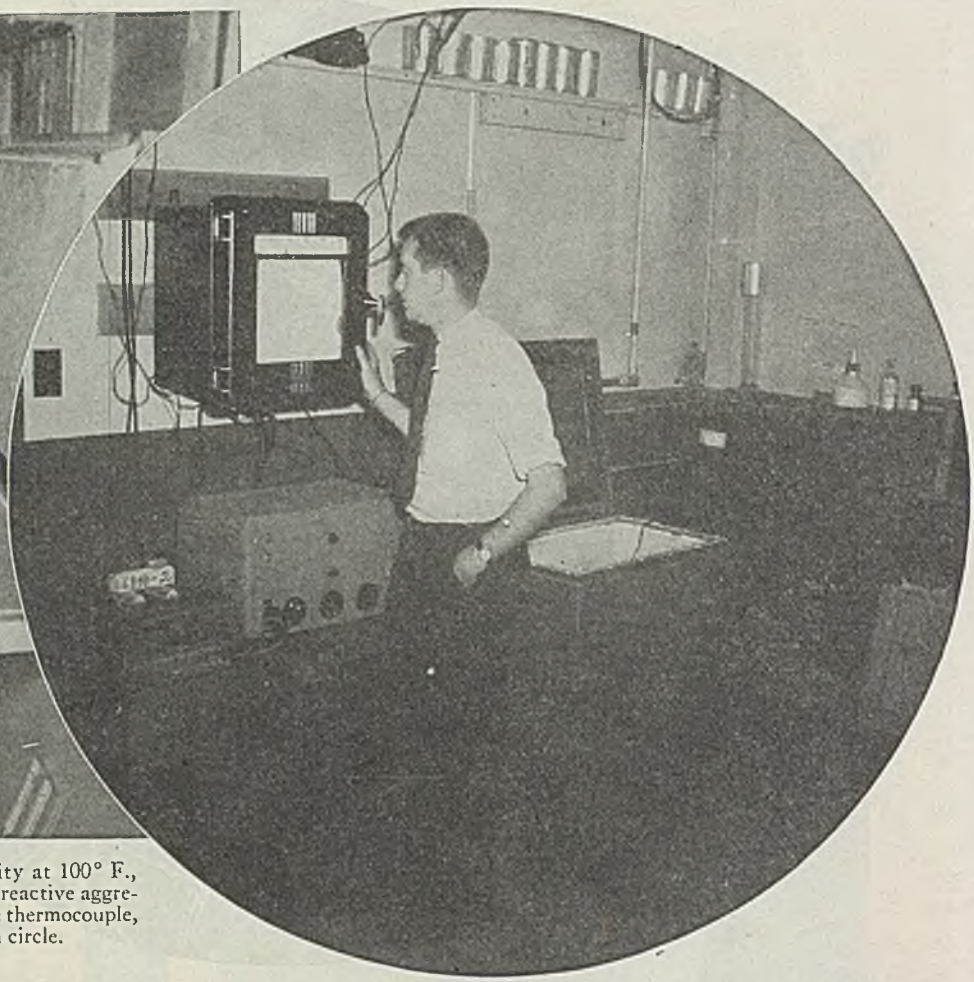

Engineer in cement laboratory of Dewey and Almy Chemical Co., Cambridge, Mass., examines 6-point Micromax Temperature Recorder used in ASTM and other cement and concrete tests.

MICROMAX

"WATCHES" ASTM TESTS IN DEWEY AND ALMY LAB

Dewey and Almy Chemical Co., in testing the cement ingredients they manufacture, find in their Micromax Recorder a usefulness for measurement and control which fits it for many testing jobs.

Serving six variously located thermocouples, the instrument is accurate and micro-sensitive across its entire range, making it especially valuable in tests which require long-time observations at or near the freezing point. The same qualities are extremely useful in calorimetry. Features such as self-standardizing safeguard the tests of such products as T.D.A. Grinding Aid, a catalyst-dispersing agent; Darex AEA, which helps air-entrained cements resist freezing and thawing; and Daraseal Compound, which keeps moisture in concrete.

Further details of the Micromax Recorder are given in Catalog N-33A, sent on request.

"Wet Room" where ASTM C-9 Tests are run under specified humidity and temperature. Test engineer is examining Micromax Recorder's thermocouple.

LEEDS & NORTHRUP COMPANY, 4920 STENTON AVE., PHILA. 44, PA.

LEEDS & NORTHRUP

MEASURING INSTRUMENTS · TELEMETERS · AUTOMATIC CONTROLS · HEAT-TREATING FURNACES

Jrl. Ad N-33A-0723(1)

INDUSTRIAL AND ENGINEERING CHEMISTRY
PUBLISHED BY
THE AMERICAN CHEMICAL SOCIETY
Analytical Edition
WALTER J. MURPHY, EDITOR

Manuscript Reviewing

No author should overlook a brief statement on the contents page of the Analytical Edition. It is his guarantee—though also a reminder of the obligations he contracts through publication—and reads: "The American Chemical Society assumes no responsibility for the statements and opinions advanced by contributors to its publications."

This is a promise to every contributor that his viewpoints—not the American Chemical Society's, the editor's, the reviewers', or the readers'—shall prevail in what is published under his authorship. By the same logic he, not they, must defend his position should his right to a place in the permanent literature ever be challenged.

With such apparent shift of credit or blame to contributors, the present rigorous review system of the Analytical Edition may seem superfluous. However, most authors, even though convinced of the value of their offerings, feel easier if they know others share their opinions. Likewise the editor, who has definite obligations to the American Chemical Society and to readers of the journal, wishes assurance from disinterested judges that a contribution merits space.

In the present system, hundreds of reviewers are called upon each year. No honorarium is provided and the privilege of prepublication reading often has dubious value, but the majority respond readily. They submit recommendations in a truly constructive spirit because of a sincere interest in maintaining and improving publication standards. They are not a fixed group maintained to review papers in each category of analytical chemistry. Instead every author, every analytical chemist, and certainly every specialist in fields touching analytical chemistry is a potential reviewer. Whether called upon frequently or infrequently, he is chosen only after several factors have been considered.

A manuscript to be reviewed is first checked on a number of points. Who beside the author is working or has worked in the field? What has been published recently? Has it been noted by the author? Has he overlooked any recent Analytical Edition articles? Are they perhaps unknown to him because they are "in press" or in an even earlier publication stage?

In answering such questions it is usually not difficult to find a number of possible reviewers. The problem then is to choose those most suitable. Advisory Board members at intervals receive a list of manuscript titles so that they can nominate appropriate critics. Authors themselves are encouraged to name those they regard as qualified. Particularly if an author feels his work has been misjudged by critics chosen originally, the editor welcomes both a rebuttal to the objectionable criticisms and suggestions as to reviewers considered competent. Every effort is made to consider all pertinent viewpoints and to reach a final decision the author can understand and endorse even if unfavorable. A disappointed author should not be a dissatisfied author.

Two reviewers are usually chosen for the initial review. One is ordinarily from the rather limited group of "authorities" in their special fields. The other may not be so widely known, but he, too, is selected for his special interest in the subject. Sometimes he can give more helpful advice, and comment in greater detail than the "authority", because of closer association with the problem discussed or even because he can give more time to the manuscript.

With each manuscript the critic receives a rating form on which he marks the contribution for originality, quality, appropriate publication place, and attention required before publication. In addition, detailed comments are requested for transmittal to the authors. Reviewers are urged to sign these, but only if they can write as freely over their signatures as otherwise.

This choice between being anonymous or named is a feature of the review system which many authors and some reviewers disparage. Any sincere critic, they reason, should not be afraid to identify himself. If unsigned comments are adverse, the apprehensive, sometimes skeptical, author often resents them and assumes such reviewers are incompetent. Such assumptions are generally erroneous. They indicate a lack of understanding of human nature and a lack of faith in the editor and his advisers.

The theory of frank and open criticism is admirable. However, situations where anonymity alone seems to guarantee honest opinions and true candor are easy to recognize. How many employers have not wished for its freedom when writing letters of recommendation? Many critics desire it when evaluating the contributions of a fellow scientist. Both the former student criticizing the work of his teacher and the nonexpert commenting on the work of an expert may experience reasonable hesitation about signing reviews even when they know their criticisms are valid. Free to say what they honestly think, they can concentrate on their reviewing without concern for what the authors' personal reactions may be.

The editor also knows that some critics cannot sign reviews because of company policies. He may question the reasonableness of such policies, but they are beyond his control. To allow them to prohibit cooperation from reviewers so restricted would surely deprive many authors of sources of superior criticism.

The anonymous review has been denounced because it fosters personal bias and indulges the acrimoniously inclined critic. These arguments can be refuted in most instances, for while the patience and good will of critics are sometimes tried by the shortcomings of authors, caustic reports are rarely submitted. Differences of opinion exist, but they are usually the result of differences in training, experience, and familiarity with Analytical Edition publication standards rather than personal bias or antagonism. Where personal prejudice exists, it can generally be detected and counteracted. It is not uncommon when reviewers submit conflicting reports, to seek the advice of a referee, to whom the manuscript and these reports are made available. One of the great advantages of the present system is the opportunity to obtain views from more than one person or group. This permits a far wider sampling of opinion than is possible with a small group of advisers, however expert each might be.

Following an initial review, comments received are passed on to the author. As a rule the editor makes no request except that reports be thoughtfully considered. The comments give the author an idea of what readers might think or say were his article published as submitted. Here is his opportunity to take care of their questions in advance. If errors have been discovered, they can be corrected. If the presentation was found obscure, it can be clarified. If a reviewer has misinterpreted data, steps can be taken to keep the reader from doing likewise.

Sometimes criticisms can be disposed of easily. Sometimes a considerable exchange of views is required before an author has justified his position or been convinced that his contribution is not suitable. Whatever the outcome, there is no attempt to coerce any author into altering his manuscript against his wishes. Any compromise he makes as a result of reviewer suggestions is his own acknowledgment of sound criticism. Any revised draft he submits is assumed to be one he, himself, approves, not one he has prepared to please the critics.

The primary purpose of the review system is maintenance of high publication standards for the Analytical Edition. It requires faith on the part of hundreds of authors and good will on the part of an even greater number of reviewers. Over many years it has proved its worth in countless instances. The editor and his assistants have faith that it will continue to do so.

Molecular Weight Distribution Data on High Polymers

Graphical Representation

R. F. BOYER

Physical Research Laboratory, The Dow Chemical Company, Midland, Mich.

This article describes the preparation and use of a series of graph papers designed to convert cumulative molecular weight distribution data for high polymers into straight lines. These graph papers are based on a theoretical two-parameter molecular weight distribution equation derived by Schulz from statistical considerations of the mechanism of vinyl-type polymerizations. It was found that most of the published molecular weight distribution data on vinyl polymers, cellulose, and cellulose derivatives will give fairly linear plots on these graph papers. In no case, however, is a perfect fit obtained. This failure, in the case of vinyl polymers, is tentatively ascribed to the simultaneous operation of several kinetic mechanisms during polymerization, and/or to faulty fractionation techniques. Various mathematical criteria for judging molecular weight distribution data are included, as is also a brief reference to the general use of these graph papers on unsymmetrical frequency distributions.

EXPERIMENTAL studies on molecular weight distributions for high-polymer systems by the method of fractional solubility (solution or precipitation) yield a series of relatively homogeneous fractions (*29*). The mass of each fraction is added up in stepwise fashion to produce an S-shaped curve of cumulative percentage against polymerization degree of the individual fractions. This curve is then differentiated to obtain the molecular weight distribution curve.

Unless a large number of fractions have been obtained, some uncertainty will exist as to the exact shape of the S-shaped curve, and this uncertainty will be multiplied by the graphical differentiation step. The resulting error may not be serious for a general characterization of the distribution curve. However, it does become important when such data are used to draw conclusions about the kinetics of polymerization. For example, Flory (*10*, *11*, *12*), Schulz (*39*, *41*, *42*), Herington and Robertson (*18*), Ginell and Simha (*15*), Stockmayer (*52*), and Hulburt *et al.* (*20*) have derived theoretical molecular weight distribution curves based on specific polymerization mechanisms. Polycondensations, branching, chain transfer, and other types of chain termination are among the reactions treated by statistical and kinetic methods. The numerical parameters appropriate to such distribution functions can in principle be obtained from an experimental distribution curve. While there is probably no substitute for a large number of narrow fractions (*34*), the question arises as to what graphical aids can be employed in handling experimental data.

The similar problem which exists in other fields, as with distribution of particle sizes or with various types of statistical data, has been discussed by Austin (*3*) and more recently by Rissik (*37*), who point out the advantage of using probability graph paper which transforms the S-shaped cumulative percentage curve into a straight line. This graph paper has the units along the cumulative percentage axis spaced according to the integral of the Gaussian distribution function, while those along the other axis may have a linear or logarithmic interval. A linear plot on such paper immediately furnishes an idea about the type of distribution involved, the general goodness of the data, and several statistical quantities such as the mean size and the standard deviation.

These graph papers, which are commercially available, yield straight lines of cumulative percentage versus molecular weight data for some high-polymer systems, but fail in many cases. A new series of graph papers was therefore designed to cover the unsymmetrical distribution curves which in theory and practice are characteristic of most high polymers. This article is concerned with the design and properties of these graph papers and with some conclusions reached in using them.

DESIGN OF GRAPH PAPERS

The preparation of the desired coordinate scales proceeds most simply by a graphical transformation based on an S-shaped curve of the correct type. This original curve may be an experimental one which is judged sufficiently accurate to serve as a model. Irany (*22*) has followed this procedure in making viscosity-concentration plots of polymers, where the lack of an adequate theory demanded a purely empirical approach. However, the theory of molecular weight distribution functions presents a number of models from which to choose.

A rather general distribution function with two adjustable parameters has been proposed on several occasions for different purposes:

$$W(P)dP = \frac{(1-\alpha)^{b+2}}{(b+1)!} P^{b+1} \alpha^{P} \, dP \qquad (1)$$

where $W(P)$ is weight the fraction of material found in the interval dP, P is polymerization degree, and α and b are constants. Equation 1 describes a family of unsymmetrical distribution curves with a single maximum and with the long tail of the distribution occurring at high values of P. The shape of the curve and the location of the maximum depend on the numerical values of α and b. As α approaches unity, and as b increases, the maximum occurs at progressively larger values of P, while as b increases the curves become sharper and more symmetrical about the maximum. For most vinyl polymers, α lies between 0.99 and unity. b, which has positive integral values including 0, is primarily responsible for the shape of the curve if α is 0.99 or greater.

There are at least three possible interpretations of Equation 1.

Schulz (*41*) first derived this equation in connection with his chain coupling theory for vinyl polymers. In this case α is the probability for chain growth, while $b + 1 = K$ is the number of growing polymer chains which combine to form the final polymer unit. Thus, when chain termination occurs by mutual coupling, $b = 1$ or $K = 2$. When b is 0, Equation 1 reverts to Schulz's original derivation for vinyl compounds (*39*) and to Flory's (*10*) derivation for linear polycondensation resins.

Later, Mark (*28*, *29*) suggested that Equation 1 might apply to branched polymers where each polymer molecule contained exactly b branches in addition to the so-called main polymer chain. This branched structure could presumably arise either through the coupling of $b + 1$ growing chains, or by the simultaneous growth of a single molecule in $b + 2$ directions.

Finally, a specific reaction mechanism or interpretation can be discarded and Equation 1 used simply to fit an experimental curve by adjusting parameters α and b. In practice it turns out that most of the existing molecular weight distribution data can be fairly well described by Equation 1. Hence, whatever the significance of the parameters, Equation 1 provides a suitable model.

Probability graph paper was therefore constructed on the basis of this equation by choosing appropriate values of α and b, calculating and plotting the distribution function of Equation 1, and integrating graphically to obtain an S-shaped cumulative percentage versus degree of polymerization curve. Regular intervals were selected along the cumulative percentage ordinate and projected, via the curve, onto the other axis. These projected points along the abscissas determined the intervals for the cumulative percentage axis of the probability paper. The other axis on the probability paper was then made linear in degree of polymerization.

Since both α and b may vary from one polymer type to another, as well as for different modes of preparation of the same polymer, it is necessary to design a range of graph papers. Fortunately, the values of α are likely to fall within a fairly narrow range. Moreover, if α is greater than 0.99, the shape of the distribution curve is practically independent of α, but is determined mainly by the value of b. Second, as b increases, the distribution curve becomes more symmetrical in shape, and its integral plots as a reasonably straight line on Gaussian probability paper for b greater than 6 to 8.

It was found, for example, that the following eight graph papers covered a wide variety of polymers and experimental conditions:

1. $\alpha = 0.99$, $b = 0, 1, 2$
2. $\alpha = 0.995$, $b = 1, 2, 3$, and 4
3. Gaussian probability paper, Codex Book Company Catalog No. 3127

To give some idea of the sensitivity of these graph papers to change in value of b, Figure 1 has been prepared. It represents theoretical cumulative percentage curves for $\alpha = 0.995$, $b = 0, 1, 2, 3$, and 4, respectively, all plotted on a graph paper designed to give a straight line for $\alpha = 0.995$, $b = 1$. It is seen that if b deviates by only one unit from the value on which the graph paper is based, the linearity is destroyed and the curve fails to pass through the origin. Depending on the accuracy of the experimental distribution data, use of this type of graph paper affords a convenient means of determining the parameter b. In addition to being straight, the line should pass through the origin with a definite slope which depends primarily on the value of b. This slope is such that the number and the weight average degree of polymerization should occur at definite cumulative percentage values which are shown below.

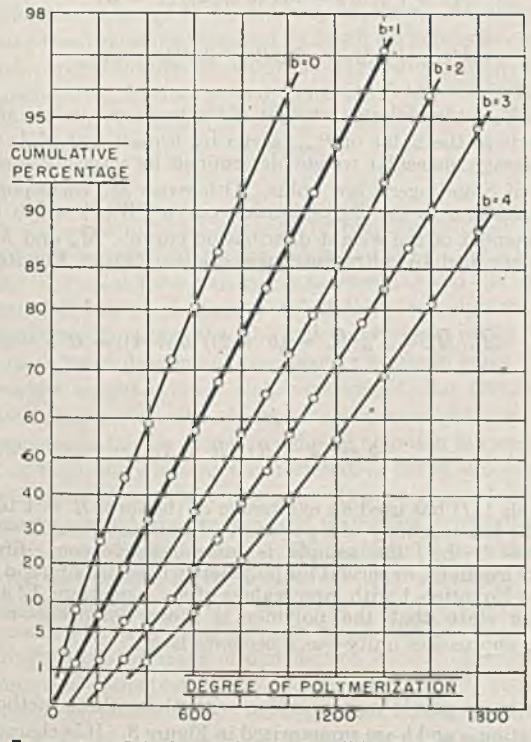

Figure 1. Calculated Cumulative Weight Percentage Curves

Based on Equation 1 for $\alpha = 0.995$, $b = 0, 1, 2, 3$, and 4, plotted on probability paper designed for $\alpha = 0.995$ and $b = 1$

Handling of Experimental Data. Following Schulz and Dinglinger (*43*) in calculating cumulative percentages, it is assumed that half the weight of each fraction is greater, half less, than the measured average molecular weight. Thus, the cumulative percentage corresponding to a given molecular weight or degree of polymerization is taken as the total weight per cent of all preceding fractions plus half the weight per cent of the fraction in question.

Once the data have been plotted on probability paper, a choice must be exercised as to the best straight line through the experimental points. Since the cumulative percentage scale is very expanded at each extremity, a large linear deviation in these regions parallel to the cumulative axis may not be serious. The linear polymerization degree scale affords a more convenient criterion for balancing deviations of the experimental points over all regions of the straight line.

The straight-line cumulative percentage curve can be differentiated numerically by employing the fact that the derivative at any point is proportional to the difference in scale reading on the cumulative percentage axis corresponding to a small, fixed interval along the degree of polymerization axis. It is more satisfactory, however, to replot values taken from the straight line back onto normal coordinate paper. This gives the S-shaped cumulative percentage curve which can be differentiated graphically, or with the aid of some mechanical device such as the tangent meter described by Richards and Roope (*36*).

There is always the danger, in work of this type, of trying to force a straight line onto data when such a procedure is not really justified by the data. The next section therefore considers certain criteria which will aid in making decisions on this point.

CALCULATION OF PARAMETERS α AND b

Before representing any molecular weight distribution data with these graph papers, it seems advisable to discuss some general features of the distribution function given by Equation 1, particularly in regard to methods of calculating parameters α and b from experimental data.

The value of b can be estimated from the type of probability paper which gives the best straight line for the experimental distribution data. There are cases when this method fails, particularly for high values of b, which require Gaussian distribution paper. In such cases, independent numerical checks on the value of b are needed. There are several general mathematical methods for finding α and b, such as the use of simultaneous equations, graphical approximations, etc. However, the unique properties of this distribution function suggest at least three special approaches to the problem.

A. Inflection Point Method. By setting the first derivative of Equation 1 equal to 0, the value of P corresponding to the maximum value of the ordinate is found to be

$$P_{max} = (b + 1)/(1 - \alpha) \qquad (2)$$

provided α is close to unity. (In general, the denominator of Equation 2 should be $-\ln_e \alpha$, which is valid for all values of α.) If b is 0, this reduces to the corresponding expression given by Flory (*10*) for condensation polymers. Next, the second deriva-

tive of Equation 1 is set equal to 0, and it is found that the inflection points come at

$$[(b + 1)/(1 - \alpha)] \pm [(b + 1)^{1/2}/(1 - \alpha)] \quad (3)$$

Thus the two inflection points are located symmetrically about P_{max}, and the separation, ΔP, between them, measured along the P axis is

$$\Delta P = 2(b + 1)^{1/2}/(1 - \alpha) \quad (4)$$

Elimination of α from Equations 2 and 4 gives an expression for b:

$$b = (2P_{max} / \Delta P)^2 - 1 \quad (5)$$

while

$$\alpha = 1 - (b + 1)/P_{max} \quad (6)$$

In theory, at least, one has merely to measure the separation between the inflection points and locate P_{max} in order to calculate both b and α. Actually it may be somewhat difficult to locate the inflection points exactly, and, since ΔP occurs as the square, the error in determining b will be correspondingly greater. Equation 4 is nonetheless a convenient criterion for inspecting distribution curves. If the curve is narrow (ΔP small) and if its maximum occurs at a high value of P, then b is large. If b is 0, there is but one inflection point on the descending side of the curve. Hence the presence or absence of an inflection point on the rising branch of the curve is immediately indicative of the general mathematical form of the distribution.

B. Areas under Distribution Curve. The total area under the weight distribution curve from $P = 0$ to ∞ is unity or 100%, but the areas from $P = 0$ to P_{max} in one case, and from $P = 0$ to $\bar{P}_w$ in the second case (where $\bar{P}_w$ is the weight-average polymerization degree), depend to a very good approximation only on the parameter b, if α is 0.99 or greater.

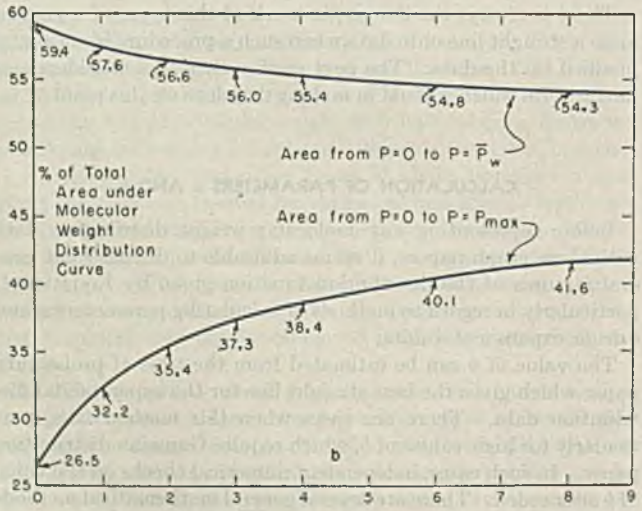

Figure 2. Areas under the Molecular Weight Distribution Curve

From $P = 0$ to P_{max} (lower curve) and from $P = 0$ to P_w (upper curve)

Specifically, by integrating Equation 1 and substituting the correct limits, it is found that:

$$\text{Area}]_0^{P_{max}} = 1 - e^{-(b+1)} \sum_0^{b+1} \frac{(b + 1)^q}{q!} \quad (7)$$

$$\text{Area}]_0^{\bar{P}_w} = 1 - e^{-(b+2)} \sum_0^{b+2} \frac{(b + 2)^q}{q!} \quad (8)$$

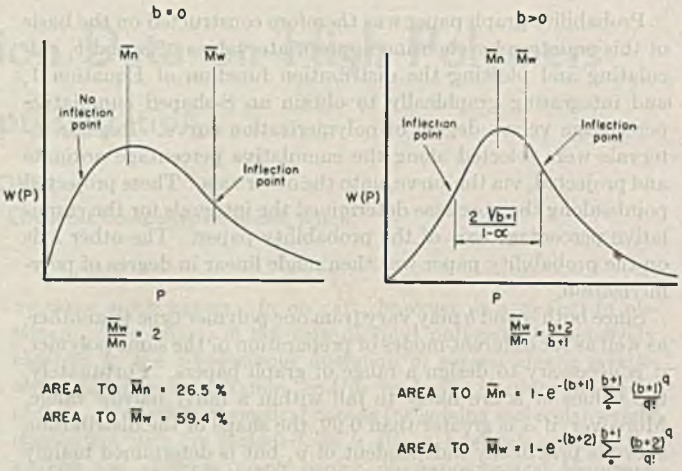

Figure 3. Characteristics of Molecular Weight Distribution Curve Described by Equation 1 for $b = 0$ and $b > 0$

These two functions have been plotted in Figure 2, from which values of b can be read if P_{max} or $\bar{P}_w$ is known. These are the relationships which fix the slope of the straight-line cumulative percentage curve mentioned above. Chowla and Auluck (*8*) have shown that the summation in Equation 7 approaches 0.5 exp $(b + 1)$ as b becomes very large. In other words, as b approaches infinity, exactly half of the area under the distribution curve is on either side of P_{max}.

C. Ratio of Weight-Average to Number-Average Molecular Weight. It is customary to calculate number, weight, and Z-average molecular weights for any molecular weight distribution function, according to the method of Lansing and Kraemer (*26*). For Equation 1, with α close to unity, there results:

$$\bar{M}_n = \bar{P}_n . M_0 = M_0 (b + 1)/(1 - \alpha) \quad (9)$$

$$\bar{M}_w = \bar{P}_w . M_0 = M_0 (b + 2)/(1 - \alpha) \quad (10)$$

$$\bar{M}_z = \bar{P}_z . M_0 = M_0 (b + 3)/(1 - \alpha) \quad (11)$$

where M_0 is the molecular weight of the monomer unit. $\bar{M}_n$ corresponds to the value of P_{max} given by Equation 2 while $\bar{M}_w$ is the average molecular weight determined by viscosity measurements if Staudinger's law holds. Otherwise $\bar{M}_w$ corresponds to the maximum in the Z-distribution curve $PW(P)$ which is the first moment of the weight distribution curve. $\bar{M}_w$ and $\bar{M}_z$ can be determined by ultracentrifuge studies. From Equations 9 and 10

$$\bar{M}_w/\bar{M}_n = \bar{P}_w/\bar{P}_n = (b + 2)/(b + 1) = R \quad (12)$$

or

$$b = (2 - R)/(R - 1) \quad (13)$$

Schulz (*41*) has used an expression of the form $R - 1$ to indicate the heterogeneity of a polymer. In his notation, $R - 1$ approaches 0—i.e., the sample is more homogeneous—first for narrow fractions, or second for polymers whose distribution curve follows Equation 1 with large values of b. Equations 12 and 13 likewise state that the polymer is more homogeneous—i.e., $\bar{P}_w/\bar{P}_n$ approaches unity—as b becomes large.

The main points in connection with these three methods of calculating α and b are summarized in Figure 3. It is characteristic of all methods that as b becomes large, the accuracy in determining its exact value diminishes. It is thus convenient to use these different methods for cross-checking. Moreover, the experi-

mental weight distribution curve can be divided and then multiplied by the degree of polymerization to give the number distribution curve and the Z-distribution curve, respectively. The number distribution curve will have a maximum at $P = b/(1 - \alpha)$ if b is 1 or greater; otherwise at $P = 0$. The Z-distribution curve will have a maximum at $P = (b + 2)/(1 - \alpha) = \bar{P}_w$. Thus, the maxima in the number, weight, and Z-distribution curves are spaced along the polymerization degree axis in the ratio of $b:(b + 1):(b + 2)$.

The exact position of the maximum for the weight distribution curve is somewhat uncertain because it arises from the graphical differentiation of the cumulative percentage curve at its steepest part. However, the maxima for the number of Z-distribution curves derive from less steep parts of the cumulative weight percentage curve and should be less subject to error. Finally, the number distribution curve can be graphically integrated to give a cumulative number distribution curve. This should plot linearly on a probability graph paper having the same α but a b value reduced by unity compared to the graph paper used for the weight distribution curve. In similar fashion the Z-distribution curve can be integrated and should plot linearly on probability paper with b one unit greater than for the weight distribution curve.

While several checks on the values of b and α may appear unnecessary, actual experience in trying to apply these various criteria to existing distribution data has not been too successful. Several of the criteria may apply in a given case but complete agreement is generally lacking.

The foregoing treatment has assumed that true molecular weights are available for the fractions under study. However, most of the existing distribution data were based on Staudinger's linear relationship between specific viscosity, η_{sp}, molecular weight, M, and concentration, c:

$$\eta_{sp} = K_s M c \tag{14}$$

where K_s is the Staudinger constant. For many polymers this equation now appears to be seriously in error. An alternative viscosity law, originally proposed by Mark (*27*) and subsequently verified experimentally by Houwink (*19*), Flory (*13*), Mathes (*30*), and Alfrey, Bartovics, and Mark (*1, 5*) has the form:

$$[\eta]_{c=0} = KM^a \tag{14A}$$

$[\eta]_{c=0}$ is the intrinsic viscosity or limiting value of η_{sp}/c as the polymer concentration approaches 0, while K and a are constants. The value for a usually lies between 0.5 and 1.0.

Flory (*13*) has emphasized the fact that for polymers whose fractions obey Equation 14A, the molecular weight of the heterogeneous polymer determined by viscosity methods is not equivalent to the weight-average molecular weight, but gives rise to what he calls a viscosity-average molecular weight. A second consequence of the use of the Staudinger equation in cases where a is less than unity is that the distribution curve is compressed along the polymerization degree axis. It appears much narrower and covers a much smaller range of molecular weights than are actually present in the material. This apparent narrowing of the observed distribution curve forces one to choose a larger value of b than is required by the true molecular weight distribution.

There are several other devices which can be employed in checking on the accuracy of distribution curves. For instance, a comparison of the plots of η_{sp}/c versus c for fractions and for the heterogeneous polymer gives another check on the value of b in Equation 1 (*50*). Secondly, a detailed study of the number, weight, and Z-distribution curves allows one to calculate α and b of Equation 1 and a in Equation 14A. Both these techniques, which assume that the true weight distribution curve is described by Equation 1 are beyond the scope of this paper, and will be treated elsewhere.

APPLICATION OF PROBABILITY PAPER TO EXPERIMENTAL DATA

Mark has recently surveyed the literature on molecular weight distribution data, particularly in regard to cellulose and its derivatives, but also including vinyl compounds (*28*). Most of the data referred to by him, as well as some appearing since his article was published, have been plotted on these special probability papers. In general, a reasonably good fit could be obtained by the proper choice of graph paper, but in no case was there the complete accord between theory and experiment that might be desired.

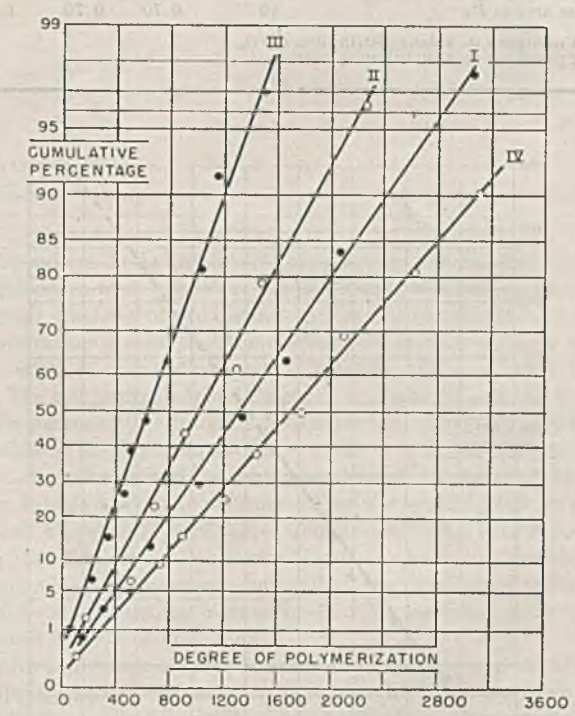

Figure 4. Cumulative Weight Percentage Curves

For four polystyrene samples of Schulz and Dinglinger listed in Table I. Probability paper has $\alpha = 0.995$, $b = 2$.

The most extensive and apparently most reliable set of results was that obtained by Schulz and Dinglinger (*43*) on four samples of polystyrene. Their data appear in Figure 4 using a graph paper with $\alpha = 0.995$, $b = 2$. Except for sample IV, all curves are reasonably satisfactory, although none of them passes through the origin. The fit for sample IV is considerably improved on a graph paper with $\alpha = 0.995$, $b = 4$. Sample II was fractionated twice, and both sets of results are in complete harmony, thus checking the consistency of their experimental technique.

Several fractions from each of these four polymers were measured for osmotic molecular weights, but the distribution curves are based on Staudinger's law. Recalculation of curves I and IV on the basis of Equation 14A (for which $a = 0.90$ was calculated from their viscosity–osmotic molecular weight data) made no perceptible improvement in the fit of the data. The straight lines still failed to pass through the origin, and still did not have the correct slope. A summary of the history of these four samples, together with calculations concerning them, is collected in Table I. It is evident that the values obtained for b show an extremely wide variation, but that the graph paper does a fair job of selecting a representative value.

Schulz and Dinglinger had concluded that these curves could

Table I. Summary of Calculations on Schulz and Dinglinger's (43) Molecular Weight Distribution Data on Polystyrene

Sample	I	II	III	IV
Polymerization temperature, ° C.	132	132	132	140
Solvent	Benzene	Benzene	Ethyl benzene	None
Styrene in solvent, %	20	20	20	100
Yield of polymer, %	11	67	69	60
$\frac{\eta_{sp}}{c}$ for polymer	7.2	5.9	3.4	9.2
$\sum\frac{\eta_{sp}}{c}$ for fractions	7.5	5.8	3.8	9.1
$\overline{P}_n$[a]	1020	815	520	1540
$\overline{P}_w$[b]	1500	1125	715	1880
b from $\overline{P}_w/\overline{P}_n$	1.15	1.60	1.65	3.55
b from probability paper	2.0	2.0	2.0	4.0
b from inflection points	2.76	2.27	3.0	3.85
b from area to $\overline{P}_{max}$	1.25	2.70	3.0	...
b from area to $\overline{P}_w$	0	0.70	0.70	1.50

[a] From peak in weight distribution curve.
[b] From peak in Z-distribution curve.

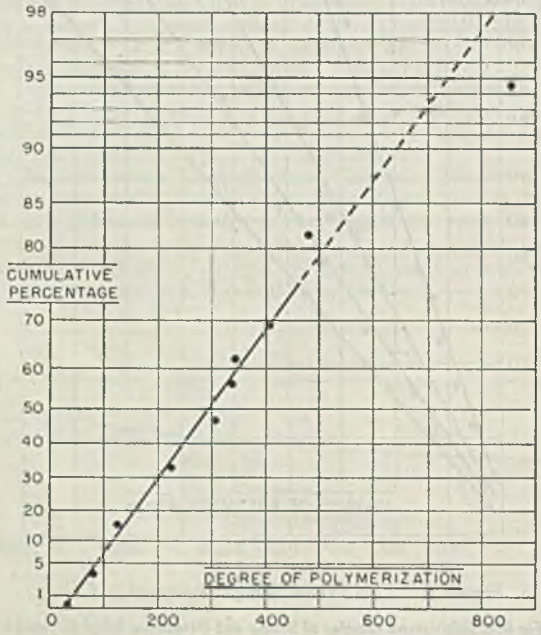

Figure 5. Cumulative Weight Percentage Curve for Polymethylmethacrylate

Data by Schulz and Dinglinger (44), graph paper of $\alpha = 0.995$, $b = 0$

be fitted with $b = 1$, and hence decided that the distribution arose from the mutual coupling of two growing chains. However, their experimental curves were sharper than their theoretical curves plotted on the same graphs (43) and calculated for $b = 1$. In fact, a b value of at least 2 is needed to account for the shape of their curves. In terms of branching, $b = 2$ means a main chain and two branches.

The same authors have also obtained a distribution curve on a sample of polymethyl methacrylate (44), polymerized as a 24% solution in toluene under air at 158° C. to a yield of 35.5%. Their data are plotted in Figure 5. With the exception of the highest molecular weight fraction, the results are reasonably well described on a graph paper for $\alpha = 0.995$, $b = 0$. Again the straight line fails to pass through the origin. The ratio between weight and number average molecular weight is approximately 2, which makes $b = 0$, but the areas under various portions of the distribution curve are not in correct proportion. Schulz and Dinglinger stated that their curve was satisfied by $\alpha = 0.99793$, $b = 2$, although their own efforts at curve fitting contradict this conclusion. For example, their plotted weight distribution curve lacks an inflection point on the rising branch, and this is consistent only with $b = 0$.

Figure 6 presents the data on 28 fractions of cellulose acetate obtained by Sookne *et al.* (49). The first fraction could not be redissolved to furnish a molecular weight. Figure 6, plotted on the

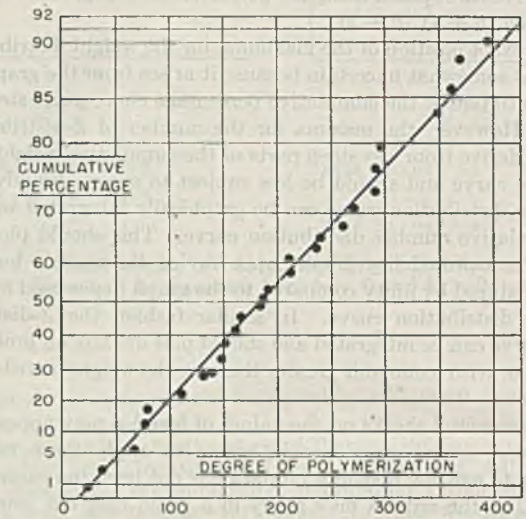

Figure 6. Cumulative Weight Percentage Curve for Cellulose Acetate (49)

Graph paper of $\alpha = 0.99$, $b = 0$

assumption that this was a true fraction, employs a graph paper with $\alpha = 0.99$, $b = 0$. If this first fraction is ignored, and the remaining fractions are spread over 100% total weight, a slightly better plot is obtained for $\alpha = 0.99$, $b = 2$. The behavior of cellulose itself is shown by Figure 7, where cumulative distribution curves for cotton cellulose and several chemically treated flax celluloses are plotted. These data, obtained by Straus and Levy (53) with cupriethylenediamine as solvent and sulfuric acid as precipitant, are best treated on Gaussian probability paper. The curves are narrow, thus corresponding to a high value for b.

There is no a priori reason for expecting cellulose and its derivatives to follow the same type of molecular weight distributions that obtain for vinyl polymers. It has been emphasized (35, 51) that Spurlin's distribution curve on cellulose nitrate is considerably narrower than a representative distribution for polystyrene. Schulz's (40) work on nitrocellulose is further confirmation of this fact. To what extent this effect is real or merely a consequence of the application of Staudinger's law cannot be decided now. Gralen and Svedberg's (16) recent ultracentrifuge studies on the molecular weights of native cellulose indicate much higher values than had previously been estimated by viscosity on extrapolation of the Staudinger law. Moreover, the degradation of native cellulose incident to purifying it or preparing its derivatives will alter the original distribution considerably. The calculations of Montroll and Simha (32) predict that a very homogeneous starting material acquires on degradation various degrees and types of heterogeneity, not necessarily represented by Equation 1.

In addition to the specific examples cited above a more general survey of the results obtained in this study is tabulated in Table II. The number of fractions, the values of b from the graph paper and also from the ratio of weight to number average polymerization degree, and a qualitative evaluation (good, fair, bad) of the fit obtained on the graph paper are included. The last two columns list, respectively, the method of determining molecular weights (ultracentrifuge, osmotic pressure, or viscosity) and the literature source.

DISCUSSION OF RESULTS

In general, most of the available molecular weight distribution data can be accommodated with some degree of satisfaction on the various probability papers which have been prepared. However, in nearly every case the agreement between theory and experiment turns out to be largely illusory. A more detailed study of the various criteria listed earlier reveals the following discrepancies, even in cases where the data lie on good straight lines.

1. The line does not pass through the origin.
2. The slope of the line is not correct.
3. Some deviation from linearity may occur at one or both ends of the distribution curve.
4. The areas under the distribution curve out to $\bar{P}_n$ and $\bar{P}_w$ are not consistent with the results given in Figure 2.
5. The ratio $\bar{P}_w/\bar{P}_n$ does not agree with the general shape of the distribution curve.

Some of these discrepancies, such as 4 and 5, are inherent in the data and have nothing to do with the use of probability paper, nor does it appear that a wider choice of graph papers would eliminate the other discrepancies. These difficulties may arise because the distribution function of Equation 1 does not and should not apply, or because the fractionation data are at fault. Several possible errors would include use of Staudinger's equation instead of the more general Equation 14A, too few fractions, too high concentrations of polymer during fractionation, degradation during the experiment, improper choice of solvents, etc.

With the vinyl polymers it may well be that a series of distribution curves is superimposed. This could arise from the simultaneous existence of two or more distinct polymerization mechanisms, such as branching and chain transfer, each of which mechanisms might give a different type of distribution curve. Herington and Robertson (*18*) have emphasized how the distribution curve will alter throughout the course of a polymerization for only one mechanism—namely, chain termination by the mutual coupling of two growing chains.

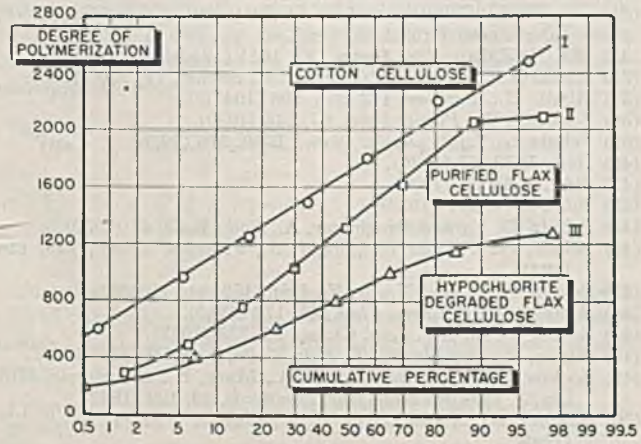

Figure 7. Cumulative Weight Percentage Curves for Several Cellulose Samples (53)

Gaussian probability paper

Table II. Summary of Fractionation Data on High Polymers

Polymer	No. of Fractions	Values of b[a] From Graph Paper	Values of b[a] From $\bar{P}_w/\bar{P}_n$	General Fit of Data[b]	Molecular Weight Method[c]	Reference
Polyisobutylene	8	0	0	F	V	(*39*)
Polymethyl methacrylate	10	0	0	F	V, O	(*44*)
Polystyrene						
Made at 90° C.	7	0	1	F	V	(*2*)
Made at 130° C.	6	∞	∞	F	V	(*2*)
Made at 132°–140° C.	8–10	2–4	1–4	F	V, O	Table I
Polyvinylchloride	5	∞	...	B	V	(*14*)
Polyvinylacetates	7	0–1	2–3	F	V	(*7*)
Polyvinylchloride-acetate	5	∞	...	F	V	(*9*)
Polymethacrylonitrile	6	...	...	B	O	(*24*)
Polyethyleneoxide	6	∞	∞	F	V	(*45*)
Buna S-benzene-soluble	..	0	...	B	U	(*23, 47*)
β-Amylose cornstarch	6	2	...	G	U	(*6*)
Gelatin	6	...	...	B	U	(*25*)
Nitrated Salep mannin	7	2	0	F	V	(*21*)
Methyl cellulose	11	2	1	G	U, V	(*48*)
Ethylcellulose	5	∞	...	F	V	(*33*)
Cellulose acetate	28	2	3	G	V, O	(*49*)
Cellulose nitrate	5	∞	2	F	V, O	(*40*)
Cellulose nitrate	66	2	2	G	V	(*35, 50*)
Nitrated cotton cellulose	6	∞	...	G	V	(*33*)
Cotton cellulose	7	∞	∞	G	V	(*53*)

[a] ∞ High value of b.
[b] B, bad; F, fair; G, good.
[c] V, viscosity; O, osmotic pressure; U, ultracentrifuge.

Several synthetic distribution curves were therefore calculated to determine their behavior. In one case it was assumed that a polymer consisted of two distinct species, each having its own distribution curve, such that there were three parts of polymer with $\alpha = 0.995$, $b = 2$, and one part of polymer with $\alpha = 0.995$, $b = 0$. The composite distribution curve was smooth and had but a single maxima. Its integral gave a perfect straight line (likely fortuitous) on graph paper of $\alpha = 0.995$, $b = 2$, but the line was rotated clockwise and did not pass through the origin. Moreover, calculation of the parameter b by the several methods previously enumerated gave values from 0 to ∞. It is thus conceivable that the observed behavior of some experimental molecular weight distribution curves may reflect the presence of different polymer species arising from several kinetic mechanisms, or from variable extents of branching.

A further source of disturbance would be a gradual increase or decline in the value of the average polymerization degree with the course of the polymerization. Thus, in Table I, polystyrene samples I and II carried to yields of 11 and 67%, respectively, differ in average polymerization degree by 20%. While there is no other apparent difference in the two distribution curves, it seems evident that each must represent the summation of many distribution curves. In this same series of polystyrene samples, the first three prepared in solvent showed on the average a lower b value than No. IV made from pure styrene. The greater prevalence of chain transfer in the presence of solvent (*31*) may well account for this difference in behavior.

In regard to branching, it seems fairly certain that if present it must affect the shape of the distribution curve. It is less certain that a fractional solubility technique will reveal the true picture of branching. Fractionation experiments isolate relatively narrow bands of molecular weights through the marked dependence of solubility on chain length (*46*). This may be rigorously selective for the members of a polymer homologous series but it may fail in the presence of branching, which would affect solubility independently of molecular weight. Thus, Baker, Fuller, and Heiss (*4*) have observed "abnormally high solubility" for slightly branched polymer molecules, as compared with linear molecules of the same chemical composition. These fractionation difficulties would be especially pronounced if one polymer contained several branched species or mixtures of branched and linear chains. Alfrey, Bartovics, and Mark (*1*) were recently able to separate a mixture of two polystyrene fractions each having the same osmotic molecular weight but coming from polymers prepared at different temperatures. While branching was not neces-

sarily involved in this experiment, some additional factor besides molecular weight affected solubility.

So long as all the branched species in a heterogeneous polymer are soluble, branching might be expected to sharpen a molecular weight distribution curve obtained by fractional precipitation. Thus, the largest molecules would on the average derive their size from numerous branches which would make such molecules more soluble than a linear molecule of the same molecular weight.

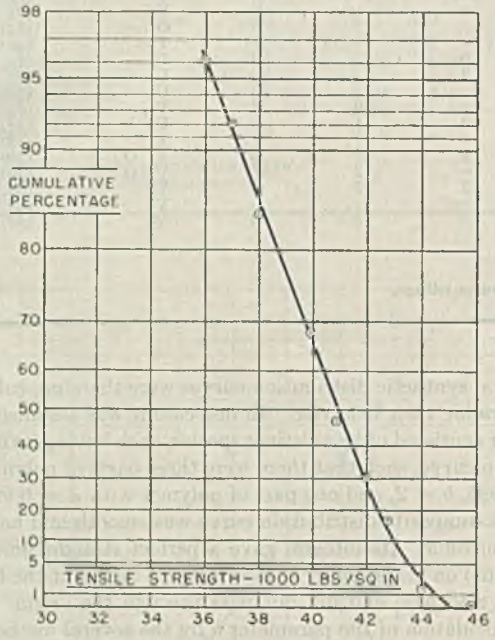

Figure 8. Distribution of Tensile Strength Values for 50 Samples of Saran Cordage

Ordinates represent percentage of samples which had not failed at indicated tensile load.

The smallest molecules would presumably be less branched and hence less soluble. The lowest and highest fractions would thus be shifted toward the center of the solubility distribution. Molecular weight determinations on such fractions might be in relative error because of the molecular complexity. It is hoped that the branching problem which is believed to exist in vinyl polymers can be treated more fully elsewhere. There is some possibility, at least with polystyrene, that branching may be connected with the activation step, but that linear molecules are also present through chain transfer.

The safest assumption concerning the distribution data treated in this report is that the probability graph papers have assisted in curve fitting, but that the data do not permit any decisive conclusions about polymerization mechanisms. (One might also say that a two-parameter equation such as Equation 1 is not sufficient to describe distributions resulting from the inhomogeneity of the kinetic process superimposed upon that inherent in the fractionation technique employed.) The existing data uniformly demonstrate the heterogeneous nature of the various high polymers studied, and do give an estimate of the approximate range of molecular weights present. It would seem advisable, however, to repeat all the experimental work under the guidance of current improvements in high-polymer theory and techniques.

APPLICATION OF PROBABILITY PAPER TO OTHER TYPES OF DATA

The special graph papers developed for molecular weight distributions can be expected to apply equally well to many other types of data which follow an unsymmetrical distribution law. One such example, given in Figure 8, applies to the range in tensile strength values obtained on breaking fifty samples of Saran cordage. Since the tail of this distribution curve runs off to the left, the cumulative percentage scale was plotted as samples that had not yet broken under a given tensile load. Harries, in his studies on glass, derived a probability law which suggested this application (*17*). The graph paper used was for $\alpha = 0.99$, $b = 0$, although these parameters do not have their usual significance in this application.

LITERATURE CITED

(1) Alfrey, T., Bartovics, A., and Mark, H., *J. Am. Chem. Soc.*, 65, 2319 (1943).
(2) Amos, J. L., and Stober, K. E., Dow Chemical Co., unpublished observations.
(3) Austin, J. B., Ind. Eng. Chem., Anal. Ed., 11, 334 (1939).
(4) Baker, W. O., Fuller, C. S., and Heiss, Jr., J. H., *J. Am. Chem. Soc.*, 63, 2142, 2148 (1941).
(5) Bartovics, A., and Mark, H., *Ibid.*, 65, 1901 (1943).
(6) Beckmann, C. O., and Landis, Q., *Ibid.*, 61, 1495 (1939).
(7) Blease, R. A., and Tuckett, R. F., *Trans. Faraday Soc.*, 37, 571 (1941).
(8) Chowla, S., and Auluck, F. C., *Math. Student*, 8, 75 (1940).
(9) Douglas, S. D., and Stoopes, W. N., Ind. Eng. Chem., 28, 1152 (1936).
(10) Flory, P. J., *J. Am. Chem. Soc.*, 58, 1877 (1936).
(11) *Ibid.*, 62, 1561 (1940).
(12) *Ibid.*, 63, 3083, 3091, 3096 (1941).
(13) *Ibid.*, 65, 372 (1943).
(14) Fuoss, R. M., *Ibid.*, 63, 2401 (1941).
(15) Ginell, Robert, and Simha, Robert, *Ibid.*, 65, 706, 715 (1943).
(16) Gralén, N., and Svedberg, T., *Nature*, 152, 625 (1943).
(17) Harries, W., *Z. tech. Physik*, 18, 48 (1937).
(18) Herington, E. F. G., and Robertson, Alan, *Trans. Faraday Soc.*, 38, 490 (1942).
(19) Houwink, R., *J. prakt. Chem.*, 157, 15 (1940).
(20) Hulburt, H. M., Harman, R. A., Tobolsky, A. V., and Eyring, Henry, *Ann. N. Y. Acad. Sci.*, 44, 397 (1943).
(21) Huseman, E., *J. prakt. Chem.*, 155, 241 (1940).
(22) Irany, E. P., *J. Am. Chem. Soc.*, 60, 2106 (1938); 61, 1734 (1939).
(23) Kemp, A. R., and Straitiff, W. G., Ind. Eng. Chem., 36, 707 (1944).
(24) Kern, W., and Fernow, H., *J. prakt. Chem.*, 160, 296 (1942).
(25) Kraemer, E. O., and Lansing, W. D., *J. Phys. Chem.*, 39, 153 (1935).
(26) Lansing, W. D., and Kraemer, E. O., *J. Am. Chem. Soc.*, 57, 1369 (1935).
(27) Mark, H., "Der feste Körper", p. 103, Leipzig, S. Hirzel, 1938.
(28) Mark, H., *Paper Trade J.*, 113, TAPPI Section, p. 28 (July 17, 1941).
(29) Mark, H., and Raff, H., "High Polymeric Reactions", pp. 47 ff., 197, New York, Interscience Publishers, 1941.
(30) Mathes, A., *J. prakt. Chem.*, 162, 245 (1943).
(31) Mayo, F. R., *J. Am. Chem. Soc.*, 65, 2324 (1943).
(32) Montroll, E. W., and Simha, R., *J. Chem. Phys.*, 8, 721 (1940); Montroll, E. W., *J. Am. Chem. Soc.*, 63, 1215 (1941).
(33) Okamura, I., *Cellulose Chem.*, 18, 135 (1935).
(34) Ott, Emil, "Cellulose and Its Derivatives", p. 883, New York, Interscience Publishers, 1943.
(35) Ott, Emil, Ind. Eng. Chem., 32, 1641 (1940).
(36) Richards, O. W., and Roope, P. M., *Science*, 71, 290 (1930).
(37) Rissik, H., *Engineer*, 172, 276, 296 (1941).
(38) Schieber, W., *Papier Fabr.*, 37, 245 (1939).
(39) Schulz, G. V., *Z. physik. Chem.*, B-30, 379 (1935).
(40) *Ibid.*, B-32, 27 (1936).
(41) *Ibid.*, B-43, 25 (1939).
(42) *Ibid.*, B-44, 227 (1939).
(43) Schulz, G. V., and Dinglinger, A., *Ibid.*, B-43, 47 (1939).
(44) Schulz, G. V., and Dinglinger, A., *J. prakt. Chem.*, 158, 136 (1941).
(45) Schulz, G. V., and Nordt, E., *Ibid.*, 155, 115 (1940).
(46) Scott, R. L., *J. Chem. Phys.*, 13, 178 (1945).
(47) Sebrell, L. B., Ind. Eng. Chem., 35, 735 (1943).
(48) Signer, R., and Liechti, J., *Helv. Chim. Acta*, 21, 530 (1938).
(49) Sookne, A. M., Rutherford, H. A., Mark, H., and Harris, Milton, *J. Research Natl. Bur. Standards*, 29, 123 (1942).
(50) Spencer, R. S., and Boyer, R. F., *Polymer Bull.*, 1, No. 6, 129 (1945).
(51) Spurlin, H. M., Ind. Eng. Chem., 30, 538 (1938).
(52) Stockmayer, W. H., *J. Chem. Phys.*, 11, 45 (1943).
(53) Straus, F. L., and Levy, R. M., *Paper Trade J.*, 114, TAPPI Section, p. 211 (April 30, 1942).

Radioactive Studies

Analytical Procedure for Measurement of Long-Lived Radioactive Sulfur, S^{35}, with a Lauritzen Electroscope and Comparison of Electroscope with Special Geiger Counter[1]

F. C. HENRIQUES, JR.[2], G. B. KISTIAKOWSKY, CHARLES MARGNETTI[3], AND W. G. SCHNEIDER[4]
Gibbs and Mallinckrodt Chemical Laboratories, Harvard University, Cambridge, Mass.

A general quantitative procedure for the measurement of S^{35} in tracer investigations is based on the oxidation of all sulfur-containing samples to the sulfate ion by the Carius procedure and subsequent precipitation as benzidine sulfate. This precipitate is collected in a specific manner and the activity therein determined with either a modified Lauritzen electroscope or a Geiger counter especially developed for soft beta-rays. A table and an equation are given for the self-absorption of the beta-particles in this precipitate. In certain respects, as compared to the Geiger counter, the modified electroscope is better suited to the routine measurement of low-energy beta-particles.

ALTHOUGH numerous investigators have used radioactive isotopes as tracers, no systematic effort has been made to develop simple quantitative procedures for determining these elements. Most investigations using radioactive tracers have been biological in nature and because of the inherent variations in biological work, analytical errors as large as 10 to 15% are not of too great import. There are four possible sources of error in the utilization of radioactive tracers in chemical and biological investigations: (1) the preparation of the sample for radioactive analysis, (2) the geometrical factors involved during detection of the disintegrations, (3) the statistical nature of the disintegration process, and (4) the detection apparatus used for determination of the radioactivity.

In numerous cases the errors resulting from the first two sources have been considerable; however, they are usually avoidable. The errors arising from the third and fourth sources have been subjected to mathematical analysis (*4, 5, 11*) and during routine radioactive analysis can be held to about 2%. Within readily recognizable limits, this error is essentially independent of the radioactivity present in the sample.

Certain radioactive elements are intrinsically more difficult to determine than others, owing to the nature and energy of their rays. Because of the low energy of the radiation, the following four radioactive elements are among the most difficult to determine quantitatively:

Element (*10*)	Maximum Energy of Emitted Particles *Mev.*	Half-Life *Days*
S^{35}	0.12 (β^-)	87
As	0.05 (I.T.e^-)	90
C^{14}	0.14 (β^-)	Approximately 1000 years
H^3	0.01 (β^-)	Approximately 30 years

Quantitative procedures (about 2% accuracy) have been worked out for the above low-energy-particle emitting isotopes—namely, the long-lived radioactive sulfur, arsenic, carbon, and tritium.

[1] First paper on subject "Radioactive Studies". Second will be found on page 354.

[2] Present address, Harvard Medical School, Boston, Mass.

[3] Present address, Massachusetts Department of Public Safety, Boston, Mass.

[4] Present address, Woods Hole Oceanographic Institute, Woods Hole, Mass.

This paper considers and evaluates in detail a routine quantitative analytical procedure that has been developed for 87-day sulfur. The radioactive sulfur used in the development of this scheme was obtained from the Radiation Laboratory, Berkeley, Calif.

The use of a radioactive isotope as a tracer depends upon the detection of a fractional number of disintegrations per unit time. In the case of S^{35} this means the accurate determination of a constant fraction of beta-particles of average energy of about 33,000 ev. This energy is so low that the betas are approximately one half absorbed by a 3 mg. per sq. cm. layer and about 95% absorbed by 10 mg. per sq. cm.

DETECTION APPARATUS

GEIGER COUNTER. The recent development of beta-ray Geiger counters (*2*) filled with helium at atmospheric pressure enables them to be constructed with extremely thin windows, which make them especially suitable for the measurement of soft radiation. This bell-type Geiger counter is shown diagrammatically in Figure 1.

The entire detection apparatus consisted of this Geiger counter, a counting rate meter (*6, 9*), and an Esterline Angus recorder (Esterline Angus Co., Indianapolis, Ind.). Two minor improvements were made on the bell-type counter: The thickness of the mica window was reduced from the usual 5 to 10 mg. per sq. cm. to 2 mg. per sq. cm. This exceedingly fragile window (2.54-cm. diameter) was protected from the radioactive sample by means of a brass guard ring (1.91 cm., diameter). Before assembly, the copper cylinder was immersed in an ammonium polysulfide solution. The resulting black sulfide surface seemed to produce better plateau characteristics than the usual bright copper or copper oxide surfaces.

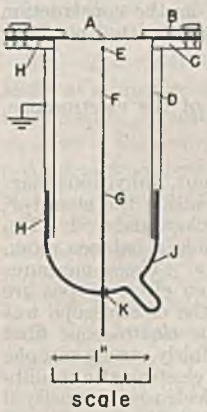

Figure 1. Bell-Type Mica Window Geiger Counter, Helium-Filled

A. Mica window (2 mg. per sq. cm.) coated with colloidal graphite
B. Brass guard ring
C. Copper support ring
D. Copper cylinder
E. 1/16 inch glass bead
F. 7-mil tungsten wire
G. 20-mil tungsten wire
H. Picein wax seal
J. Pyrex tube
K. Tungsten-to-glass seal

This counter had a threshold at about 1600 volts and a 180-volt plateau. It recorded about 60% of the S^{35} beta-particles impinging upon the mica window. When placed inside a 2.5-cm. (1 inch) thick lead box, the natural background (cosmic and local radiations) was 20 to 40 counts per minute.

MODIFIED LAURITZEN QUARTZ FIBER ELECTROSCOPE (*7*). An electroscope detects beta-particles through measurement of the ionization produced by the inelastic collisions of these particles with the air molecules inside the electroscope chamber. Since the path length of the low-energy S^{35} beta in air is not too long, a considerable fraction of the total ionization possible can be collected by the

electroscope unit. In fact, when samples are placed inside the electroscope chamber, the sensitivity to S^{35} of the Lauritzen electroscope is about the same as of the best designed bell-type Geiger counter.

A simple procedure for introducing the radioactive samples inside the electroscope chamber was worked out.

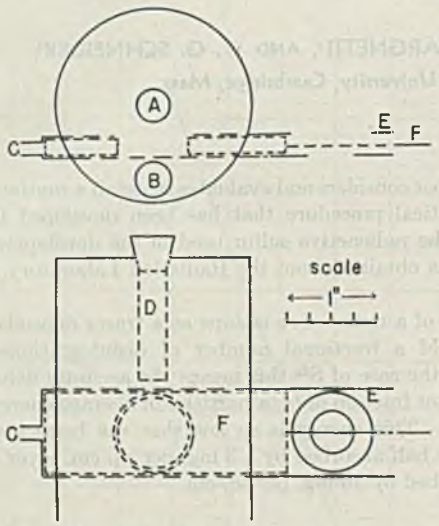

Figure 2. Modified Lauritzen Electroscope Case

A. Window
B. Opening for boat
C. To drying tube (magnesium perchlorate)
D. Boat for drying agent
E. Sleeve for sliding bar
F. Sliding bar for introducing brass disks

First the region of maximum sensitivity within the electroscope chamber was determined by placing a radioactive sample at various positions inside the chamber. Then a simple brass case was constructed which combined the usual cover of the ionization chamber with a sliding-bar device. This sliding-bar device enabled brass disks containing the radioactive samples to be introduced in the most sensitive location within the chamber in a reproducible manner. Brass was chosen as the construction material, since only about 6 alpha-particles are emitted per hour per sq. cm. of surface (*1*).

In order to increase the reproducibility of the electroscope, certain precautions were necessary:

1. A small boat filled with the drying agent, anhydrous magnesium perchlorate, was kept continuously inside the chamber; this resulted in much lower and steadier backgrounds. 2. The electroscope was kept in a balance case inside a balance room. The illuminating lamp burned continuously. These measures minimized temperature fluctuations to which electroscopes are somewhat sensitive. 3. When not in use the electroscope was kept continuously charged. Before use the electroscope fiber was discharged 2 or 3 times by means of a fairly strong sample. These measures ensured rapid attainment of electrostatic equilibrium. The power pack used to charge the electroscope consisted of a simple voltage-doubler circuit (25Z6 tube).

A diagrammatic representation of the modified case of the Lauritzen quartz fiber electroscope is given in Figure 2.

PREPARATION OF RADIOACTIVE SULFUR FOR MEASUREMENT

For accurate radioactive measurement, the low energy of the emitted beta-particles necessitates the isolation of a sulfur-containing compound in a pure state and the collection of this compound in a uniform and reproducible manner. The procedure described was developed with this in mind.

All the sulfur-containing samples are oxidized to the sulfate ion by the Carius method and the sulfur precipitated as benzidine sulfate; this quantitative procedure is described in detail by Niederl *et al.* (*8*). Instead of being evaporated to dryness under reduced pressure as suggested by these investigators, the Carius tube solution is transferred to a 30-cc. beaker and evaporated by means of either an infrared lamp or an inverted hot plate. Through experimentation it has been found that 6 to 7 mg. is a convenient amount of precipitate to handle. Thus enough inactive sulfur, usually as sulfate ion, was added to keep the benzidine sulfate weight above 6 mg.

A previously weighed filter paper circle, 2.22 cm. in diameter, and prepared from Munktell's No. OK paper, is placed over a fritted-glass filtering disk of coarse porosity. The paper is wetted down with water, the water pump is turned on, and the glass cylinder is clamped in place with small springs; thus when assembled the filter apparatus resembles an Allihn filter tube (see Figure 3). This apparatus is somewhat similar to that described by Tarver and Schmidt (*12*). The benzidine sulfate is now rapidly washed into the glass cylinder. Final rinsings are made with 95% alcohol. The cylinder is removed and the water pump is turned off. The paper containing the precipitate is placed in a desiccator and reweighed, then permanently mounted by centering on a brass disk (19 mm. in diameter) and pressing on a brass ring which fits snugly over the disk (Figure 4). The activity of the precipitate is then determined by placing the assembled disk either inside the electroscope chamber by means of the sliding bar, or face down on the guard ring of the mica window of the bell counter.

Benzidine hydrochloride is superior to barium chloride as a precipitant, owing to the uniformity of the resulting matlike precipitate. The combination of Munktell's filter paper and the Corning fritted disk of C porosity results in a very uniformly distributed precipitate which adheres firmly to the filter paper. Numerous kinds of filter papers and fritted disks were tried before the above result was obtained. The filter paper with and without precipitate is reweighed after standing in a desiccator for one hour. Under these conditions the weights are reproducible to 0.05 mg. In order to prevent loss of weight due to handling, it is necessary that the filter paper have sharp edges; this is most readily accomplished by having the circles cut by a commercial stationery concern.

The importance of the above factors cannot be overemphasized. The energies of the emitted beta-rays are so low that a considerable fraction of these particles are absorbed in the benzidine sulfate. The uniformity of the precipitate reduces this self-absorption to a reproducible factor and the weighing of the precipitate enables this factor to be taken into account.

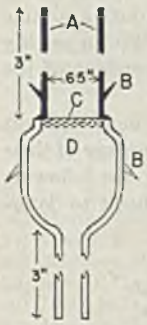

Figure 3. Benzidene Sulfate Precipitating Apparatus

A. Pyrex cylinder
B. Glass ears for springs
C. Munktell's No. OK filter paper circle
D. Fritted disk of coarse porosity, prepared from Corning GYCRY crucible

The procedure described above is well suited to routine use in both chemical and biological tracer work, since the Carius method enables a large number of samples to be oxidized simultaneously. By using a large-capacity electric furnace and a time clock, these oxidations can be done at night, thus enabling one person to make S^{35} analyses on about 20 to 40 samples per day.

Table I illustrates a typical set of S^{35} analyses for both a Lauritzen electroscope and a Geiger counter. Computations pertinent to columns 7, 8, and 9 are considered below.

RELATIVE ACCURACY AND SENSITIVITY OF RADIOACTIVE ANALYTICAL METHOD

The appearance of a beta-particle inside a Geiger counter produces a discrete impulse or "count" which is recorded by an auxiliary apparatus. Thus, the number of counts per minute minus the natural

Table I. Typical Set of S^{35} Analyses with Modified Lauritzen Electroscope and Bell-Type Mica Window Geiger Counter

Carius No.	Disk No.	Weight of Ppt., Mg.	Electroscope Reading Initial	Electroscope Reading Final	Time, t, Sec.	Total Activity $(d/t)_s$ $\times 10^2$	Net Activity $[(d/t)_s - (d/t)_b]$ $\times 10^2$	Weight Correction Factor (See Table III)	S, γ	S, γ per Unit Net Activity
				Electroscope 97, Expt. 19-P, 3/24/43						
	Std-1	7.00	45	55	173.1	5.74	5.68	1.000	3.200	0.563
			45	55	174.4					
	Std-2	7.00	45	55	292.4	3.41	3.35	1.000	1.900	0.567
			45	55	293.4					
12	7	8.70	45	55	312.1	3.21	3.15	0.895	1.99	...
			45	55	311.0					
14	9	6.07	45	55	100.5	9.91	9.85	1.065	5.27	...
			45	55	101.1					
17	11	11.25	45	50	1840	0.273	0.214	0.780	0.16	...
21	12	8.18	45	50	7100	0.070	0.011	0.925	0.007	...
	Background		45	50	8500	0.059	Nil	...	...	...
	Std-1	...	45	55	175.6	5.71	5.65	...	3.200	0.566
			45	55	174.6					
	Std-2	...	45	55	295.7	3.40	3.34	...	1.900	0.569
			45	55	292.1					
									Av.	0.566
				Geiger Counter C and Counting Rate Meter, Expt. 19-P, 3/24/43						
			Scale Reading		Total Activity, Counts per Min.	Net Activity $(c/m)_s - (c/m)_b$				
..	Std-1	...	3	69	3450	3420		1.000	3.200	1070
..	Std-2	...	3	41	2050	2020		1.000	1.900	1060
	Background		7	15	30	Nil		...	...	...
12	7	8.70	3	41	2050	2020		0.925	2.04	...
14	9	6.07	2	58	5800	5770		1.045	5.16	...
17	11	11.25	7	82	164	134		0.815	0.15	...
21	12	8.18	7	20	40	10		0.945	0.01	...
..	Std-1	...	3	68	3400	3370		...	3.200	1050
..	Std-2	...	3	42	2100	2070		...	1.900	1090
									Av.	1070

background is a relative measure of the amount of radioactivity present. This quantity will be denoted as

$$(c/m)_s - (c/m)_b \qquad (1)$$

where c denotes counts, m minutes, s sample, and b background. The appearance of the beta-particle in the neighborhood of the charged repelling post of a Lauritzen electroscope produces ionization which discharges the gold-plated quartz fiber at a faster rate than its natural (background) rate of discharge. Thus the reciprocal of the time for the fiber to move a certain number of scale divisions in the presence of a radioactive sample minus the reciprocal of the time for the fiber to move the same number of scale divisions in the absence of the sample (background) is a measure of the amount of radioactivity present. This quantity will be denoted as

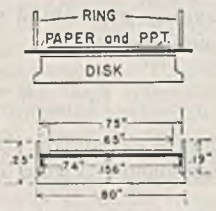

Figure 4. Brass Measuring Disks

Above. Unassembled
Below. Assembled

$$(d/t)_s - (d/t)_b \qquad (2)$$

where d is the distance traversed by the fiber in time t in seconds, s sample, and b background.

The relative sensitivity of the Geiger counter and electroscope may be defined for comparative purposes by the following equations:

$$\frac{(c/m)_s - (c/m)_b}{\overline{(c/m)_b}} \qquad (3)$$

$$\frac{(d/t)_s - (d/t)_b}{\overline{(d/t)_b}} \qquad (4)$$

where the bar in the denominator denotes average value. The sensitivity as defined by Equation 4 is essentially the same for all Lauritzen quartz fiber electroscopes. These electroscopes usually possess an absolute sensitivity such that 1 millicurie of radium at a distance of 1 meter produces a movement of 2 to 5 scale divisions per minute. Under these conditions all Lauritzen electroscopes discharge at a rate of about 60 times "natural" background. Thus the absolute sensitivity is of small import, since there is no appreciable loss in accuracy in allowing the fiber of the electroscope possessing a low absolute sensitivity to discharge 10 scale divisions instead of the 20 scale divisions one would use with electroscopes of greater absolute sensitivity.

The determination of experimental values for Equations 3 and 4 as a function of relative concentration of radioactive sulfur contained in a constant weight (7 mg.) of benzidine sulfate is a measure of the accuracy and relative sensitivity of the radioactive analytical procedure for S^{35} with both the electroscope and Geiger counter. The concentration of the radioactive sulfur was progressively diluted previous to precipitation by mixing known volumetric aliquots of both inert (carrier) sulfate ion and sulfate ion containing S^{35}.

Table II tabulates the results of duplicate determinations for both the electroscope and counter. The concentration of the weakest radioactive sample measured has been arbitrarily taken as unity. The data show that satisfactory radioactivity analyses can be made with samples containing activities 5 to 200 times the background. Since radioactive sulfur is readily obtainable with high specific activity, this is not a serious limitation of the procedure. The data indicate that the electroscope is somewhat more accurate than the counting apparatus used in this investigation. However, this difference would disappear on substitution of a well-designed scaling circuit for the counting rate meter. The relative sensitivities of the instruments are essentially identical; that of the electroscope could be increased somewhat by surrounding it with lead, 2.5 cm. thick.

The absolute sensitivity of both instruments is such that 10^{-4} microcurie of S^{35} will be of the order of the background in ac-

Table II. Radioactivity Measurements as a Function of S^{35} Content of Sulfate

(Dilution experiments. S^{35} concentration in least active sample is chosen as unity. Radioactivity measurements are expressed as ratio of net activity to average background.)

Modified Lauritzen Electroscope				Relative S^{35} Concentration	Bell-Type Mica Window Geiger Counter			
Radioactive Measurements			Average deviation, %		Radioactive Measurements			Average deviation, %
Observed R_i	Av.	Expected[a] R_i		C_i	Observed R_i	Av.	Expected[a] R_i	
206	205	207	1.0	1000	253	254	254	0.0
204					255			
162	164	166	1.5	800	210	208	203	2.2
165					205			
103	103	104	1.0	500	125	126	127	0.8
103					127			
82.3	83.0	83.2	0.2	400	98	98.5	102	3.4
83.6					99			
41.8	42.0	41.6	0.8	200	50.2	50.6	50.8	0.4
42.1					51.0			
21.0	20.9	20.8	0.5	100	25.0	25.4	25.4	0.0
20.8					25.7			
17.2	16.9	16.6	1.5	80	21.3	20.8	20.3	2.2
16.5					20.2			
10.3	10.4	10.4	0.5	50	11.8	12.0	12.7	5.5
10.4					12.2			
8.23	8.15	8.32	2.0	40	11.0	10.7	10.2	4.4
8.07					10.3			
4.30	4.20	4.16	0.8	20	5.39	5.33	5.08	5.1
4.11					5.27			
2.07	2.15	2.07	3.6	10	2.39	2.48	2.54	2.4
2.22					2.56			
1.73	1.69	1.66	1.8	8	1.97	1.98	2.03	2.7
1.65					1.98			
1.12	1.09	1.04	4.3	5	1.35	1.31	1.27	2.8
1.05					1.26			
0.90	0.88	0.83	6.0	4	0.91	0.97	1.02	5.4
0.85					1.02			
0.41	0.44	0.42	4.8	2	0.46	0.50	0.51	2.0
0.47					0.54			
0.16	0.19	0.21	9.5	1	0.23	0.28	0.25	12
0.22					0.32			

[a] $R_i = \frac{C_i \Sigma (R_i/C_i) \log C_i}{\Sigma \log C_i}$. This equation expresses the fact that accuracy of measurement increases somewhat with concentration of radioactivity.

tivity. Thus 10^{-3} microgram of any sulfur compound can be readily determined if the specific activity is 1 millicurie of S^{35} per 10 mg. of compound.

CORRECTION FOR WEIGHT OF BENZIDINE SULFATE PRECIPITATE

Since the beta-particles emitted from S^{35} have a maximum energy of only 0.12 Mev., a considerable fraction of these particles are absorbed in the benzidine sulfate precipitate. Thus it is necessary to refer all radioactive measurements to a predetermined weight, which was arbitrarily chosen as 7.00 mg. or 3.25 mg. per sq. cm.

A correction chart was obtained by determining the radioactivity of constant concentrations of S^{35} as a function of the weight of the benzidine sulfate precipitate; the range was 1 to 25 mg. in 1-mg. intervals. All data are the averages of triplicate determinations (Table III). The values are not quite the same with the electroscope and the Geiger counter. Since the beta-particles are far from monochromatic and the Geiger counter counts each particle that enters the counter, while the electroscope measures the ionization resulting from a particle, the difference in the above results is to be expected. Further, the electroscope data are independent of the electroscope used, while the counter data depend upon the thickness of the mica window of the bell-type counter.

A consideration of the magnitude of these correction factors shows that the error due to self-absorption is not appreciable in radioactive analytical work, since the benzidine sulfate precipitate is weighable to better than 0.1 mg.

The self-absorption is expressed to an excellent approximation by the following equation (*3*):

$$I/I_0 = (1 - e^{-\alpha d})/2\alpha d \qquad (5)$$

where I_0 is a constant but may be considered the "true" total activity present in the benzidine sulfate precipitate, d is the "thickness" of the sample in milligrams per sq. cm., and α is an average exponential absorption coefficient of the following numerical value:

$$\alpha = 0.32 \text{ sq. cm. per mg.} \qquad (6)$$

for the electroscope data. This equation is derived in the following manner (Figure 5):

Let $2S$ be the "true" specific activity per unit weight (mg.) of precipitate. Assuming exponential absorption ($I = I_0 e^{-\alpha x}$), the measurable activity from the weight element, AdX, is

$$SAe^{-\alpha x}dx \qquad (7)$$

since $^1/_2$ of the disintegrations are directed downward.

Thus the total measurable activity is

$$I = SA \int_0^d e^{-\alpha x}dx = SA(1 - e^{-\alpha d})/\alpha \qquad (8)$$

Since "true" total activity is

$$I_0 = 2SAd \qquad (9)$$

we have by substituting (9) in (8),

$$I/I_0 = (1 - e^{-\alpha d})/2\alpha d \qquad (10)$$

All the approximations made in this derivation are trivial as compared to the assumption of exponential absorption of the beta-particles. This equation for the self-absorption of low-energy beta-particles which arise from radioactive disintegration seems to be experimentally valid to within 2 to 5%.

EVALUATION OF GEIGER COUNTER AND ELECTROSCOPE

The data given above show that accurate analytical results can be obtained with either the modified Lauritzen electroscope or

bell-type mica window counter. In fact, on the basis of accuracy and sensitivity they are essentially equivalent. Both instruments will readily detect 10^{-4} microcurie of S^{35}. In laboratories where there are a limited number of personnel trained in electronics, an electroscope is preferable in view of its ruggedness and simplicity of design. It has been the authors' experience that during routine use the entire counting apparatus is considerably more erratic in behavior than an electroscope. An electroscope will give continuous reproducible results until the gold plating on the quartz fiber becomes broken; this phenomenon is readily recognizable. Further, the cost of a complete counting apparatus is more than tenfold that of an electroscope. The average life of an electroscope under the somewhat drastic conditions of placing radioactive samples inside the ionization chamber is about one year; thus it is advisable to own two electroscopes.

Two statements are sometimes made regarding the relative merits of the Geiger counter and the electroscope which require consideration:

1. Since it is capable of detecting each individual disintegration, a Geiger counter is intrinsically more sensitive than an electroscope. This statement is certainly true of the theoretical counter. Unfortunately it does not apply to the practical case of measuring low-energy beta-particles, since the routine placement of radioactive samples inside Geiger counters is not conducive to reproducible counting.
2. Since the accuracy of measuring activities of the order of background depends in part upon the reproducibility of this background, a Geiger counter is more accurate for these determinations than an electroscope. This deduction is based essentially upon the fact that the time variation in the number of cosmic and local rays entering a counter is less than the time variation in the total ionization produced by these same rays as measured by the electroscope (*4, 5, 11*). Actually the statistical variations in the background of the electroscope are somewhat less than that of counters developed for the detection of soft beta-particles. This is due to the large difference in the "effective background detection area" of the instruments; the beta-ray counter enclosed in a lead box records about 30 background counts per minute, while the electroscope is measuring the ionization produced by at least 200 "background" rays per minute. During two years, numerous background determinations have been made both with the electroscope and beta-ray Geiger counter. On a basis of 1-hour determinations, the daily variations in background were with few exceptions never greater than 10% with the beta-ray counter and 6% with the electroscope. Accurate determinations on samples containing activity of the order of the background can be made by measuring the sample, background, sample and background, respectively; this is how the activities in samples of concentration 1 to 8 in Table II were determined.

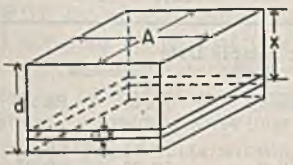

Figure 5

Since the sensitivity with respect to background and the reproducibility of this background of the modified electroscope and bell-type mica window counter are essentially identical, the times required to measure any radioactive sample to the desired accuracy with either instrument are equal. It is of interest to indicate the actual time of measurement. Samples with radioactivity of the order of the background necessitate 1 to 3 hours to determine to about 5%; however, with these samples this accuracy is usually not necessary and 15 minutes will suffice for most investigations. The maximum accuracy for both counter and electroscope will be with samples at least 10 times background. The time required to measure these samples is a matter of minutes. Because of the necessity of equilibrating the position of the quartz fiber, accurate results with samples containing radioactivity in excess of 250 times background cannot be expected; depending on the electroscope, an activity of this order will discharge the fiber at a rate of 10 to 20 small divisions per minute. The maximum counting rate for a Geiger counter depends on the over-all quenching circuit time constant. For the specific counter and auxiliary apparatus used in these investigations, this rate was 12,000 counts per minute (~400 times background).

Table III. Self-Absorption of S^{35} Beta-Particles

(Reciprocal correction factors for weight of benzidine sulfate precipitate for both an electroscope and Geiger counter. Net measured activity is to be divided by these factors. The factor for 7.00 mg. of precipitate is defined as unity.)

Electroscope Reciprocal Weight Correction Factor	Total Weight of Benzidine Sulfate Ppt. *Mg.*	Weight of Ppt. *Mg./sq. cm.*	Geiger Counter Reciprocal Weight Correction Factor
1.595	1	0.46	1.370
1.465	2	0.93	1.290
1.350	3	1.40	1.205
1.245	4	1.85	1.150
1.155	5	2.30	1.095
1.070	6	2.80	1.050
1.000	7	3.25	1.000
0.935	8	3.70	0.955
0.880	9	4.15	0.910
0.830	10	4.65	0.865
0.780	11	5.10	0.825
0.750	12	5.55	0.790
0.715	13	6.00	0.754
0.680	14	6.50	0.715
0.650	15	6.95	0.680
0.625	16	7.40	0.650
0.595	17	7.90	0.625
0.570	18	8.35	0.600
0.545	19	8.80	0.575
0.520	20	9.25	0.555
0.500	21	9.75	0.535
0.480	22	10.20	0.520
0.465	23	10.70	0.500
0.450	24	11.10	0.480
0.435	25	11.60	0.465

It will be shown in subsequent publications that the Lauritzen electroscope with certain modifications is well suited for the measurement of other radio elements emitting low-energy particles. Further, it is to be recommended for use with radioelements emitting high-energy particles, since it is usually not difficult to obtain these elements with sufficiently high specific activity at a reasonably low cost. If necessary, the electroscope chamber could be made gas-tight and filled with a high-density vapor such as sulfur dioxide or methyl iodide, thus increasing the ionization produced by the high-energy particles.

ACKNOWLEDGMENT

R. S. Halford of the Harvard Chemical Laboratories collaborated with the senior author in designing the modified case of the Lauritzen electroscope.

LITERATURE CITED

(1) Bearden, J. A., *Rev. Sci. Instruments*, 4, 271 (1933).
(2) Brown, S. C., Good, W. M., and Kip, A. F., *Ibid.*, 17, in press (1946).
(3) Dodson, R. W., private communication.
(4) Evans, R. D., *Rev. Sci. Instruments*, 6, 99 (1935).
(5) Evans, R. D., and Neher, H. V., *Phys. Rev.*, 45, 144 (1935).
(6) Kip, A. F., Bousquet, A. G., Evans, R. D., *et al.*, *Rev. Sci. Instruments*, 17, in press (1946).
(7) Lauritzen, C., and Lauritzen, T., *Ibid.*, 8, 483 (1937).
(8) Niederl, J. B., Baum, H., McCoy, J. S., and Kuck, J. A., Ind. Eng. Chem., Anal. Ed., 12, 428 (1940).
(9) Radioactivity Center, Mass. Institute of Technology, Cambridge, Mass.
(10) Seaborg, G. T., *Rev. Mod. Phys.*, 16, 1 (1944).
(11) Strong, J., "Procedures in Experimental Physics", pp. 245–8, 298–304, New York, Prentice-Hall, 1938.
(12) Tarver, H., and Schmidt, C. L., *J. Biol. Chem.*, 130, 67 (1939).

Work done under Contract No. NDCrc-169 between the president and fellows of Harvard College and the Office of Scientific Research and Development, which assumes no responsibility for the accuracy of statements contained herein.

Determination of Acetone

An Ultraviolet Spectrophotometric Method

G. L. BARTHAUER, F. V. JONES, AND A. V. METLER
Field Research Department, Magnolia Petroleum Company, Dallas, Texas

A method is described for the determination of acetone in mixtures with diisopropyl ether, isopropyl alcohol, and low-molecular weight mono-olefins. Essentially the procedure involves suitable dilution of the sample with 2,2,4-trimethylpentane, followed by measurement of the optical density of the diluted material at 280 millimicrons.

IN CONNECTION with the production of propylene by the catalytic dehydration of isopropyl alcohol, it was necessary to develop a rapid and accurate method for measuring acetone produced as a by-product of the main reaction. Low-molecular weight mono-olefins, diisopropyl ether, and unreacted isopropyl alcohol were also present in considerable quantities in the solutions to be investigated.

From the standpoint of both rapidity and accuracy, a photometric method, based on the absorption of ultraviolet light by acetone, appeared to be the most promising approach to the problem.

Hartley (*4*) has reported the complete absence of ultraviolet bands (above the Schumann region) for isopropyl alcohol. Bielecki and Henri (*1*) detected a very slight continuous absorption for *n*-propyl alcohol but, in the light of subsequent work by Massol and Faucon (*5*) who showed that the degree of absorption of a secondary alcohol was lower than that of the corresponding primary, it appeared that this absorption could be regarded as insignificant from an analytical viewpoint.

Carr and Walker (*2*) have thoroughly investigated the ultraviolet spectra of mono-olefins in the low-molecular weight range. In no case does the absorption become significant above 260 millimicrons, a wave length well below the acetone absorption maximum.

Despite a thorough search of the literature, no data on the absorption of diisopropyl ether were found. The absence of significant bands, however, has been proved experimentally.

The absorption of ultraviolet light by acetone has been the subject of much study and the authors' work has only verified previous reports (*6–9*).

EXPERIMENTAL

REAGENTS AND EQUIPMENT. Acetone, Commercial Solvents (C.P.).

Diisopropyl ether, Eastman Kodak No. 1193. This material was purified by successive fractionation and chemical treatment until only a very faint trace of acetone remained.

Isopropyl alcohol, Eastman Kodak No. 212, treated like the diisopropyl ether.

1-Octene, Connecticut Hard Rubber Company. Approximately 99% pure, the remainder consisting of close-boiling isomers.

2,2,4-Trimethylpentane (Iso-octane), Rohm and Haas material, carefully purified prior to use by means of silica gel (*3*).

All spectral measurements were made with a Beckman DUV spectrophotometer equipped with a hydrogen discharge source. The wave-length scale was calibrated with a mercury vapor lamp to within ±0.1 millimicron just prior to use. Matched quartz cuvettes (10 mm.) were employed to contain the sample and the 2,2,4-trimethylpentane reference solution.

SCANNING AND CALIBRATION. Figure 1 is a plot of experimentally obtained transmittancies against wave length for a solution of each component in the mixture. A band width of 0.5 millimicron was used throughout the entire wave-length range.

As can be seen, acetone showed a broad band centered at approximately 280 millimicrons. A calibration curve prepared at this wave length by plotting the so-called "optical densities" $\left(\log \frac{I_0}{I_x}\right)$ against the corresponding concentrations of acetone in 2,2,4-trimethylpentane showed no significant deviation from Beer's law.

CALCULATION AND INTERPRETATION

The molecular extinction coefficient, k, of each compound was calculated from the foregoing data, using the familiar modified form of the Beer-Lambert equation,

$$I_x = I_0 10^{-klc}$$

where l represents cell length (cm.), c the molar concentration, and I_0 and I_x the incident and emergent light intensity, respectively. These data are shown in Table I.

SYNTHETIC SAMPLES

A series of synthetic samples containing varying amounts of the pure components was analyzed for acetone content. Each sample

Table I. Molecular Extinction Coefficients at 280 Millimicrons

Compound	Concentration Vol. %	Transmittancy %	k
Acetone	1	5.0	9.58
Olefin	10	87.8	0.09
Diisopropyl ether	25	93.8	0.02
Isopropyl alcohol	25	90.0	0.01

Table II. Synthetic Sample Data

Sample Composition				Results	
Alcohol %	Ether %	Olefin %	Acetone %	Acetone found %	Error %
95.0	...	...	5.0	5.38	+0.38
...	...	90.0	10.0	10.22	+0.22
...	85.0	...	15.0	14.86	−0.14
50.0	15.0	15.0	20.0	20.31	+0.31
10.0	50.0	15.0	25.0	25.40	+0.40
10.0	10.0	50.0	30.0	29.68	−0.32

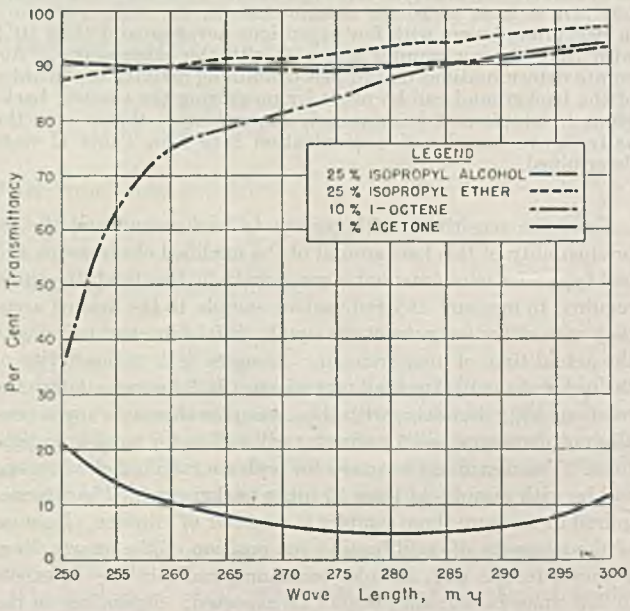

Figure 1. Experimentally Obtained Values

was accurately diluted with 2,2,4-trimethylpentane until the optical density obtained fell within the range of the calibration curve. Reference to the curve and the application of the appropriate dilution factor readily permitted calculation of the acetone concentration in the original sample.

All values shown in Table II were calculated from the equation of the best-fitting calibration line. This equation was obtained by the method of least squares.

As can be seen from Figure 1, the rate of change of the extinction coefficient of acetone is small at its absorption maximum. This would suggest the ready application of filter photometers for transmittancy measurements despite the relatively broad wave bands usually associated with such instruments.

SUMMARY

Acetone may be determined in the presence of alcohols, ethers, and mono-olefins of low molecular weight by measurement of the spectral transmittancy at 280 millimicrons. The data indicate that a low-cost filter photometer may be employed for obtaining satisfactory transmittancy values.

LITERATURE CITED

(1) Bielecki, G., and Henri, V., *Compt. rend.*, 155, 456–8 (1912).
(2) Carr, E. P., and Walker, M. K., *J. Chem. Phys.*, 4, 751–5 (1936).
(3) Graff, M. M., O'Connor, R. T., and Skau, E. L., Ind. Eng. Chem., Anal. Ed., 16, 556–7 (1944).
(4) Hartley, W. N., *J. Chem. Soc.*, 39, 153–73 (1881).
(5) Massol and Faucon, *Bull. soc. chim.*, 11, 931–5 (1912).
(6) Purvis, J. E., *J. Chem. Soc.*, 127, 9–14 (1925).
(7) Rice, F. O., *Proc. Roy. Soc.*, 91, 76 (1914).
(8) Walls, H. J., and Ludlam, E. B., *Trans. Faraday Soc.*, 33, 776–81 (1937).
(9) Washburn, E. W., "International Critical Tables", Vol. V, pp. 369, 371, 374, 376, 377, New York, McGraw-Hill Book Co., 1929.

Amperometric Titration of Chloride, Bromide, and Iodide Using the Rotating Platinum Electrode

H. A. LAITINEN, W. P. JENNINGS, AND T. D. PARKS[1], Noyes Chemical Laboratory, University of Illinois, Urbana, Ill.

Chloride, bromide, and iodide can be titrated rapidly in dilute solution with silver nitrate, using a rotating platinum electrode as the indicator electrode in amperometric titrations. Wide variations in the concentration of acid or salts present do not affect the results. A tendency toward low results is observed with increasing dilution. Chloride can be titrated in 10^{-4} *N* solution in 75% acetone, bromide in 50% acetone, and iodide in water.

THE use of a rotating platinum electrode in amperometric titrations (*4*) of arsenite with bromate (*6*), silver with chloride (*6*), and mercaptans with silver (*3*) has been described. Halides can be titrated in a simple manner by measurement of the diffusion current of silver ions during the course of the titration. The end point is determined graphically from a plot of current against titration volume.

Salomon (*7, 8, 9*) made a study of "galvanometric titrations" using two silver electrodes in dilute potassium chloride with an e.m.f. of 0.1 volt applied across the electrode. When the potassium chloride was titrated with silver nitrate, practically no current flowed until an excess of silver had been added. The end point was taken as the point where the sudden current increase occurred.

The dead-stop end point of Foulk and Bawden (*1*) is based upon the sudden polarization or depolarization of one or both electrodes of an electrolytic cell in the presence of the first small excess of reagent.

Both the galvanometric and dead-stop end points are very similar in principle to the amperometric end point. However, the important new feature of the amperometric titration is that the current is measured in general on a diffusion current region of a current-voltage curve. On such a region, the current is independent of the potential of the electrode because of an extreme state of concentration polarization at the indicator electrode. Since the concentration of material undergoing electrode reaction is maintained at a value practically equal to zero, the current is limited by the supply of fresh material to the electrode surface by diffusion. The rate of diffusion, and hence the current, is proportional to the concentration of diffusing substance in the bulk of the solution. By using a rotating electrode, the diffusion layer thickness is decreased, thereby increasing the sensitivity and the rate of attainment of a steady diffusion state. It is evident that a titration curve of diffusion current against volume of reagent is, in general, a straight line. (Strictly speaking, a correction for dilution is necessary to attain a linear relation between current and volume of reagent, but by working with a reagent which is tenfold more concentrated than the solution being titrated, the correction becomes negligibly small.)

In titrating halides with silver, the potential of the rotating electrode is made negative enough to plate out silver ions, leaving the layer of solution next to the electrode depleted of silver ions. The potential, however, must not be negative enough to give an appreciable current due to the reduction of dissolved oxygen. The range of permissible potential is strictly limited, as is evident from an examination of the current-voltage curves of silver-ion reduction and oxygen reduction using a silver-plated electrode (*6*). The potential of the saturated calomel electrode happens to lie in the permissible range, so that it is necessary only to short-circuit the rotating electrode through a suitable current measuring instrument to a saturated calomel electrode of relatively large area. Titrations in ammoniacal medium are carried out at a more negative potential, to deposit the complex diammine silver ions. Fortunately, the reduction curve of oxygen is shifted to more negative potentials in ammoniacal solution, and all that is necessary is to substitute for the saturated calomel electrode a reference electrode of more negative potential.

In the previous work on the amperometric titration of silver with chloride (*6*), a large irregularly fluctuating current was observed even in the presence of a large excess of chloride where the silver ion concentration should be very low. This current was attributed to a depolarization of the platinum cathode by colloidally dispersed silver chloride particles. It was found that the abnormal current could be decreased by flocculating the precipitate by the addition of electrolyte, and eliminated by the addition of gelatin. The gelatin causes the precipitate to become peptized by protective colloid action, but the gelatin-coated particles no longer are reducible at the cathode. The gelatin also changed the character of the plated silver from a coarsely crystalline to a finely divided, adhering deposit. With the coarsely deposited silver, a slowly drifting diffusion current was observed, while electrodes plated in the presence of gelatin gave constant diffusion currents for long periods of time. The drifting effect is unimportant in amperometric titrations if a freshly cleaned platinum electrode is used.

[1] Present address, Shell Development Co., Emeryville, Calif.

Table I. Titration of 100 Ml. of Chloride

Normality of Cl^-	Normality of $AgNO_3$	Galvanometer Sensitivity	$AgNO_3$ Used Theory	$AgNO_3$ Used Experimental	Error
			Ml.	*Ml.*	%
		Aqueous Solution, 0.8 *N* Nitric Acid			
0.100	0.500	1/50	20.00	20.00, 19.68	0.0, −1.6
				19.74, 19.87	−1.3, −0.6
0.0100	0.100	1/50	10.00	9.99, 9.99	−0.1, −0.1
				9.95, 9.99	−0.5, −0.1
0.0100	0.0500	1/20	20.00	19.82, 19.81	−0.9, −1.0
				19.79, 19.86	−1.1, −0.7
0.0100	0.0500	1/50	20.00	19.99, 20.00	−0.1, 0.0
				20.00, 19.99	0.0, −0.1
				19.97	−0.2
0.0050	0.0500	1/50	10.00	10.01, 10.02	+0.1, +0.2
				9.99, 9.99	−0.1, −0.1
0.0020	0.0100	1/50	20.00	20.00, 19.68	0.0, −1.6
				19.74, 19.87	−1.3, −0.6
0.0020	0.0100	1/20	20.00	19.45, 19.46	−2.8, −2.7
0.0010	0.0100	1/20	10.00	9.36, 9.16	−6.4, −8.4
				9.41, 9.10	−5.9, −9.0
0.0005	0.0100	1/20	5.00	4.25, 4.29	−15.0, −14.2
				4.19, 4.20	−16.2, −16.0
		50% Acetone, 0.8 *N* Nitric Acid			
0.1000	0.500	1/50	20.00	20.00, 19.97	0.0, −0.2
				19.98	−0.1
		1/20	20.00	19.95	−0.2
0.0100	0.100	1/20	10.00	9.94, 9.94	−0.6, −0.6
				9.93, 9.95	−0.7, −0.5
0.0100	0.0500	1/50	20.00	19.90, 19.89	−0.5, −0.6
		1/20	20.00	19.95, 19.96	−0.2, −0.2
				19.94, 19.96	−0.3, −0.2
0.0050	0.0100	1/50	10.00	9.96	−0.4
		1/20	10.00	9.95, 9.95	−0.5, −0.5
				9.94	−0.4
0.0020	0.0100	1/50	20.00	19.81, 19.83	−1.0, −0.8
				19.82, 19.83	−0.9, −0.8
0.0010	0.0100	1/20	10.00	9.71, 9.71	−2.9, −2.9
				9.73, 9.73	−2.7, −2.7
0.00050	0.0100	1/20	5.00	4.84, 4.83	−3.2, −3.4
				4.83, 4.80	−3.4, −4.0
0.00020	0.0010	1/20	20.00	19.20, 18.70	−4.0, −6.5
		1/10	20.00	18.87, 18.83	−5.7, −5.9
0.0001	0.0010	1/10	10.00	9.33, 9.05	−6.7, −9.5
				9.08, 9.05	−9.2, −9.5
0.00020[a]	0.0010	1/10	20.00	19.45, 19.47	−2.8, −2.7
0.00010[a]	0.0010	1/10	10.00	9.75, 9.95	−2.5, −0.5

[a] In 75% acetone.

EXPERIMENTAL

Several types of rotating microelectrodes have been used, but the most satisfactory one in the authors' experience was made from a cone-drive laboratory stirring motor essentially as previously described (*6*). A sturdy piece of platinum wire (No. 18) was sealed into 6-mm. soft-glass tubing to form an electrode 5 to 10 mm. long. The tubing was bent at right angles about 2 cm. from the end. A drop of mercury inside the tube served to make electrical contact to a copper wire inside the glass tube, and connected at its other end to a brass sleeve inside the chuck provided with the motor. The electrical contact is very important and sliding or bearing contacts should be avoided. By inverting the shaft of the Sargent cone-drive stirrer, a small cup is formed at the top end of the shaft. A drop of mercury in the cup makes direct metallic contact between the rotating shaft and the frame of the motor which is provided with binding posts.

The sensitivity of the current-measuring device is of some importance, especially in chloride titrations. Owing to the solubility of the precipitate, an appreciable current passes through the cell at the end point and if a very sensitive galvanometer is used without shunting, a tendency toward low results is observed. A very convenient instrument for current measurements is the Fisher Electropode, which was designed for use with the dropping mercury electrode. It contains a multiple mirror lamp and scale galvanometer, provided with an Ayrton shunt which permits choice of a wide range of sensitivities. A microammeter of 15- or 30-microampere range, or a small enclosed lamp and scale type galvanometer, provided with a variable shunt, has been found entirely satisfactory. In general, the lowest sensitivity consistent with accurate readings has given the best results.

Care should be taken to arrange a reference electrode of large area (to prevent polarization by the passage of current) and salt bridges of low resistance. In the present work the electrode and salt bridge were of the type described by Hume and Harris (*2*). The agar plugs were replaced by plugs of sintered glass, prepared from powdered Pyrex (*5*). For titrations in ammoniacal medium, the mercury–mercuric iodide–potassium iodide cell, described by Kolthoff and Harris (*3*), of potential −0.23 volt *vs.* saturated calomel electrode, was used. In typical titrations, the entire cell had a resistance of the order of 1500 to 2000 ohms.

TITRATION OF CHLORIDE

Standard solutions of sodium chloride and silver nitrate were prepared accurately, using reagent quality salts which had been powdered and dried at 110° for 2 hours. Curves for the titration of 0.1 *N* and 0.001 *N* chloride are shown in Figures 1 and 2.

In a series of titrations of 0.01 *N* chloride, the concentration of gelatin was varied between 0.01 and 0.4%, nitric acid was added in concentrations between 0.08 *N* and 3.2 *N*, and sulfuric acid was added in concentrations between 0.08 *N* and 9.2 *N*. The maximum variation in results observed was 0.5%. Titrations of 0.002 *N* chloride in the presence of 0.2 *M* barium nitrate or 2 *M* potassium nitrate did not show interference by the added salts in the presence of 0.1% gelatin.

Table I shows data obtained for various concentrations of chloride in aqueous solution and in 50% acetone. In all these titrations, 100 ml. of chloride solution, 0.8 *N* in nitric acid, and 0.1% gelatin were used. The galvanometer sensitivity indicates the fraction of the full sensitivity (0.01 microampere per mm.) used in each titration.

According to Table I, satisfactory results can be obtained down to 0.002 *N* chloride in aqueous medium, but low results were found for lower concentrations (15% low at 0.0005 *N*). In general, the lowest galvanometer sensitivity consistent with accurate readings gave the best results, since the observations were taken relatively far from the end point in titration of dilute solutions.

Using 50% acetone as the titrating medium the solubility of silver chloride is reduced to such a point that 10^{-4} *N* chloride solution can be titrated with a 10% error. In 75% acetone, the error with 10^{-4} *N* chloride is reduced to 3%. However, the diluting effect of the additional acetone must be considered in making a comparison, since the original sample would be diluted fourfold using 75% acetone and only twofold using 50% acetone.

In general, the use of 50% acetone as a titrating medium is recommended for chloride concentrations below about 0.005 *N*.

TITRATION OF BROMIDE

The precision and accuracy of bromide titrations were checked under conditions very similar to those found suitable for chloride. Gelatin was added in the present experiments, although later

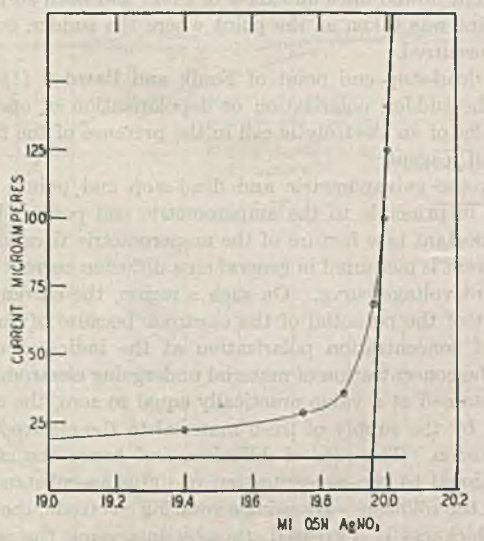

Figure 1. Titration Curve

100 ml. of 0.100 *N* NaCl, 0.8 *N* HNO_3, 0.1% gelatin, with 0.500 *N* $AgNO_3$

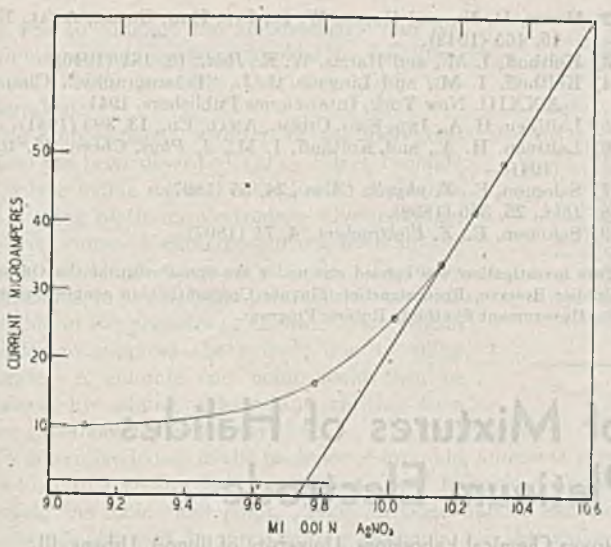

Figure 2. Titration Curve

100 ml. of 0.001 *N* NaCl, 0.8 *N* HNO_3, 0.1 % gelatin, in aqueous solution with 0.0100 *N* $AgNO_3$

work showed that the addition of gelatin was unnecessary. The bromide titration curves were similar in shape to those for chloride, except that a smaller current was observed before the end point, allowing a higher galvanometer sensitivity to be used.

Pure potassium bromide was prepared by thermal decomposition of reagent quality potassium bromate in an electrically heated tube furnace at about 400°. Gravimetric standardization checked within 0.1% the normality of bromide solution prepared by using the potassium bromide as a primary standard substance.

Titration data for various concentrations of bromide in aqueous solution and in 50% acetone using 0.8 *N* nitric acid and 0.1% gelatin are given in Table II. The results in general were somewhat low. In aqueous medium, 0.001 *N* bromide can be titrated, while in 50% acetone, 0.0001 *N* bromide gave a 3% error.

To prevent the interference of chloride, titrations in the presence of 0.01 to 0.02 *N* ammonia were tried. It was found that 0.01 *N* ammonia could be added without affecting the bromide end point, using bromide concentrations as low as 0.001 *N*.

Table II. Titration of 100 Ml. of Bromide

Normality of Br^-	Normality of $AgNO_3$	Galvanometer Sensitivity	$AgNO_3$ Used Theory *Ml.*	$AgNO_3$ Used Experimental *Ml.*	Error %
Aqueous Solution, 0.8 *N* Nitric Acid					
0.009991	0.0500	1/20	19.98	19.80, 19.86	−0.9, −0.6
				19.84, 19.92	−0.7, −0.3
0.005115	0.0500	1/20	10.23	10.12, 10.13	−1.1, −1.0
				10.08	−1.5
0.002046	0.0100	1/20	20.46	19.96, 19.93	−2.5, −2.6
				19.94	−2.6
0.001023	0.0100	1/20	10.23	9.90, 9.96	−3.3, −2.7
				9.88	−3.5
0.000512	0.0100	1/20	5.12	4.91, 4.89	−4.1, −4.5
				4.92	−3.9
Silver Nitrate, 50% Acetone, 0.8 *N* Nitric Acid					
0.01023	0.0500	1/20	20.46	20.21, 20.18	−1.2, −1.4
				20.32, 20.15	−0.7, −2.0
				20.36, 20.28	−0.5, −0.9
0.005115	0.0500	1/20	10.23	10.17, 10.14	−0.6, −0.9
				10.15, 10.05	−0.8, −1.8
				10.09, 10.14	−1.4, −0.8
0.002046	0.0100	1/20	20.46	19.95, 19.98	−2.6, −2.3
				19.93, 19.95	−2.7, −2.6
				20.11, 19.95	−1.8, −2.6
0.001023	0.0100	1/20	10.23	9.88, 9.90	−3.5, −3.3
				9.91, 9.92	−3.2, −3.1
				9.92, 9.92	−3.1, −3.1
0.000512	0.0100	1/20	5.12	4.98, 4.97	−2.7, −2.9
				4.95	−3.3
0.00010	0.0010	1/5	10.00	10.22, 10.26	+2.2, +2.6
				10.03	+0.3

Later work showed that if bromide titrations are carried out in the absence of gelatin, chloride does not interfere, because a current is caused by silver chloride particles.

TITRATION OF IODIDE

A solution of sodium iodide was prepared from a Baker and Adamson reagent quality product and standardized by oxidation with nitrite, destruction of the excess nitrite with urea, and titration with thiosulfate.

The results of titrations in aqueous medium, 0.8 *N* nitric acid, and 0.1% gelatin are given in Table III. As with bromide, the addition of gelatin was found later to be unnecessary.

The effect of various concentrations of ammonia on the titration of iodide is shown in Table IV. With 0.01 *N* iodide, even 1 *N* ammonium hydroxide had no effect, while with 0.001 *N* iodide a 10% error was found using 0.5 *N* ammonia although 0.1 *N* ammonia had no effect. By adding 0.1 to 0.3 *N* ammonia, the interference of bromide and chloride can be prevented.

It is concluded that iodide can be successfully titrated in nitric acid, neutral, or dilute ammoniacal medium.

DISCUSSION

The amperometric method is useful for the rapid titration of halides in dilute solution and in the presence of large concentrations of acid or salt. A titration can be completed in 3 to 5 minutes, because the points of most interest on the titration curve are those lying beyond the end point. Although not a highly accurate method in dilute solution, results accurate to ±0.1% can be obtained in 0.1 *N* solutions.

Compared with the Mohr and Fajans procedures, the amperometric method has the advantages of applicability at high dilutions and in acid or alkaline solution. Compared with the Volhard method, it has the obvious advantage of a direct titration over a back-titration method.

Table III. Titration of 100 Ml. of Iodide

Normality of I^-	Normality of $AgNO_3$	Galvanometer Sensitivity	$AgNO_3$ Used Theory *Ml.*	$AgNO_3$ Used Experimental *Ml.*	Error %
Silver Nitrate, Aqueous Solution, 0.8 *N* Nitric Acid					
0.0100	0.0500	1/20	20.00	19.81, 19.95	−0.9, −0.3
				19.88, 19.91	−0.6, −0.5
				19.96, 19.93	−0.2, −0.4
				19.92	−0.4
0.00500	0.0500	1/20	10.00	9.97, 9.95	−0.3, −0.5
				9.97	−0.3
0.00200	0.0100	1/10	20.00	19.77, 19.75	−1.1, −1.2
				19.75	−1.2
0.00100	0.0100	1/10	10.00	9.83, 9.85	−1.7, −1.5
				9.83	−1.7
0.00050	0.0100	1/10	5.00	4.88, 4.87	−2.4, −2.6
				4.87	−2.6
0.000050	0.0010	1/2	5.00	4.35, 4.53	−13.0, −9.4
				4.82	−3.6
0.000020	0.0010	1/2	2.00	1.77, 1.80	−11.5, −10.0
				1.77	−11.5
Blank	0.0010	1/2	0.00	0.05	.....

Table IV. Titration of 100 Ml. of Iodide

Normality of I^-	Normality of $AgNO_3$	Normality of NH_4OH	Galvanometer Sensitivity	$AgNO_3$ Used *Ml.*	Error %
Aqueous Medium, Various Concentrations of Ammonia					
0.0100	0.0500	0.01	1	19.64	−1.8
			1/2	19.78, 19.67	−1.1, −1.6
		0.02	1/2	19.60, 19.80	−2.0, −1.0
				19.65	−1.8
		0.10	1/2	19.64, 19.63	−1.8, −1.9
		0.50	1/5	19.70, 19.58	−1.5, −2.1
				19.72	−1.4
		1.0	1/2	19.64, 19.65	−1.8, −1.8
0.00100	0.0100	0.01	1/10	9.85, 9.86	−1.5, −1.4
			1/5	9.92, 9.89	−0.8, −1.1
		0.02	1/5	9.89, 9.84	−1.1, −1.6
		0.10	1/5	9.76, 9.84	−2.4, −1.6
				9.86	−1.6
		0.50	1/2	9.01, 9.24	−9.9, −7.6
		1.0	1	8.44, 8.49	−15.6, −15.1

The potentiometric method can be applied in dilute solutions and in general is more accurate than the amperometric method, but is considerably slower. To obtain reliable results potentiometrically it is necessary that solubility equilibrium be reached at each point of the curve, especially in the near vicinity of the end point. By titrating to an equivalence potential, the potentiometric method can be made more rapid, but the attainment of equilibrium must be experimentally proved.

LITERATURE CITED

(1) Foulk, C. W., and Bawden, A. T., *J. Am. Chem. Soc.*, 48, 2045 (1926).
(2) Hume, D. N., and Harris, W. E., Ind. Eng. Chem., Anal. Ed., 15, 465 (1943).
(3) Kolthoff, I. M., and Harris, W. E., *Ibid.*, 18, 161 (1946).
(4) Kolthoff, I. M., and Lingane, J. J., "Polarography", Chapter XXXIII, New York, Interscience Publishers, 1941.
(5) Laitinen, H. A., Ind. Eng. Chem., Anal. Ed., 13, 393 (1941).
(6) Laitinen, H. A., and Kolthoff, I. M., *J. Phys. Chem.*, 45, 1079 (1941).
(7) Salomon, E., *Z. physik. Chem.*, 24, 55 (1897).
(8) *Ibid.*, 25, 366 (1898).
(9) Salomon, E., *Z. Elektrochem.*, 4, 71 (1897).

This investigation was carried out under the sponsorship of the Office of Rubber Reserve, Reconstruction Finance Corporation, in connection with the Government Synthetic Rubber Program.

Amperometric Titration of Mixtures of Halides Using the Rotating Platinum Electrode

H. A. LAITINEN, W. P. JENNINGS, T. D. PARKS[1], Noyes Chemical Laboratory, University of Illinois, Urbana, Ill.

Iodide, bromide, and chloride can be successively titrated in mixtures with silver nitrate, using the rotating platinum electrode as an amperometric indicator electrode. Ammonia is added for the iodide titration, an excess of acid is added for the bromide titration, and gelatin is added for the chloride titration. Multivalent metallic ions added as flocculating agents do not appreciably affect the titration of bromide in bromide-chloride mixtures, indicating that mixed crystal equilibrium is not reached during the rapid addition of silver nitrate. The amperometric method is much more rapid than the potentiometric method for mixtures of halides, although not always as accurate.

CONSIDERABLE work has been done in the titration of mixtures of halides, especially by potentiometric titrations.

Bromide and iodide mixtures were first titrated potentiometrically by Behrend (*1*), who added sufficient ammonia to keep silver bromide in solution. He was unable to determine bromide in the presence of chloride. Dutoit and von Weisse (*4*) and Pinkhof (*14*) titrated iodide in the presence of bromide without adding ammonia.

In attempts to titrate bromide in the presence of chloride, Pinkhof (*14*) added ammonium carbonate to prevent the precipitation of silver chloride. By using the proper reference electrode, the titration was carried out until the bromide concentration was 10^{-3} *N*, and a correction of this amount was added to the result.

Liebich (*12*) attempted to titrate mixtures of halides. Titration of iodide gave high results in the presence of bromide, but accurate results were obtained in the presence of barium nitrate. Similar high results were found for iodide in the presence of chloride, and bromide in the presence of chloride. The addition of barium nitrate or alum was shown to improve the results. Clark (*2*, *3*) found about a 1% error in bromide titrations in the presence of an equal concentration of chloride in the presence of 5% barium nitrate. He also titrated mixtures of bromide and iodide in the presence of barium nitrate, and chloride-iodide mixtures without salt addition.

The high results obtained for the more insoluble halide in chloride-bromide or bromide-iodide mixtures have been attributed by Liebich (*12*) and Müller (*13*) to the formation of mixed crystals of silver halides as shown by Kuster (*10*) and Thiel (*16*) and studied in detail by Kolthoff and Eggertsen (*8*). Clark (*2*, *3*), however, considered adsorption to be responsible. Flood (*5*) calculated the theoretical error due to ideal mixed crystal formation assuming (*a*) that the entire precipitate is in equilibrium with the solution at all times and (*b*) that the precipitate coagulated upon formation, and only the part being precipitated at each instant is in mixed crystal equilibrium. Flood and Bruun (*6*) applied the results assuming "ideal inhomogeneous mixed crystal formation" (case *b*) to chloride-bromide mixtures, and calculated correction factors to be applied to the results as a function of mole fraction of bromide in the mixture. Thus for an equimolar mixture, the bromide result should be 1.2% high and the chloride result an equal amount low. Flood and Bruun concluded that mixed crystal formation accounted largely for the experimental results but that adsorption also was a contributing factor. They suggested that increased dilution would diminish the error due to adsorption.

Zintl and Betz (*17*) titrated mixtures of halides in very dilute solution (about 0.001 *N*). Bromide could barely be titrated in the presence of 10 times as much chloride, iodide in the presence of 60 times as much bromide, and iodide in the presence of 5000 times as much chloride. Flood and Sletten (*7*) and Schütza (*15*) worked out techniques for detecting potentiometric end points in chloride-bromide mixtures which require empirical corrections depending upon the composition of the mixture.

The potentiometric titration method suffers from the inherent difficulty that the potential break for bromide in the presence of chloride is only about 0.1 volt (*13*).

[1] Present address, Shell Development Co., Emeryville, Calif.

Table I. Effect of Multivalent Cations on Bromide Titration in Absence and Presence of Chloride

Normality of Br^-	Normality of Cl^-	Normality of $AgNO_3$	Electrolyte Present	$AgNO_3$ Used *Ml.*	Error %
0.01	...	0.1	.....	9.96, 9.90	−0.4, −1.0
			0.2 *M* Ba^{++}	9.95, 9.96, 9.97	−0.5, −0.4, −0.7
			0.005 *M* Al^{+++}	10.04, 9.96	0.4, −0.4
			0.005 *M* Al^{+++}, 0.8 *N* HNO_3	9.93, 9.94	−0.7, −0.6
			0.02 *M* Al^{+++}, 0.8 *N* HNO_3	10.00	0.0
			0.002 *M* Th^{+4}	10.05, 9.95	0.5, −0.5
0.001	...	0.01	.....	10.01	0.1
			0.002 *M* Th^{+4}	9.95, 10.04	−0.5, 0.4
0.01	0.1	0.1	0.8 *N* HNO_3	10.03, 10.03, 10.07	0.3, 0.3, 0.7
			0.2 *M* Ba^{++}	9.93, 9.92, 9.93	−0.7, −0.8, −0.7
			0.002 *M* Al^{+++}, 0.8 *N* HNO_3	10.03, 10.06	0.3, 0.6
			0.005 *M* Al^{+++}, 0.8 *N* HNO_3	10.02, 10.09	0.2, 0.9
			0.02 *M* Al^{+++}, 0.8 *N* HNO_3	10.00, 10.04	0.0, 0.5
			0.01 *M* Th^{+4}, 0.8 *N* HNO_3	10.05, 10.07	0.5, 0.7
			0.02 *M* Th^{+4}, 0.8 *N* HNO_3	10.07, 10.12, 10.12	0.7, 1.2, 1.2
0.01	0.02	0.1	0.8 *N* HNO_3	10.24, 10.20	2.4, 2.0
				10.08[a], 10.01[a]	0.8, 0.1
			0.2 *M* Ba^{++}, 0.8 *N* HNO_3	10.07, 10.06	0.7, 0.6
			0.02 *M* Al^{+++}	10.26, 10.22	2.6, 2.2
			0.02 *M* Th^{+4}	10.07, 10.12	0.7, 1.2
0.002	0.002	0.02	0.8 *N* HNO_3	9.71	−2.9
			0.2 *M* Ba^{++}	9.82, 9.58	−1.8, −4.2
			0.02 *M* Al^{+++}, 0.8 *N* HNO_3	9.43, 9.65	−5.7, −3.5

[a] 2 minutes stirring after each ml. of $AgNO_3$ added.

It was to compare the amperometric and potentiometric end points as applied to the titration of halide mixtures that this study was undertaken.

The amperometric titration of the individual halides has been described (*11*). Silver bromide and silver iodide do not cathodically depolarize the rotating platinum electrode. Silver chloride, however, causes a cathodic current even in the presence of a large excess of chloride. Therefore it is possible, in principle, to titrate either bromide or iodide in the presence of chloride if no gelatin is added to suppress the current due to silver chloride. A chloride end point could then be obtained by adding gelatin and shifting to a lower galvanometer sensitivity.

To determine iodide in the presence of bromide, ammonia can be added to increase the solubility of silver bromide without affecting the iodide end point. Thus all three halides can be successively titrated by first adding ammonia for the iodide titration, then adding an excess of acid and titrating the bromide, and finally adding gelatin for the chloride end point.

EXPERIMENTAL

The effect of adding multivalent metallic ions as flocculating agents on the titration of bromide in the absence and presence of chloride is shown in Table I. The apparatus and experimental procedure have been described (*11*).

Although a trend toward higher results for bromide in the presence of increasing amounts of chloride is noticeable, the flocculating ions in general had no effect on the end point. It is possible that under the conditions of the amperometric titration in which the end point is rapidly passed (the entire titration takes only 3 to 5 minutes), mixed crystal equilibrium is not reached even though the precipitate is colloidally dispersed. In two experiments (Table I), the titration was delayed for 2 minutes after the addition of each milliliter of reagent. Contrary to expectation, the results were lower than for the same titration run rapidly. The presence of five or ten times as much chloride as bromide led to a flat titration curve with no bromide end point. For solutions less than 0.002 *N* in both bromide and chloride, low results were obtained for bromide. At higher concentrations, a balancing of errors occurs, the "normal" low result for the amperometric bromide titration being balanced by a positive error caused by mixed crystal formation.

In Table II, data are given for several titrations of iodide-bromide mixtures in the presence of various concentrations of ammonia. It appears that 0.2 *N* ammonia is too concentrated for solutions of iodide more dilute than 0.01 *N*. In general, a concentration of 0.1 *N* ammonia is suitable for all but the most dilute iodide solutions.

Table II. Titration of Iodide in Presence of Bromide in Ammoniacal Solution

Normality of I^-	Normality of Br^-	Normality of $AgNO_3$	Normality of NH_3	$AgNO_3$ Used	Error
				Ml.	%
0.01	....	0.1	..	9.94	−0.6
0.01	0.01	0.1	0.1	9.94, 9.93, 9.94	−0.6, −0.7, −0.6
			0.2	9.90, 9.96, 9.92	−1.0, −0.4, −0.8
0.01	0.05	0.1	0.2	9.88, 9.83, 9.82	−1.2, −1.7, −1.8
0.001	0.001	0.01	0.1	9.99, 9.93	−0.1, −0.7
			0.2	9.64, 9.58	−3.6, −4.2
0.001	0.01	0.01	0.1	9.80, 9.80, 9.88[a]	−2.0, −2.0, −1.2
0.0001	0.0001	0.001	0.05	10.07, 9.95	0.7, −0.5
			0.1	9.46, 9.31[a]	−5.4, −6.9
			0.2	8.77[a]	−12.3

[a] 0.1% gelatin added.

Table III. Titration of Mixtures of Iodide, Bromide, and Chloride

Sample	Normality of Halide	Normality of $AgNO_3$	Medium	Galvanometer Sensitivity	$AgNO_3$ Used	Error
					Ml.	%
1	0.01 *N* I^-	0.1	0.1 *N* NH_3	1/2	9.97, 9.94	−0.3, −0.6
	0.01 *N* Br^-	0.1	0.8 *N* HNO_3	1/5	10.10, 10.01	1.0, 0.1
	0.01 *N* Cl^-	0.1	0.1 % gel.	1/20	9.86, 9.73	−1.4, −2.71
2	0.18 *N* I^-	0.1	0.1 *N* NH_3	1/2	17.91	−0.5
	0.009 *N* Br^-	0.1	0.8 *N* HNO_3	1/5	8.92, 8.81	−0.9, −2.1
	0.003 *N* Cl^-	0.05	0.1 % gel.	1/20	6.06, 6.01	1.2, 0.2
3	0.003 *N* I^-	0.05	0.1 *N* NH_3	1/2	5.86, 5.93	−2.3, −1.2
	0.018 *N* Br^-	0.1	0.8 *N* HNO_3	1/5	18.10, 18.12	0.3, 0.6
	0.009 *N* Cl^-	0.1	0.1 % gel.	1/20	8.91	−1.0
4	0.009 *N* I^-	0.1	0.1 *N* NH_3	1/2	8.98	−0.2
	0.003 *N* Br^-	0.05	0.8 *N* HNO_3	1/5	6.07	1.2
	0.018 *N* Cl^-	0.1	0.1 % gel.	1/20	17.75	−1.4

The results obtained in titrations of all three halides are shown in Table III. As indicated, a 0.1 *N* ammonia medium was used for the iodide titration, followed by 0.8 *N* ammonia for the bromide and 0.1% gelatin for the chloride. The galvanometer sensitivity of about 0.01 microampere per mm. was cut by means of an Ayrton shunt to $^1/_2$ for the iodide, $^1/_5$ for the bromide, and $^1/_{20}$ for the chloride titration to obtain a suitable residual current line in each titration. As a reference electrode, the mercury–mercuric iodide–potassium iodide cell of Kolthoff and Harris (*9*, potential −0.23 volt *vs.* saturated calomel electrode) was used for the iodide titration in ammoniacal medium, followed by a saturated calomel reference electrode for the bromide and chloride titrations.

No difficulty was encountered except in the bromide titration of sample 4, when only about 10% of the total halide present was bromide. In this case, the bromide curve was flat with an indistinct end point.

In Table IV, data are shown for the analysis of three synthetic halide mixtures of varying composition, made by one worker as unknowns and analyzed by another.

The amperometric method shows promise as a rapid method for the determination of halides in mixtures, although it is not always as accurate as the slower potentiometric method.

Table IV. Analysis of Unknown Halide Mixtures

Sample	Present			Found		
	I^-	Br^-	Cl^-	I^-	Br^-	Cl^-
	Mg./100 ml.			*Mg./100 ml.*		
1	15.15	155.1	0.43	15.0	153.8	0.62
2	2.54	73.5	312.0	2.0	76.2	305.6
3	121.8	17.6	21.3	121.3	15.3	21.4

LITERATURE CITED

(1) Behrend, R., *Z. physik. Chem.*, 11, 466 (1893).
(2) Clark, W., *J. Am. Chem. Soc.*, 48, 749 (1926).
(3) Clark, W., *J. Chem. Soc.*, 1926, 768.
(4) Dutoit, P., and von Weisse, G., *J. chem. Phys.*, 9, 578 (1911).
(5) Flood, H., *Z. anorg. allgem. Chem.*, 229, 76 (1936).
(6) Flood, H., and Bruun, B., *Ibid.*, 229, 85 (1936).
(7) Flood, H., and Sletten, E., *Z. anal. Chem.*, 15, 30 (1938).
(8) Kolthoff, I. M., and Eggertsen, F. T., *J. Am. Chem. Soc.*, 61, 1036 (1939).
(9) Kolthoff, I. M., and Harris, W. E., Ind. Eng. Chem., Anal. Ed., 18, 161 (1946).
(10) Kuster, F. W., *Z. anorg. Chem.*, 19, 81 (1899).
(11) Laitinen, H. A., Jennings, W. P., and Parks, T. D., Ind. Eng. Chem., Anal. Ed., 18, 355 (1946).
(12) Liebich, C., dissertation, Dresden, 1920.
(13) Müller, E., "Elektrometrische Massanalyse", p. 115, Dresden, Steinkopf, 1932.
(14) Pinkhof, J., dissertation, Amsterdam, 1919.
(15) Schütza, H. S., *Angew. Chem.*, 51, 55 (1938).
(16) Thiel, A., *Z. anorg. Chem.*, 24, 1 (1900).
(17) Zintl, E., and Betz, K., *Z. anal. Chem.*, 74, 330 (1928).

This investigation was carried out under the sponsorship of the Office of Rubber Reserve, Reconstruction Finance Corporation, in connection with the Government Synthetic Rubber Program.

Centrifugal Sedimentation Method for Particle Size Distribution[1]

A. E. JACOBSEN AND W. F. SULLIVAN, Titanium Division, National Lead Company, Research Laboratory, Sayreville, N. J.

The centrifugal sedimentation method for particle size distribution of materials in a dispersed system is reviewed. A preferred method has been used which is analogous to Odén's method of tangential intercepts for gravitational sedimentation. This procedure yields the same results as those obtained by the variable suspension height method but is more convenient from the practical point of view. Examples are given to show practical applications of the beaker-type centrifuge to the study of relative dispersion of titanium dioxide pigment in paint systems. The method is of limited usefulness for the determination of specific surface area or the relative efficiency of light-diffusing properties of materials which are either aggregated or irregularly shaped, since Stokes' law is based on the assumption of an equivalent spherical particle. Electron micrographs supplement the sedimentation studies.

THE determination of the particle size distribution of finely divided material is of practical and fundamental importance in physicochemical studies. In particular, centrifugal sedimentation has proved very valuable in determining the relative distribution of pigments in paint vehicles (*7*). The theory underlying the application of sedimentation data for the calculation of the particle size distribution has been worked out (*3, 8, 9*) and verified by comparison with the results obtained by other methods (*4, 5*).

From the practical point of view the use of a suitable dispersion technique for the particulate material is of significance, since the sedimentation data are of little value unless a satisfactory dispersion has been attained. Hence, cognizance must be taken of the nature of the dispersing agent used, and the particular technique employed in preparing the dispersion. A further limitation is the effect of particle shape. The concept of "equivalent spherical diameter" has been used in all applications of Stokes' law, but it is known from electron microscope studies that the particles are rarely spherical, often being irregular aggregates of primary particles. In extreme conditions poor correlation may exist between specific surface as calculated from particle size distribution data and specific surface as determined by independent methods.

THEORETICAL

The gravitational method of sedimentation has proved suitable for determining the particle size distribution of particles in suspensions where the size range is from about 1 to 50 microns. The procedure used involves the application of Stokes' law (*4, 5, 11*) and Odén's method of tangential intercepts (*8, 9*).

The equating of the frictional force, as given by Stokes' law, to the gravitational force on the particle yields the relation

$$D = \sqrt{\frac{18\eta h}{(d_1 - d_0)gt}} \qquad (1)$$

where D = equivalent spherical diameter of the particle
η = coefficient of viscosity of the suspension medium
h = height of suspension
d_1 = density of particle
d_0 = density of suspension medium
g = gravitational acceleration
t = time of settling

Since the usual method of obtaining data on a polydisperse suspension is to determine the sedimentation-time curve, it is apparent that in time t, all particles having a diameter equal to or greater than D_m will settle through height h. In addition, a certain fraction of the particles having a diameter less than D_m will settle through a height less than h. The deduction of the sedimented "fines" may be accomplished by Odén's method of tangential intercepts in which

$$\int_0^{D_m} F(D)dD = (1 - p) + t\frac{dp}{dt} \qquad (2)$$

where p = total weight fraction sedimented
$F(D)dD$ = weight fraction of particles having a diameter between D and $D + dD$

For materials with a particle size range of approximately 0.1 to 1 micron, the ordinary beaker-type centrifuge has been employed to determine the distribution. The essential point of divergence from gravitational sedimentation is that the force acting on the particle increases with the settling distance. As first shown by Svedberg and Nichols (*12*) the gravitational equation must then be modified to

$$D = \sqrt{\frac{18\eta \ln x_2/x_1}{(d_1 - d_0)\omega^2 t}} \qquad (3)$$

where x_1 = distance from the center of rotation to a point in the suspension
x_2 = distance from the center of rotation to a second point in the suspension
ω = angular velocity in radians per second

The calculation of the particle size distribution from the sedimentation-time curve was apparently first accomplished by Romwalter and Vendl (*10*) who arrived at the equation

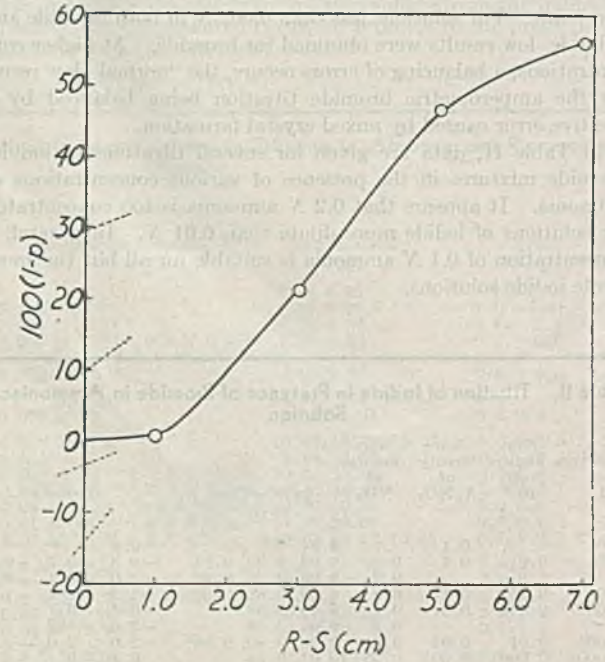

Figure 1. Sedimentation of Titanium Dioxide in Dutch Oil Z2

Variable suspension height method

[1] Three papers presented in the Symposium on Measurement and Creation of Particle Size at the Twelfth Annual Chemical Engineering Symposium of the Division of Industrial and Engineering Chemistry are presented here, pages 360–73. Other papers in the symposium will be published in the July issue of the INDUSTRIAL EDITION.

$$\int_0^{D_m} F(D)dD = \frac{R^2 - S^2}{S^2} \frac{1}{\ln R^2/S^2} t \frac{dp}{dt} \quad (4)$$

where R = distance from center of rotation to bottom of cup
S = distance from center of rotation to surface of suspension

However, this equation was shown by Brown (*3*) to be invalid and this conclusion has been confirmed by the authors. Thus, since R and S are constants, the weight fraction of particles having diameters between 0 and D_m is given by

$$\int_0^{D_m} F(D)dD = K \times t \frac{dp}{dt} \quad (4')$$

Therefore the value of the integral must run from 0 to 1 as the particle diameter is increased from 0 to ∞. Direct application of the sedimentation-time curve, however, shows that the term $t \frac{dp}{dt}$ and hence the integral $\int_0^{D_m} F(D)dD$ go through a maximum, since at low values of t, $t \frac{dp}{dt}$ equals a small number and, at high values of t, it is again a small number since the slope $\frac{dp}{dt}$ approaches 0.

Brown was unable to find a mathematical solution for the distribution function $F(D)$ when the time of centrifuging was used as a variable, but did arrive at a satisfactory solution when the suspension height $(R - S)$ was varied. His equation for cylindrical centrifuge tubes is:

$$\int_0^{D_m} F(D)dD = (1 - p) + (R - S) \frac{dp}{dS} \quad (5)$$

This equation has been used by the authors, and results have been expressed as a cumulative curve, $\int_0^{D_m} F(D)dD$ *vs.* D_m rather than as the distribution function itself, $F(D)$ *vs.* D_m, since the latter would involve second derivatives, a procedure which is probably not justified by the experimental accuracy achieved.

In actual practice, however, it has been found somewhat more convenient to use a modified method for the determination of the cumulative weight per cent curve. The principle of this method, which has already been pointed out in the work of both Brown (*3*) and Martin (*7*), is that centrifugal sedimentation can be made to approach gravitational sedimentation by making the height of suspension $(R - S)$ small. This means that the centrifugal force on the particle is taken to be approximately constant over the settling distance. Hence, the mathematical procedure is identical with the gravitational calculations, except that the gravitational acceleration, g, is replaced by the centrifugal acceleration, $\omega^2 R$. The results obtained by this method have been found to check closely those obtained by the variable suspension height method for many pigment dispersions.

There are two reasons for preferring to use a small height of suspension with variable time rather than variable suspension height and constant time. First, the former method requires considerably less sample, which is an important factor where limited quantities are available and, secondly, a wider particle size range can be covered without having to readjust the centrifuge conditions. Thus, using the variable suspension height procedure, two or more analyses may be necessary at different centrifuge speeds in order to cover adequately the particle size range usually encountered. From the physical viewpoint the requirement of sector-shaped tubes is also more closely approached when the suspension height is made small. On the negative side it must be considered that the relative experimental error involved in measuring the height is larger when the height is small. However, by carefully calibrating the centrifuge cups on a volume basis, the error seems to have been minimized as judged by the reproducibility of the results, and their agreement with other methods.

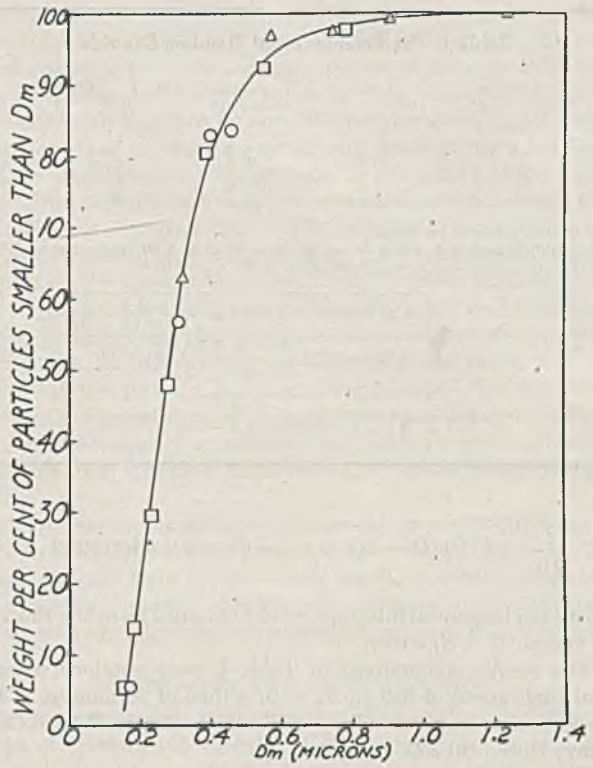

Figure 2. Cumulative Weight Per Cent Curve for Titanium Dioxide in Dutch Oil Z2

○ Variable suspension height method, 650 r.p.m.
△ Variable suspension height method, 350 r.p.m.
□ Modified gravitational method

EXPERIMENTAL

Apparatus. The apparatus used was an International centrifuge, size I, Type SB, equipped with 115-volt Transtat voltage regulator which was designed to improve the constancy of the rotational speed. The centrifuge head holds eight chromium-plated cylindrical cups (9.20 × 3.58 cm.) each having a cover to prevent solvent evaporation. The distance, R, from the center of rotation to the bottom of the centrifuge cup was 21.3 cm. The centrifuge speed was measured with a General Radio Strobotac and the time of acceleration and deceleration allowed for by the method of Marshall (*6*). For the centrifuge speed used in the experiments described, the correction was one minute.

The pigment dispersions were prepared by mixing titanium dioxide with an organic vehicle in the ratio of 100 to 54 grams in a mechanical mixer for 60 minutes. The mixture was then put through a three-roll laboratory paint mill with the rolls set at 0.075 mm. (0.003 inch) and finally diluted to approximately 3% solids with mineral spirits. The pigment suspension was analyzed by pipetting a 10-ml. aliquot into a weighed crucible, burning off the organic matter, and weighing the ignited residue as titanium dioxide. In the case of the centrifuged samples the supernatant suspension was carefully separated from the sedimented material and mixed before sampling. Since the suspension is dilute, the per cent sedimented may be calculated in the following manner:

$$\% \text{ sedimented} = 100p = \frac{\text{weight of sediment}}{\text{weight of total}} \times 100 =$$

$$\frac{\text{weight of total} - \text{weight in suspension}}{\text{weight of total}} \times 100$$

$$\approx \frac{(C_{TiO_2})_{\text{initial}} - (C_{TiO_2})_{\text{suspension}}}{(C_{TiO_2})_{\text{initial}}} \times 100$$

where (C_{TiO_2}) = concentration of TiO_2 in grams per liter.

Comparisons of Methods. In applying the variable suspension height method it was found convenient to modify Equation 5 to

Table I. Sedimentation of Titanium Dioxide

$R - S$	$100 \times (1 - p)$	$2 \times 100(1 - p)$	Tangential Intercept[a]	$100 \int_0^{D_m} F(D)dD$	D_m[b]
Cm.	%	%	%	%	μ
1.00	0.94	1.9	− 3.5	5.4	0.17
3.00	21.1	42.2	−14.5	56.7	0.30
5.00	46.6	93.2	10.0	83.0	0.40
7.00	56.0	112.0	29.5	83.5	0.46

[a] Values taken from Figure 1.
[b] From Equation 3, using $X_1 = S$, $X_2 = R$, $d = 4.20$ grams per cc., $d_0 = 0.80$ grams per cc. and $\eta = 0.0096$ poise at 25° C. we have:

$$D_m = \sqrt{\frac{18 \times 0.0096 \times 2.303 \log \frac{21.3}{21.3 - (R - S)}}{(4.20 - 0.80)\left(\frac{2\pi \times 650}{60}\right)^2 30 \times 60}}$$

$$D_m = \sqrt{1.400 \log \frac{21.3}{21.3 - (R - S)}} \text{ microns}$$

$$\int_0^{D_m} F(D)dD = 2(1 - p) - \text{tangential intercept} \qquad (5')$$

where the tangential intercept is that obtained from the $100(1 - p)$ versus $(R - S)$ curve.

The results summarized in Table I were obtained using a centrifuge speed of 650 r.p.m. with a time of 30 minutes. The dispersion medium was a linseed oil vehicle (National Lead Company, Dutch Oil Z2).

These results, however, cover only the particle size interval from 0.17 to 0.46 micron and leave an appreciable fraction of the distribution unaccounted for. Hence, with the variable suspension height method, a second analysis was necessary using different conditions—viz., 350 r.p.m. and a time of 30 minutes. The end results are expressed together with those of Table I in the form of a cumulative weight per cent curve (Figure 2).

The modified gravitational method, using $(R - S) = 1$ cm. was carried out with the previous suspension, so that a comparison between the two methods might be made. In order to apply the intercept method, Equation 2 was changed to

$$\int_0^{D_m} F(D)dD = 1 - \text{tangential intercept} \qquad (2')$$

and Equation 1 to

$$D_m = \sqrt{\frac{18\eta(R - S)}{(d_1 - d_0)\omega^2 Rt}} \qquad (1')$$

The results are summarized in Table II.

The cumulative weight per cent curve is also shown in Figure 2. The close agreement with the variable suspension height method is evident. It should be mentioned in connection with the precision of the modified gravitational method that a check analysis on a portion of the original suspension showed an absolute error not greater than 1%.

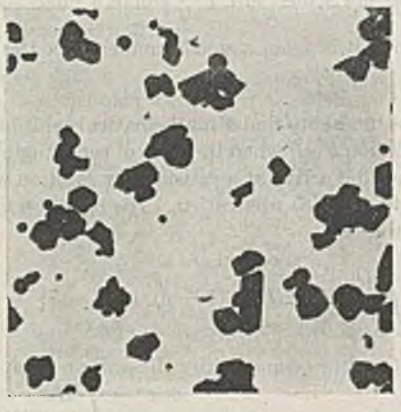

Figure 4. Electron Micrograph of Titanium Dioxide, × 15,000

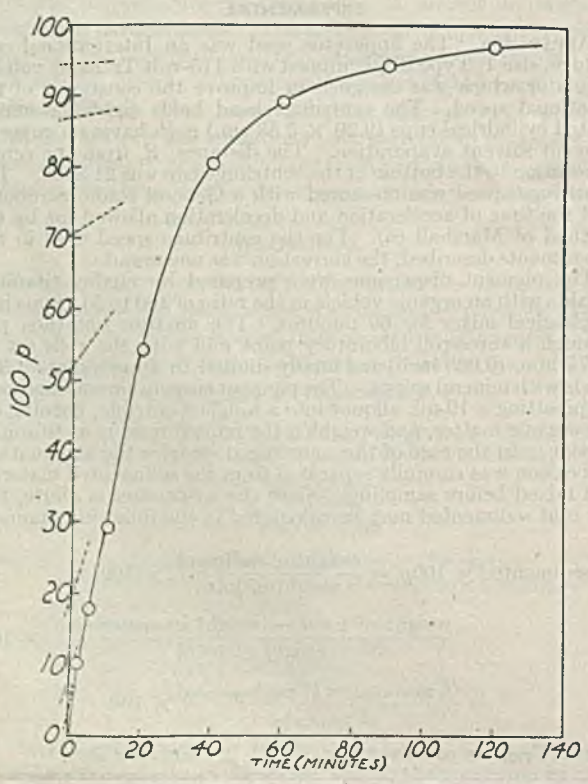

Figure 3. Sedimentation Curve of Titanium Dioxide in Dutch Oil Z2

Modified gravitational method

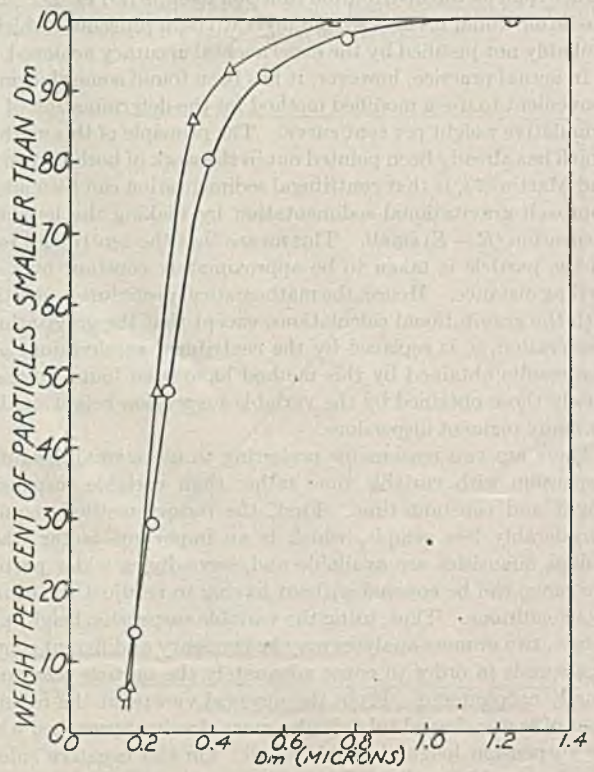

Figure 5. Cumulative Weight Per Cent Curve for Titanium Dioxide in Dutch Oil Z2

○ Modified gravitational method
△ Electron micrograph count method

Table II. Sedimentation of Titanium Dioxide

Time	$100 \times p$	Tangential Intercept[a]	$100 \int_0^{D_m} F(D)dD$	D_m[b]
Min.	%	%	%	μ
2	10.3	0	100	1.24
5	17.8	2.5	97.5	0.78
10	29.2	7.5	92.5	0.55
20	54.3	19.5	80.5	0.39
40	80.8	52.0	48.0	0.28
60	89.0	70.5	29.5	0.23
90	94.5	87.0	13.0	0.18
120	97.0	94.5	5.5	0.15

[a] Values taken from Figure 3.
[b] From Equation 1′ using $\eta = 0.0096$ poise, $(R - S) = 1$ cm., $d_1 = 4.20$ grams per cc., $d_2 = 0.80$ gram per cc., $R = 20.8$ cm., $\omega = \frac{2\pi \times 350}{60}$ radians per second.

Table III. Effect of Milling

Milled		Not Milled	
$100 \int_0^{D_m} F(D)dD$	D_m	$100 \int_0^{D_m} F(D)dD$	D_m
%	μ	%	μ
14.3	0.20	5.6	0.20
45.0	0.30	29.2	0.30
67.2	0.40	55.7	0.40
81.0	0.50	75.0	0.50
96.7	1.00	95.0	1.00

Although the agreement between the two methods lends credence to the fundamental "correctness" of the distributions arrived at by means of the centrifuge, it was thought advisable to check the results by an independent method. A series of electron micrographs was taken of the pigment from which a particle size distribution was made by the count method (*1*). Over 500 particles were counted. The specimens for the electron microscope were made by incorporating a small amount of the original paint with collodion which was used as a supporting film. A typical micrograph is shown in Figure 4. The particle size distribution is represented graphically in Figure 5 for comparison with the centrifuge data. The comparative results are in reasonable agreement, considering the divergence in technique.

PRACTICAL APPLICATIONS

Effect of Milling. To illustrate that the method of preparing the dispersion is of fundamental importance and has to be considered with any data given on particle size distribution, two dispersion procedures were used for the same pigment. In both cases a 60-minute mix was carried out in a small mechanical mixer using a linseed oil–tung oil vehicle (known to the paint trade as VM-1215, which was developed by the Technical Service Laboratories of the Titanium Pigment Corp., New York, N. Y.). One half of the pigment paste was subsequently put through the laboratory paint mill and the other half was not. The cumulative weight per cent distributions, as determined by the modified gravitational method, are given in Table III. These data show that milling has the effect of producing a finer particle size d stribution.

Nature of Dispersing Vehicle. Since in the practical preparation of paint dispersions, a wide variety of vehicles are available, the distribution obtained will depend also on the vehicle used. As an example another titanium dioxide pigment was dispersed according to the previously described procedure in both a Dutch Oil Z2 and a linseed oil–tung oil vehicle (VM-1215). The cumulative weight per cent distributions, as determined by the modified gravitational method, are given in Table IV.

These data again emphasize the relationship between the particle size distribution and the dispersion conditions.

Influence of Particle Shape. Electron micrograph studies of various titanium dioxide pigments have shown that the pigment particles are invariably aggregates of primary particles. As an extreme case it is possible to have approximately the same particle size distribution for two different pigments, one of which is composed of aggregates having very small primary particles and the other composed of aggregates having large primary particles. The cumulative weight per cent distributions, using a linseed oil–tung oil vehicle (VM-1215), are summarized in Table V.

Electron micrographs (Figure 6) indicate that the particulate material in the pigment composed of small primary particles has a more open structure and hence considerably more specific surface.

The particle shape may also be a factor where the number of particles in an aggregate is approximately the same, but the shapes of the primary particles differ widely. The following example shows the cumulative weight per cent distribution for a pigment composed of acicular primary particles and one having approximately spherical particles. The vehicle is again VM-1215.

The corresponding electron micrographs, as shown in Figure 7, illustrate the difference in particle shape. Surprisingly enough, those pigments have approximately the same hiding power (*2*). It is therefore apparent that complete reliance on sedimentation data would again lead to error in the evaluation of these products.

CORRELATION WITH OTHER PROPERTIES

Specific Surface. An estimate of the specific surface from a study of electron micrographs in comparison with the specific

Table IV. Effect of Dispersing Vehicle

Dutch Oil Z2		Linseed Oil–Tung Oil (VM-1215)	
$100 \int_0^{D_m} F(D)dD$	D_m	$100 \int_0^{D_m} F(D)dD$	D_m
%	μ	%	μ
12.0	0.15	3.0	0.15
41.5	0.20	20.0	0.20
71.5	0.30	51.5	0.30
87.0	0.40	72.5	0.40
93.0	0.50	84.5	0.50
100.0	1.00	97.5	1.00

Table V. Influence of Particle Shape

Large Primary Particles		Small Primary Particles	
$100 \int_0^{D_m} F(D)dD$	D_m	$100 \int_0^{D_m} F(D)dD$	D_m
%	μ	%	μ
11.2	0.20	13.1	0.20
42.1	0.30	38.2	0.30
59.9	0.40	59.1	0.40
75.9	0.50	69.7	0.50
92.8	1.00	90.8	1.00

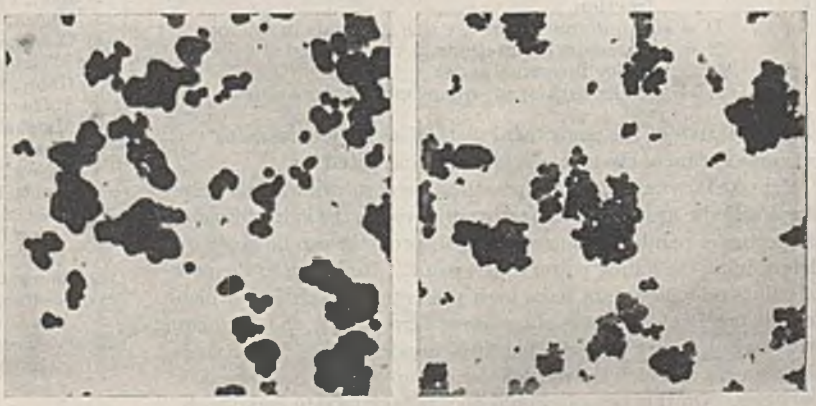

Figure 6. Electron Micrographs of Titanium Dioxide, ×15,000

Left. Large primary particles. *Right.* Small primary particles

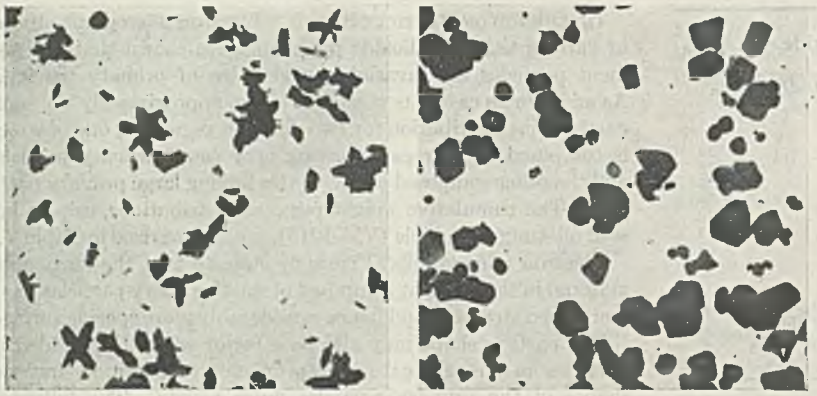

Figure 7. Electron Micrographs of Titanium Dioxide, ×15,000

Left. Acicular particles. *Right.* Approximately spherical particles

Table VI. Influence of Particle Shape

Acicular		Approximately Spherical	
$100\int_0^{D_m} F(dD)D$	D_m	$100\int_0^{D_m} F(D)dD$	D_m
%	μ	%	μ
30.0	0.20	9.7	0.20
49.3	0.30	62.7	0.30
67.1	0.40	81.0	0.40
73.0	0.50	86.8	0.50
88.7	1.00	98.0	1.00

Table VII. Specific Surface

	Large Primary Particles	Small Primary Particles
	Sq. m. per gram	
Centrifugal sedimentation method	4.7	4.8
Electron micrograph method	5	10

surface calculated from centrifugal sedimentation data is given in Table VII. In the case of the former a particle size distribution by the count method was made considering as far as possible only the primary particles. Figure 8, which is a second electron micrograph of the pigment shown in Figure 6 (right), was used for the count. This differs from the latter figure in that the dry pigment was vigorously ground in an agate mortar in order to deaggregate it as much as possible. The equation employed for the determination of specific surface from size distribution data is

$$S = \frac{6}{100d}\sum\frac{W\%}{D}$$

where $W\%$ = per cent by weight of the total pigment per given fraction
D = mean diameter for the size intervals in microns
Σ = summation of fractions in the size distribution
d = density in grams per cc.
S = specific surface in square meters per gram

A limitation of the centrifugal method as far as disclosing the inherent nature of the material is clearly indicated here.

Hiding Power. From a practical point of view, aggregate shape and size are important factors involved in the light-diffusing properties of paints. A measure of this property can be made by determining the hiding power of the paint. Referring to the pair of paints on which data have been presented in Table V (which for all practical purposes show close agreement), the pigment with large primary particles has 10% greater hiding power than the pigment in which the particles are composed of small primary particles. On this basis it would be a fallacy to rely completely on sedimentation studies for depicting light-diffusing qualities of particulate materials.

SUMMARY

The centrifugal sedimentation method is based on proved fundamental principles, thus making it suitable for determining cumulative particle size distribution of particulate material in dilute suspensions.

A modified centrifugal sedimentation procedure has been employed in which the analytical results agree with the results obtained by the variable suspension height method and with electron micrographic count.

Examples have been presented to show the practical use of the method for physicochemical studies dealing with the dispersion of titanium dioxide pigments in organic vehicles.

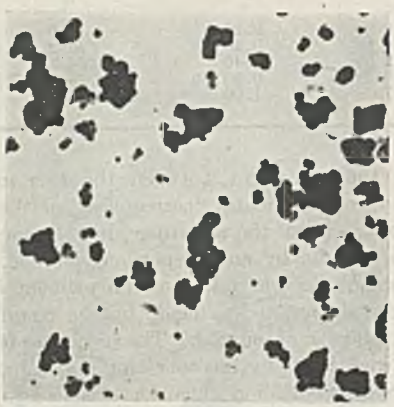

Figure 8. Electron Micrograph of Titanium Dioxide, ×15,000

Small primary particles, ground in agate mortar

Limitations of the sedimentation method for the determination of specific surface area and the hiding power of particulate material which are aggregated or nonspherical in shape have been emphasized.

ACKNOWLEDGMENT

Appreciation is expressed to R. Dahlstrom, director of research, National Lead Company, Titanium Division, for his interest and suggestions.

LITERATURE CITED

(1) Am. Soc. Testing Materials, Standards, Part II, p. 1575 (1944).
(2) *Ibid.*, Part II, p. 882 (1944).
(3) Brown, C., *J. Phys. Chem.*, 48, 246 (1944).
(4) Gessner, H., "Die Schlämmanalyse", Leipzig, Akademische Verlagsgesellschaft, 1931.
(5) Hahn, F. V. von, "Dispersoidanalyse", pp. 271–2, Dresden, Theodor Steinkopff, 1928.
(6) Marshall, C. E., *Proc. Roy. Soc.* (London), **A126**, 427 (1930).
(7) Martin, S. W., Am. Soc. Testing Materials, Symposium on New Methods for Particle Size Determinations in the Subsieve Range, Philadelphia, Pa., 1941.
(8) Odén, S., in J. Alexander's "Colloid Chemistry", Vol. I, p. 861, New York, Chemical Catalog Co., 1926.
(9) Odén, S., *Kolloid. Z.*, 18, 33 (1916).
(10) Romwalter, A., and Vendl, M., *Kolloid Z.*, **72**, 1 (1935).
(11) Svedberg, T., "Colloid Chemistry", New York, Chemical Catalog Co., 1928.
(12) Svedberg, T., and Nichols, J. B., *J. Am. Chem. Soc.*, 45, 2910 (1923).

Presented before the Division of Industrial and Engineering Chemistry, American Chemical Society, Symposium on Measurement and Creation of Particle Size, Brooklyn, N. Y., December, 1945.

Particle Size by Spectral Transmission

EMERSON D. BAILEY
E. I. du Pont de Nemours & Co., Inc., Wilmington, Del.

A simple method has been developed for determining two-parameter size distributions from transmissions measured in the visible and near infrared parts of the spectrum. It is based on an empirical relationship between scattering, particle size, refractive index, and the wave length of light. The method was developed for essentially nonabsorbing materials and was originally based on particle size measurements made with the low-speed Svedberg ultracentrifuge.

THE spectral transmission method of particle size analysis is a technique for obtaining information on the particle size distributions of finely divided colorless powders from the amount of light they transmit in completely deflocculated dilute suspensions. Usually the only data required are a series of transmissions measured over a spectral range of 0.4 to 2.0 microns. The method is limited to colorless materials and to particle sizes for which optimum scattering occurs in the range over which the transmissions can be measured.

Light scattering has been used in the study of particle size since Rayleigh (*7*) did his fundamental work nearly 50 years ago. Pfund (*6*) and Gamble and Barnett (*3*) have made use of Rayleigh's equation in the study of comparatively large particles by carrying out their measurements in the near infrared. Stratton and Houghton (*8*), and very recently Barnes and La Mer (*2*), have described theoretical curves which apply to scattering systems when the particle size is of the same order as the wave length of the radiation. Both of these curves are based on the equations of Mie (*5*) and apply only to a specific value of the relative refractive index of the particle. The basis for the present particle size method is a more general empirical relationship which was derived during studies on scattering systems carried out with a low-speed Svedberg ultracentrifuge (*9*). A brief description of the basic relationship is given below to aid in the discussion of the method of particle size analysis and a more complete description of the work on scattering systems is planned for later publication.

DERIVATION OF SCATTERING FUNCTION

As far as possible the terms used in the following discussion are defined according to established convention.

Specific extinctions are calculated from the measured transmissions of scattering suspensions according to the Beer-Lambert law as illustrated in Equation 1

$$\frac{I}{I_0} = e^{-\bar{E}_M c t} \qquad (1)$$

where I is the intensity of the transmitted light; I_0, the intensity of the incident light; $\bar{E}_M$, the average specific extinction for the particle size distribution involved; the subscript, M, refers to a function determined by the relative refractive index of the particle and the wave length of the radiation used; c, the volume concentration of the suspension in units of 0.01 cc. of suspended material per 100 cc. of suspension; and t, the cell thickness in centimeters. Particle size is measured as particle radius and the unit used for both particle radius and wave length of radiation is 1 micron. One micron is 10^{-4} cm. or 10^4 Ångström units. Relative refractive index is the refractive index of the particle divided by the refractive index of the suspension medium. In the distributions used the areas under the distribution curve correspond to the volume of material in a given size range and not to the number of particles.

The primary variables which determine specific extinction in a scattering system are the size and relative refractive index of the suspended particles and the wave length of the incident radiation. These variables were studied by fractionating four nearly colorless minerals covering a refractive index range of 1.36 to 2.45 into 6 to 9 relatively homogeneous samples. The particle size distributions and the specific extinctions of each of the fractionated samples were determined at the same time in a Svedberg low-speed untracentrifuge, in a suspension medium whose refractive index was 1.47. The radiation used covered a band of wave lengths from 0.400 to 0.480 micron and the average wave length was calculated to be 0.450 micron.

The four curves shown in Figure 1, in which specific extinction is plotted as function of particle size, were then derived from these data. In this step a set of simultaneous integral equations was solved for each group of samples with an instrument called the moment-product integrator (*9*). When the coordinates of Figure 1 were transformed, so that the product of specific extinctions and radius were plotted against the product of the Lorentz refractive index coefficient, $\frac{m^2 - 1}{m^2 + 2}$, and the radius, the four curves were very nearly superimposed. In the refractive index term m is the relative refractive index. A comparison of measured and calculated transmissions over the wave-length range of 0.7 to 2.0 microns showed that if the abscissa unit were assumed to be $\left[\frac{m^2 - 1}{m^2 + 2}\right]\frac{n_0}{\lambda}$ multiplied by the radius, a satisfactory agreement was obtained. In the final term n_0 is the refractive index of the suspension medium and λ is the wave length of the radiation in air. For convenience the factor which modifies the particle radius has been called M.

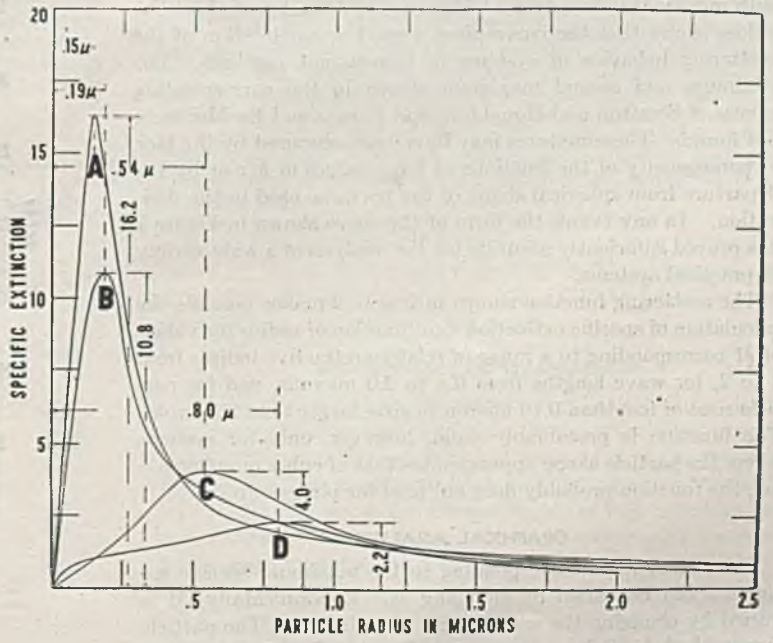

Figure 1. Mineral Series

A. Sphalerite, n = 2.47 *C.* Barytes, n = 1.66
B. Cerussite, n = 2.03 *D.* Cryolite, n = 1.37 λ = 0.450μ

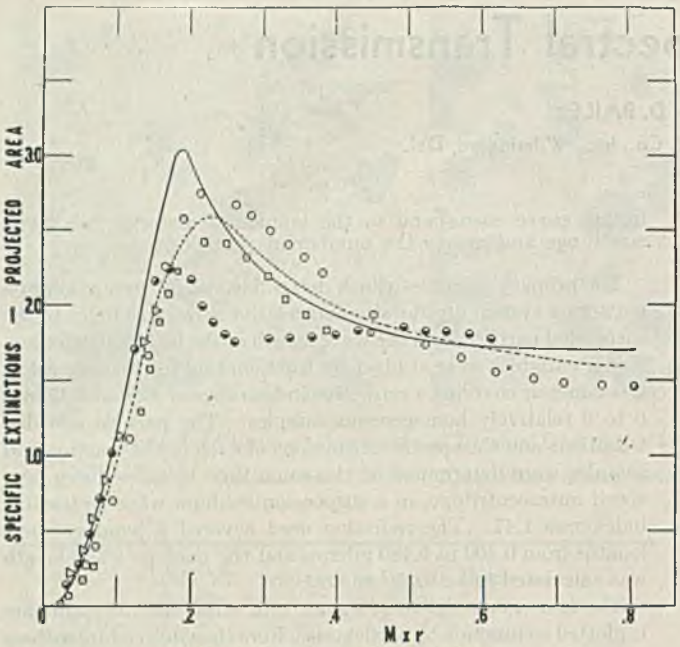

Figure 2. Scattering Function

——— Adjusted for monochromatic light
- - - - Original function
⊙ Sphalerite. ◒ Cerussite. △ Cryolite. ⊡ Barytes.

Figure 2 shows the data plotted on the new basis. The dotted curve shows the original form of the curve and the solid curve shows the form adopted after new measurements had been made and corrections had been applied to compensate for the use of heterochromatic light in obtaining the original data (*1*). In Figure 2 the specific extinctions are no longer on a volume basis but on a basis which corresponds to the volume of particles divided by the particle radius and called specific extinction per unit projected area. The spread of the points near the maximum is probably due to the indirect method which had to be used in constructing the curves of Figure 1. The deviation of the cerussite curve from the barytes and sphalerite curves is due largely to the double refraction of this mineral. The agreement between specific extinctions calculated from the solid curve of Figure 2 with measured values over a wide range of M and particle radius values shows that the curve gives a good approximation of the scattering behavior of systems of transparent particles. The minimum and second maximum shown in the corresponding curves of Stratton and Houghton, and Barnes and La Mer were not found. These features may have been obscured by the lack of homogeneity of the fractions at large values of Mr or by the departure from spherical shape of the particles used in the derivation. In any event, the form of the curve shown in Figure 2 has proved sufficiently accurate for the analysis of a wide variety of practical systems.

The scattering function shown in Figure 2 makes possible the calculation of specific extinction as a function of radius for values of M corresponding to a range of relative refractive indices from 1 to 2, for wave lengths from 0.4 to 2.0 microns, and for particle sizes of less than 0.10 micron to sizes larger than 2 microns. The function is presumably valid, however, only for systems where the particle shape approximates that of cubes or spheres—i.e., the function probably does not hold for plates or rods.

GRAPHICAL ANALYSIS

The radius value corresponding to the maximum specific extinction can be varied by changing M. Experimentally, M is varied by changing the wave length of radiation. The particle size method depends on the fact that each wave length emphasizes a different part of the particle size distribution. In order to make rapid analyses possible a graphical comparison method has been adopted which involves the use of the two-parameter distribution function shown in Figure 3 and first used by Lansing and Kraemer for molecular weight analysis (*4*).

In the analytical expression r_0 is the radius value of the maximum of the distribution and B is a nonuniformity coefficient. A B value of 0 corresponds to a sample which is completely homogeneous with respect to particle size. As B increases, the spread of the curve becomes greater and a B value of unity corresponds to a very polydisperse material. Figure 3 shows graphically the way in which the distribution is affected as the B value is changed. As Lansing has shown, any of the usual averages can be expressed in terms of the two parameters r_0 and B. The expression which modifies the exponential term is derived so that the area under the distribution curve will be unity for all values of the parameters. The weight average radius, $\bar{r}$, which is usually used to characterize the distribution, is calculated by multiplying r_0 by $e^{3B^2/4}$.

The average specific extinction, $\bar{E}_M$, for a polydisperse sample is calculated by multiplying the ordinates of the differential particle size distribution by the corresponding ordinates of the appropriate specific extinction–radius relation. If the area under the distribution is unity before the multiplication, the area under the product curve is numerically equal to $\bar{E}_M$. The specific extinction–radius relation is derived from Figure 2 by substituting the numerical value of M in the abscissa function and dividing the ordinates of the solid curve by the resulting values of particle radius.

It can be shown by a consideration of the integral implied in the argument above that when the values of $\bar{E}_M$ which result from the use of the distribution function of Figure 3 are divided by M and plotted against M on double logarithmic paper, a curve with a single maximum is obtained whose shape is independent of the r_0 value used. Changes in r_0 in this type of plot merely translate the curve parallel to the M axis. Changes in B on the other hand do change the shape of the curve. As B increases (uniformity decreases) the curve becomes flatter and the change in shape is accompanied by a vertical and horizontal displacement of the maxima of the curves. Since the shape of the curve depends only on

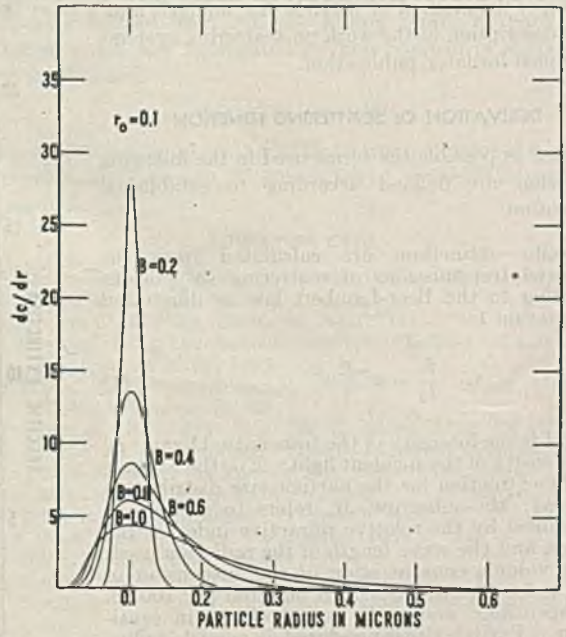

Figure 3. Distribution Function

$$\frac{dc}{dr} = \frac{e^{-\left[\frac{1}{B}\ln\frac{r}{r_0}\right]^2}}{\sqrt{\pi}\, r_0 B e^{0.25B^2}}$$

the nonuniformity coefficient, B, this parameter of an experimental distribution can be determined by superimposing the experimentally determined $\frac{E_M}{M}$ *vs.* M curve on a curve calculated for the same degree of nonuniformity. It is easy to show that the ratio of the M values of the maxima of two curves calculated for different values of r_0 but the same value of B is equal to the ratio of the r_0 values. The r_0 value of an experimental curve can therefore be determined by the magnitude of the translation on the logarithmic scale which is required to bring it into coincidence with a curve calculated for an r_0 value of unity and the same B value.

In order to make the comparisons suggested above, a chart has been constructed in which $\frac{E_M}{M}$ has been plotted against M on double logarithmic paper from values calculated for a single value of r_0 and a range of B values. In order to make the graphical operation as simple as possible, the family curves corresponding to the various B values have been plotted with a common maximum value. Correction scales are used to compensate for the translations which were required to make the maxima coincide. Table I shows the values of $\frac{E_M}{M}$ and M which were used in constructing the chart which is shown in Figure 4.

In Figure 4 the solid curves near the top and slightly to the right of center are the comparison curves. The maxima of all the curves have been made to agree with the maximum calculated for the curve corresponding to a B value of 0. The horizontal M scale is shown near the center of the figure. The r_0 scale above the M scale is required because an r_0 value of 0.1 micron was used in the standard calculations in order to keep the chart as small as possible.

The experimentally determined points are plotted on transparent tracing paper, which is placed over the coordinate system of the chart, so that these points can be translated easily into coincidence with the standard family curves after they have been plotted. The tracing paper is supported by a light Lucite frame which is provided with reference lines to orient the frame with the chart and correction scales to compensate for the translations which were required to bring the maxima of the standard family together. The shaded frame in the figure shows the frame in the plotting position.

Table I. Numerical Values Used in Constructing Standard Comparison Curves

M	$\frac{E_M}{M}$ $B = 0$	$B = 0.2$	$B = 0.4$	$B = 0.6$	$B = 0.8$	$B = 1.0$
0.5	6.0	6.4	7.2	7.5	8.8	9.3
0.6	7.1	7.5	8.3	9.0	9.8	10.1
0.7	8.2	8.6	9.4	10.2	10.7	10.3
0.8	9.3	9.7	10.5	11.2	11.2	10.4
0.9	10.5	10.8	11.6	12.0	11.7	10.4
1.0	11.6	11.9	12.5	12.5	11.8	10.4
1.1	12.7	13.0	13.4	12.8	11.8	10.3
1.2	13.7	13.9	13.9	13.0	11.6	10.1
1.3	14.6	14.7	14.2	12.9	11.4	9.9
1.4	15.5	15.3	14.4	12.8	11.1	...
1.5	16.2	15.7	14.4	12.6	10.85	...
1.6	16.7	15.9	14.1	12.2	10.5	...
1.7	16.8	15.7	13.8	11.8	10.1	...
1.8	16.6	15.2	13.4	11.5	9.8	...
1.9	15.7	14.5	12.9	11.0	9.4	...
2.0	14.6	13.8	12.4	10.6	...	...
2.1	13.5	13.0	11.8	10.2	...	...
2.2	12.6	12.2	11.1	9.8	...	...
2.3	11.7	11.4	10.6	9.3	...	...
2.5	10.1	9.9	9.6	8.5	...	...
2.8	8.3	8.2	8.3	7.5	...	...

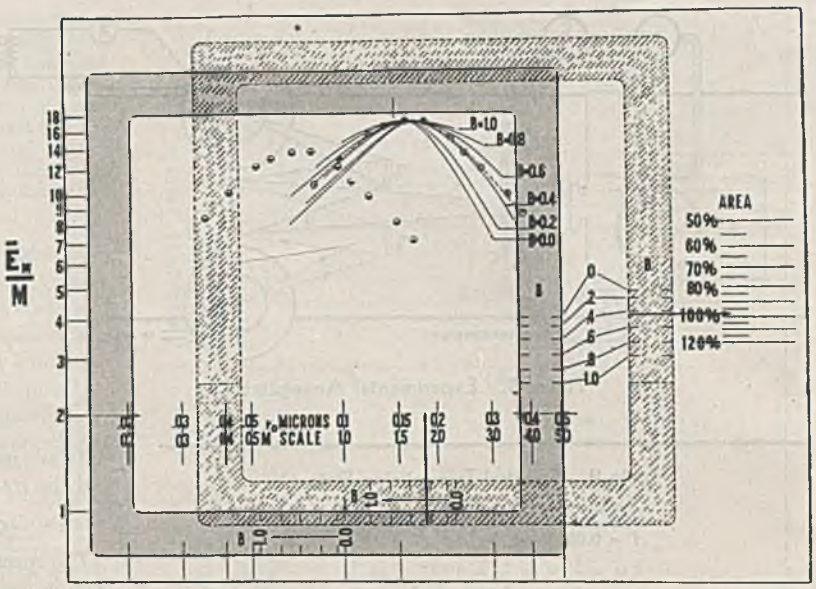

Figure 4. Standard Chart

To orient the frame for plotting, the horizontal reference lines are placed in coincidence with an $\frac{E_M}{M}$ value of 2.0 and the vertical reference lines are adjusted to agree with an M value of 1.0. The half-shaded points shown were determined for a sample of the anatase form of titanium dioxide in a suspension medium of an alkyd varnish. These points were plotted with frame in the position indicated by the shaded rectangle. After the points have been plotted the frame is translated vertically and horizontally until the maximum of the experimental curve agrees with the maximum of the standard family, always keeping the edges of the frame parallel with the coordinate system of the chart. The translated position of the frame is shown by the cross-hatched rectangle in Figure 4. The position of the experimental points in the standard family is indicated by the open points.

The B value is determined by inspection and the r_0 value is read on the r_0 scale opposite the selected B value on the horizontal correction scale on the frame. The value read on the vertical scale to the right opposite the selected B value on the vertical correction scale shows the fraction of the material in the suspension which contributed appreciably to the scattering. When a sample contains a fraction of very small or very large material, the vertical scale readings are less than 100%. When the form of the true distribution of the sample is appreciably different from the function shown in Figure 3, the shape of the experimental curve differs from that of the standard family, and when the true distribution is more symmetrical than the distribution function the vertical scale readings are usually greater than 100%. This results from the fact that in a more symmetrical distribution there is more than the calculated amount of material in the most effective size range. In such cases the parameters are determined from the arm of the experimental curve which agrees better with the standard family.

When B has a value of 0.5 the range of r_0 which can be determined by the method varies from 0.08 to 0.5 micron for a material with a refractive index of 2.7 to 0.10 to 0.8 micron for a material with a refractive index of 2.0.

MEASUREMENT OF TRANSMISSIONS

The significance of the measurement is entirely dependent on the degree of deflocculation attained in the suspensions prepared. The suspension media are chosen to promote good dispersion and, in addition, if required, special deflocculating agents are added. The suspension media are always liquids of high viscosity to retard settling. Water-white glycerol and certain alkyd varnishes give excellent results with many materials.

The suspensions usually are prepared with a carefully ground mortar and pestle. Weighed amounts (0.01 to 0.05 gram) of the material to be suspended are transferred to the mortar and the medium is added drop by drop at start. The degree of defloccu-

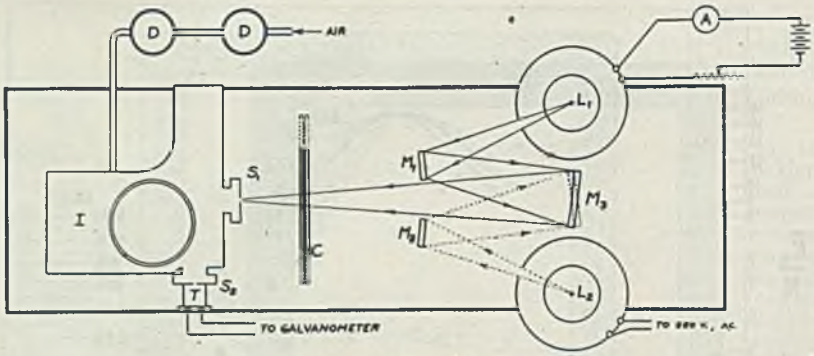

Figure 5. Experimental Arrangement

Table II. Spectral Transmission Data

Cell thickness = 0.08 cm.
Concentration = 1.19×10^{-4} cc./cc.
$ct = 0.0955$ ($c_0t_0 = 10^{-4}$)

$$\bar{E}_M = \frac{1}{ct} \times \ln \frac{1}{T} = 10.47 \times \ln \frac{1}{T}$$

Wave length, Micron	$\frac{1}{T}$	$\ln \frac{1}{T}$	$\bar{E}_M$	M	$\frac{\bar{E}_M}{M}$
0.405	3.19	1.16	12.15	1.71	7.11
0.436	3.24	1.18	12.32	1.51	8.19
0.546	2.30	1.16	12.17	1.10	11.16
0.500	3.16	1.16	12.07	1.23	9.81

lation attained depends on the amount of working that is given the paste with pestle as the first drops are added. When 1 cc. of suspension medium has been added the dilution is carried on more rapidly until the required weight of liquid has been added. The concentration is adjusted so that transmission in the blue part of the spectrum has a value of about 20%. The suspensions used in determining the distributions shown below were prepared following a time schedule in which the total time required was 0.5 hour.

Careful measurements have shown that the particle size distribution does not change with dispersion time when the time of preparation is longer than 0.5 hour. This indicates that no true grinding is done and that the degree of deflocculation is satisfactory.

A very thin cell of accurately known thickness is used in the measurements because most suspension media absorb at wave lengths between 1.5 and 2.0 microns and the effect of this absorption can be minimized by increasing the suspension concentration and reducing the cell thickness. The cell thickness now used for most of the measurements is about 0.075 cm.

The data required for the analysis are a series of 14 transmissions measured over the wave-length range of 0.4 to 2.0 microns. Figure 5 shows the experimental arrangement which has been used for such measurements.

L_1 is an incandescent lamp and L_2 is an H-3 mercury arc. M_1 and M_2 are plane mirrors which permit interchanging the sources and M_3 is a concave mirror which produces an image of the source at the monochromator slit, S_1. The monochromator, I, is based on a Gaertner Type L 235 infrared spectrometer which was modified by manufacturer to cover the full spectral range given above. T, the receiver, may be either a vacuum thermopile or a photocell. According to the present operating practice a photocell is used with an amplifier and meter for the visible spectrum and a thermopile-galvanometer combination used for the spectral region from 0.7 to 2.0 microns. The mercury arc is used in the blue and violet parts of the spectrum. The incandescent lamp is used for wave lengths of 0.5 micron and longer. The cell block containing three cells, two for suspensions and one for the clear suspension medium, is shown at C.

The specific extinctions are calculated from the measured transmissions in the manner indicated in Table II.

The factor which converts the logarithm of reciprocal transmission to specific extinction is calculated from the values of concentration and cell thickness as indicated at the top of the table. Column 2 shows the reciprocal of the transmissions measured at the wave lengths of column 1. Columns 3 and 4 show the calculation of specific extinction. The M values of column 5 are calculated for anatase in an alkyd varnish and 6 is obtained by dividing 4 by 5. Columns 5 and 6 are plotted as shown in Figure 4.

The method of analysis is rather rapid, the complete operation requiring but 2 hours, and the operations involved are simple enough for a technician to carry out satisfactorily. The results are usually reported as average radius, the B value found, and the fraction of the material found in the distribution.

COMPARISONS WITH ULTRACENTRIFUGE DATA

The spectral transmission method of particle size analysis has been in use for several years and during that time its reliability has been reasonably well tested. Figures 6 and 7 show the way in which the method has operated with practical systems.

Figure 6 illustrates the effectiveness of B as a measure of nonuniformity.

Distributions calculated from the values of r_0 and B are compared with distributions determined with the ultracentrifuge for the same materials. In both samples of anatase shown the value of r_0 is about 0.2 micron. Anatase A has a B value of 0.2 as a result of careful laboratory fractionation, while anatase B has a B value of 0.6 and is comparable with the material which was fractionated to obtain distribution A. The distribution for the bentonite clay has a B value of 0.95. The agreement obtained indicates that B is a satisfactory measure of uniformity.

The anatase form of titanium dioxide has a refractive index of 2.5 at the D line, while bentonite has a refractive index of about 1.5 and was measured in a medium whose refractive index was 1.4 Figure 7 shows a continuation of distribution comparisons for materials of different refractive index. The section at the left shows a sample of the rutile form titanium dioxide, the refractive index of which is about 2.7 at the D line. The center section shows an experimental sample, the refractive index of which

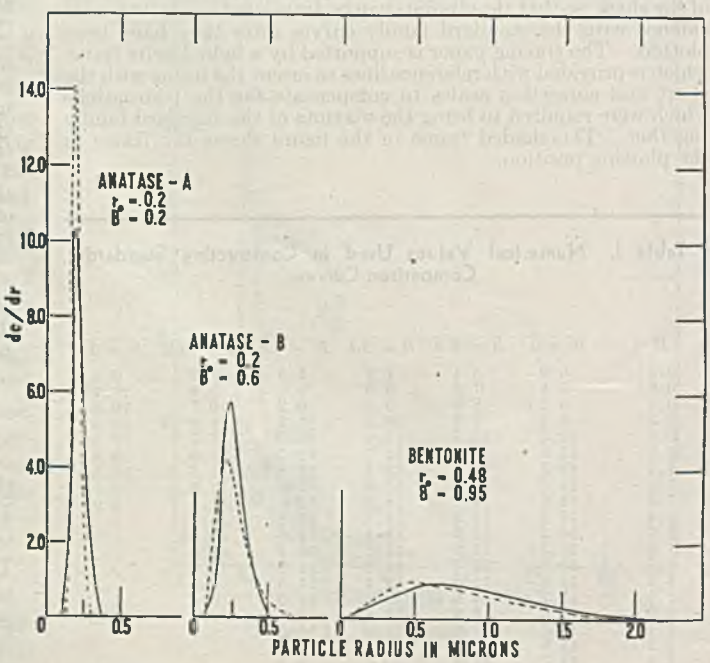

Figure 6. Comparison of Particle Size Distributions

——— Ultracentrifuge
- - - - Spectral transmission

was found to be 2.25 at the D line, and the distributions shown were used in determining this refractive index. The section at the right shows a comparison for a sample of zinc oxide, the relative refractive index of which is about 2.0 at the D line. The spectral transmission distribution for the zinc oxide sample was measured in a solid medium. The sample was prepared by dispersing the pigment in partially polymerized methyl methacrylate resin and the distribution determined when the polymerization was complete. This example illustrates the fact that the method is not limited to liquid media.

The method can be useful with unstable systems. Measurements for such systems have been made with a recording spectrophotometer similar to the instrument now made by the General Electric Company. The time required for the measurement of the full spectral range curve of the instrument is only 3 minutes and this speed of measurement makes such analyses possible. The restricted wave-length range of this spectrophotometer, however, makes it advisable to use the more cumbersome apparatus described earlier for routine measurements.

While different operators will choose values of B which will vary by 0.1, or in some cases more, the corresponding differences in r_0 usually compensate. The work which has been carried out indicates that the average radius is reproducible to within 5%.

REFRACTIVE INDEX

It has previously been assumed that the M value for each wave length of radiation in the range of measurement was known. In order to calculate such M values it is necessary to know the refractive index of both particle and suspension medium over the wave length range of 0.4 to 2.0 microns. The refractive indices of most materials of interest are given in literature for the visible part of the spectrum. In the work reported, the values for the infrared have been calculated by the simple Hartmann dispersion formula $n = n_0 + \frac{c}{\lambda - \lambda_0}$ where n_0, c, and λ_0 are arbitrary constants. In Figure 8 the indices of several materials are shown to illustrate the use of this method, and the corresponding M values are plotted against wave length below. Satisfactory results have been obtained by using the average index of anisotropic materials, so long as the particle index is not close to that of the suspension medium. When one index of a material with multiple indices nearly matches the medium, the method does not give reliable results.

When no refractive index data are available for materials whose refractive index is above 2.0, there has been no very reliable method for determining the index if the material is available only in finely divided form. A method for making such determinations has been worked out which makes use of the graphical technique described.

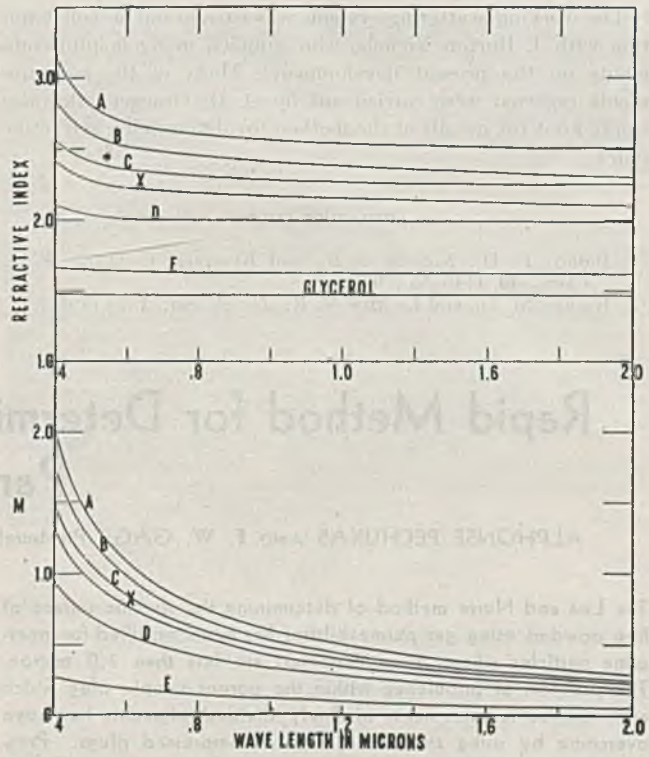

Figure 8. Refractive Index and M vs. Wave Length

A. Rutile, TiO_2 *D.* Cassiterite, SnO_2
B. Anatase, TiO_2 *E.* Barytes, $BaSO_4$
C. Sphalerite, ZnS *X.* Experimental sample

In order to make this evaluation it is necessary to determine the particle size distribution of the material by another method, such as ultracentrifugal analysis. An approximate value of M is then calculated from the average radius and a measured specific extinction. Using this value an M vs. λ curve is interpolated in the series of curves of Figure 8 and the graphical method applied with the measured specific extinction vs. wave length curve. The distribution calculated with the trial values of M usually is in error but it does provide a basis for selecting a better value of M to use in a second attempt. By continuing this process of successive approximations, it is possible to calculate a reasonably accurate curve showing M as function of wave length. When the vertical scale reading in Figure 4 is very nearly 100% for an M vs. λ curve which gives parameters which agree with the known distribution, it is fairly certain that the dispersion deduced is accurate. The refractive indices can, of course, be calculated from the M values.

The curves marked X in Figure 8 were determined in this way. The agreement obtained between the ultracentrifuge distribution and the distribution calculated by the graphical analysis using the final M values is shown in the middle section of Figure 7.

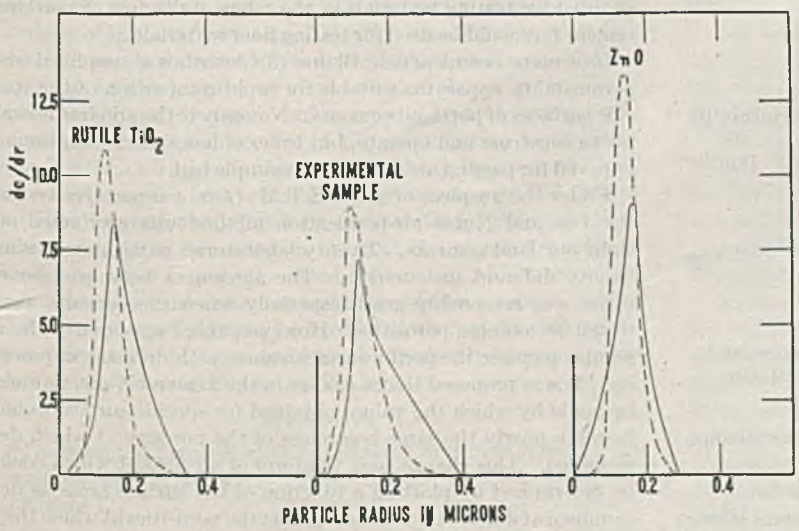

Figure 7. Comparison of Particle Size Distributions

——— Ultracentrifuge
- - - - Spectral transmission

ACKNOWLEDGMENTS

Grateful acknowledgment is made of the important contribution which Elmer O. Kraemer made to this development. All the work on scattering systems referred to here was carried out in the research group which he headed and much of what was accomplished was due to his active participation.

The work on scattering systems was carried out in collaboration with J. Burton Nichols, who supplied many helpful comments on the present development. Many of the measurements reported were carried out by O. H. Graeger, who also worked out the details of the method for determining refractive index.

LITERATURE CITED

(1) Bailey, E. D., Nichols, J. B., and Kraemer, E. O., *J. Phys. Chem.*, 40, 1149–55 (1936).
(2) Barnes, M. D., and La Mer, V. K., *J. Coll. Sci.*, 1, 79 (1946).
(3) Gamble, D. L., and Barnett, C. E., Ind. Eng. Chem., Anal. Ed., 9, 310 (1937).
(4) Lansing, W. D., and Kraemer, E. O., *J. Am. Chem. Soc.*, 57, 1369 (1935).
(5) Mie, G., *Ann. Physik*, 25, 377 (1908).
(6) Pfund, A. H., *J. Optical Soc. Am.*, 24, 143 (1934).
(7) Rayleigh, Lord (Strutt, J. W.), *Phil. Mag.*, 47, 377 (1899).
(8) Stratton, J. A., and Houghton, H. G., *Phys. Rev.*, 38, 159 (1931).
(9) Svedberg and Pederson, "The Ultracentrifuge", pp. 338–42, Oxford, Clarendon Press, 1940.

Presented before the Division of Industrial and Engineering Chemistry, American Chemical Society, Symposium on Measurement and Creation of Particle Size, Brooklyn, N. Y., December, 1945. Contribution 208 from the Chemical Department, E. I. du Pont de Nemours and Company.

Rapid Method for Determining Specific Surface of Fine Particles

ALPHONSE PECHUKAS AND F. W. GAGE, Pittsburgh Plate Glass Co., Columbia Chemical Division, Barberton, Ohio

The Lea and Nurse method of determining the specific surface of fine powders using gas permeabilities has been modified for measuring particles whose mean diameters are less than 1.0 micron. The problem of turbulence within the porous sample plug which accompanies measurements of finely divided pigments has been overcome by using small-bore, highly compressed plugs. Pressure differentials of 1 atmosphere have been substituted for the lower pressures of Lea and Nurse to overcome the resistance to air flow offered by the more highly compressed plugs. The method is rapid and simple in operation and is reproducible, the specific surface values being fairly constant over a range of porosities. An apparatus suitable for routine work and plant control is described.

During the past several years the permeability method of determining the specific surface of fine particles has received considerable attention from workers interested in a rapid and accurate means of measuring the particle size of pigments in the subsieve range. The theory of the permeability method and details of experiments conducted to test its validity have been discussed by Carman (*4–6*), who showed that the specific surface of a powder could be expressed by the equation

$$S_0 = 14\sqrt{\frac{1}{K_1} \times \frac{\epsilon^3}{(1-\epsilon)^2}} \qquad (1)$$

where

S_0 = specific surface of the powder in sq. cm. per cc.
K_1 = proportionality constant representing the permeability of the porous medium
ϵ = porosity or fractional void of the bed of powder

Based on laws of fluid flow, K_1 can be expressed by

$$K_1 = \frac{Q_1 \eta L}{A \times \Delta P} \qquad (2)$$

where

Q_1 = rate of flow of the percolating fluid in ml. per second
A = cross-sectional area of the porous medium in sq. cm.
η = viscosity of the fluid in poises
L = thickness of porous medium in cm.
ΔP = pressure difference driving the fluid through the medium in grams per sq. cm.

Carman has shown that for the same powder at different porosities the porosity function, $\epsilon^3/(1-\epsilon)^2$, is accurate over a fairly wide range of porosities.

Carman worked for the most part with liquids rather than air, being of the opinion that surface area values from air permeabilities tended to be high, owing to incomplete dispersion of the powder in the bed. However, he recognized that not only was it difficult to select a liquid that would give reasonably good dispersion and wetting, but adsorption of the liquid at the particle surface might tend to decrease the effective porosity, giving a low permeability and therefore a high surface area value.

Lea and Nurse (*9*) have evolved a highly developed gas-permeability method which is appreciably more rapid than the liquid-permeability method and is extremely reproducible. They have shown that gas permeabilities are consistent for different gases and that corresponding values of particle size with gases are more in accord with sedimentation particle size analysis than with liquids.

Gooden and Smith (*7*) have also successfully used air permeabilities for measuring various sized fractions of powdered silica. However, for the more finely divided fractions, agreement was poor between the air permeability particle size and that calculated from microscopic measurements.

Blaine (*2*) has devised an air-permeability apparatus similar to that of Lea and Nurse which he found well adapted to comparing the specific surfaces of powdered materials. His procedure was fast and simple and the test results were reproducible. He concluded that the air-permeability apparatus was not only well adapted for testing materials in the range of fineness of portland cement but could be used for testing finer materials.

In a more recent article Blaine (*3*) describes a simplified air-permeability apparatus suitable for rapid comparison of the specific surfaces of portland cements. Not only is the apparatus simple to construct and operate, but times of less than 3 minutes are required for passing air through the sample bed.

Under the auspices of the A.S.T.M. (*1*) a comparative test of the Lea and Nurse air-permeation method was conducted on eight portland cements. Twenty laboratories participated using twenty different instruments. The agreement between laboratories was reasonably good, especially when the cements were tested at average porosities. However, there appeared to be a regular increase in specific surface values with decrease in porosity. It was proposed that a change in the Lea and Nurse formula be made by which the values obtained for specific surface would be more nearly the same regardless of the porosity at which determined. This change took the form of a constant which could be determined by plotting a function of the surface areas as determined at different porosities against the porosities at which they were determined and extrapolating the straight line obtained to zero surface area. The intersection at the zero surface area line is apparently a constant for each type of material. This constant

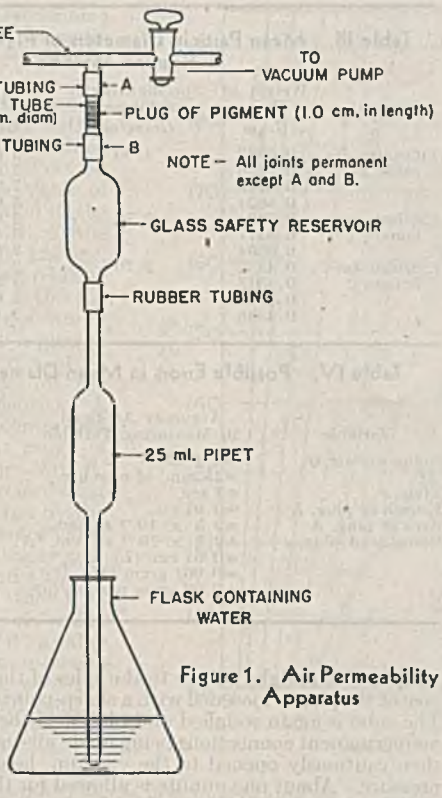

Figure 1. Air Permeability Apparatus

can be used to correct the Lea and Nurse formula so that calculated specific surface areas are not affected by the porosity at which the powder is tested.

From a theoretical point of view the permeability method should be valid within experimental errors down to a particle diameter of 0.1 micron. However, it has been constantly recognized that the method has certain limitations which might not permit its being applied to the measurement of particle size diameters much below 2 microns. Lea and Nurse (*9*) have stated that the method may be limited to particles of 10 microns or larger. Work (*10*) has found that the porosity function, $\epsilon^3/(1-\epsilon)^2$, is very critical and is not proportional to the permeability over a very wide range in some cases. Thus in making tests of various materials it is necessary to determine the porosity at which this function is proportional to the permeability.

However, because of its relative simplicity and apparent reproducibility the method definitely merits consideration.

A need arose in this laboratory for a rapid, reproducible method for determining the relative particle sizes of pigments in the range of 0.1 to 2.0 microns. Microscopic methods were tedious and only semiquantitative, since with even a dark-field microscope the smaller particles are often overlooked and a true evaluation cannot be made. Adsorption methods are also time-consuming and often lead to erroneous results, especially with particles of irregular surfaces. Attention was therefore turned to an air-permeation method. An investigation of the method detailed by Lea and Nurse (*9*) demonstrated that some modifications would have to be made before it could be used satisfactorily to measure the specific surface of pigments having mean diameters less than 1.0 micron. Air flow rates much in excess of 10 ml. per minute were to be avoided since turbulence resulted, invalidating the equation developed by Carman (*4*) for Poiseuille flow. It was also found necessary to compact the pigment tightly in small-bore tubes in order to avoid channeling, which resulted if only relatively light pressures and large beds were used. These highly compressed pigment beds resisted air flow to such an extent that measured rates could be obtained only by using a full atmosphere pressure drop across the bed.

APPARATUS

The essential features of the apparatus first developed for determining the surface area of finely divided pigments are shown in Figure 1.

It consists of an Erlenmeyer flask filled with water, a 25-ml. pipet connected to a glass safety reservoir with a permanent heavy rubber connection, and the sample tube, having an internal diameter of 0.634 cm. and constructed of precision-bore tubing.

In making a determination a plug of pigment of known volume is formed in the sample tube. This is packed in by hand, using two short cylindrical lengths of metal which fit snugly inside the sample tube and extend beyond it at each end. The length of the plug is measured with a micrometer which spans the plug and the two metal pieces of known length. To simplify calculations the pigment plugs are all formed to a constant length of 1.00 cm. This is done by adding or subtracting pigment until the well packed plug is slightly too long and then making a final adjustment by compressing to the exact length.

The sample tube is then weighed and placed in the apparatus. The flask of water is drawn to one side, so the pipet tip is no longer immersed in the water, and the vacuum pump started. The stopcock on the vacuum line is then opened slowly to avoid sudden application of vacuum to the sample plug. The pressure differential is noted by means of a mercury gage (not shown in Figure 1) and maintained at approximately 740 mm. of mercury. After permitting the system to come to equilibrium, the rate of flow of air through the sample plug is measured by moving the flask of water back to position and timing accurately the interval required to draw 25 ml. of water into the pipet.

With the data obtained it was possible to calculate the specific surface of the sample. Equations 1 and 2 may be combined and modified to yield the following equation:

$$S_t = 14\sqrt{\frac{At \times \Delta P}{Q_2 \eta L} \times \frac{\epsilon^3}{(1-\epsilon)^2}} \qquad (3)$$

where

Q_2 = volume of air in ml. flowing through sample plug in time t

or

$$S_w = \frac{S_v}{\rho} = \frac{14}{\rho}\sqrt{\frac{At \times \Delta P}{Q_2 \eta L} \times \frac{\epsilon^3}{(1-\epsilon)^2}} \qquad (4)$$

where

S_w = specific surface of the pigment in sq. cm. per gram
ρ = specific gravity of pigment

Since ρ, A, ΔP, η, and L are known constants, Equation 4 may be put in the following form:

$$S_w = K_2\sqrt{\frac{t}{Q_2} \times \frac{\epsilon^3}{(1-\epsilon)^2}} \qquad (5)$$

where

$$K_2 = \frac{14}{\rho}\sqrt{\frac{A \times \Delta P}{\eta L}}$$

K_2 will, of course, have a unique value for each type of pigment. The porosity may be expressed mathematically as

$$\epsilon = 1 - \frac{W}{\rho A L} \qquad (6)$$

where

W = weight of pigment in plug in grams

Having measured t, Q_2, and W, it is a very simple task to combine Equations 5 and 6 to calculate the specific surface, S_w

It is clear from the foregoing that the apparatus required and technique are very simple. The method is also rapid, requiring less than an hour for one determination. If it is desired, more than one apparatus may be run off the same vacuum manifold.

The reproducibility is good, as is indicated in Table I. Small variations in ΔP which are experienced because of fluctuations in the barometric pressure have little effect on the specific surface values. Although no attempt is made to use the same weight of pigment for each determination, the porosities are fairly uniform in duplicate determinations with the same pigment.

Because of the critical nature of the porosity function, $\epsilon^3/(1-\epsilon)^2$, the actual values of surface area may not agree too well with those obtained by this method. However, since no known method can be relied upon to yield infallible surface area measurements, comparisons with other methods, while not precise, serve to indicate whether the method yields results of the right order of magnitude. Harkins and Gans (*8*) using an adsorption method obtained values of 38,000 and 57,300 sq. cm. per gram on two titanium dioxide pigments, which compare very favorably with the results in Table I. Apparently the air-permeation method described here can be relied upon to give values of the correct order of magnitude.

Table I. Surface Area of Titanium Dioxide Pigment

Pigment	Porosity	Surface Area, Sq. Cm. per Gram
Titanium dioxide 1	0.7194	36,600
	0.7337	36,200
	0.7286	35,400
	0.7167	34,900

Table II. Comparison of Mean Cross-Sectional Diameter Values

(Calculated from specific surface value of a titanium dioxide pigment, assuming various particle shapes. Specific surface area, 36,000 sq. cm. per gram)

Assumed Shaped of Particles	Mean Diameter, Micron
Spherical	0.42
Rod-shaped, length 1.5 times diameter	0.37
Rod-shaped, length 2 times diameter	0.35
Rod-shaped, length 3 times diameter	0.33
Rod-shaped, length 4 times diameter	0.31

APPARATUS FOR ROUTINE CONTROL WORK

Although this method was highly satisfactory as a research tool, it soon became desirable to modify it for routine and more rapid determinations. Therefore, the apparatus was redesigned so that shorter times would be required for making a determination, and calculation of the particle size would be simplified.

This modified apparatus, diagrammed in Figure 2, consists of a 150-ml. beaker filled with water, an inverted 10-ml. graduated pipet with the tip cut off, a calcium chloride tube, the sample tube, and a stopcock, which is connected to a source of high vacuum. The sample tube is a stainless steel tube carefully machined and having an internal diameter of 0.579 ± 0.0025 cm. All connections are made with heavy, tightly fitting sections of rubber tubing and are all made permanent except those between the calcium chloride tube and the rubber stopper and between the sample tube and the rubber connection.

In making a determination the sample tube is weighed and then placed over the bottom plunger of the hand press shown in Figure 3. The sample is transferred to the sample tube by means of a funnel and packed into the tube, using the top section of the hand press. When the plug is reasonably firm the sample tube is reversed. This prevents the tube from coming in contact with either the top or bottom of the hand press, thus ensuring that the plug length is exactly that between the two plungers. Sample is added until a firm, solid plug is obtained. Any portion of the sample which might adhere to the sides of the tube above the surface of the plug is loosened with a sharp-pointed wire and removed. The tube is again weighed and placed in the apparatus, the two nonpermanent connections being made air-tight. The stopcock is then cautiously opened to the vacuum, held at less than 5-mm. pressure. About one minute is allowed for the system to come to equilibrium, after which the time for a measured amount of air to pass through the plug is determined. The quantity of air is chosen so that the time required is between 2 and 5 minutes.

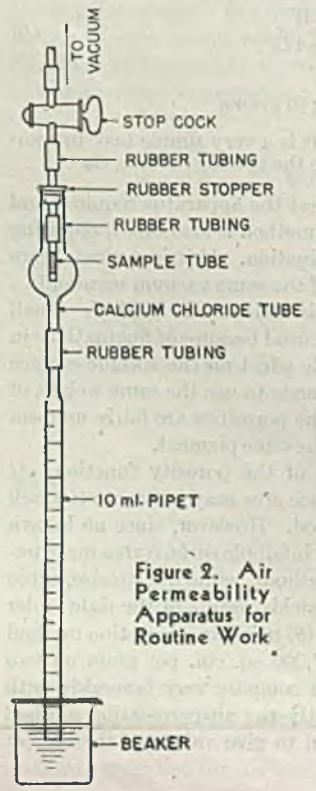

Figure 2. Air Permeability Apparatus for Routine Work

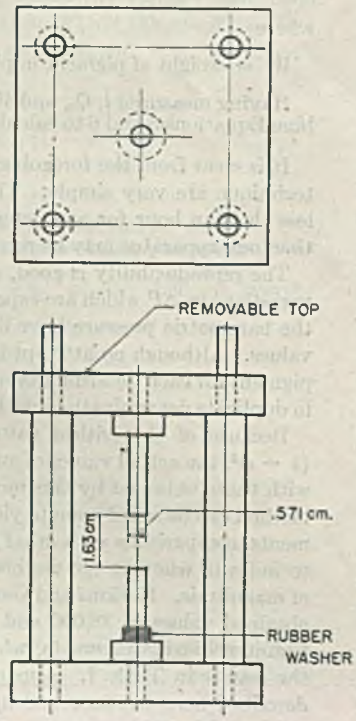

Figure 3. Hand Press

Table III. Mean Particle Diameters of Pigments, Using Rapid Routine Method

Pigment	Weight of Plug, *Gram*	Specific Gravity of Pigment, *Gram/ml.*	Volume of Air, *Ml.*	Time, *Sec.*	d_m, *Micron*
Titanium dioxide 2	0.6963	4.00	5.0	151	0.74
	0.7376		5.0	169	0.78
	0.6623		7.0	161	0.78
	0.6624		5.0	116	0.78
Calcium carbonate 1	0.3424	2.70	3.0	181	0.30
	0.3177		3.0	156	0.28
	0.3394		3.0	195	0.28
Calcium carbonate 2	0.4432	2.70	2.5	177	0.43
	0.4313		2.5	186	9.40
	0.4225		3.0	218	0.38
	0.4346		3.0	224	0.40

Table IV. Possible Errors in Mean Diameter Determination

Variable	Accuracy Assumed in Measuring Variable	Maximum % Deviation in d_m Due to Error in Measuring Variable
Volume of air, Q_2	±0.1 ml.	±1.0
ΔP	±25 mm. of mercury	±1.7
Time, t	±1 sec.	±0.4
Length of plug, L	±0.01 cm.	±0.3
Area of plug, A	$\pm 2.3 \times 10^{-3}$ sq. cm.	±0.5
Porosity of plug, ϵ	$\pm 2.3 \times 10^{-3}$ sq. cm. (A)	±2.0
	±0.01 cm. (L)	±2.0
	±0.001 gram (W)	±0.5
	±0.02 gram per ml. (ρ)	±1.2

CALCULATION OF PARTICLE SIZE

For routine control it is convenient to express the specific surface area of the pigment in terms of mean diameter. This is usually done by assuming a spherical shape for each particle. However, whether a spherical shape or a rodlike shape is assumed does not change the order of magnitude of the mean cross-sectional diameter, and in fact does not change the actual value appreciably. This is demonstrated in Table II, in which the mean cross-sectional diameters of a titanium dioxide pigment calculated on the basis of several assumed particle shapes are presented.

Assuming a spherical particle, Equation 4 becomes

$$S_w = \frac{6}{d_m \rho} \tag{7}$$

where

d_m = mean cross-sectional diameter in cm.

By combining Equations 4 and 7 and expressing d_m in microns, the following equation is obtained:

$$d_m = \frac{30{,}000}{7} \times \sqrt{\frac{Q_2 \eta L (1-\epsilon)^2}{\epsilon^3 A t \Delta P}} \tag{8}$$

By suitable mathematical expansion Equation 8 becomes

$$d_m = \left[\left(\frac{3 \times 10^4}{7} \times L \sqrt{\frac{\eta}{\Delta P}}\right)\left(\frac{W/\rho}{(LA - W/\rho)^{3/2}}\right)\right]\sqrt{\frac{Q_2}{t}} \tag{9}$$

$$= K_3 \sqrt{\frac{Q_2}{t}}$$

where

$$K_3 = \left(\frac{3 \times 10^4}{7} \times L \sqrt{\frac{\eta}{\Delta P}}\right)\left(\frac{W/\rho}{(LA - W/\rho)^{3/2}}\right) \tag{9A}$$

or

$$\frac{K_3^2}{d_m^2} = \frac{t}{Q_2} \tag{10}$$

By employing Equations 9A and 10 the value of d_m may be calculated by a simple graphical method. How this can be accomplished is shown in Figure 4.

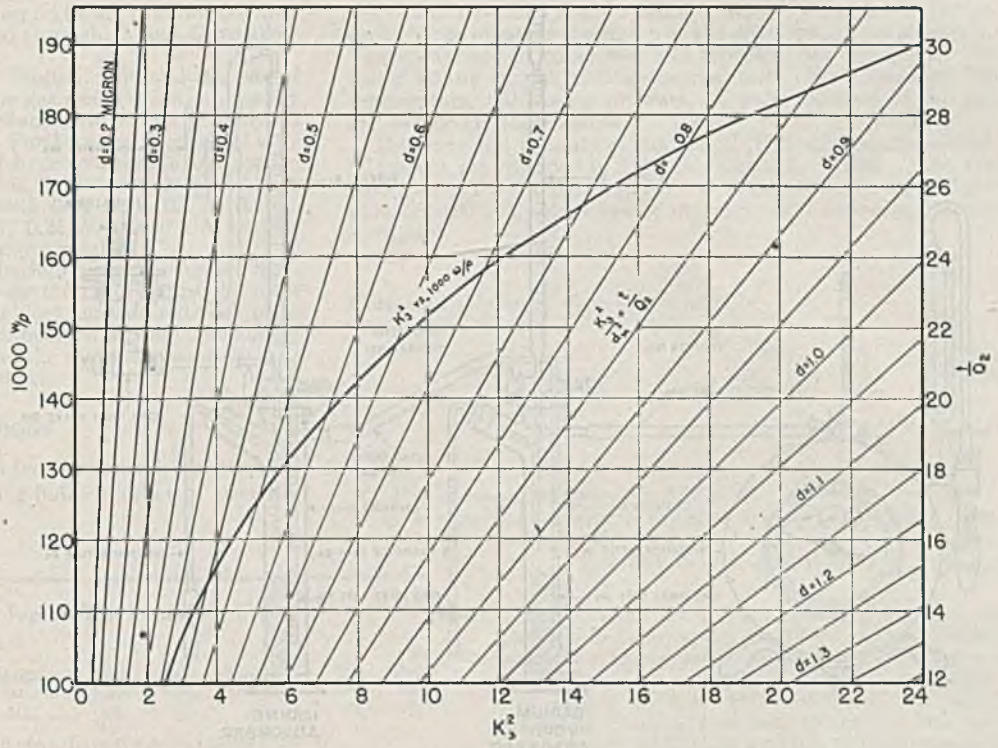

Figure 4. Chart for Determining Mean Cross-Sectional Diameter

Since L, η, and A are constants and ΔP is held within limits, variations within which have only negligible effect on the value of d_m, the value of K_3, or K_3^2, is a function of the ratio of the weight, W, of the sample to its specific gravity, ρ, and a curve is drawn relating these two functions. On the same graph is drawn a family of curves in which K_3^2 is plotted versus t/Q_2 for a series of d_m values covering those of the pigments being measured. A few preliminary measurements will determine what range of t/Q_2 and W/ρ values will be encountered and therefore what ranges must be covered by the graph. To determine the value of d_m for any particular pigment, ratios W/ρ and t/Q_2 are calculated. Using the W/ρ versus K_3^2 curve, the K_3^2 value corresponding to the W/ρ value is determined. The intersection of this K_3^2 value with the t/Q_2 ratio is then found and the value of d_m obtained by interpolation.

This method is reproducible, as is demonstrated in Table III. It was recognized that there would be several sources of error in a measurement of this type. Reference to Table IV will demonstrate, however, that if all errors were cumulative the maximum deviation in the value of d_m would be 9.6%, owing to experimental errors. In actual practice the maximum deviation is approximately 5% of the value of d_m. This does not appear too large in light of the errors accompanying measurements of mean cross-sectional diameters by other methods.

SUMMARY

A method for determining the specific surface area of pigments in the range of 0.1 to 1.0 micron has been described. The method is reproducible and is easily modified for rapid control work. Although the specific surface values obtained may not be true values, accurate comparisons of similar pigment types may be made.

LITERATURE CITED

(1) Am. Soc. Testing Materials, Working Committee on Fineness, Committee C-1 on Cement, *Bull.* 118, 31 (1942).
(2) Blaine, R. L., *Ibid.*, *Bull.* 108, 17 (1941).
(3) *Ibid.*, *Bull.* 123, 51 (1943).
(4) Carman, P. C., *J. Soc. Chem. Ind.*, 57, 225T (1938); 58, 1T (1939).
(5) Carman, P. C., Am. Soc. Testing Materials, Symposium on New Methods for Particle Size Determination in the Subsieve Range, p. 24, 1941.
(6) Carman, P. C., *Trans. Inst. Chem. Engrs.* (London), 15, 150 (1937).
(7) Gooden, E. L., and Smith, C. M., Ind. Eng. Chem., Anal. Ed., 12, 479 (1940).
(8) Harkins, W. D., and Gans, D. M., *J. Am. Chem. Soc.*, 53, 2804 (1931).
(9) Lea, F. M., and Nurse, R. W., *J. Soc. Chem. Ind.*, 58, 277T (1939).
(10) Work, L. T., discussion of paper by P. C. Carman, "Shape and Surface of Fine Powders by the Permeability Method", Am. Soc. Testing Materials, Symposium on New Methods for Particle Size Determination in the Subsieve Range, p. 24, 1941.

Presented before the Division of Industrial and Engineering Chemistry, American Chemical Society, Symposium on Measurement and Creation of Particle Size, Brooklyn, N. Y., December, 1945.

Simultaneous Determination of Hydrogen Sulfide and Carbon Dioxide in a Continuous Gas Stream

CLYDE L. BLOHM AND FRED C. RIESENFELD, The Fluor Corp., Ltd., Los Angeles, Calif.

A method is described for the simultaneous determination of hydrogen sulfide and carbon dioxide in a continuous stream of natural gas. The two acidic gases are absorbed in standardized iodine and barium hydroxide solutions. Only simple laboratory equipment is required.

IN THE course of one of the research projects of this laboratory, it was found necessary to analyze a stream of natural gas for hydrogen sulfide and carbon dioxide in such a manner that a large number of analyses could be taken which, at the end of the operation, could be integrated into a quantitative over-all balance.

Various methods are known for determining hydrogen sulfide and carbon dioxide in natural gas. Hydrogen sulfide is most commonly determined by the Tutweiler method (*2, 4, 9*), or by one of the cadmium sulfide methods (*3, 5*). The carbon dioxide content of the gas is usually measured by absorption in sodium hydroxide solution in an Orsat (*2, 6, 8*) or Orsat-type apparatus, or may be determined by absorption in barium hydroxide solution as described by Martin and Green (*7*). When both hydrogen sulfide and carbon dioxide are present, the total acid gas content

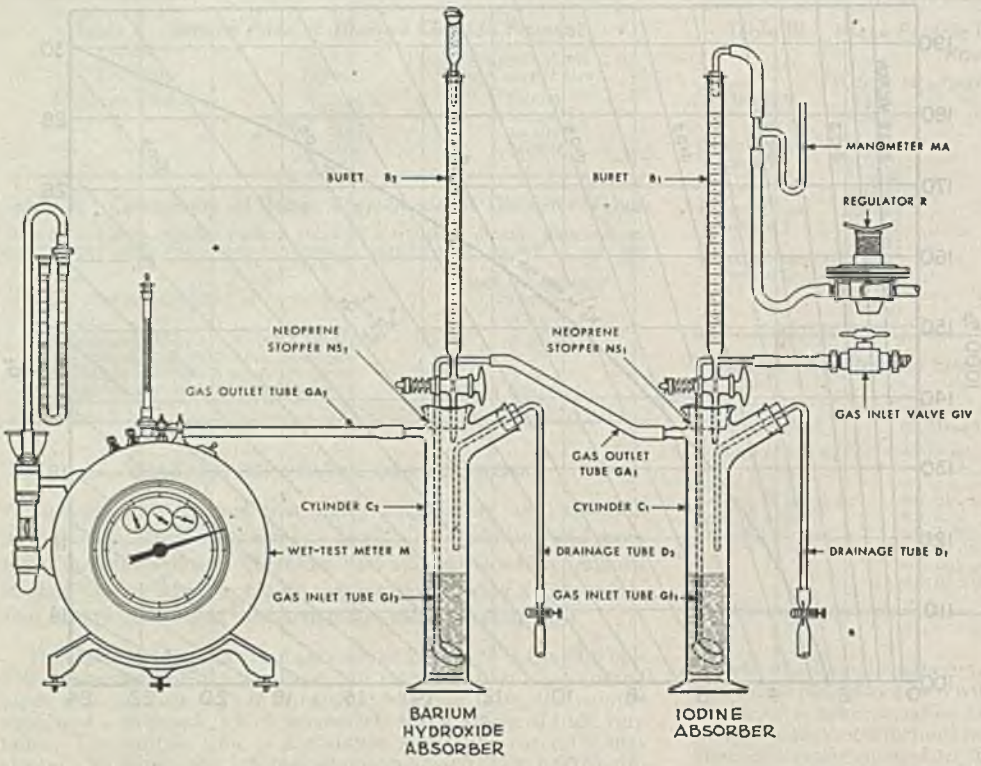

Figure 1. Diagram of Apparatus

is measured by absorption in sodium hydroxide, the hydrogen sulfide determined by one of the methods mentioned, and the carbon dioxide found by difference.

These methods were not satisfactory for the project under investigation, mainly because they did not provide means for analyzing the gas stream continuously and simultaneously for both hydrogen sulfide and carbon dioxide. Results obtained by the Orsat and Tutweiler methods represent merely individual spot analyses, and do not indicate gradually occurring changes of the hydrogen sulfide and carbon dioxide content. For the same reason, the over-all balance which is calculated from such analyses is inaccurate. By using the cadmium sulfide method, the gas stream can be analyzed continuously for hydrogen sulfide, but the carbon dioxide content still has to be found by spot analyses. Furthermore, the equipment specified by the C.N.G.A. (*5*) for this method is complicated and difficult to clean, which causes some difficulties in an operation that requires many analyses.

The method which this laboratory has developed consists of titrating the hydrogen sulfide with standard iodine and the carbon dioxide with standard barium hydroxide solution, using starch and phenolphthalein as the respective indicators. The chemical reactions upon which this method is based are:

$$H_2S + I_2 = 2HI + S \quad (1)$$

$$Ba(OH)_2 + CO_2 = BaCO_3 + H_2O \quad (2)$$

The advantage of this method is that any chosen volume of gas can be analyzed by appropriate variation of the increments and the strength of the titrating fluids, the gas stream can be observed at any given moment, and occurring changes detected immediately. However, the method does not distinguish between hydrogen sulfide and mercaptans or other reducing agents. If such are present, the "apparent" hydrogen sulfide content is determined. Furthermore, any acidic constituents, other than carbon dioxide, which would be absorbed by barium hydroxide are also disturbing factors.

EXPERIMENTAL PROCEDURE

Reagents. Iodine solution, 0.1 *N*, is prepared by dissolving approximately 60 grams of pure potassium iodide in 50 ml. of water, to which 13 grams of pure iodine are then added. This solution is made up to a final volume of 1 liter with distilled water.

The iodine solution is standardized with arsenic trioxide, Standard Sample 83a, or subsequent samples, of the National Bureau of Standards, according to the procedure indicated in the provisional certificate of analysis of Standard Sample 83a.

Barium hydroxide solution, 0.25 *N*, is prepared by dissolving 79 grams of pure barium hydroxide octahydrate in 1 liter of distilled water free of carbon dioxide.

The barium hydroxide solution is standardized with 0.1 *N* hydrochloric acid, which has been standardized against 0.1 *N* sodium hydroxide. Acid potassium phthalate Standard Sample 84b, or subsequent samples, of the National Bureau of Standards is used as primary standard for the sodium hydroxide solution. The procedure to be followed is specified in the provisional certificate of analysis of Standard Sample 84b.

Starch solution, 0.4%.

Phenolphthalein solution, 0.1%.

Apparatus. The equipment used in this method (Figure 1) consists of two 500-ml. Pyrex hydrometer cylinders, C_1 and C_2, modified by the addition of a side arm, into the top of each of which a two-holed neoprene stopper, NS_1 and NS_2, is inserted. One of the holes holds the gas inlet, GI_1 and GI_2, which is a sintered-glass dispersion tube; through the other hole a 50-ml. buret, B_1 and B_2, is inserted in such a manner that its tip reaches into the cylinder. The side arm, GA_1 and GA_2, serves as gas outlet. D_1 and D_2 are drainage tubes, through which liquid can be siphoned from the cylinder.

B_1 is filled with the standard iodine solution for the titration of the hydrogen sulfide. Inasmuch as the gas dispersion tube in the barium hydroxide absorber creates some back pressure in the iodine absorber, it is necessary to drive the iodine solution from the buret by means of air or neutral gas at a pressure of from 150 to 250 mm. of mercury which is controlled by the regulator, *R*, and the manometer, *MA*. This pressure necessitates the use of a spring-loaded stopcock on the iodine buret. B_2 is filled with standard barium hydroxide solution for the titration of the carbon dioxide. It is necessary to close the top of B_2 with a soda-lime tube to protect the barium hydroxide from contact with carbon dioxide in the air.

The connection between the gas source, the two cylinders, and the gas meter, *M*, are made by neoprene tubing. Rubber tubing absorbs small amounts of hydrogen sulfide which causes inaccuracy in the analysis and, therefore, the use of neoprene tubing and stoppers is recommended. It is desirable to use as short lengths of this tubing as convenient, using glass tubing to span any very great distances.

The gas meter, *M*, can be any suitable displacement meter graduated in 0.01 liter or 0.001 cubic foot.

Procedure. Before the test is started, C_1 and C_2 are loaded with 150 ml. of carbon dioxide-free distilled water, 5 ml. of 0.4% starch solution and sufficient standard iodine solution to produce a slight but permanent blue coloration in the solution are added to C_1, and 5 ml. of 0.1% phenolphthalein solution are placed in C_2. B_1 and B_2 are filled with the respective titration fluids.

A measured amount of iodine and barium hydroxide solution is now added to the respective cylinders and the flow is started at the gas inlet valve, *GIV*, at a rate of 1 to 2 cubic feet per hour. As soon as the iodine or barium hydroxide solution is exhausted, which is indicated by a color change of the indicator, the gas volume read on the meter is recorded and fresh titration fluid is added. This procedure is continued throughout the entire test

period. Whenever the amount of liquid in the cylinder becomes too large, sufficient liquid is drained through D_1 and D_2 to allow the operation to be continued.

By decreasing the increments of titration fluid and the rate of gas flow, rather rapid changes in the gas composition can readily be detected. If gas of rather constant composition is analyzed larger increments should be used. Furthermore, in cases of very low or very high concentrations of hydrogen sulfide and carbon dioxide, the strength of the titration fluids may be varied. In this laboratory, experiments run with 0.01 N, 0.025 N, 0.1 N, and 0.5 N iodine, and with 0.1 N, 0.25 N, and 0.5 N barium hydroxide solutions yielded satisfactory results.

The sulfur formed in C_1 and the barium carbonate formed in C_2 during the analysis somewhat impair the detection of the color change of the indicator and tend to block the sintered-glass plate in the gas dispersion tube. Both difficulties can be overcome by some experience in the operation and the choice of coarse (such as Corning "C" porosity) sintered plates.

CALCULATIONS

The calculations of three typical test runs, using gas mixtures of different composition and titrating fluids of different strength, are shown in Table I.

Column 1 is a list of the readings taken on the flowmeter at each change of either the starch or the phenolphthalein indicator. The values are in cubic feet and represent the reading of the meter at the end of each absorption test. No corrections for temperature, barometric pressure, or water content of the gas are included in these values.

The corrected volumes of gas passing through each increment of reagent are recorded in liters in column 2. These values are corrected to the standard conditions customary in the natural gas industry (60° F., 30 inches of mercury, dry) according to the formula:

$$\text{Corrected volume} = \text{observed volume} \times \frac{520}{460 + t} \times \frac{p}{30} \times \frac{p - pw}{p}$$

where

t = observed temperature in ° F.
p = observed barometric pressure in inches of mercury
pw = vapor pressure of water at observed temperature in inches of mercury

These values are further corrected for the acid gas absorbed during the analysis. If gas of rather constant acid gas content is analyzed, this correction is found by calculating the hydrogen sulfide and carbon dioxide absorbed from the total volume of titrating fluid used in the test run and subsequently adding an average prorated volume to each increment. In cases of varying acid gas concentration, the acid gas volume to be added to the discharge volume has to be prorated from increment to increment. The error in both methods is very small and well below the reading error on the meter. Finally, there must be subtracted from the volume read on the meter the gas displaced from each absorber on the addition of titrating fluid. For convenience in computation, the input gas volume is calculated in liters, since all other volume measurements are made in metric units.

The corrected volumes of gas passing through the apparatus for each test are recorded in liters in columns 3 and 4.

Columns 5 and 8 indicate the increments of standard iodine and barium hydroxide solution in milliliters.

Columns 6 and 9 show the calculated volumes of hydrogen sulfide and carbon dioxide corresponding to each increment of titrating fluid:

1 ml. of 0.1 N iodine = 1.183 ml. of hydrogen sulfide at 60° F. and 30 inches of mercury
1 ml. of 0.1 N barium hydroxide = 1.183 ml. of carbon dioxide at 60° F. and 30 inches of mercury

In columns 7 and 10, the hydrogen sulfide and carbon dioxide contents of the gas are listed in volume per cent.

For purposes of comparison, results of analyses by the Tutweiler and C.N.G.A. methods for hydrogen sulfide and by the Orsat method for carbon dioxide are given in footnotes *a*, *b*, and *c*.

If it is desired to express the hydrogen sulfide value in grains per 100 standard cubic feet the percentage has to be multiplied by 628.9.

Table I. Typical Test Runs

Total Metered Flow	Gas Tested	Gas per H_2S Test	Gas per CO_2 Test	Iodine Increment	H_2S Calcd.	H_2S Content	$Ba(OH)_2$ Increment	CO_2 Calcd.	CO_2 Content
Cu. feet	*Liters*	*Liters*	*Liters*	*Ml.*	*Ml.*	*%*	*Ml.*	*Ml.*	*%*
Run 1, Iodine Normality 0.0984, $Ba(OH)_2$ Normality 0.4226[a]									
0.089	2.533	2.384	...	25.0	29.1	1.15	...	...	...
0.098	2.763	...	2.600	...	...	...	25.0	125.0	4.52
0.181	2.336	...	2.198	...	...	...	25.0	125.0	5.35
0.182	2.621	2.466	...	25.0	29.1	1.11	...	...	...
0.263	2.307	...	2.171	...	...	...	25.0	125.0	5.42
0.273	2.563	2.412	...	25.0	29.1	1.14	...	...	...
0.345	2.307	...	2.171	...	...	...	25.0	125.0	5.42
0.365	2.592	2.439	...	25.0	29.1	1.12	...	...	...
0.425	2.251	...	2.118	...	...	...	25.0	125.0	5.55
0.458	2.621	2.466	...	25.0	29.1	1.11	...	...	...
0.507	2.307	...	2.171	...	...	...	25.0	125.0	5.42
0.549	2.563	2.412	...	25.0	29.1	1.14	...	...	...
0.588	2.278	...	2.144	...	...	...	25.0	125.0	5.49
0.642	2.621	2.466	...	25.0	29.1	1.11	...	...	...
0.671	2.336	...	2.198	...	...	...	25.0	125.0	5.35
0.735	2.621	2.466	...	25.0	29.1	1.11	...	...	...
0.753	2.307	...	2.171	...	...	...	25.0	125.0	5.42
0.826	2.563	2.412	...	25.0	29.1	1.14	...	...	...
0.835	2.307	...	2.171	...	...	...	25.0	125.0	5.42
0.918	2.563	2.412	...	25.0	29.1	1.14	...	...	...
Run 2, Iodine Normality 0.00955, $Ba(OH)_2$ Normality 0.2306[b]									
0.0085	2.302	2.244	...	25.0	2.83	0.12	...	...	...
0.129	3.508	...	3.419	...	...	...	25.0	68.2	1.94
0.181	2.604	2.538	...	25.0	2.83	0.11	...	...	...
0.227	2.658	...	2.591	...	...	...	25.0	68.2	2.56
0.277	2.604	2.538	...	25.0	2.83	0.11	...	...	...
0.324	2.631	...	2.564	...	...	...	25.0	68.2	2.59
0.375	2.658	2.591	...	25.0	2.83	0.11	...	...	...
0.423	2.686	...	2.618	...	...	...	25.0	68.2	2.54
0.473	2.658	2.591	...	25.0	2.83	0.11	...	...	...
0.523	2.718	...	2.645	...	...	...	25.0	68.2	2.51
0.571	2.658	2.591	...	25.0	2.82	0.11	...	...	...
0.623	2.718	...	2.645	...	...	...	25.0	68.2	2.51
0.669	2.658	2.591	...	25.0	2.82	0.11	...	...	...
0.722	2.686	...	2.618	...	...	...	25.0	68.2	2.54
0.768	2.686	2.618	...	25.0	2.82	0.11	...	...	...
0.823	2.740	...	2.671	...	...	...	25.0	68.2	2.49
0.867	2.686	2.618	...	25.0	2.82	0.11	...	...	...
0.923	2.718	...	2.645	...	...	...	25.0	68.2	2.51
0.965	2.658	2.591	...	25.0	2.82	0.11	...	...	...
1.022	2.718	...	2.645	...	...	...	25.0	68.2	2.51
Run 3, Iodine Normality 0.3431, $Ba(OH)_2$ Normality 0.1052[c]									
0.093	2.513	...	2.458	...	...	...	25.0	31.2	1.24
0.099	2.678	2.623	...	20.0	81.6	3.05	...	...	...
0.186	2.513	...	2.458	...	...	...	25.0	31.2	1.24
0.200	2.731	2.676	...	20.0	81.6	2.99	...	...	...
0.275	2.406	...	2.351	...	...	...	25.0	31.2	1.30
0.299	2.678	2.623	...	20.0	81.6	3.05	...	...	...
0.364	2.406	...	2.351	...	...	...	25.0	31.2	1.30
0.399	2.705	2.650	...	20.0	81.6	3.02	...	...	...
0.452	2.380	...	2.325	...	...	...	25.0	31.2	1.31
0.499	2.705	2.650	...	20.0	81.6	3.02	...	...	...
0.540	2.380	...	2.325	...	...	...	25.0	31.2	1.31
0.600	2.731	2.676	...	20.0	81.6	2.99	...	...	...
0.625	2.300	...	2.245	...	...	...	25.0	31.2	1.35
0.702	2.758	2.703	...	20.0	81.6	2.96	...	...	...
0.711	2.326	...	2.271	...	...	...	25.0	31.2	1.34
0.803	2.731	2.676	...	20.0	81.6	2.99	...	...	...
0.826	2.300	...	2.245	...	...	...	25.0	31.2	1.35

[a] H_2S, %. Tutweiler, 1.14; C.N.G.A., 1.14. CO_2, %. Orsat, 5.46.
[b] H_2S, %. Tutweiler, 0.11; C.N.G.A., 0.11. CO_2, %. Orsat, 2.59.
[c] H_2S, %. Tutweiler, 3.03; C.N.G.A., 3.03. CO_2, %. Orsat, 1.32.

DISCUSSION

As can be seen from Table I, the results obtained by the proposed method check well with values from analyses by the customary methods. The probable accuracy of the Orsat method, with good equipment is dependent largely on buret reading error. This is stated to be of the order of 0.05 to 0.1 ml. (*8*). Thus, on a gas con-

taining 10% acidic constituents, the percentage error would be ±0.5 to 1.0% on a 100-ml. sample. The C.N.G.A. method is said to be accurate to within 5% (presumably ±5%, *4*), but here again the percentage error is dependent on the total amount of material measured. The accuracy of the Tutweiler method is dependent largely upon the iodine buret reading error. If this error is ±0.05 ml., the use of 5 ml. of iodine solution would give a percentage error of ±1%. Thus it is seen that the method herein described has a probable accuracy of the same order of magnitude as that of the customary methods.

The first value in a series of determinations has to be discarded because some gas is consumed for the saturation of the liquids in the absorption cylinders, which causes erroneous meter readings. Subsequently, the variations between successive determinations should not be greater than ±2.5%. This accuracy holds for a wide range of acid gas concentrations and diminishes only if the acid gas content is very low and very small increments of titrating fluids have to be used. The method is applicable to practically every concentration of hydrogen sulfide and carbon dioxide occurring in natural gas, since accurate analyses can be obtained by appropriate variations of the strength and the increments of the titrating solutions.

The method is readily adapted to routine field testing by measuring the solutions into the absorption cylinders by accurately calibrated pipets, and then passing the gas through the solution until the indicators change color. From the meter readings and the amount of standard solutions used, the acid gas content of such spot samples may be calculated. However, the increments of iodine and barium hydroxide have to be chosen in such a manner that the barium hydroxide is exhausted first in order to avoid erroneous results due to absorption of hydrogen sulfide in the barium hydroxide solution.

CONCLUSIONS

An analytical method has been developed for the continuous and simultaneous determination of hydrogen sulfide and carbon dioxide in a stream of natural gas, using standard iodine and barium hydroxide solutions as titrating fluids.

The results found by this method are accurate and compare favorably with results obtained by methods customary in the gas industry.

Slightly modified, the method can be used for routine work in the field.

LITERATURE CITED

(1) American Gas Chemists' Handbook, 3rd ed., New York, Chemical Publishing Co., 1929.
(2) *Ibid.*, p. 462.
(3) API Code No. 50-A, Section V, "Code for Measuring, Sampling, and Testing Natural Gas", American Petroleum Institute, Division of Production, Dallas, Texas.
(4) Bureau of Mines, *Rept. Investigation* 3128 (1931).
(5) California Natural Gasoline Association, 510 West 6th St., Los Angeles, Calif., *Bull.* TS-431 (1943).
(6) *Ibid.*, *Bull.* TS-342.
(7) Martin, W. McK., and Green, J. R., Ind. Eng. Chem., Anal. Ed., 5, 114-18 (1933).
(8) Matuszak, M. R., "Fisher Gas Analysis Manual", New York, Fisher Scientific Co.
(9) Tutweiler, C. C., *J. Am. Chem. Soc.*, 23, 173 (1901).

Analysis for Naphthene Ring in Mixtures of Paraffins and Naphthenes

M. R. LIPKIN, C. C. MARTIN, AND S. S. KURTZ, JR., Sun Oil Company, Experimental Division, Norwood, Pa.

A new method based on the temperature coefficient of density and either density or refractive index is recommended for the analysis of ring content in mixtures of paraffins and naphthenes. When tested on pure compound data it shows an average deviation of 8% due mainly to isomer effect. The accuracy of the method is dependent to some extent on the degree of condensation of the naphthene rings, and is unsatisfactory for bridged ring naphthenes and single naphthene rings containing more than eight carbon atoms in the ring. The new method is compared with the older methods of Davis and McAllister, and Vlugter, Waterman, and van Westen.

THIS paper continues a general investigation of the interrelationship of physical properties and their use in analytical methods for hydrocarbons (*7, 9–14, 17, 22*) and is concerned with the determination of weight per cent ring carbon atoms in mixtures of paraffins and naphthenes. Per cent ring is arbitrarily defined as 100 times the ratio of the ring carbon atoms to the total carbon atoms, and must be distinguished from per cent naphthenes which is the percentage of naphthenic molecules and includes both ring and side chain.

Two methods for obtaining a naphthene ring analysis have been published. The method developed by Davis and McAllister (*2*) is based on molecular volume and molecular weight and gives number of ring carbon atoms. This method requires two properties, density and molecular weight, and the accuracy is dependent to some extent on the degree of condensation of the naphthene rings. Schiessler *et al.* (*18*) have pointed out the systematic deviation of this equation for high molecular weight hydrocarbons and have worked out a correction for use in this range. This systematic deviation is not surprising in view of the meager pure compound data available in 1930 when the Davis and McAllister paper was published.

The method for per cent naphthene ring developed by Vlugter, Waterman, and van Westen (*20, 21*) is based on a correlation of Lorentz-Lorenz specific refraction and molecular weight, and requires three properties, density, refractive index, and molecular weight. The use of three physical properties instead of two, as in the Davis and McAllister method, introduces an additional variable involving a knowledge of the size of the naphthene rings (cyclopentane or cyclohexane types). Thus, in the analysis of petroleum fractions by the Waterman method it becomes necessary to make assumptions regarding the size and degree of condensation of the naphthene rings. It is usually assumed that the naphthene rings are condensed cyclohexanes, since for this correlation that type of ring structure best represents the average for all naphthenes.

In the initial stages of this work it was found that there were many combinations of physical properties which would give a correlation for determining weight per cent ring. The method presented is based on the temperature coefficient of density and density or refractive index. No other combinations of properties were found which gave a better correlation. The temperature coefficient of density is derived from molecular weight (*13*), which is easily determined from other laboratory inspection tests by means of the correlations of Hirschler (*7*), or Mills, Hirschler, and Kurtz (*17*).

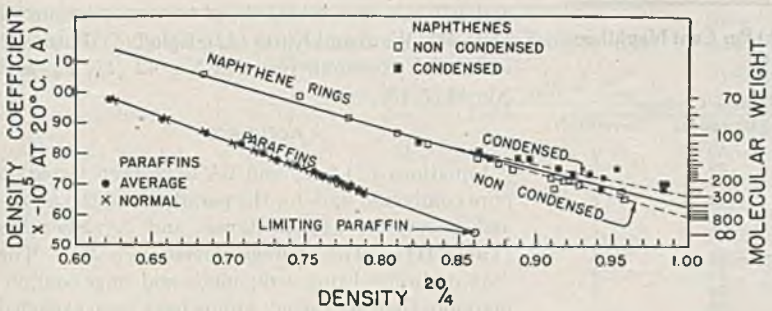

Figure 1

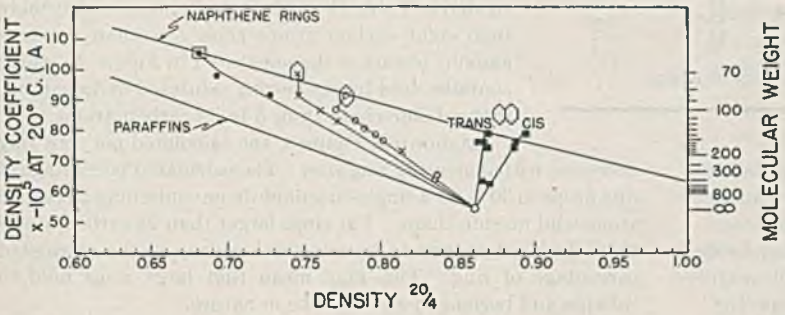

Figure 2

Table I. Relation of Molecular Weight and Temperature Coefficient of Density

Molecular Weight	A^a	Molecular Weight	A^a	Molecular Weight	A^a	Molecular Weight	A^a
70	98.4[b]	92	89.0	140	78.5	260	68.5
71	97.9[b]	94	88.4	143	78.0	271	68.0
72	97.4	96	87.8	147	77.5	284	67.5
73	96.9	98	87.3	150	77.1	297	67.0
74	96.4	100	86.7	153	76.7	310	66.5
75	96.0	102	86.1	156	76.3	324	66.0
76	95.5	104	85.6	159	75.9	340	65.5
77	95.0	106	85.1	163	75.5	357	65.0
78	94.5	108	84.6	167	75.0	374	64.5
79	94.1	110	84.1	172	74.5	394	64.0
80	93.6	112	83.7	177	74.0	415	63.5
81	93.2	114	83.2	182	73.5	439	63.0
82	92.8	116	82.8	187	73.0	467	62.5
83	92.3	118	82.4	193	72.5	499	62.0
84	91.9	120	82.0	199	72.0	538	61.5
85	91.5	122	81.6	205	71.5	586	61.0
86	91.1	125	81.0	213	71.0	643	60.5
87	90.7	128	80.5	221	70.5	718	60.0
88	90.4	131	80.0	229	70.0	805	59.5
89	90.0	134	79.5	239	69.5	902	59.0
91	89.4	137	79.0	249	69.0		

[a] $A = -10^5 \times \alpha$ (temperature coefficient of density at 20° C.).
[b] These values are probably less accurate than the others.

DERIVATION OF EQUATIONS

It was found on plotting density versus the temperature coefficient of density for paraffins and noncondensed naphthene rings containing no chain (Figure 1), that linear relationships exist for each of these two classes of hydrocarbons. A third straight line branching from the noncondensed naphthene ring line can be drawn through the data for condensed naphthene rings.

As shown in Figure 2, the addition of a side chain to a naphthene ring causes the properties to approach those of a paraffin of infinite molecular weight and the degree of approach is roughly proportional to the percentage of chain. The density of the paraffin of infinite molecular weight, sometimes known as the limiting paraffin, is 0.861 (*10*). For mixtures of paraffins and naphthenes in the region below 0.861 density, an equation was derived assuming the percentage of paraffin plus paraffin side chain can be obtained by interpolation between the paraffin line and the naphthene ring line, along a line of constant density. Thus, for d < 0.861

$$\text{Weight \% ring} = \frac{A + 190.0d - 217.9}{0.593d - 0.249} \quad (1)$$

where

d = density at 20° C.

$A = -10^5 \times$ temperature coefficient of density (α) derived from molecular weight (see Table I)

Figure 3 demonstrates that this method of interpolation is satisfactory for naphthenic hydrocarbons; the deviations of the calculated from the experimental weight per cent ring for the alkyl cyclohexanes and alkyl cyclopentanes are shown. The greatest deviations seem to be in the initial members of the series; this irregularity is common to most physical properties of these hydrocarbons.

Table II demonstrates that the method is also satisfactory for mixtures of paraffins and naphthenes. In three examples hypothetical properties for binary mixtures of a paraffin and a naphthene at several different concentrations have been calculated. Hydrocarbons which agree fairly well with the correlation were chosen for these calculations. Two sets of the mixtures shown consist of hydrocarbons which would not ordinarily be encountered together, but the results on these serve to indicate that the method is useful for samples of wide boiling range.

In the region above 0.861 density, saturated petroleum fractions consist mainly of naphthenes as shown by the work of Mair, Willingham, and Streiff (*16*), which indicates that paraffins do not exist in lubricating oils. A second equation was derived for this region, assuming that the percentage of paraffin plus paraffin side chain can be obtained by interpolation between the naphthene ring line and the limiting paraffin point along a straight line drawn through the point representing the sample. Thus, for d > 0.861

$$\text{Weight \% ring} = \frac{A + 102.8d - 142.8}{0.262} \quad (2)$$

Above 0.861 density, the naphthene ring line is a compromise line midway between the condensed and noncondensed naphthene rings. This assumes an equal distribution of the condensed and noncondensed types and introduces an uncertainty which becomes larger with increasing number of rings per molecule. If one type predominates in the tri- and tetracyclic range, the error may be as great as 5 to 10%. When our state of knowledge is sufficiently advanced that we know the relative amounts of con-

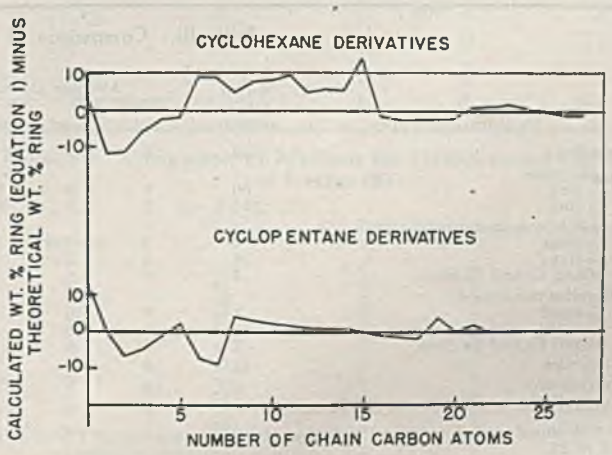

Figure 3

Table II. Agreement of Calculated with Theoretical Weight Per Cent Naphthene Ring for Hypothetical Binary Mixtures

Hypothetical Mixtures	Mole % of Paraffin	Molecular Weight	d_4^{20} [a]	A	% Ring Carbons Calcd.	Theoretical	Deviation
1-Methyl-2-amyl	0	168.3	0.8146	74.9	50	50	0
cyclohexane	20	171.5	0.8028	74.5	40	39	1
($C_{12}H_{24}$) with	40	174.8	0.7917	74.2	30	29	1
5-butylnonane	60	177.9	0.7814	73.9	21	19	2
($C_{13}H_{28}$)	80	181.2	0.7717	73.6	11	9	2
	100	184.4	0.7624	73.3	1	0	1
2-Ethyldecalin	0	166.3	0.8702	75.1	83	83	0
($C_{12}H_{22}$) with	25	149.8	0.8346	77.1	72	70	2
3,3-dimethyl-	50	133.2	0.7940	79.6	57	53	4
pentane (C_7H_{16})	75	116.7	0.7474	82.7	35	30	5
	100	100.2	0.6933	86.6	2	0	2
Cyclohexane	0	84.2	0.7786	91.8	102	100	2
(C_6H_{12}) with n-	20	101.4	0.7683	86.3	70	67	3
dodecane	40	118.6	0.7612	82.3	45	43	2
($C_{12}H_{26}$)	60	135.9	0.7559	79.2	25	25	0
	80	153.1	0.7519	76.7	9	11	−2
	100	170.3	0.7488	74.7	−5	0	−5

[a] Densities calculated on volume % basis assuming no volume change on mixing.

densed and noncondensed naphthenes in different petroleum fractions, we can replace Equation 2 with two separate equations for condensed and noncondensed naphthene rings.

A plot similar to the density versus A correlation may be derived by plotting refractive index against A, and an alternative set of equations have been derived in terms of these properties

For $n < 1.478$

$$\text{Weight \% ring} = \frac{A + 374.1n - 607.2}{1.152n - 1.471} \qquad (1A)$$

For $n > 1.478$

$$\text{Weight \% ring} = \frac{A + 232.9n - 398.4}{0.232} \qquad (2A)$$

Where n = refractive index at 20° C. for the D line of sodium.

The authors recommend use of Equations 1 and 2 derived in terms of temperature coefficient of density and density. Equations 1A and 2A appear to be slightly less accurate, but may be used as an alternative when it is more convenient to obtain refractive index than density. Inspection of these equations indicates that weight per cent ring can also be calculated from density and refractive index alone. This calculation has been found to give considerably greater error and is not recommended.

The four equations were derived from the physical property data on the normal paraffins and naphthene rings without side chain. A slight adjustment, however, was necessary to obtain a better fit with the data for the whole mass of paraffins and naphthenes. Therefore the final equations do not agree exactly with the lines shown in Figures 1 and 2. The data on pure hydrocarbons were assembled from the compilations of Doss (*3*), Ward and Kurtz (*22*), Egloff (*5*), Eaton (*4*) and A.P.I. Research Projects No. 42 (*18, 24*) and No. 44 (*1, 19*).

ACCURACY

Equations 1, 1A, 2, and 2A have been tested on pure compound data for the paraffins and the mono- and polycyclic cyclopentanes and cyclohexanes (Table III). The average deviation is 8%. The data on bridged ring compounds and rings containing more than six carbon atoms have been excluded from Table III because the bridged ring compounds show more than the true amount of ring as demonstrated in Table IV, and single rings containing more than eight carbon atoms show less than the true amount of ring as demonstrated in Figure 4; which contains data for single-ring saturated hydrocarbons without side chain from 5 to 34 carbon atoms.

As shown in Figure 4, the calculated per cent ring decreases with increasing ring size. The calculated percentage of ring drops to 30% for a single-ring naphthene containing 25 carbon atoms and no side chain. For rings larger than 25 carbon atoms there does not appear to be any further drop in the calculated percentage of ring. This may mean that large rings tend to collapse and become more chainlike in nature.

In the analysis of petroleum fractions we need not expect too much trouble from these anomalies, since rings larger than six carbon atoms have not yet been isolated from petroleum, and the

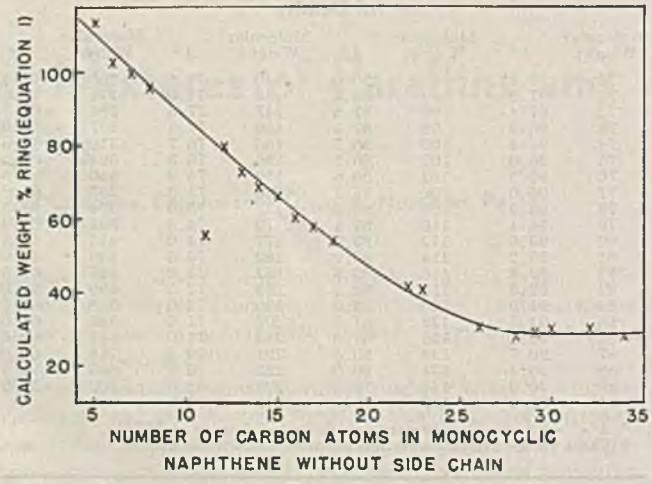

Figure 4

Table III. Comparison of Methods for Pure Compound Data

Hydrocarbon Types	No. of Compounds	Calculated Weight Per Cent Ring: Average Deviation[a] A–d[c]	A–n[d]	Davis	Waterman	Deviation of Average[b] A–d	A–n	Davis	Waterman	Maximum Deviation A–d	A–n	Davis	Waterman
Paraffins	224	7	7	9	6	0	0	6	3	−55	−68	−63	121
Monocyclics													
C_5 ring	56	6	9	11	5	−2	−7	−7	−2	−19	−27	−20	−14
C_6 ring	115	8	9	10	11	1	1	−1	−10	+28	+44	−91	+51
Dicyclics noncondensed													
C_5 rings	7	2	5	6	6	−1	−4	−2	−4	−6	+27	−15	−9
C_6 rings	26	5	7	7	21	−4	2	2	−17	−13	+16	39	51
Mixed C_5 and C_6 rings	7	6	6	6	15	−6	−6	−6	−15	−13	+31	−11	−19
Dicyclics condensed													
C_5 rings	4	8	10	8	13	6	1	1	10	+14	+12	−12	19
C_6 rings	32	6	5	9	8	5	6	8	−7	+18	+37	25	−51
Mixed C_5 and C_6 rings	7	8	6	7	10	8	5	7	4	+12	+9	10	16
Tricyclics	13	10	10	9	18	−3	−2	4	−12	+25	+39	36	−41
Tetracyclics	6	10	9	8	19	−6	0	5	−17	−14	+18	22	−59
Average (according to No. of compounds)		7	8	8	12	0	0	2	−6	..	..	..	..

[a] Without regard to sign. [b] Taking sign into account. [c] (A–d) refers to calculation by Equations 1 or 2. [d] (A–n) refers to calculation by Equations 1A or 2A.

Table IV. Comparison of Methods for Saturated Bridged Ring Compounds

Compounds	Deviation of Calculated Weight % Ring			
	A–d	*A*–*n*	Davis	Waterman
	14	11	12	8
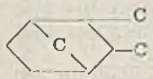	25	22	27	24
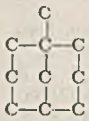	−7	−16	18	14
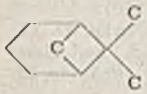	25	20	31	28
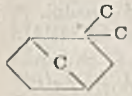	9	−1	38	35
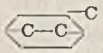	23	20	31	29
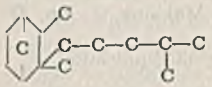	14	11	25	24
	29	25	53	52
	24	5	81	78
	23	18	54	54

bridged ring structures which have been shown to be present are probably in small concentration in most crudes.

As shown in Table III, accuracy of the recommended method is only slightly better than obtained with the Davis-McAllister and Waterman methods when compared on the basis of the whole mass of pure compound data. (The Waterman method in this case has been used, assuming the condensed cyclohexane type of ring structure is the predominant polycyclic naphthene type.) However, a comparison on hydrocarbon fractions of higher molecular weight shows a pronounced difference between the recommended method and these other methods. In general, the Davis-McAllister method gives results which are on the average as much as 10% higher than the *A*-density method, and the Waterman method gives results which are as much as 5% lower (see Tables V, VI, VII). Work done by A.P.I. Project No. 42 (*18*, *24*) shows that the *A*-density method is accurate within 2 to 3% on the pure compounds of high molecular weight. This indicates the recommended method is probably the most accurate in the high molecular weight range.

The Davis and McAllister method and the *A*-density method both use the same physical properties, molecular weight and density, so that it is not reasonable to believe that one would be subject to more variables than the other. It is only because the present correlators had more and better data that the new correlation shows less deviation.

An example of the accuracy of this method for unusual materials is demonstrated on three petroleum wax fractions originally reported by Ferris, Cowles, and Henderson (*6*), and later analyzed for carbon and hydrogen content by Mair and Schicktanz (*15*). A comparison is made of weight per cent ring calculated from Equation 1 with values calculated from carbon and hydrogen content, assuming a variety of possible naphthene ring structures in mixtures with paraffin, where the carbon and hydrogen value show naphthene to be present. As shown in Table VIII, the agreement is good.

In the routine use of this method for the high melting point waxes, weight per cent ring can be determined from melting point and refractive index in the liquid state, usually at 80° C. The molecular weight is then calculated from refractive index and melting point by the method of Mills, Hirschler, and Kurtz (*17*), and the refractive index is corrected to 20° C. using Equations 1 and 2 (*13*). The latter equation is sufficiently accurate for the purpose of this paper, although it is not in general recommended for correcting refractive index over a wide range of temperature. The application of this type of analysis to aromatic rings is being studied.

ACKNOWLEDGMENT

The statistical data contained in this paper have been completely revised since its presentation at the 1941 Atlantic City meeting of the American Chemical Society. The authors wish to acknowledge the assistance of H. P. Spain in carrying out many of the calculations.

LITERATURE CITED

(1) Am. Petroleum Inst., Research Project 44, National Bureau of Standards. Selected Values of Properties of Hydrocarbons as of June 30, 1945.

Table V. Comparison of Methods for Hydrogenated Lube Oil Extracts of Mair, Willingham, and Streiff (*16*)

Fractions	Weight % Ring *A*–d	Deviation from *A* – d Method *A*–*n*	Davis	Waterman
B-12-H	74	3	10	−5
B-16-H	72	3	10	−6
B-19-H	70	3	5	−7
C-1-H	78	4	10	−3
C-7-H	77	3	13	−5
C-13-H	75	3	11	−5
C-20-H	69	3	11	−5
C-(26 + 27)-H	60	3	11	−4
C-30-H	56	2	10	−6
C-33-H	51	2	9	−6
C-35-H	47	2	7	−7
C-37-H	43	2	7	−10
C-res-H	34	0	4	−10
E-1-H	75	4	12	−7
E-25-H	50	3	12	−4
Deviation of average		3	10	−6

Table VI. Comparison of Methods for Hydrogenated Olefin Polymers of Waterman, Leendertse, and Makkink (*23*)

Fractions	Weight % Ring *A*–d	Deviation from *A*–d Method *A*–*n*	Davis	Waterman
II	6	−1	5	0
IV	5	0	7	−2
I′	11	1	7	−4
II′	13	1	6	−4
III′	12	1	6	−4
IV′	17	1	5	−6
V′	16	0	6	−5
VI′	18	1	6	−7
Deviation of average		1	6	−4

Table VII. Comparison of Methods for Hydrogenated Gas Oils of Kreulen (*8*)

Fractions	Weight % Ring *A*–d	Deviation from *A*–d Method *A*–*n*	Davis	Waterman
1	68	−4	−1	−8
2	66	−2	2	−4
3	65	0	5	−4
4	47	−5	1	−5
6	49	−5	1	−5
5	42	−4	2	−6
11	43	−3	−6	−8
7	45	−5	1	−5
8	31	−3	3	−4
9	28	−3	4	−2
10	33	−3	3	−5
Deviation of average		−3	1	−5

Table VIII. Accuracy of Calculation for Three Wax Fractions Refined by Ferris et *al.* (*6*)

	Weight Per Cent Ring				
		Calculated from Empirical Formula[a] Determined by Mair and Schicktanz (*15*), Assuming Mixtures of Paraffins with Naphthenes of Following Types:			
Fraction	Calcd. by Equation 1	One or more cyclohexane rings per molecule	One or more 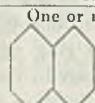 groups per molecule	One or more cyclopentane rings per molecule	One or more 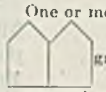 groups per molecule
6A	−4[b]	−2[b]	−2[b]	−2[b]	−2[b]
6I	9	14	11	11	9
6J	12	15	13	13	10

[a] Mair and Schicktanz analyzed samples prepared by Ferris, Cowles, and Henderson after these had been in storage for some time. A correction to x in formula C_nH_{2n+x} was made to allow for loss of hydrogen due to slight oxidation while in storage. Mair and Schicktanz state that they have probably overcorrected for this loss of hydrogen, which would result in slightly low values for the weight per cent ring calculated from empirical formula.

[b] Hypothetical negative value for per cent ring is reported for a strict comparison of accuracy. In practice, negative values for calculated weight per cent ring would be reported as 0.

(2) Davis, G. H. B., and McAllister, E. N., Ind. Eng. Chem., 22, 1326 (1930).
(3) Doss, M. P., "Physical Constants of the Principal Hydrocarbons", 4th ed., Texas Co., 1943.
(4) Eaton, J. L., "Science of Petroleum", Vol. II, London, Oxford University Press, 1938.
(5) Egloff, G., "Physical Constants of Hydrocarbons", Vols. I and II, New York, Reinhold Publishing Corp., 1940.
(6) Ferris, S. W., Cowles, H. C., and Henderson, L. M., Ind. Eng. Chem., 23, 681 (1931).
(7) Hirschler, A. E., *J. Inst. Petroleum*, 32, 133 (1946).
(8) Kreulen, D. J. W., *J. Inst. Petroleum Tech.*, 23, 253 (1937).
(9) Kurtz, S. S., Jr., and Lipkin, M. R., *J. Am. Chem. Soc.*, 63, 2158 (1941).
(10) Kurtz, S. S., Jr., and Lipkin, M. R., Ind. Eng. Chem., 33, 779 (1941).
(11) Kurtz, S. S., Jr., and Ward, A. L., *J. Franklin Inst.*, 224, 583, 697 (1937).
(12) Lipkin, M. R., and Kurtz, S. S., Jr., paper presented before Petroleum Division, American Chemical Society, Detroit, 1940.
(13) Lipkin, M. R., and Kurtz, S. S., Jr., Ind. Eng. Chem., Anal. Ed., 13, 291 (1941).
(14) Lipkin, M. R., and Martin, C. C., *Ibid.*, 18, 380 (1946).
(15) Mair, B. J., and Schicktanz, S. T., Ind. Eng. Chem., 28, 1056 (1936).
(16) Mair, B. J., Willingham, C. B., and Streiff, A. J., *J. Research Natl. Bur. Standards*, 21, 565 (1938).
(17) Mills, I. W., Hirschler, A. E., and Kurtz, S. S., Jr., Ind. Eng. Chem., 38, 442 (1946).
(18) Schiessler, R. W., Cosby, J. N., Clarke, D. G., Rowland, C. S., Sloatman, W. S., and Herr, C. H., *Proc. Am. Petroleum Inst., Refining*, 23, III, 15 (1942).
(19) Taylor, W. J., Pignocco, J. M., and Rossini, F. D., *J. Research Natl. Bur. Standards*, 34, 413 (1945).
(20) Vlugter, J. C., Waterman, H. I., and van Westen, H. A., *J. Inst. Petroleum Tech.*, 18, 735 (1932).
(21) *Ibid.*, 21, 661 (1935).
(22) Ward, A. L., and Kurtz, S. S., Jr., Ind. Eng. Chem., Anal. Ed., 10, 559 (1938).
(23) Waterman, H. I., Leendertse, J. J., and Makkink, J. Ph., *J. Inst. Petroleum Tech.*, 22, 333 (1936).
(24) Whitmore, F. C., A.P.I. Project 42, private communication.

Presented before the Division of Petroleum Chemistry at the 102nd Meeting of the American Chemical Society, Atlantic City, N. J.

Equation Relating Density, Refractive Index, and Molecular Weight for Paraffins and Naphthenes

M. R. LIPKIN and C. C. MARTIN, Sun Oil Company Experimental Division, Norwood, Pa.

An equation is presented relating refractive index for the sodium *D* line, density, and temperature coefficient of density, each at 20° C., for paraffins, naphthenes, and mixtures of saturated hydrocarbons in the liquid state. The temperature coefficient of density at 20° C. is obtained from molecular weight using the correlation of Lipkin and Kurtz (*9*). The equation correlates density and refractive index for all saturated hydrocarbons more accurately than previous equations, but is not accurate for the calculation of molecular weight. It may be applied to hydrocarbon mixtures, such as saturated petroleum fractions, because it does not require a knowledge of molecular formula or structure. Refractive index may be calculated from density and the temperature coefficient of density with an accuracy of ±0.002 for pure hydrocarbons and ±0.001 for petroleum fractions. Likewise, density may be calculated from refractive index and the temperature coefficient of density with an accuracy of ±0.004 and ±0.002, respectively. The equation provides the basis for further correlations which will serve as tools in the analysis of hydrocarbon mixtures.

THIS paper is part of a general investigation (*6–11*) of the relationship between density, refractive index, and other physical properties of hydrocarbons and the relationship of these properties to hydrocarbon structure.

Lipkin and Kurtz (*9*) have shown that the variation of density, refractive index, and the temperature coefficient of density with temperature is related to molecular weight. More recently Lipkin, Martin, and Kurtz (*11*) demonstrated in Figure 1 of their paper the relationship of density at 20° C. and the temperature coefficient of density at 20° C. to hydrocarbon structure. Figure 1 of this paper shows the similar relationship for refractive index and the temperature coefficient of density. From these two correlations which differ in only one variable, density in the first and refractive index in the second, it was possible to derive Equation 1 for calculating refractive index from density and the temperature coefficient of density.

$$n = \frac{69.878d - 0.4044Ad - 0.797A + 136.566}{5.543d - 0.746A + 126.683} \quad (1)$$

For the calculation of density this relation may be put in the form of Equation 2.

$$d = \frac{126.683n - 0.746An + 0.797A - 136.566}{-5.543n - 0.4044A + 69.878} \quad (2)$$

In these equations

n = refractive index at 20° C. for the *D* line of sodium
d = density at 20° C.
A = $-10^5 \times$ temperature coefficient of density (α), which is obtained from the approximate molecular weight (Table I, *11*)

The derivation was originally based on data for eight *n*-paraffins and fourteen monocyclic and noncondensed polycyclic naphthenes without side chains. Slight adjustments were then made to obtain better agreement with the average data on almost 600 hydrocarbons.

Since accurate determination of the temperature coefficient of

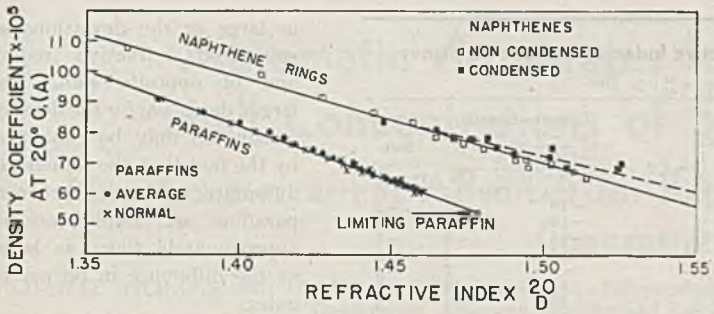

Figure 1

density is difficult, this property is derived from molecular weight (*9*). The average molecular weight for mixtures of hydrocarbons may be obtained experimentally, or from correlations with other physical properties. In this laboratory, molecular weights are obtained either from the boiling point–density correlation of Mills, Hirschler, and Kurtz (*14*) or from the correlation of Hirschler (*4*) using the viscosities at 100° and 210° F.

Approximate molecular weights are adequate for the calculation of refractive index or density especially in the molecular weight range above 100. The effect of a 5% error in the molecular weight on the calculation of refractive index is shown in Table I. The data are calculated for paraffins (*6*). The error in the calculated refractive index decreases from 0.0014 at 70 molecular weight to 0.0002 at 400 because of the asymptotic nature of the relation (*9*) between molecular weight and temperature coefficient of density.

COMPARISON WITH OTHER EQUATIONS

Equation 1 differs from other equations for the calculation of refractive index from density and molecular weight in that it does not contain constants the evaluation of which requires a knowledge of molecular structure.

Table II presents a comparison of the accuracy of density and refractive index values for the C_5–C_9 isoparaffins calculated by Equations 1 and 2 and by the method of Taylor, Pignocco, and Rossini (*15*). The latter method requires a knowledge of the exact structure of the isoparaffins and the calculation of the hydrocarbon's density and refractive index is based on the values of those properties for the normal isomer. The data indicate that this method is slightly more accurate for the C_5–C_8 isoparaffins but that Equations 1 and 2 are slightly better for the C_9 isoparaffins.

Kurtz *et al.* (*7, 8*) have discussed the relative accuracy of the various equations relating refractive index and density. Comparison of the accuracy of Equation 1 with that of the older equations of Newton, Gladstone and Dale, Sellmeier-Drude, and Eykman as applied to the calculation of the refractive index of the isomeric C_7 paraffins is given in Table III. For these older equations the authors have used (1) specific refraction constants calculated from the average properties of the whole group of C_7 paraffin isomers, (2) Lorentz-Lorenz specific refractions calculated from both the average properties of the isomers and from the Eisenlohr atomic refractions, and (*3*) the constants developed by Kurtz and Lipkin (*7*) for the Sellmeier-Drude equation. The data in Table III demonstrate that only the Newton and Sellmeier-Drude equations provide results comparable in accuracy with Equation 1.

The deviations between the best literature values for refractive index and refractive index calculated by a particular equation for a group of isomers can sometimes be correlated with a particular physical property. In several of the older equations this deviation apparently varies with density; the deviations obtained by using Equation 1 seem to vary with the aniline points of the hydrocarbons. The authors have no explanation for these facts at present.

Table I. Difference in Calculated Refractive Index of Paraffins, Assuming 5% Error in Molecular Weight

Molecular Weight True	Molecular Weight Assumed	d_4^{20}	Δn
70	73.5	0.623	0.0014
100	105.0	0.686	0.0008
150	157.5	0.738	0.0005
200	210.0	0.765	0.0004
300	315.0	0.796	0.0003
400	420.0	0.810	0.0002

EXPERIMENTAL DATA

Equations 1 and 2 have been tested with data for a large number of paraffins and naphthenes and saturated fractions from petroleum.

The pure hydrocarbon data are identical with those used previously (*11*). Data on petroleum fractions include the hydrogenated cracked paraffin waxes of Kreulen (*5*), the hydrogenated polymerized pentenes of Waterman (*18*), the acid-treated oils of Bestushew (*2, 17*), the hydrogenated and solvent-extracted oils of Mair (*12, 13*), and the hydrogenated oils of Vlugter *et al.* (*16*). Data were obtained in this laboratory on virgin gasolines, gas oils, and fractions of a catalytically cracked gas oil, all acid-treated to remove aromatics and olefins.

Table II. Comparison of Methods for Calculating Density and Refractive Index for Isoparaffin Data

	Deviation of Calculated Properties			
	$d_4^{20} \times 10^4$		$n_D^{20} \times 10^4$	
	Equation 2	N.B.S. method (*15*)	Equation 1	N.B.S. method (*15*)
	C_5 to C_8 Isomers[a]			
Average deviation	11	7	4	4
Maximum deviation	42	24	17	11
	C_9 Isomers[b]			
Average deviation	13	15	6	
Maximum deviation	40	38	16	22

[a] Six C_5—C_8 isoparaffins not included in tabulation because four normal isomers are used as reference standards in N.B.S. method, neopentane is a gas at 20° C., and 2,2,3,3-tetramethylbutane is a solid at 20° C.
[b] *n*-Nonane, 2,2,3,3-tetramethylpentane, and other nonanes for which (*1*) does not list accurate data excluded from tabulation.

The sources of the molecular weights necessary for the calculation of the temperature coefficient of density were as follows: pure hydrocarbons, theoretical values; oil fractions reported in the literature, experimental values in the reference; gasoline and gas oil fractions from the authors' laboratory, from the density–boiling point relationship of Mills, Hirschler, and Kurtz (*14*).

ACCURACY

The accuracy with which refractive index and density can be calculated by Equations 1 and 2 is demonstrated in Table IV, where the deviations of the calculated from the experimental values for the entire mass of data are tabulated. Calculated refractive indices show an average deviation (without regard to sign) of 0.002 for pure compounds and 0.001 for petroleum fractions. Calculated densities show an average deviation of 0.004 gram per ml. for pure compounds and 0.002 gram per ml. for petroleum fractions. In general, the properties of petroleum fractions may be calculated much more accurately than those of pure compounds because in a mixture of hydrocarbons there is a tendency toward cancellation of the isomer and molecular structure effects found in calculations involving the individual hydrocarbons.

Table III. Comparison of Equations for Calculation of Refractive Index of Isomeric Heptanes

(Calculated − Observed n_D^{20}) × 10^4

	Equation 1	Newton, $\frac{n^2-1}{d} = C^a$	Gladstone and Dale, $\frac{n-1}{d} = C^a$	Eykman, $\frac{n^2-1}{n+0.4} \times \frac{1}{d} = C^a$	Lorentz-Lorenz, $\frac{n^2-1}{n^2+2} \times \frac{1}{d} = C$ C^a	C^b	Sellmeier Drude[c]
2,4-Dimethylpentane	12	0	−10	−12	−19	−11	−2
2,2-Dimethylpentane	10	−2	−11	−15	−19	−11	−4
2-Methylhexane	4	−5	−10	−12	−15	−8	−7
n-Heptane	−4	−9	−10	−13	−11	−4	−11
3-Methylhexane	−1	−3	−2	−1	−1	7	−5
2,2,3-Trimethylbutane	3	4	7	9	11	18	2
3,3-Dimethylpentane	2	5	11	13	16	24	3
2,3-Dimethylpentane	0	4	11	16	18	26	1
3-Ethylpentane	−2	5	15	19	23	32	2
Av. deviation	4	4	10	12	15	16	4
Deviation of av.	3	0	0	0	0	8	−2
Maximum deviation	12	9	15	19	23	32	−11

[a] C calculated from average properties for isomeric heptanes: $d_4^{20} = 0.6859$ and $n_D^{20} = 1.3879$ (*15*).
[b] C calculated from Eisenlohr atomic refraction constants.
[c] Using constants for average paraffins developed by Kurtz and Lipkin (7).

Table IV. Accuracy of Calculated Densities and Refractive Indices

	Number	Refractive Index $n_D^{20} \times 10^4$ Av. dev.	Dev. of av.	Max. dev.	Density $d_4^{20} \times 10^4$ Av. dev.	Dev. of av.	Max. dev.
Pure compounds							
Paraffins	230	10	−4	46	22	6	−108
Monocyclics	217						
C_3 ring	15	28	11	73	68	−28	179
C_4 ring	10	20	10	48	48	−26	−116
C_5 ring	56	18	15	52	43	−37	−114
C_6 ring	111	20	−13	−138	47	30	329
C_7 ring	5	26	−26	141	65	65	141
C_8–C_{10} rings	20	41	−41	−109	98	96	263
Dicyclics	105						
Noncondensed	43	26	−17	−93	64	40	223
Condensed	46	23	+1	−156	56	−2	223
Bridged rings	16	31	+31	+121	70	−70	−291
Tri- and tetracyclics	24	40	22	+126	95	−69	−304
Av.	576	19	−3	−156	44	5	−304
Petroleum fractions							
Lubricating oil	78	11	+3	19	26	−7	−50
Gas oil	24	2	0	−6	5	−1	−15
Gasoline	7	3	+2	+6	9	−8	−15
Av.	109	9	+2	19	20	−6	−50

The accuracy with which molecular weight may be calculated from Equation 1 (by calculating temperature coefficient of density at 20° C. and converting to molecular weight by means of Table I, *11*) has been investigated. The magnitude of deviations increases rapidly with increasing molecular weight, and may be ascribed to the rapidly increasing $\frac{\Delta \text{ molecular weight}}{\Delta \alpha}$. The equation is not satisfactory for the calculation of molecular weight, especially when the molecular weight is greater than 150.

The accuracy of calculations by these equations is nearly independent of the structure of the saturated hydrocarbons, but there are a few noticeable trends. These are difficult to evaluate quantitatively because the experimental inaccuracies of the data are frequently of the same order of magnitude as the deviations in the calculation.

The qualitative discussion of trend is confined to the refractive index calculations as shown in Table IV. The paraffin hydrocarbons have the smallest deviation of all classes. Monocyclic naphthenes show an increasing negative deviation with increasing ring size; the deviation of the average (taking sign into account) of the alkylcyclopentanes is +0.0015 and the alkylcyclohexanes is −0.0013. Since petroleum fractions contain both cyclopentane and cyclohexane derivatives (*3, 10*), the deviations tend to cancel each other. The condensed dicyclic naphthenes show no trend, but the noncondensed dicyclics show a systematic deviation of −0.0017.

The deviations of calculated density are approximately twice as large as the deviations of calculated refractive index, and of opposite sign. The larger deviation for the density calculation may be explained by the fact that the numerical difference in density between paraffins and naphthenes is approximately twice as large as the difference in refractive index.

Many of the deviations in the calculated densities and refractive indices may be attributed to errors in the reported properties of the pure hydrocarbons. These errors are frequently of the order of ±0.001 and may be due to impure products, inaccurate determination of properties, or the determination of properties on two different samples, not necessarily of the same purity. It has been frequently observed that physical properties calculated by Equations 1 and 2 for a set of hydrocarbon fractions from some one laboratory show small systematic deviations from the experimental values. This may be attributed to a predominant molecular structure type in these fractions or to the fact that the experimental precision of the data is better than the accuracy.

By means of the equation shown in this paper and the correlations shown in (*9*) it is possible to correlate at any temperature, where the hydrocarbons are in the liquid state, the density, refractive index, and temperature coefficient of density for saturated hydrocarbons. The significance of the application of this equation to olefins and aromatics will be discussed in a subsequent paper.

ACKNOWLEDGMENT

The authors wish to express their appreciation to Stewart S. Kurtz, Jr., for his guidance in the preparation of this paper.

LITERATURE CITED

(1) Am. Petroleum Inst., Research Project 44 at National Bureau of Standards, Selected Values of Properties of Hydrocarbons as of June 30, 1945.
(2) Bestushew, M., *Erdol und Teer*, 7, 159 (1931).
(3) Forziati, A. F., Willingham, C. B., Mair, B. J., and Rossini, F. D., *J. Research Natl. Bur. Standards*, 32, 11 (1944).
(4) Hirschler, A. E., *J. Inst. Petroleum Tech.*, 32, 133 (1946).
(5) Kreulen, D. W., *Ibid.*, 24, 554 (1938).
(6) Kurtz, S. S., Jr., and Lipkin, M. R., Ind. Eng. Chem., 33, 779 (1941).
(7) Kurtz, S. S., Jr., and Lipkin, M. R., *J. Am. Chem. Soc.*, 63, 2158 (1941).
(8) Kurtz, S. S., Jr., and Ward, A. L., *J. Franklin Inst.*, 224, 583, 697 (1937).
(9) Lipkin, M. R., and Kurtz, S. S., Jr., Ind. Eng. Chem., Anal. Ed., 13, 291 (1941).
(10) Lipkin, M. R., and Kurtz, S. S., Jr., paper presented before Petroleum Division, ACS, Detroit, 1940.
(11) Lipkin, M. R., Martin, C. C., and Kurtz, S. S., Jr., *Ibid.*, 18, 376 (1946).
(12) Mair, B. J., and Schicktanz, S. T., Ind. Eng. Chem., 28, 1450 (1936).
(13) Mair, B. J., Willingham, C. B., and Streiff, A. J., *J. Research Natl. Bur. Standards*, 21, 565 (1938).
(14) Mills, I. W., Hirschler, A. E., and Kurtz, S. S., Jr., Ind. Eng. Chem., 38, 443 (1946).
(15) Taylor, W. J., Pignocco, J. M., and Rossini, F. D., *J. Research Natl. Bur. Standards*, 34, 413 (1945).
(16) Vlugter, J. C., Waterman, H. I., and van Westen, H. A., *J. Inst. Petroleum Tech.*, 21, 661 (1935).
(17) Ward, A. L., Kurtz, S. S., Jr., and Fulweiler, "Science of Petroleum"; ed. by Dunston, Nash, Brooks, and Tizard, Vol. 14, p. 2582, London, Oxford University Press, 1938.
(18) Waterman, H. I., Leendertse, J. J., and Makkink, J. P., *J. Inst. Petroleum Tech.*, 22, 333 (1936).

Automatic Apparatus for Determination of Small Concentrations of Sulfur Dioxide in Air

New Countercurrent Absorber for Rapid Recording of Low and High Concentrations

MOYER D. THOMAS AND JAMES O. IVIE, Department of Agricultural Research, AND T. CLEON FITT, Western Smelter Research Department, American Smelting and Refining Company, Salt Lake City, Utah

A simple countercurrent absorber is described in which practically complete absorption of the water-soluble gases such as sulfur dioxide, ammonia, and hydrogen chloride may be obtained with gas flow rates ranging from less than 10 to more than 5000 times the liquid rates. This absorber, when used in conjunction with a conductivity flow cell of small volume, gives a rapid recording of the concentration from a few parts per billion to several per cent. With the lower gas concentrations, the record is a running average, covering 1 to 2 minutes. An alternative absorber containing conductivity electrodes can reduce this time to 10 to 15 seconds, but absorption is not complete. A simple pump for delivering small volumes of liquid is also described. Equipment embodying this absorber has been applied to the measurement of atmospheric contamination, to the chemical control of a pilot plant making elemental sulfur from sulfur dioxide, and to the rapid measurement of sulfur dioxide in flue gases in the presence of carbon dioxide.

IN THE automatic apparatus for the determination of small concentrations of sulfur dioxide in air previously described (*6–9*), a uniform air stream is aspirated through a measured volume of absorbing solution for a definite time, after which the air stream is changed to a second absorber that has been automatically charged with fresh solution while the first absorber was aspirating. The sulfur dioxide is oxidized to sulfuric acid by hydrogen peroxide, and the course of the absorption is followed by measuring continuously the conductivity of the solution on a recording Wheatstone bridge. The record thus gives primarily the average gas concentration over a given time period, but it also shows a considerable part of the variability of the concentration during that period, represented by differences in the slope of the conductivity curve.

It has been recognized that a more or less "instantaneous" method of recording the gas concentration would be advantageous in many applications, though the average values of short intervals (20 to 30 minutes) are indispensable for any practicable summation of the record over long periods of time. Such instantaneous recordings have heretofore been precluded by lack of a suitable absorber to handle the large ratio of gas volume to liquid volume (about 5000 to 1) required for this analysis.

APPARATUS

Starting with an observation of one of the authors (J.O.I.) that the movement of gas and liquid in opposite directions in a small tube is greatly facilitated by inserting into the tube a pair of twisted-together wires, absorbers have been constructed utilizing the principle of countercurrents, which fulfill the following conditions: (1) The gas and liquid move in opposite directions without bubbling. (2) The walls of the absorber are uniformly wet by liquid which flows in a continuous capillary stream following the wire, from one end of the absorber to the other without forming isolated wet or dry spots. (3) Absorption of sulfur dioxide is practically complete in any range of concentration, from a fraction of a part per million to several per cent, depending on the dimensions of the absorber. (4) The conductivity of effluent liquid can be determined continuously in a small flow cell to give a running, short-time, average measure of the gas concentration.

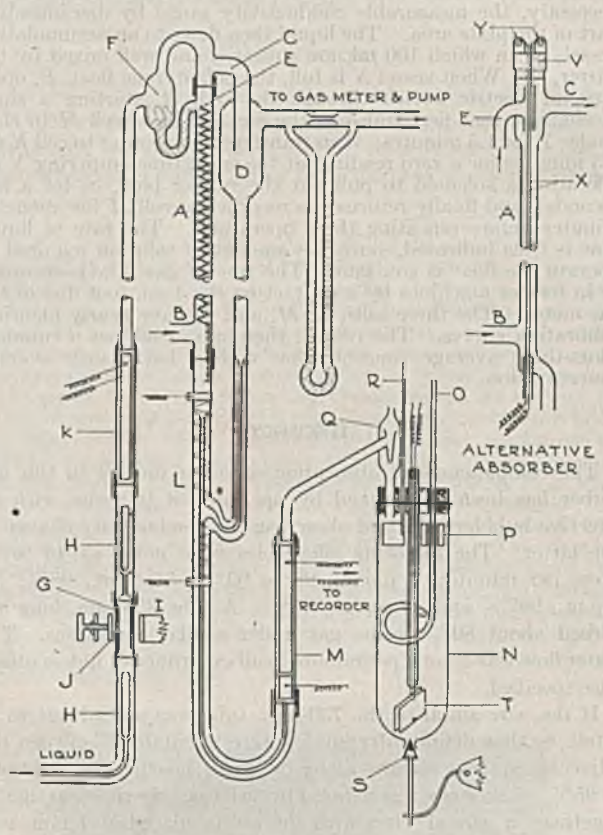

Figure 1. Diagram of Field Sulfur Dioxide Autometer

It is shown below that the indicated concentration at any moment is an average value covering a period which may be as long as 1 or 2 minutes, following the lag representing the time required for the liquid to flow from the absorber to the cell. In an alternative, less efficient absorber, the total time for the analysis may be reduced to 10 to 15 seconds.

Figure 1 is a diagram and Figure 2 is a photograph of an assembly designed to determine sulfur dioxide in the atmosphere in the concentration range up to about 3 to 5 p.p.m., with provision for automatically increasing this range severalfold if necessary. The absorber, *A*, is a 730-mm. length of glass tubing 7.6 to 7.8 mm. in inside diameter, with T-connections near each end. The tube is packed with a helix consisting of two strands of No. 26 B. & S. gage wire, twisted loosely together, then coiled into a 6-pitch spiral which fits snugly against the inside wall. The wire preferably should be of platinum, but Nichrome will withstand a long period of operation before it is seriously corroded, if the hydrogen peroxide concentration is not too high.

The air sample enters the absorber through *B* and leaves at *C*. A convenient rate is 12 to 15 liters per minute. The absorbing solution (2 to 4 $\times 10^{-3}$ *M* hydrogen peroxide in 5 $\times 10^{-5}$ *N* sulfuric acid) is pumped into the tube at *E* at the rate of 3.3 ml. per minute. Trap *D* is provided in case bubbling should occur which would carry part of the liquid over with the gas. A satisfactory liquid pump is obtained by squeezing slightly at 1-second intervals a piece of 6.3-mm. heavy-walled rubber tubing, *G*, mounted

between two glass check valves, *H*. Delivery from the pump is controlled by adjusting stop *J* against the movement of plunger *I*. The reservoir, *F*, eliminates most of the pulsation in the flow. A stainless steel Zenith gear pump, such as is used in the rayon industry, also gives an excellent controlled flow of liquid, but unfortunately the metal is slightly attacked by the solution.

The solution, after emerging from the absorber, is warmed to room temperature by low-voltage current through a resistance wire on the tube at *L*. This also reduces the amount of dissolved gas in the liquid. The solution flows through a 2-mm. capillary U-tube into the conductivity cell, *M*, which has two platinum plates, 5 × 75 mm., mounted parallel in polystyrene with a spacing of 1.8 mm. and a capacity of 0.7 ml. One of the plates may be cut into two pieces, one piece, say, four times the length of the other, and provided with separate leads in order to increase, if necessary, the measurable conductivity range by disconnecting part of the plate area. The liquid then flows to an accumulating vessel, *N*, in which 100 ml. are collected and well mixed by the stirrer, *O*. When vessel *N* is full, the polystyrene float, *P*, operates an electric switch through the rod, *R*, starting a clock mechanism that first transfers the recorder from cell *M* to electrodes *T* for 1.5 minutes; then transfers the recorder to cell *K* for 1.5 minutes for a zero reading, at the same time emptying *N* by operating a solenoid to pull out the rubber plug, *S*, for a few seconds; and finally returns the recorder to cell *M* for about 27 minutes before repeating these operations. The rate of liquid flow is thus indicated, since the amount of solution required to operate the float is constant. The rate of gas flow is recorded as in former machines by a contact on the 1 cu. foot dial of the gas meter. The three cells, *K*, *M*, and *T*, have nearly identical calibration curves. The record, therefore, combines a running, short-time, average concentration with a half-hourly average concentration.

EFFICIENCY

The completeness of absorption of sulfur dioxide in this absorber has been determined by operating it in series with an effective bubbler tube and observing the conductivity change in the latter. The following efficiencies were noted at 15 to 18 liters per minute: 2 p.p.m., 98 to 99%; 5 p.p.m., 98%; 15 p.p.m., 96%; and 24 p.p.m., 95%. A tube 350 mm. long absorbed about 80% of the gas under similar conditions. The water flow was 3.3-ml. per minute in all experiments, unless otherwise specified.

If the wire spiral in the 730-mm. tube was spread out to 4-pitch, so that definite dry spaces were maintained between the adjacent capillary streams along the wire, the efficiency fell to 90 to 95%. Efficiency was reduced by twisting the wires too tightly together; a pair of wires with the twists spaced at 1 mm. was slightly less efficient than a pair with twists 3 mm. or more long. Efficiency was also reduced if the size of the tube was increased. For example, a 730-mm. length of 8.6-mm. inside diameter tubing had an absorption efficiency of 90 to 95% at 15 to 25 liters per minute. Presumably a longer length of this tubing was needed for complete absorption. Efficiency of absorption in the larger tubes was reduced a little by using 30- or 32-gage instead of 26-gage wire, probably because the smaller wire induced less turbulence in the gas stream. A tube of 7-mm. bore exhibited high efficiency but it could not be operated at rates above 10 liters per minute, whereas the 8.6-mm. bore tube would readily carry 25 liters per minute. The 7-mm. bore tube could carry 6 liters per minute when the liquid rate was 15 ml. per minute. Carrying capacity could be increased appreciably by adding 1% butyl alcohol to depress the surface tension of the solution, but the efficiency was not changed.

The absorber has also been used effectively for gas concentrations up to 8% by increasing the water flow and reducing the gas rate in 5 to 7-mm. bore tubes. Evidently almost any condition of absorption can be met by the proper choice of bore and length of tube.

An excess of hydrogen peroxide is essential. The stock solution is stable, but about 10% of the peroxide is catalytically decomposed by the platinum black in each cell, making an over-all decomposition of 30% on passing through the system, in addition to that used up by reaction with sulfur dioxide, although only one cell precedes the absorber. Solutions stronger than 0.004 *M* evolve an appreciable amount of oxygen in the cells, which may interfere somewhat with the conductivity measurements. For this reason, when it is necessary to use more peroxide, a flow cell, with dip electrodes, as shown in Figure 5, may be used.

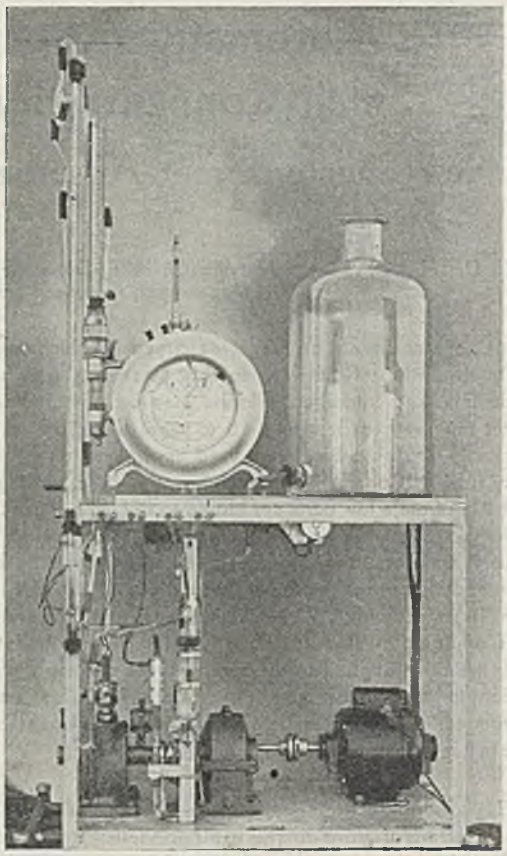

Figure 2. Field Sulfur Dioxide Autometer

A number of tests were made with different amounts of peroxide. When a fivefold excess was present, the efficiency of absorption was not appreciably increased by making the excess 15-fold. Even a slight excess seemed to be very effective. In an experiment with 15 p.p.m. of sulfur dioxide which used up nearly all the peroxide in a 0.002 *M* solution the efficiency of absorption was 93%, as compared with 96% in a 0.006 *M* solution. When the gas concentration was increased to 24 p.p.m., nearly all the excess sulfur dioxide beyond the capacity of the 0.002 *M* peroxide passed through the absorber, whereas the 0.006 *M* solution absorbed 95% of the gas.

RATE OF RESPONSE

Two factors need to be considered in determining the rate of response of the system to changes in the sulfur dioxide content of the air. The first is the lag due to the volume of liquid in the cell and in the U-tube ahead of the cell. This will depend on the length and bore of the tube, and the dimension of the cell. Obviously the recorder will lag behind any absorber by the time required to displace this solution. In addition, if the absorption takes place in some degree over the whole area of the absorber, full response of the recorder will be determined by the time required for complete displacement of the capillary liquid in the absorber.

A large number of empirical tests were made in which a sudden change of concentration was produced in the absorber, by alternately making connection at *B*, Figure 1, to a steady mixture of sulfur dioxide in air, or to a soda-lime tube. It required about 25 to 30 seconds before the recorder gave its initial response. This

represented displacement of the liquid in the U-tube. In addition, about 14 seconds were required to displace the 0.7 ml. in the cell. However, the absorber contained about 4 ml. of capillary water which required more than a minute for displacement. It was noted that about 35 seconds after the recorder showed its initial response to the change of gas concentration, 50% of the change was registered on the recorder. Similarly, 80% of the change was registered in about 60 seconds; 90% in 90 seconds; and 95% in 120 seconds. Complete response usually required 4 to 5 minutes. For practical purposes the record can therefore be considered to be a running average concentration of 1 to 2 minutes' duration—that is, being registered about 2 minutes after the time of sampling. Smaller tubes and higher rates of liquid flow will, of course, increase the rate of response.

"INSTANTANEOUS" ABSORBER

If more rapid and more detailed registration of a variable gas concentration than can be obtained with the regular absorber in Figure 1 is desired, a tube of the type illustrated as an alternative absorber in Figure 1 may be used, in which rapidity of response is obtained at the expense of efficiency of absorption.

It consists of two No. 26 gage platinized platinum wires, *X*, stretched taut by the screws, *Y* in the center of a 10-mm. outside diameter tube, and spaced about 1 to 1.5 mm. The absorbing liquid is led onto the wires at *E* which then serve not only as the capillary path of the liquid but also as conductivity electrodes. Platinum wire has sufficient tensile strength to maintain a nearly permanent calibration, but platinum-clad steel wire strung on a steel frame to avoid undue strain on the glass would be a preferable arrangement. The absorbing liquid forms a continuous capillary film between the two wires if the liquid flow exceeds a minimum value (1.5 ml. per minute for 750-mm. wire length). The response of this absorber to a change of gas concentration is nearly as rapid as a micromax recorder can follow. With a liquid flow of 3.3 ml. per minute, recorder response is nearly complete in 5 to 10 seconds, and 10 to 15 seconds suffice for complete response. Efficiency of absorption is 20 to 40%, depending primarily on the gas rate. This absorber requires empirical calibration with known gas concentrations.

APPLICATIONS

Several units of the equipment have been operated in the field, and it is evident that the new method can generally replace, to advantage, the older "accumulation" method for field sulfur dioxide analyses. Figure 3 illustrates the type of record that may be obtained.

Points *A* give the initial conductivity of the absorbing solution, displaced a little for ease of identification. Points *B* give the conductivity of the accumulated solution at 50-minute intervals. Between points *A* and *B* the flow cell is registering, indicating considerable fluctuation of the concentration. It may be noted that nearly every point *B* falls about where one would expect the average value of the preceding short-time readings to occur.

At point *C*, the concentration threatened to go beyond the range of the recorder. The latter accordingly operated a latching relay switch which disconnected the longer portion of the divided plate in the conductivity cell (Figure 1). The registration fell back to *D* and continued to rise, then fell off to *E*, when the accumulating cell was switched in. If the registration had fallen off a few more divisions beyond *E*, the recorder would have reconnected the plate in the conductivity cell. This actually occurred during the change from *B* to *A*. Definite proof that the recorder operated in the high concentration range is furnished by the track which registered gas volume along the right-hand edge of the chart. At *F*, the volume pen moved from right to left. When the low concentration range was registered, the pen moved from left to right.

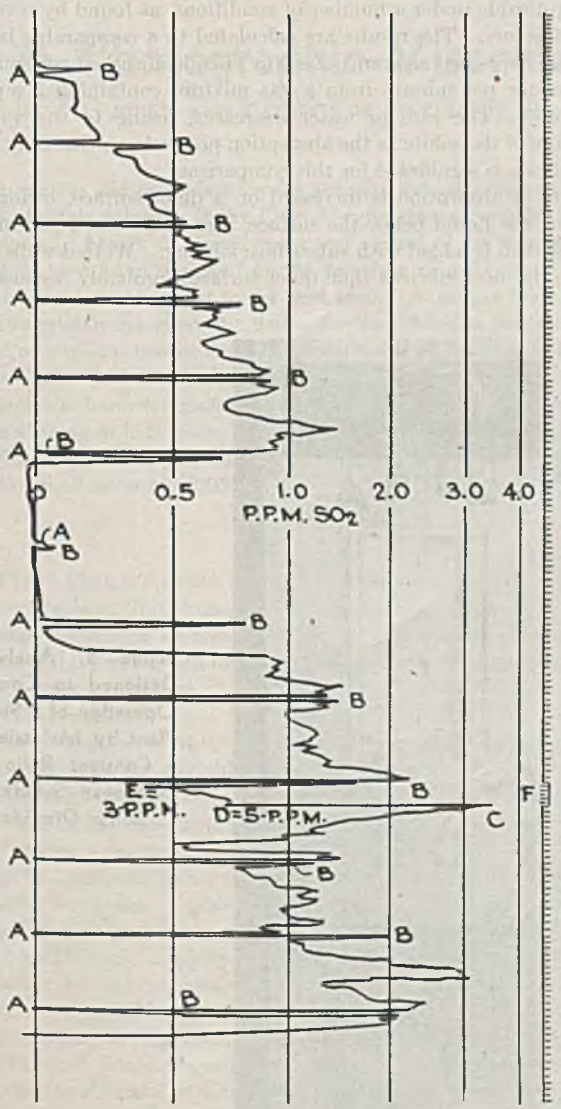

Figure 3. Type of Record Obtained with Field Autometer

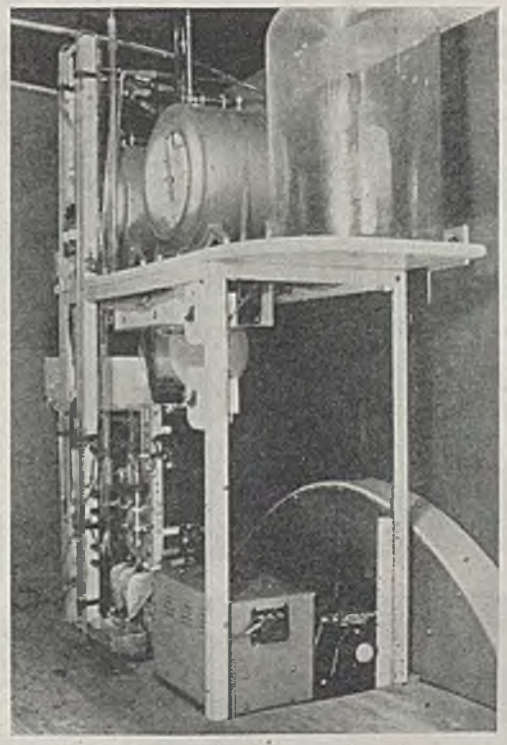

Figure 4. Double Autometer with Facilities for Igniting One Sample. Equipment Mounted in Truck

The new absorber also works satisfactorily with other soluble gases like ammonia (*4*) and hydrogen chloride, but it is ineffective with carbon dioxide. This is to be expected because of the relative solubilities of these gases (*10*). However, the optimum absorber dimensions for ammonia and hydrochloric acid have not been worked out.

Because accurately timed mechanical valves are not used, the new system is easily adapted to the multiple analyses previously described (*9*) for sulfur dioxide, hydrogen sulfide, organic sulfur, hydrogen chloride, and organic chlorine. A double unit has been constructed similar to Figure 2, in which one of the air samples may be ignited. Two clock-switching mechanisms are provided, one of which alternates every minute the connection between the two flow cells and the recorder; the other causes the registration of the two "accumulation" cells and the "feed" cell during 4 minutes of each half hour. Figure 4 is a photograph of this machine mounted in an insulated truck for ready transportability. The instrument can be used only where a source of power is available.

Another machine has been built at the suggestion of E. P. Fleming to control the operation of a pilot plant making elemental sulfur. This plant burns sulfur dioxide from metallurgical processes with sufficient natural gas to combine with all the oxygen, both in the sulfur dioxide and in the free state. The furnace is operated at about 1200° C., and hydrogen sulfide and sulfur dioxide are the principal reaction products. The desired ratio of these gases is two volumes of hydrogen sulfide to one of sulfur dioxide. The latter then react in a catalyst chamber to give sulfur and water vapor.

Figure 5 is a double photograph of the analyzer as seen from two directions.

Measured samples of gas from the plant containing 0.5 to 3.0% total sulfur are drawn through the system by two slow-moving piston pumps provided with mercury check valves, while a third smaller pump adds a definite proportion of oxygen to the samples. The gas is filtered to remove sulfur. The hydrogen sulfide in one of the samples is burned to sulfur dioxide by contact with a faintly glowing platinum coil before absorption. The hydrogen sulfide in the other sample passes through its absorber unchanged. Practically complete absorption of sulfur dioxide is obtained in a 350-mm. length of 5-mm. bore tubing, using a liquid flow of 6 ml. and a gas flow of 100 ml. per minute. Drying bottles and soda-lime tubes are provided following the absorbers to protect the mercury check valves and the pumps. The conductivity flow cells are connected as two arms of a Leeds & Northrup recording Wheatstone bridge. Any departure from a predetermined ratio of the conductivities of the two solutions then causes a valve on the natural gas supply to open or close, thus modifying the reaction in the furnace in the desired direction. With a variable sulfur dioxide supply, this machine and a modification of it, employing larger rates of gas and liquid flow, have played an important role in the successful operation of the plant.

Finally, a simple compact apparatus has been constructed, using Zenith gear pumps, for the analysis of high concentrations (up to 10% or more) of sulfur dioxide, which is comparable in speed, accuracy, and simplicity to the conventional "hot wire" method, but is not affected by admixture of carbon dioxide.

DISCUSSION

It is well established that at the interface between a liquid and a gas there are thin layers of the two substances with physical properties different from those in the body of either liquid or gas. These layers have been referred to as "stationary films" (*5*), and absorption of a solute by a liquid from a gas is largely determined by the manner in which the solute molecules traverse these films.

Table I gives the values for the initial rate of absorption of sulfur dioxide under a number of conditions, as found by several investigators. The results are calculated to a comparable basis and are expressed as grams of sulfur dioxide absorbed per square centimeter per minute from a gas mixture containing 2 p.p.m (volume). The rate in water decreases, owing to the vapor pressure of the solute as the absorption proceeds, so that only the initial rate is significant for this comparison.

Rate of absorption is increased on a quiet surface, owing to stirring the liquid below the surface, and is increased still more when alkali is added with subsurface stirring. Wetted walls are evidently more efficient than quiet surfaces, probably because of

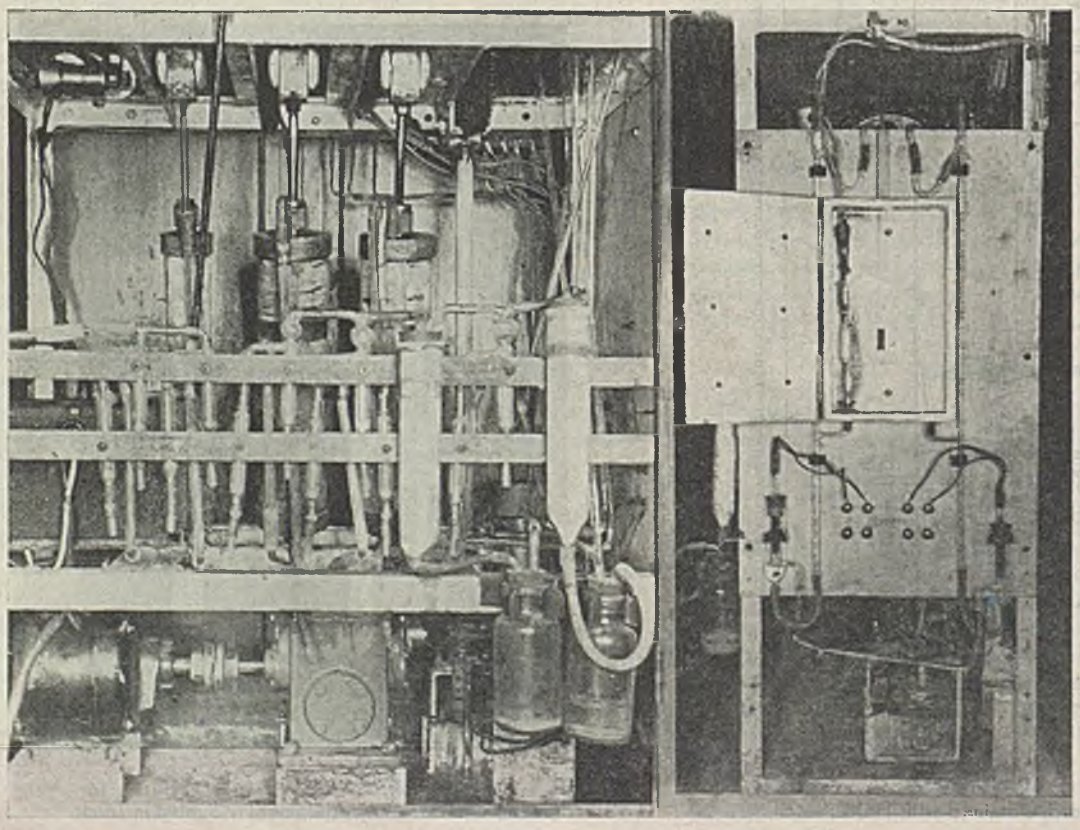

Figure 5. Analyzer Designed to Control Operation of a Sulfur Plant by Maintaining a Constant Ratio of Hydrogen Sulfide to Sulfur Dioxide

Table I. Initial Rates of Absorption of Sulfur Dioxide

Partial Pressure, Atmosphere	Liquid	Surface	Absorption Rate[a]	Observer
1.0	Water, not stirred	Quiet	0.10	Becker (*1*)
0.03	Water, stirred	Quiet	0.15	Whitman and Davis (*10*)
0.5	1.8 *M* KOH, stirred	Quiet	0.63	Davis and Crandall (*2*)
0.1	Water flowing	Wetted wall tower[b]	1.2	Haslam *et al.* (*3*)
2×10^{-6}	0.002 *M* H_2O_2	Wetted wall tube[c]	3.5	This paper

[a] Grams of SO_2 per sq. cm. per min. $\times 10^7$, calculated to a partial pressure of 2×10^{-6} atmosphere in each case.
[b] Flow: gas, 121 liters per min.; liquid, 1800 cc. per min. in 76-mm. tube (10° C.).
[c] Flow: gas, 15 liters per min.; liquid, 3.3 cc. per min. in 7.6-mm. tube (15° C.).

the continuous formation of new films on the former. The absorption rate in the 7.6-mm. tube is three times more rapid and the ratio of gas to liquid flow 65-fold greater than in the 76-mm. tower. This difference in rate is explained by the presence of hydrogen peroxide in the small tube and is in accord with the observation that the latter is a poor absorber after all the peroxide is used up. The behavior of this tube suggests that most of the liquid is present in an absorbing film, since efficiency is affected only slightly by varying the excess of peroxide. The average film thickness is about 0.02 cm.

No data could be found in the literature giving the initial absorption rate of sulfur dioxide from bubbles. Carbon dioxide (*2*) is absorbed 70 times as rapidly from a bubble surface as from a subsurface-stirred quiet surface. If sulfur dioxide behaves similarly, the estimated rate of absorption from bubbles would be about 3 times the value given for the new absorber in Table I. This would explain the high efficiency of the simple bubbler previously described (*8*).

LITERATURE CITED

(1) Becker, H. G., Ind. Eng. Chem., 16, 1220 (1924).
(2) Davis, H. S., and Crandall, G. S., *J. Am. Chem. Soc.*, 52, 3769 (1930).
(3) Haslam, R. T., Hershey, R. L., and Keen, R. H., Ind. Eng. Chem., 16, 1224 (1924).
(4) Hendricks, R. H., Thomas, M. D., Stout, M., and Tolman, B., Ind. Eng. Chem., Anal. Ed., 14, 23 (1942).
(5) Lewis, W. K., and Whitman, W. G., Ind. Eng. Chem., 16, 1215 (1924).
(6) Thomas, M. D., Ind. Eng. Chem., Anal. Ed., 4, 253 (1932).
(7) Thomas, M. D., and Abersold, J. N., *Ibid.*, 1, 14 (1929).
(8) Thomas, M. D., and Cross, R. J., Ind. Eng. Chem., 20, 645 (1928).
(9) Thomas, M. D., Ivie, J. O., Abersold, J. N., and Hendricks, R. H., Ind. Eng. Chem., Anal. Ed., 15, 287 (1943).
(10) Whitman, W. G., and Davis, D. S., Ind. Eng. Chem., 16, 1233 (1924).

A Photographic-Viscometric Apparatus and Technique

JESSE L. RILEY AND GEORGE W. SEYMOUR, Research Department, Celanese Corporation of America, Cumberland, Md.

An apparatus and procedure for the accurate determination of flow times of dilute solutions in the Ostwald-type viscometer have been developed. Means of measurement and control of the viscometric variables have been designed on the principle of making approximately equal contributions to the final error. A unique feature of the apparatus is the automatic timing device. Motion pictures are made of meniscus transits in the viscometer and of the virtual image of an accurate, electronically operated clock. Times of transit are interpolated from the pictures to 0.001 second. Corrected flow times of three or four check runs for each of three cellulose acetate solutions in dioxane ranging from 0.01 to 0.3% concentration fall within a time range of 0.005%.

IMPROVEMENT of the accuracy of the measurement of the flow times of dilute high-polymer solutions in conjunction with suitable calibration or correction of the viscometer will provide viscosity data which will make possible a more critical evaluation of the several methods of extrapolation (*6, 7, 9*) for obtaining intrinsic viscosities.

The realization of this end is, of course, based on a proper appreciation of the variables involved (*1, 4, 5, 10, 13*) and the development of apparatus embodying the inferred degrees of precision in the measurement or control of these variables. An outstanding treatment of this problem has already been provided by Jones and Talley (*8*). Perhaps the most notable feature of their work was a photoelectric timing device which automatically recorded flow times to a precision of 0.01 second. In the present work, a photographic timing device is used, which possesses several advantages not inherent in the photoelectric timing device. The entire timing record of a run, including identification, is contained on about 0.5 meter of 16-mm. film. The times of transit of the initial and final marks on the viscometer may be obtained by interpolation from six to twenty pre- and post-transit readings. The standard deviation of reading the transit time of any run may be made subject to calculation by statistical means.

ANALYSIS OF VISCOMETRIC ERROR

Design of the apparatus was based on an analysis of error with the intent that error contributions from the several variables controlled and measured would be of the same magnitude. To achieve a given coefficient of variation $\frac{s}{\bar{x}}$ for an individual result the permissible error contributions of the variables may be calculated from the equation

$$\frac{s}{\bar{x}} = \sqrt{\left(\frac{s_x}{\bar{x}_x}\right)^2 + \left(\frac{s_y}{\bar{x}_y}\right)^2 + \left(\frac{s_z}{\bar{x}_z}\right)^2 + \cdots\cdots}$$

The primary variables, considering the case of the Ostwald viscometer, are three: time, temperature, and pressure. The volume of flow and the dimensions of the capillary are constant. Pressure may be analyzed into three subordinate variables: sample volume, sample density, and viscometer alignment. To obtain a coefficient of variation for this five-variable condition of 0.01% the contribution of each variable should be 0.004%. An aim of 0.003% was set for the measurement or control of each of the five variables to provide a reasonable margin to cover small oversights or the failure quite to meet the specification on some one variable. The required magnitudes are shown in Table I, calculated for an assumed 100-second flow time in an Ostwald viscometer of conventional proportions.

Table I. Permissible Error Contributions of Variables

Variable	Corresponding to ±0.003%
Time	±0.003 second per 100 seconds
Temperature	±0.002° C. for dioxane at 25° C.
Sample volume	±0.001 ml.
Sample density	±0.3 mg. for 10-gram pycnometer sample
Viscometer alignment	±30 seconds of arc in plane of limbs of viscometer

Drainage and surface tension errors, which affect volume of flow and pressure, are best limited through proper design of the viscometer (*3*). They are not given explicit consideration in this analysis. The effect such errors would have on the relative viscosities of dilute solutions in a single solvent can be assumed to be substantially less than other contributions to error.

The components in the apparatus are described in the same order as the variables to which they relate. A schematic diagram of the assembled components of the apparatus is shown in Figure 1.

PHOTOGRAPHIC TIME RECORDER

An electrical 60-cycle frequency standard, *A*, accurate to ±0.001% provides the basis of time measure. (The frequency standard was specially made by American Time Products, Inc. It has an output at 115 volts of 40 watts.) Current from this frequency standard is used to operate 60-cycle, 115-volt synchronous motors which drive a 25-cm. (10-inch) dial, sweep second clock, and a 5-inch dial conventional electric clock, *B*. (The 10-inch dial sweep second clock consumes 5 watts alternating current. It is made by the Standard Electric Time Company.) This timing combination is calibrated by audio-visual comparison to standard time signals broadcast by WWV, the National Bureau of Standards radio station, and received on radio *W*. Error of 0.001% corresponds to 0.3 second in 8 hours, a readily observable difference.

The 5-inch dial clock is mounted in front of and concentric to the 10-inch dial clock by means of three fine wires (see Figure 2 for detail). The clocks are so placed that a spherical mirror, *C*, establishes a virtual image of the clocks in juxtaposition to the measuring bulb of an Ostwald-type viscometer, *D*, immersed in a thermostatically controlled water bath, *L*. A 16-mm. motion picture camera, *E*, operated at 32 frames per second, is focused to photograph the virtual image of the clocks and the measuring bulb of the viscometer. The clocks operate continuously. The exposure lever of the camera is manually operated during the transits by the meniscus of the two graduations of the viscometer. (Functional relations of camera, clocks, mirror, and viscometers are shown in Figure 3.) To "stop" the second hand of the clock a 0.001-second exposure time is required. It was obtained by using a disk shutter with a 12° opening in place of the shutter with a 167½° opening supplied with the camera. Lighting demands, using 80 Weston (tungsten) film and an *f*1.9 lens, are moderate.

The necessarily rapid passage of the upper graduation of the Ostwald viscometer by the meniscus is secured by reduction of the internal diameter of the upper tube to about 1 mm. Smaller diameters permit spanning and resultant bubble formation in the upper tube.

THERMOSTAT

The thermostatically controlled water bath is simple in construction but can be made to operate with a variation as small as ±0.001° C.

The water bath, *L*, is constructed of copper, lagged with cork, and contains a 0.6-cm. (0.25-inch) plate glass front. The capacity is 120 liters. Circulation is provided by means of an Aminco centrifugal pump-type stirrer. The pattern of flow is stabilized by means of the glass vane, *T*. Flow from the pump is directed on the cooling coil, *O*, and heating coil, *P*, which are grouped together. A highly sensitive Aminco mercury-in-glass thermoregulator is placed directly in the wake of the heating and cooling coils. This reduces to a minimum the lag in the heating-cooling cycle. The rate of heating of the 200-watt heating coil is controlled by the variable transformer, *S*. The average heat consumption is about 50 watts. An adjustable constant rate of cooling is obtained by use of a constant-level device, *Z*, on the cooling water supply. The optimum adjustment requires that the rate of cooling, heater off, be slow, about 0.006° C. per minute, and that the rate of heating, heater on, be approximately equal. Under these conditions thermal lag in the thermoregulator is reduced to a minimum. The critical element is the thermoregulator. It must have a well-defined cycle of on-off operation within 0.001° C. If these conditions are met, the temperature control indicated will result. The true temperature of the bath was determined by reference to a thermometer with corrections certified to 0.01° C. by the National Bureau of Standards.

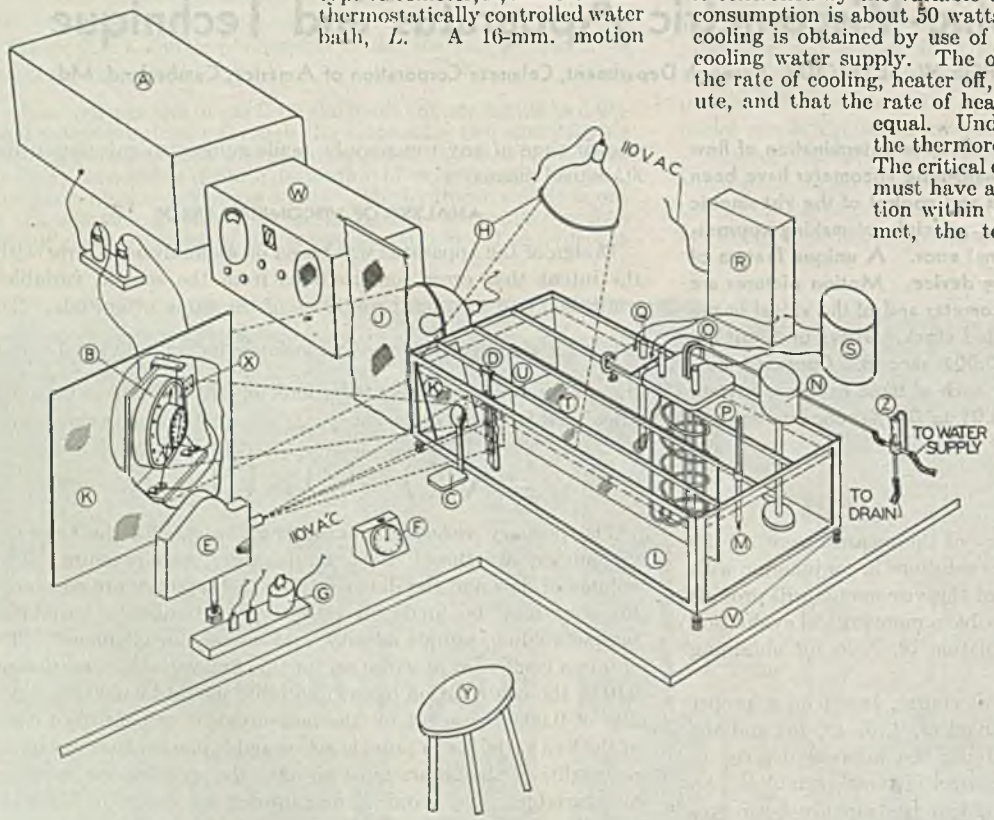

Figure 1. Schematic Diagram of Photographic Viscometer

A. Standard 60-cycle, 115-volt source
B. Clock assembly
C. Spherical, surface-silvered mirror
D. Viscometer and clamp
E. 16-mm. motion picture camera
F. Stop watch for rough checks
G. Switch for photographic illumination
H. Photoflood lamps and reflectors
J. Cheesecloth diffusion screen
K. Opal glass diffusion plates
L. Thermostat bath
M. Beckmann thermometer
N. Circulating pump
O. Cooling coil
P. Heating coil
Q. Sensitive thermoregulator
R. Electronic relay
S. Variable transformer for regulation of heating rate
T. Glass vane for directing circulation
U. Level, lapped brass bar for supporting viscometer clamps
V. Leveling screws
W. Short-wave radio receiver
X. Run identification tag
Y. Operator's position
Z. Constant-level water supply for cooling coil

SAMPLE VOLUME AND DENSITY

Analytical Balance, Pipet, Pycnometer. The sample volume is roughly determined by a pipet, then accurately calculated from the density and the weight increase of the loaded viscometer determined on an analytical balance. The loaded viscometer is also weighed after the viscosity determination. The time rate of change in charge volume due to volatile loss is calculated. From this rate the average solvent loss per run is obtained and a corrected volume calculated for each trial.

The sample density is determined in a 10-ml. Ostwald-type pycnometer, thermostatically controlled to ±0.001° C. and weighed to 0.1 mg.

VISCOMETER CLAMP, LEVEL, AND VISCOMETER

A viscometer holder consisting of a screw clamp, two brass V-blocks, and a spring clamp, all securely attached to a stainless steel column, *D*, is used. The heavy brass bar, *U*, upon which it is mounted is secured to the thermostat frame. The vertical alignment of the clamp is checked by means of a highly sensitive level, 30 seconds of arc per 0.1 inch, mounted perpendicular to a rod, which is held as the viscometer is held. Adjustment in level is made by turning the bolts, *V* (Figure 1) which function as legs for the thermostat. (Figure 4 shows the viscometer clamp in detail and illustrates the use of the level in the alignment test.)

The viscometer in present use is the Ostwald type, capillary length, 12.5 cm., diameter 0.5 mm. Bulb capacity is approximately 3 ml. and the charge volume about 6 ml. Diameter of the upper capillary is about 1 mm.

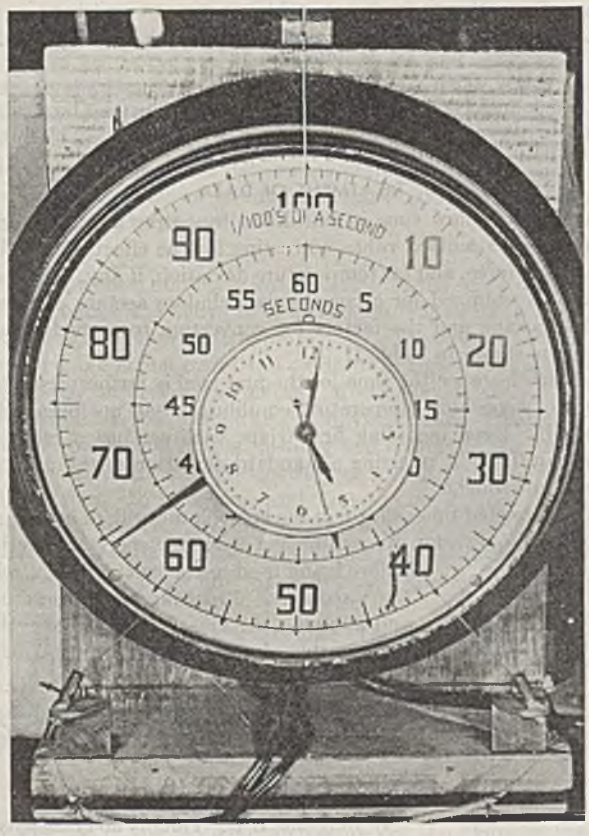

Figure 2. Clock Assembly

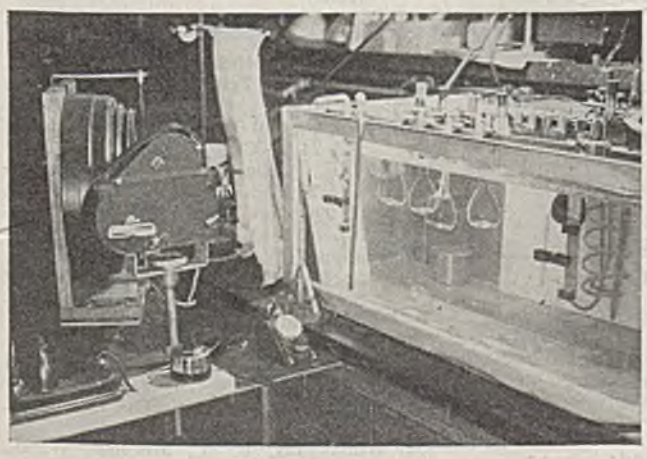

Figure 3. Functional Positions of Clocks, Mirror, Viscometer and Camera

Any viscometer that can be made to photograph satisfactorily can be used. A Ubbelohde viscometer would eliminate the sample volume considerations. Minor modifications would adapt the apparatus for use with the Hoeppler or other falling ball viscometers.

PROCEDURE

The most necessary single element in a flow time determination is the avoidance of dust particles in the viscometer. All cleaning fluids entering the viscometer pass through a fine sintered plate funnel (Figure 5). The viscometer is dried with air drawn through the same sintered plate. Cleaning fluids and air are propelled through the viscometer by attachment of the effluent side to a vessel maintained at reduced pressure, *B'*.

Once cleaned and dried, the viscometer is stoppered with dust-free rubber stoppers and weighed. The sampling pipet is cleaned and dried similarly.

The sample is drawn into the pipet through a fine sintered plate filter stick (Figure 5). A flash evacuation of the pipet, by proper manipulation of stopcock *A'*, suffices to draw in the sample. Concentration changes caused by volatile loss may be shown by calculation to be negligible.

The filtered sample is transferred from the pipet to the weighed viscometer, and is shaken to assure air saturation and to put any dust which may be present in motion so that it may be seen. The presence of visible particles disqualifies a sample. If the liquid appears dust-free, the sample weight is obtained.

The viscometer, equipped with inverted tubes at both openings to keep out dust, is placed in the clamp in the thermostat and let stand for 10 minutes. The sample is then drawn up slowly by an aspirator bulb to above the top graduation. Clocks and viscometer are illuminated by operation of switch *G* (Figure 1). The sample is let flow and the transit of the upper graduation by the meniscus is photographed. Photographic illumination is immediately turned off. It is turned on again to photograph the

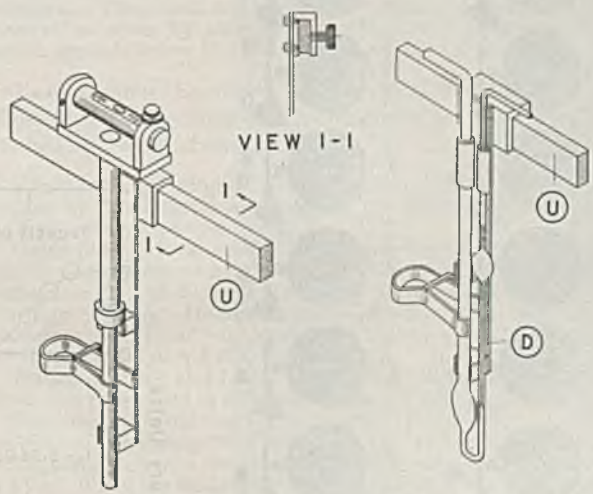

Figure 4. Sensitive Level, Clamp, and Viscometer

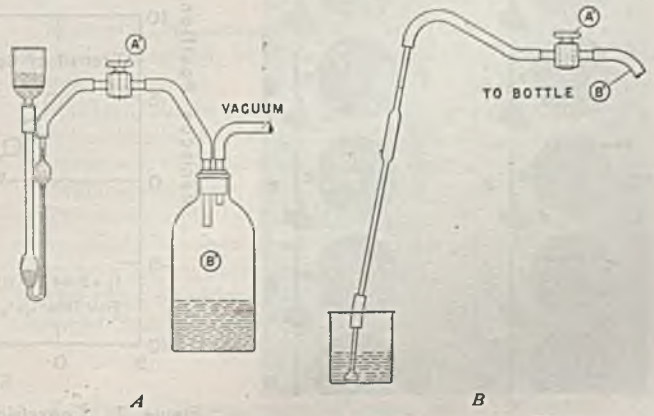

Figure 5. Cleaning Device for Viscometer and Pipet

Table II. Flow Times of Cellulose Acetate Solutions in Dioxane

Mark	Concn.	Observed Time	Observed Temp.	Sample Volume	Correction Factors: Temp.[a]	Correction Factors: Sample volume[b]	Correction Factors: Density[c]	Corrected Time
	% w/w	Sec.	° C.	Ml.				Sec.
64	0.009707	366.299	24.994	5.9846	0.999894	1.000152	1.000040	366.331
		366.308	24.994	5.9840	0.999894	1.000169	1.000040	366.346
		366.315	24.992	5.9834	0.999859	1.000187	1.000040	366.347
		366.308	24.992	5.9828	0.999859	1.000203	1.000040	366.345
55	0.09749	425.832	25.001	5.9987	1.000018	0.999758	1.000292	425.861
		425.806	25.002	5.9981	1.000035	0.999773	1.000292	425.848
		425.809	25.001	5.9975	1.000018	0.999791	1.000292	425.851
62	0.2934	589.728	24.997	5.9869	0.999947	1.000090	1.000808	590.227
		589.711	24.996	5.9863	0.999930	1.000110	1.000808	590.211
		589.690	24.996	5.9857	0.999930	1.000133	1.000808	590.204

[a] Based on temperature coefficient of viscosity for dioxane of $\frac{1.76\%}{°\,C.}$.

[b] Read from calibration curve relating flow time to sample volume for dioxane. Factor is unity for sample volume of 5.9900 ml.

[c] Solution density referred to density of dioxane solvent of 1.02781 grams per ml. at 25.00° C.

transit of the bottom graduation. (If illumination is left on for more than several seconds, the bath temperature is measurably increased.) Temperature during the trial is recorded. At least three checks are made. The viscometer is removed from the thermostat and dried and the final sample weight obtained.

The negative film is developed and projected on a microfilm reader. A plot of the distance of the meniscus from the graduation versus time may be used to give, by interpolation, the time of transit to an apparent ±0.001 second. Time of flow is the difference in upper and lower transit times. A photographic record of a single run and a plot of the data read from it are shown in Figures 6 and 7. As the relation of meniscus position to time is linear, an analytical expression may instead be used to treat the data from which the time of transit and the standard deviation of a reading may be calculated.

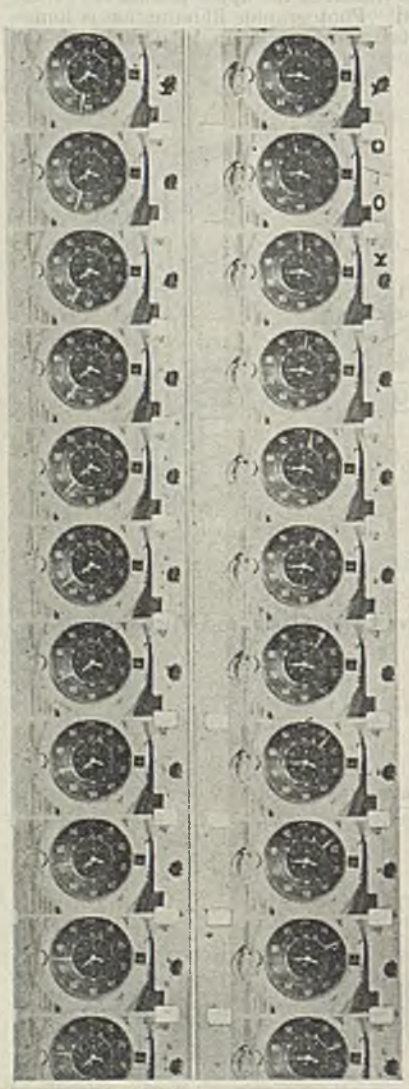

Figure 6. Photographic Timing Record

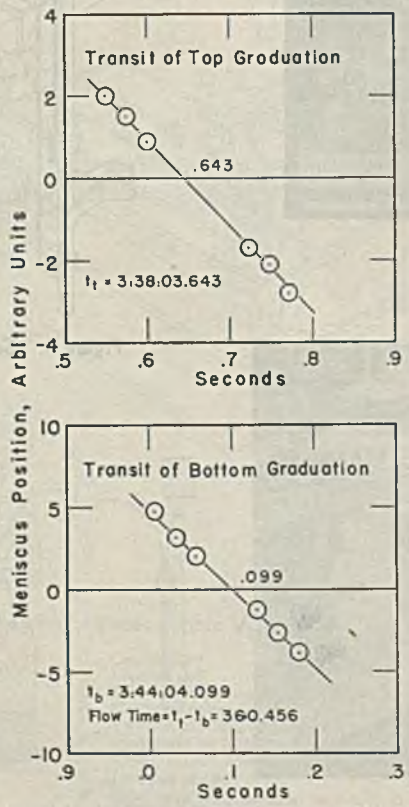

Figure 7. Conversion of Photographic Timing Data to Transit Times

TREATMENT OF DATA

A corrected flow time is calculated by correcting the charge volume to a standard value, correcting for the effects of density on driving force, and for temperature deviation, if any.

Results obtained for a commercial cellulose acetate dissolved in 1,4-dioxane and the factors for converting to corrected flow times are shown in Table II.

In each instance the time for the first trial is farthest from the average, suggesting temperature equilibrium had not been quite attained. Even including first trials, each set has a range of less than 0.005%, inferring a standard deviation of the order of magnitude sought.

The corrected times shown in the last column will, of course, require the application of a calibration or kinetic energy correction before being used in the calculation of relative viscosities. Procedures for determining and applying the kinetic energy correction are reported elsewhere (*2, 5, 11, 12, 14*).

LITERATURE CITED

(1) Barr, G., "A Monograph of Viscometry", Chaps. II, III, and V, London, Oxford University Press, 1931.
(2) *Ibid.*, pp. 125–7.
(3) *Ibid.*, pp. 127–36.
(4) Bingham, E. C., "Fluidity and Plasticity", New York, McGraw-Hill Book Co., 1922.
(5) Cannon, M. R., and Fenske, M. R., Ind. Eng. Chem., Anal. Ed., 10, 297–301 (1938).
(6) Coppick, S., *Paper Trade J.*, 117, No. 7, 25–9 (1943).
(7) Howlett, F., Minshall, E., and Urquhart, A. R., *J. Textile Inst.*, 35, T133–68 (1944).
(8) Jones, G., and Talley, S. K., *Physics*, 4, 215–24 (1933).
(9) Ott, E., "Cellulose and Cellulose Derivatives", High Polymer Series, Vol. V, p. 996, New York, Interscience Publishers, 1943.
(10) Philippoff, W., "Viskosität der Kolloide", pp. 52–8, Dresden and Leipzig, Theodor Steinkopf, 1942 (Ann Arbor, Mich., J. W. Edwards, 1944).
(11) *Ibid.*, pp. 53–5.
(12) Schulz, G. V., *Z. Elektrochem.*, 43, 481–4 (1937).
(13) Smith, C. H. G., *Australian Chem. Inst. J. Proc.*, 10, 47–51 (1943).
(14) Willihnganz, E. A., McCluer, W. B., Fenske, M. R., and McGraw, R. V., Ind. Eng. Chem., Anal. Ed., 6, 231–4 (1934).

Electron Diffraction and Electron Microscope Study of Oxide Films Formed on Metals and Alloys at Moderate Temperatures

Stripped Oxide Films of Metals

R. T. PHELPS[1], EARL A. GULBRANSEN, AND J. W. HICKMAN, Westinghouse Electric Corporation, Pittsburgh, Pa.

The oxidation process occurring on metals has been studied by electron diffraction and electron microscopy, using oxide films stripped by procedures suggested by Evans and co-workers. The apparatus and techniques are briefly described. The metals studied include chromium, cobalt, copper, iron, molybdenum, nickel, aluminum, columbium, and tungsten. The electron micrographs and electron diffraction patterns are presented and discussed. The oxide films are shown to consist of small oxide crystals ranging in size from 100 to 2500Å.

THE physical and chemical structure of the oxide films formed on metals and alloys is of considerable interest in our understanding of their protective properties. The authors (*10, 14*) have studied the structure of the oxide films formed on metals and alloys by the reflection method of electron diffraction. These studies show that chemical and physical transformations occur during the formation and heating and cooling of the oxide film. Inasmuch as the reflection method samples only the outer surface of the film, the information obtained is incomplete. The bulk structure and composition may be considerably different from that on the outer surface. In addition, the nature and size of the crystals in the oxide film can only be approximated by the reflection technique.

This paper presents electron microscope and electron diffraction evidence concerning the structure of electrochemically and chemically stripped films from a series of nine metals which had been oxidized under known conditions: iron, nickel, cobalt, chromium, molybdenum, tungsten, columbium, aluminum, and copper.

ELECTRON MICROSCOPE TECHNIQUE

The use of the electron microscope for the study of the submicroscopic fine structure of matter is well known (*1*). Commercial instruments are available with a resolving power of less than 40 Å. Thus, the shape of particles and the nature of the mosaic structure of a system of crystals may be approximated for particles of 150 Å. or larger. The low penetrating power of 60-kv. electrons in matter limits its direct use to oxide films of the order of 500 Å. in thickness. The preparation of such films requires the use of electrochemical or chemical methods for stripping the oxide film from the metal.

SURVEY OF THE LITERATURE

STRIPPING OF FILM. The presence of a film on passive iron was proved by Evans (*4*) who stripped films too thin to show interference colors from metals.

His first method was based on electrochemical action, using the oxidized metal as the anode in order to dissolve the metal underlying the film. This method was applied to oxidized electrolytic iron, copper, and aluminum to secure films which were examined with the light microscope. The second method was based on direct chemical attack of the underlying metal by a saturated solution of iodine in 10% potassium iodide.

Later Evans and Stockdale (*5*) extended and modified the electrochemical method to remove oxide films from iron, copper, nickel, carbon steel, and stainless steel. For removal of the film from iron, saturated potassium chloride in a hydrogen atmosphere was used as the electrolyte. Hydrogen prevented contamination of the removed film by secondary reaction products caused by oxidation of the dissolved iron.

Vernon, Wormwell, and Nurse (*23*) modified Evans' iodine method by using the reagent developed by Rooney and Stapleton (*19*) to remove oxide films from iron and carbon steel. In this technique both oxygen and water were eliminated as possible contaminating agents by employing a solution of iodine in anhydrous methyl alcohol in a nitrogen atmosphere.

Several chemical methods have been successful in removing films from different metals. Withey and Millar (*26*) developed an analytical method of estimating the oxide in or on aluminum which has been applied by several workers to the removal of the oxide film. Aluminum metal is removed from its oxide film by treatment with hydrogen chloride at 300° to 400° C.; the oxide film is retained intact. Wernick (*24*) and Fischer and Kurtz (*6*) removed oxide film from aluminum by scratching the film and immersing in saturated mercuric chloride solutions. Kutzelnigg (*16*) dissolved tin foil away from its oxide by a 10% ferric chloride solution. Tammann and Arntz (*22*) rendered visible the film present on silver by placing on the surface a drop of mercury, which spreads below the film, raising it from the metal.

TRANSMISSION ELECTRON DIFFRACTION OF OXIDE FILMS. Most of the oxide films on massive pieces of metal have been studied by the reflection method.

Darbyshire (*3*) studied stripped oxide films of nickel and copper by the transmission method; the patterns were identified as NiO and Cu_2O, respectively.

Oxide films of iron, nickel, and copper were stripped from the metals and examined by Smith (*20*). Air-heated, first-order interference colored films of iron gave patterns corresponding to Fe_3O_4 or γ-Fe_2O_3. Heating of one of the films to 600° C. gave a pattern which resembled more nearly that of γ-Fe_2O_3 as prepared by dehydration of γ-FeOOH.

Iitaka, Miyake, and Iimori (*15*) claimed that the film stripped from iron passivated in dichromate was γ-Fe_2O_3, not Fe_3O_4.

Steinheil (*21*) obtained transmission patterns of aluminum oxides after stripping from the metal. At room temperature the oxide formed was a face-centered cubic structure with A_0 = 5.35 Å. When the oxide was formed by heating in a small flame it conformed to the x-ray structure of γ-Al_2O_3.

White and Germer (*25*) measured the rate of oxidation of thin copper films by transmission of both the copper and cuprous oxide.

ELECTRON MICROSCOPY OF OXIDE FILMS. Henneberg (*13*) showed micrographs of the oxide films stripped from iron, aluminum, and nickel.

Mahl (*17*) obtained micrographs of stripped oxide films of electrolytic iron and aluminum. The iron oxide films showed a granular structure, while those of aluminum showed both granular and amorphous structures, depending on the treatment of the metal.

The micrographs by Fischer and Kurtz (*6*) of stripped aluminum oxide films show a definite granular structure. The films were prepared by electrolytic oxidation by either direct or alternating current and by using sulfuric or oxalic acid. The film was stripped from the metal by the mercuric chloride technique.

APPARATUS

ELECTRON DIFFRACTION CAMERA WITH FURNACE. This apparatus is described in previous papers (*8, 10, 14*). The polished metal sample is oxidized under controlled conditions of tem-

[1] Present address, American Cyanamid Company, Stamford, Conn.

perature, time, and oxygen pressure in the electron diffraction furnace. The progress of the oxidation is studied in situ by electron diffraction at the temperature of the reaction.

Electrolytic Apparatus for Removing Oxide Films. Two modified versions of the apparatus described by Evans (*5*) are used to remove the oxide film from the metal by electrolysis.

The apparatus shown in Figure 1 consists essentially of three parts, cell *A* for electrolysis in an hydrogen atmosphere, reservoir *B* with oxygen-free wash water, and hydrogen purifying parts *C* and *G*.

A has three side arms, fitted with stopcocks. T_2 leads directly to the source of purified hydrogen. Electrolytic tank hydrogen is purified by passing the gas over copper turnings at 300° C. and through a solution of sodium bicarbonate in *C*. Hydrogen pres sure is used to force the wash water from *B* through T_3 into cell *A*. The electrolyte and washings are removed by T_2. The cell is divided into two compartments by a fritted-glass filter.

Boiled, saturated potassium chloride solution is placed in *A*. Purified hydrogen from *C* is bubbled alternately through the solutions in both arms by a tube (not shown in Figure 1) leading directly from *C* into the cell at the openings at the top. After this preliminary blow-out of the air, the purified hydrogen enters T_2 to sweep out the air above the solution continuously during the electrolysis. The oxidized metal, *D*, is installed as the anode and is held in place by the rubber stopper, *F*, which has a small vent for escape of hydrogen. The cathode, *E*, is the same metal as *D*, or platinum.

The source of current is 110 volts direct current. The current passed through the cell is controlled by a potentiometer-rheostat and a second rheostat in series with the electrodes. The electrolysis is started at a current of 10 ma. and increased gradually to 60 ma. if the film is not loosened after one hour. The time necessary to remove the film varies from 0.5 to 1.5 hours.

As the electrolysis proceeds the loosened film detaches itself or is freed by lightly tapping the electrode. The film is recovered as squares 1 mm. on an edge because the oxidized surface had been ruled previously in such a manner. Washing of the pieces of film is accomplished by draining through T_1 and forcing wash water through T_3 with T_2 closed. After washing, the cell is disconnected at T_2 and T_3 to invert and to remove the pieces of film to a small dish.

Electron Microscope. A type EMB-4 microscope, equipped with an electron diffraction unit, is used.

CALIBRATION

Electron Diffraction. The use of the electron diffraction adapter of the electron microscope has been described in detail by Picard (*18*). Magnesium oxide is used as a diffraction standard. In the calibration procedure, the diameters, *D*, of the transmission diffraction rings are recorded. The lattice spacings, d_{hkl}, are obtained from x-ray diffraction tables (*11*). The calibration constant, Dxd_{hkl}, is calculated for the several rings, and the value is found to be 27.3. From the measured diameters of the unknown diffraction pattern, the values of the lattice spacings, d_{hkl}, are readily obtained.

Electron Microscope. The magnification is determined by establishing a relationship between the lower magnification range of the electron microscope with optical measurements on the same object. A 10.67-micron tungsten wire is used as the object. Having established this relationship, the higher magnifications can be calibrated by comparison of the distance between two particles at the high magnification with the same distance at a lower magnification where the relationship with the light instrument has been established. Dispersed titanium dioxide particles are used in this study.

PREPARATION OF SPECIMENS

The specimens are machined from bars of the metals to cylinders 0.92 cm. (0.375 inch) in diameter and 0.375 inch long, and

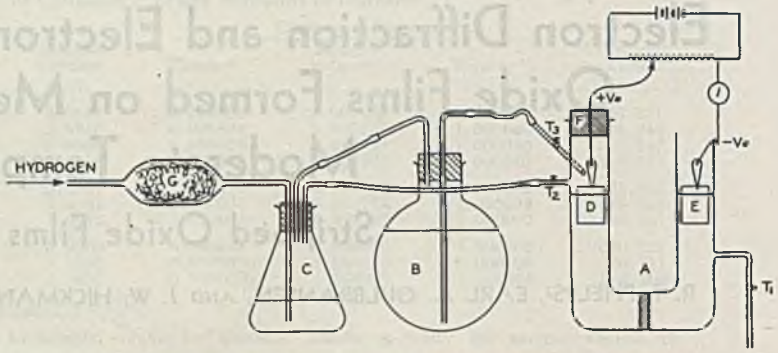

Figure 1. Electrolytic Apparatus for Removing Oxide Films

after cleaning, are heat-treated at elevated temperatures in dissociated ammonia gas or in wet hydrogen. The details of the heat treatment and subsequent metallographic polish are shown in Table I. The specimens are stored in a desiccator over anhydrous calcium chloride.

The metal specimen is placed in the electron diffraction camera furnace (*8, 10, 14*) and heated to the proper temperature. Oxygen to a pressure of 0.1 atmosphere is admitted and the specimen is oxidized for a predetermined time. The time and temperature

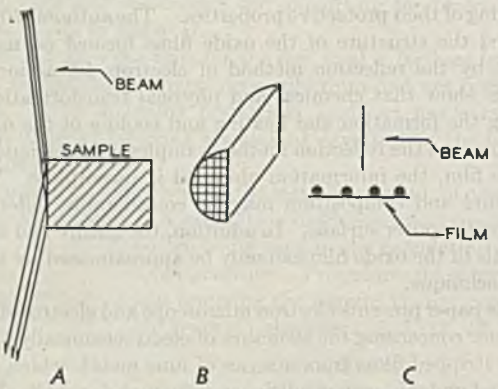

Figure 2. Specimen before and after Electrolysis

A. Reflection diffraction
B. Film on metal
C. Film mounted for electron microscopy

Table I. Analysis and Preparation of Metal Specimens

Metal	Analysis	Heat Treatment	Polishing
Cr	Electroplated on polished oxygen-free high conductivity Cu	None	Emery paper No. 1, 320 wax wheel, chrome rouge, No. 1 alumina
Co	Electrolytic P 0.003, Al 0.033, Al_2O_3 0.004, C 0.0015	1000° C. for 15 hours in dissociated ammonia gas	Emery paper No. 1, 320 wax wheel, chrome rouge, No. 3 alumina
Cu	Oxygen-free, high conductivity	900° C. for 15 hours in dissociated ammonia gas	Emery papers through 000, chrome rouge, No. 3. alumina
Fe	Research Puron, 99.96%	1000° C. for 15 hours in wet H_2	Emery papers through 000, chrome rouge, No. 3 alumina with 95% alcohol
Mo	99.95+%	1200° C. for 1 hour in dissociated ammonia gas	Emery papers through 000 chrome rouge, Nos. 1 and 3 alumina
Ni	Commercial grade, C 0.02, Mn 0.29, Si 0.02, Cu 0.07, Co 0.80, Fe 0.15	1000° C. for 12 hours in dissociated ammonia gas	Emery paper No. 1, 320 wax wheel, chrome rouge, No. 3 alumina
Al	99.986%	None	Emery papers through 000, chrome rouge, Nos. 1 and 3 alumina
Cb	99.9+%	None	Emery papers through 000, chrome rouge, Nos. 1 and 3 alumina
W	99.9+%	10 hours at 1200° C. dry H_2	Emery paper through 000, chrome rouge, Nos. 1 and 3 alumina

Figure 3. Study of Oxidation of Nickel

a. Light micrograph, polished
b. Light micrograph, oxidized
c. Electron micrograph, stripped oxide film
d. Electron micrograph, replica, oxidized surface

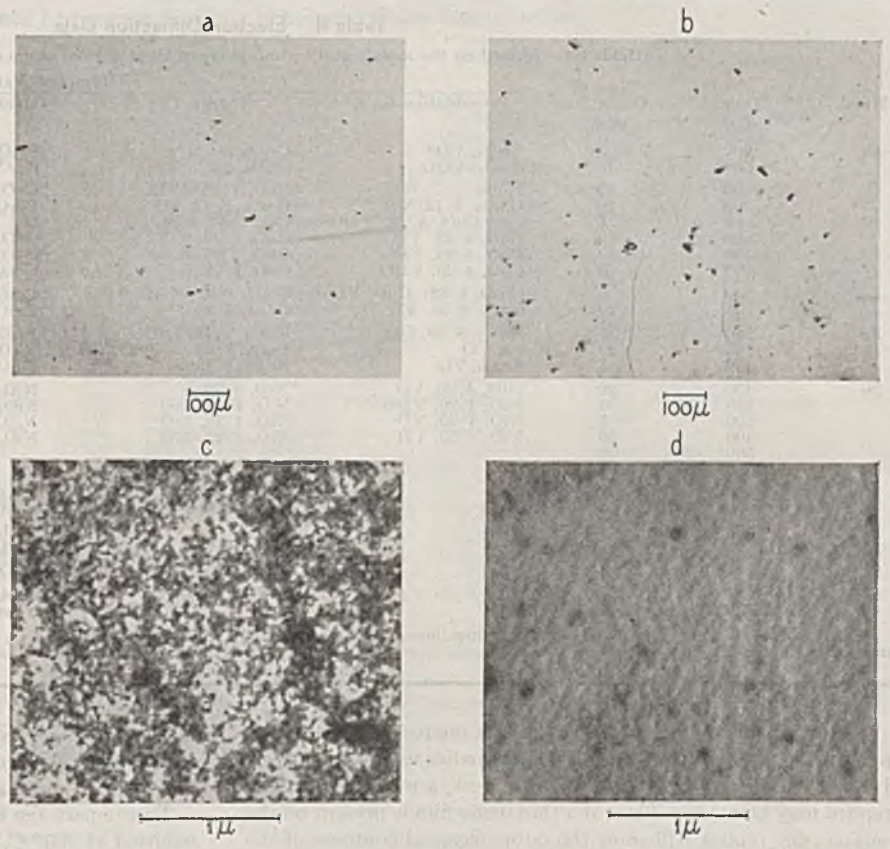

conditions of the oxidation are estimated from rate measurements where available. Oxide film thicknesses of the order of 1.0 to 3.0 micrograms per sq. cm. weight of oxygen can be studied effectively. Where rate measurements are not available, it is necessary to make intelligent guesses as to the oxidation conditions.

Electron diffraction reflection patterns are taken of the sample after oxidation and after cooling in vacuo to room temperature. The specimen is removed and cut carefully in two portions; one portion is used for making photomicrographs at 100 and 1000×.

A thin film of Parlodion is formed on the surface of the other portion by placing a small drop of 0.01% solution of Parlodion in amyl acetate on the surface and draining off the excess solution. After the film is dry, the surface is scratched with a sharp point of a needle into 1-sq. mm. sections. To protect the sides and bottom of the sample from electrochemical or chemical action, these parts are painted with a protective coating. The details of this part of the sample preparation are shown in Figure 2.

The sample is now placed either in the electrolytic cell shown in Figure 1 or in a beaker for chemical attack for removal of the film. Chemical or electrochemical attack occurs at the scratches where the metal is exposed. As the attack develops the film is gradually loosened from the metal. The films are washed by hot oxygen-free distilled water in the electrochemical cell or in the beaker. The small squares are now ready for mounting on the specimen screens and are placed in the microscope for study after drying in a vacuum chamber at room temperature.

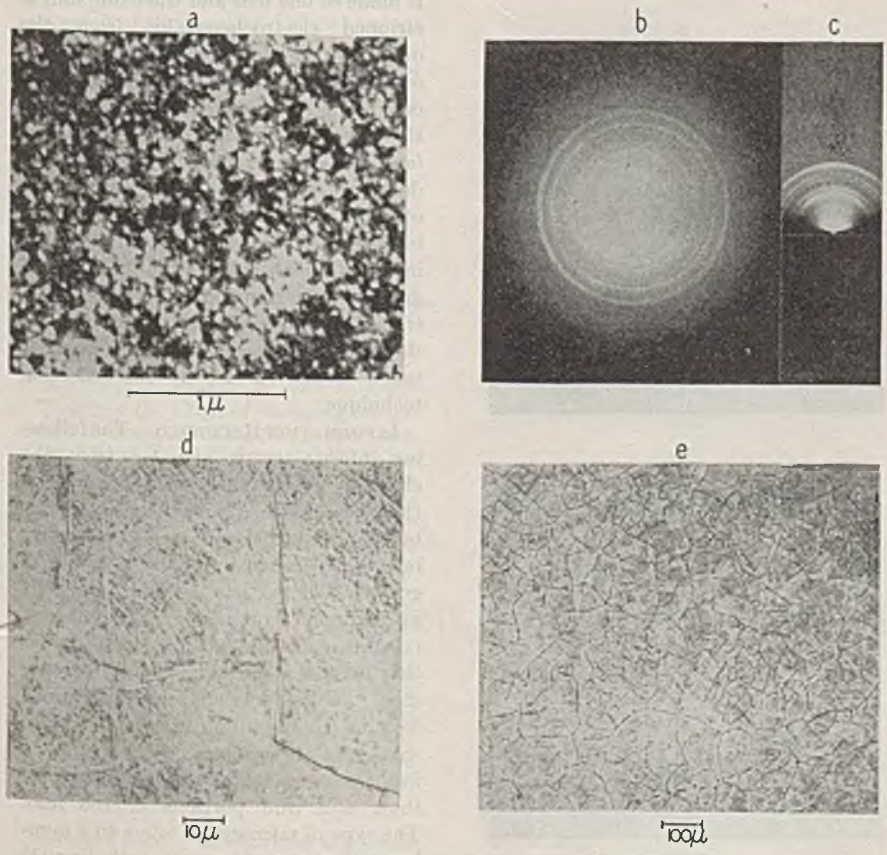

Figure 4. Oxide Film of Chromium, Cr 5–600

a. Electron micrograph stripped film
b. Electron diffraction transmission stripped film
c. Electron diffraction reflection film on metal
d, e. Light micrograph film on metal

METHOD OF INTERPRETING DATA

Electron Diffraction. The electron diffraction reflection method has been discussed in previous papers (*8, 10, 14*). The methods used in the interpretation of data by the transmission technique are similar to those used for the reflection method. In the transmission technique the specimen is the sample of stripped film. The diffraction patterns obtained are a series of concentric rings instead of half circles as in the reflection method.

The transmission method possesses several advantages over the reflection method. The diffraction rings are sharper and the background of incoherent scattering is less. The transmission method also yields information on the structure of the whole film, while the reflection method indicates only the structure of the outer surface. This is important, since the surface structure is probably different from the structure of the body on the film.

Table II. Electron Diffraction Data

(Oxide films formed on the metals at 0.1 atmosphere of O_2 at various times at various temperatures)

Metal	Temp. ° C.	Time of Oxidation Min.	Diffraction Patterns: Preoxidation by R[a]	Oxidized by R	Oxidized at 25° C. by R	Stripped by T
Cr	600	5	Cr_2O_3, VD[a]	Cr_2O_3, S	Cr_2O_3, S	Cr_2O_3, M
	600	30	Cr_2O_3, VDO	Cr_2O_3, SO	Cr_2O_3, SO	Cr_2O_3, D
Co	200	50	None	CoO, 4.28[a], VD	CoO, 4.28, VD	CoO, 4.24; Co_3O_4, 8.07, D
	300	10	Co_3O_4, 8.12, VD	Co_3O_4, 8.12, SO	Co_3O_4, 8.12, DO	CoO, 4.25; Co_3O_4, 8.06, S
	400	5	Co; CoO, 4.28, VDO	Co; CoO, 4.28, SO	Co; CoO, 4.28, SO	CoO, 4.24, MO
	400	10	CoO, 4.22, VD	CoO, 4.22, S	CoO, 4.22, S	CoO, 4.23, M
	400	30	CoO, 4.28, VDO	CoO, 4.28, S	CoO, 4.28, S	CoO, 4.24, MO
	500	5	CoO, 4.29, VDO	CoO, 4.29, S	CoO, 4.29, S	CoO, 4.24, MO
Cu	200	5	Cu_2O, 4.32; CuO, VD	Cu_2O, 4.32; CuO, S	Cu_2O, 4.32; CuO, S	Cu_2O, 4.23, MO
	200	30	Cu_2O, 4.33, VD	Cu_2O, 4.33, S	Cu_2O, 4.33, S	Cu_2O, 4.24, DO
Fe	250	5	Fe_3O_4, 8.49, DO	Fe_3O_4, 8.49, DO	Fe_3O_4, 8.49, DO	Fe_3O_4, 8.35, M
	250	30	Fe, VD	Fe_3O_4, 8.44; α-Fe_2O_3, SO	Fe_3O_4, 8.44; α-Fe_2O_3, SO	Fe_3O_4, 8.35; α-Fe_2O_3, SO
	300	5	Fe_3O_4, VD	Fe_3O_4, 8.43, S	Fe_3O_4, 8.43, S	Fe_3O_4, 8.37, DO
Ni	400	20	NiO, 4.20, VD	NiO, 4.20, S	NiO, 4.20, S	NiO, 4.17, SO
	450	5	NiO, 4.20, VDO	NiO, 4.20, MO	NiO, 4.20, MO	NiO, 4.15, DO
	500	5	NiO, 4.20, VD	NiO, 4.20, MO	NiO, 4.20, MO	NiO, 4.15, SO
	500	20	NiO, 4.22, VD	NiO, 4.22, MO	NiO, 4.22, MO	NiO, 4.15, MO
	500	60	....	....	....	NiO, 4.17, DO
	550	5	....	....	....	NiO, 4.19, SO
Mo	450	5	None	Mo_2O_3, S	Mo_2O_3, S	Mo_2O_3, M
	500	5	None	Mo_2O_3, MoO_3, S	Mo_2O_3, MoO_3, S	Mo_2O_3, M
Al	500	5	None	α-Al_2O_3 γ-Al_2O_3, VD	α-Al_2O_3 γ-Al_2O_3, VD	γ-Al_2O_3; α-Al_2O_3 VD
Cb	400	5	None	CbO, M	CbO, M	Cb_2O_5; CbO, SO
W	400	5	None	None	None	WO_3, D
	450	5	None	None	None	WO_3, D

[a] Key: R, reflection; T, transmission; S, sharp lines; M, medium lines; VD, very diffuse lines; D, diffuse lines; O, oriented pattern. Numbers refer to unit cell size.

Electron Microscope. The electron microscope can be applied to the study of surfaces of opaque bodies in two ways: (1) If the structure of the surface is of interest, a polystyrene-silica replica may be made. Thus, if a thin oxide film is present on the surface, the replica will show the outer physical contours of the oxide film. A comparison of a micrograph of this replica with one made before oxidation would be interesting. (2) By use of the stripped film technique the details of crystals making up the body of the oxide can be studied.

To compare the two methods a specimen of polished nickel is oxidized at 400° C. for 20 minutes in 0.1 atmosphere of oxygen. The sample is divided into two parts. A polystyrene-silica replica is made of one half and the oxide film is stripped electrochemically from the other half. Figure 3 shows a comparison of the results achieved by the two methods. The replica shows more detail of the physical structure of the outer surface, while the stripped film shows more detail of the crystal structure of the oxide film. The stripped film technique is used in this study. Not only is more information obtained from the micrographs of the stripped film but the electron diffraction pictures of the body of the film may be compared with that taken of the surface by the reflection technique.

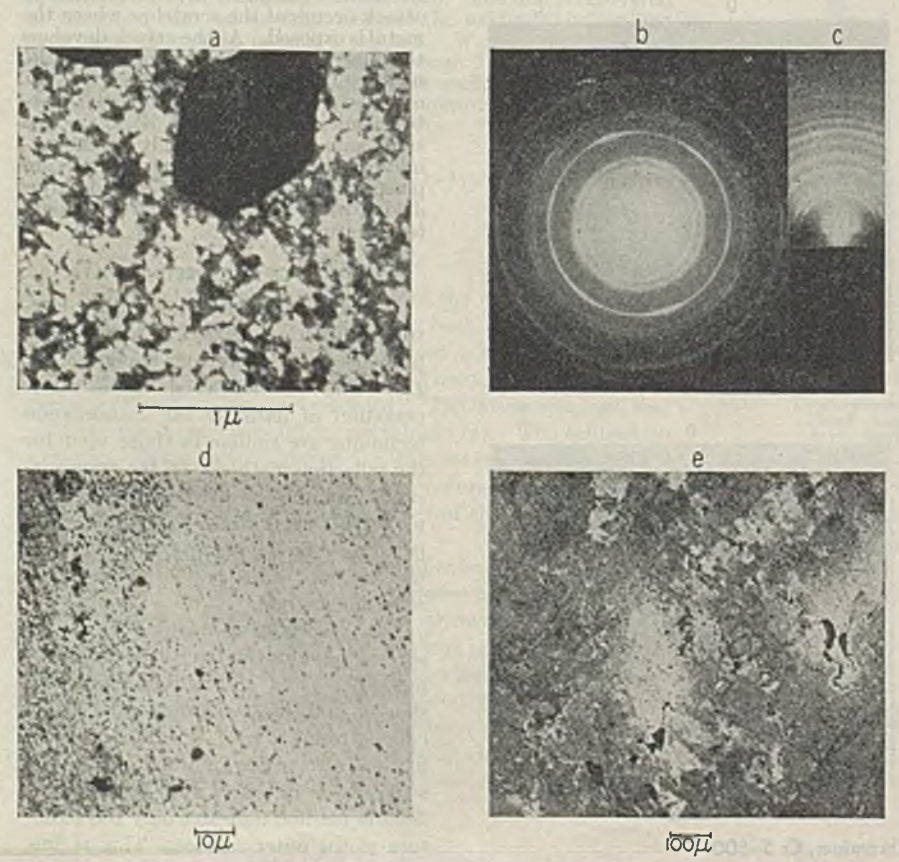

Figure 5. Oxide Film of Cobalt, Co 5–400

a. Electron micrograph stripped film
b. Electron diffraction transmission stripped film
c. Electron diffraction reflection film on metal
d, e. Light micrograph film on metal

Information Recorded. The following information is recorded from the electron micrographs of the stripped film: (1) particle size, (2) particle size distribution, (3) particle shape, (4) uniformity in film thickness, and (5) type of micrograph. The particle size is obtained by averaging measurements on a number of crystals, while the particle size distribution indicates the variation in particle size. The particle shape is determined from an examination of the more typical shapes in the pattern. Uniformity in film thickness refers to the presence of thick and thin portions of the film. The type of micrograph refers to a number of features of interest, including (1) the sharpness of the crystal edges, (2) the presence of overlapping crystals, and (3) the presence of extraneous material.

Table III. Electron Microscope Analyses of Stripped Oxide Films of Metals

Metal	Temp. °C.	Time of Oxidation Min.	Color of Film on Metal	Micrograph	Particle Size Å.	Size Distribution Å.	Shape	Uniformity	Type of Micrograph
Cr	600	5	Greenish yellow	4	400	250 to 750	Irregular	Fairly uniform	Medium sharp, overlapping crystals
	600	30	Mauve	[a]	400	250 to 750	Irregular	Nonuniform	Diffuse, overlapping crystals
Co	200	50	Light yellow	[a]	450	300 to 700	Irregular	Fairly uniform	Diffuse, overlapping crystals
	300	10	Mauve-blue	[a]	300	200 to 400	Irregular	Uniform	Medium sharp
	400	5	Blue and yellow	5	450	250 to 1000	Irregular	Fairly uniform	Sharp, overlapping crystals
	400	10	Pink and green	6	600	300 to 1500	Irregular and square, angular	Nonuniform	Sharp, overlapping crystals
	400	30	Greenish blue	[a]	600	300 to 1500	Irregular, angular	Nonuniform	Sharp, overlapping crystals
	500	5	Silver-pink II	[a]	1000	600 to 2000	Irregular, angular	Nonuniform	Sharp, overlapping crystals
Cu	200	5	Yellow	7	500	300 to 900	Irregular	Nonuniform	Medium sharp, overlapping crystals
	200	30	Brown	[a]	750	450 to 1500	Irregular	Nonuniform	Medium sharp, overlapping crystals
Fe	250	5	Light blue I	[a]	350	250 to 500	Irregular	Nonuniform	Diffuse
	250	30	Pink blue II	8	1200	500 to 1800	Irregular, angular	Fairly uniform	Sharp, overlapping crystals
	300	5	Silver-blue II	[a]	400	300 to 600	Irregular, angular, some large slender crystals	Nonuniform	Diffuse, overlapping crystals
Mo	450	5	Yellow-mauve I	9	500	250 to 1000	Irregular, angular	Nonuniform	Medium sharp
Ni	400	20	Yellow-mauve I	10	400	300 to 600	Irregular squares	Nonuniform	Sharp, overlapping crystals
	450	5	Silver-yellow	[a]	500	300 to 800	Irregular	Fairly uniform	Diffuse
	500	5	Yellow II	[a]	600	400 to 1000	Irregular	Uniform	Diffuse
	500	20	Yellow-red II	11	600	300 to 1500	Irregular	Nonuniform	Medium sharp
	500	60	Yellow-red II	[a]	600	300 to 1500	Irregular, angular	Nonuniform	Medium sharp
	550	5	Silver-yellow II	[a]	600	300 to 2000	Irregular	Nonuniform	Sharp, overlapping crystals
Al	500	5	Light yellow and metallic	12	500	100 to 2500	Large regular, small irregular	Nonuniform film discontinuous	Sharp, particles overlap
Cb	400	5	Dark blue and light purple	13	250	100 to 600	Very irregular	Nonuniform cracks	Medium, patchwork of thick and thin sections
W	400	5	Light reddish yellow	14	150	100 to 400	Round, irregular	Fairly uniform	Sharp, replica of metal grains

[a] Micrographs not shown.

These features are important in classifying a micrograph but are less definite in their interpretation.

RESULTS

Preliminary Experiments. The methods used for the stripping of oxide films from metals are well known, but several points concerning the general technique appear to need clarification. Are extraneous reaction products formed as a result of chemical or electrochemical action? Is it necessary to use a hydrogen atmosphere in the electrochemical cell? Does the stripping technique affect the chemical and physical structure of the oxide film?

Several stripping experiments have been made using both an air and a hydrogen atmosphere. Electron micrographs made from these films show more extraneous matter from the films stripped in an air atmosphere. A hydrogen atmosphere is adopted in the standard technique.

To study the effect of stripping on the chemical structure of the film, a specimen of Nichrome V is polished and then oxidized in the electron diffraction camera furnace. After cooling to room temperature, a reflection pattern is taken. The sample is now subjected to the stripping procedure. Before the film is completely loosened, the sample is removed, washed, and dried. It is placed in the electron diffraction camera and a reflection picture of the surface layer is again taken. No change in the chemical structure is noticed. This evidence, together with the fact that hydrated oxides of the metals have not been observed, indicates that the electrochemical stripping procedure does not affect the surface appreciably.

Oxide Films. In studying the oxide films formed on the metals at 0.1 atmosphere of oxygen for various times at various temperatures, the samples are heat-treated and polished as described in Table I before being placed in the electron diffraction camera furnace for oxidation. For most of the metals several oxidations are made under different time and temperature conditions. Results of electron diffraction study are shown in Table II.

Three reflection patterns and one transmission pattern are taken of the oxide film. The first reflection pattern is taken of the

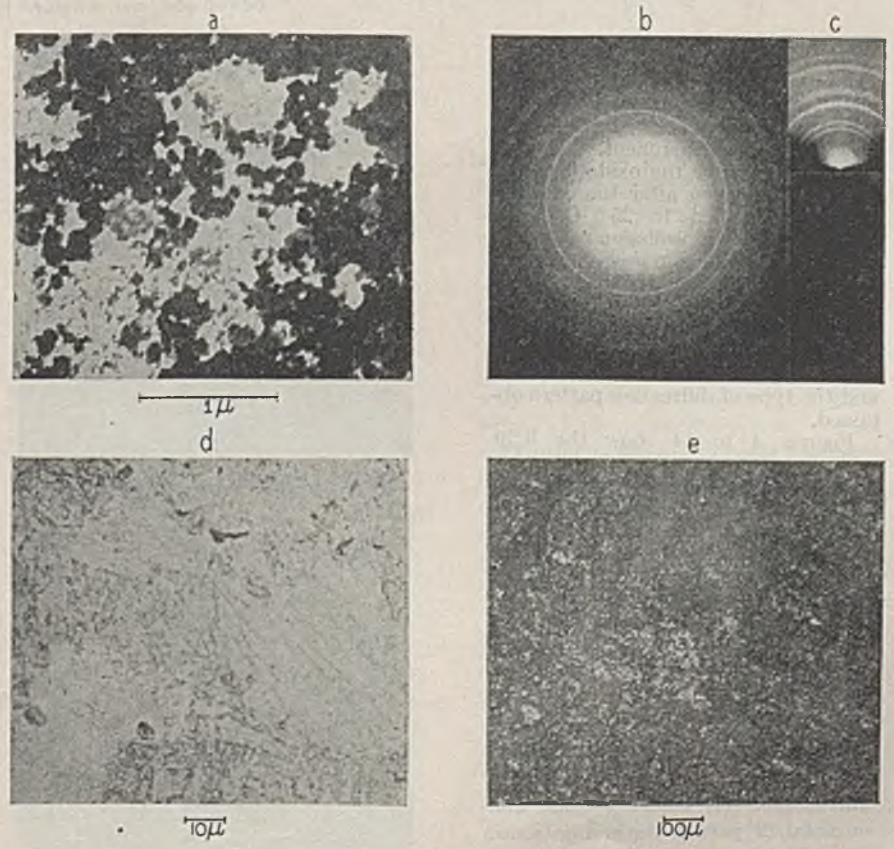

Figure 6. Oxide Film of Cobalt, Co 10–400

a. Electron micrograph stripped film
b. Electron diffraction transmission stripped film
c. Electron diffraction reflection film on metal
d, e. Light micrograph film on metal

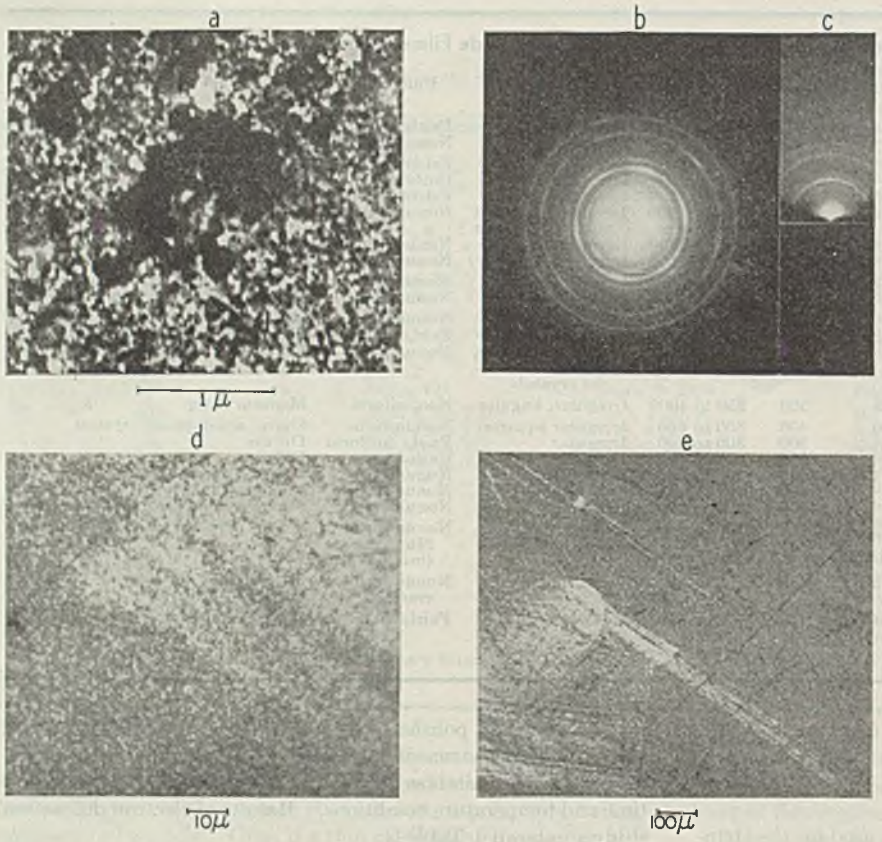

Figure 7. Oxide Film of Copper, Cu 5–200

a. Electron micrograph stripped film
b. Electron diffraction transmission stripped film
c. Electron diffraction reflection film on metal
d, e. Light micrograph film on metal

metal in the vacuum of the camera before oxidation and at the temperature of the experiment. The second is taken after the oxidation, and the third is taken after the oxidized sample is cooled to 25° C. in a vacuum. The transmission pattern of the stripped oxide film is also included, in order to compare the body structure of the film with its surface structure. Table II shows the chemical structure of the surface oxide, the unit cell size where readily calculable, and the type of diffraction pattern obtained.

Figures 4 to 14 show the light micrographs, electron micrographs, electron diffraction transmission patterns, and electron diffraction reflection patterns for the metal specimens. The lengths of 1, 10, or 100 microns are shown on the photographs. The light micrographs were taken of the unstripped oxide film at 100 and 1000×, while the electron micrographs were taken at 6800× and enlarged optically to 34,000×.

Table III summarizes the information recorded from the electron microscope: (1) color of oxide film on metal, (2) particle size in Ångströms, (3) particle size distribution, (4) particle shape, (5) film uniformity, and (6) type of micrograph.

DISCUSSION

Electron Diffraction. The experimental d_{hkl} values are compared to the values obtained from x-ray data and the patterns identified. The d_{hkl} values also are used to calculate the lattice parameters, *a*, for oxides of the cubic types. The x-ray data, used for identification purposes, are shown in Table IV. The lattice parameters for Mo_2O_3, CbO, and Cb_2O_5 have not been determined from the x-ray data.

Table V shows a comparison of the electron diffraction results obtained in this study with the x-ray parameters. The composition of the oxide films, with several exceptions in the cobalt and copper oxidation experiments, is shown to be similar by the transmission and the reflection methods. The oxides found can be correlated with known oxide structures. With the exception of several oxidation experiments on cobalt and copper, the oxides fit fairly well with the predictions of the time-temperature existence regions previously studied (*10, 14*). Differences may be expected due to the polishing procedures employed and to the pressure influence on the existence chart.

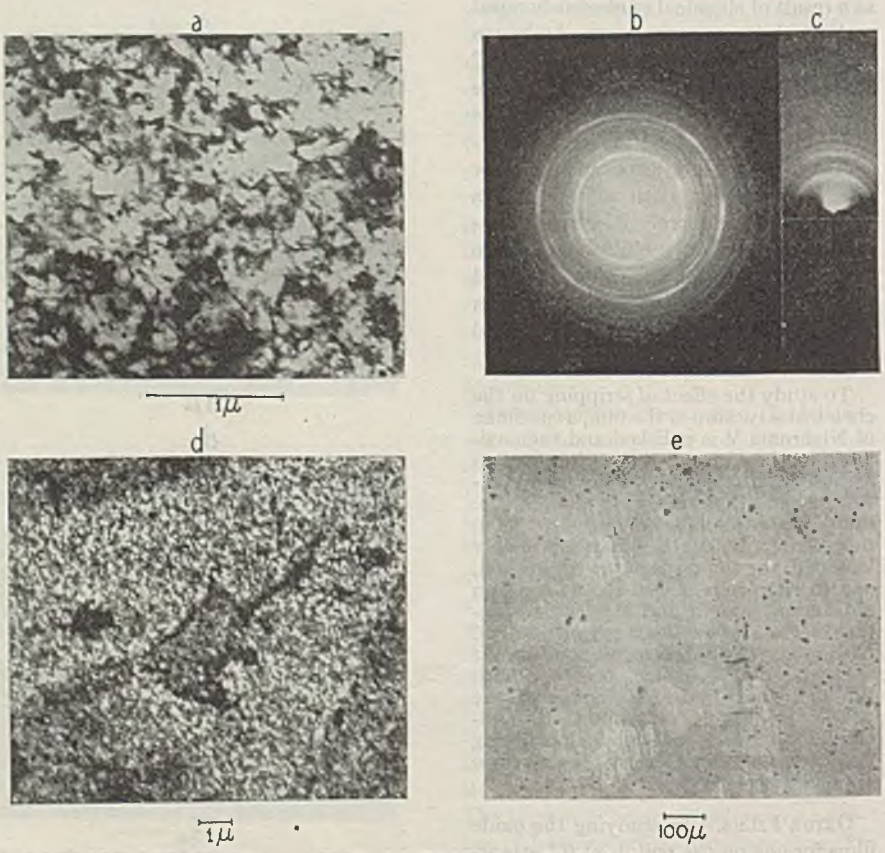

Figure 8. Oxide Film of Iron, Fe 30–250

a, d. Electron micrograph stripped film
b. Electron diffraction transmission stripped film
c. Electron diffraction reflection film on metal
e. Light micrograph film on metal

The lattice parameters of the oxide structures shown in Table V indicate deviations from the accepted x-ray data. A previous work (*10*) indicated that the electron diffraction reflection method yielded lattice parameters slightly larger than the x-ray values. This positive deviation was attributed to either the presence of metal in solid solution in the oxide lattice or strains set up as a result of the formation of the oxide film.

Positive deviations are also noticed in the reflection measurements of this study. The transmission data show small negative deviations. A breakdown of the average deviations on a percentage basis of the oxide lattice parameters from the x-ray values is shown in Table VI. The precision involved in the measurement of the lattice parameters is about 0.25% for the transmission patterns and about 0.4% for the reflection patterns.

The reflection method yields lattice parameters which average 0.7% high, while the transmission method gives values which average 0.2% low. A cross calibration of the instruments was made by taking patterns of the same specimen of stripped oxide film. The transmission electron diffraction pattern taken with the electron microscope gave an average deviation of d_{hkl} values from the x-ray values of less than 0.1%, while the electron diffraction high-temperature camera gave an average deviation of 0.2%. This cross calibration indicated either that the positive deviations noticed on the reflection patterns are real or that some unknown factor is affecting the reflection experiments. The improbability of relating this unknown factor to a variable specimen to plate distance in the reflection technique has been discussed (*10*).

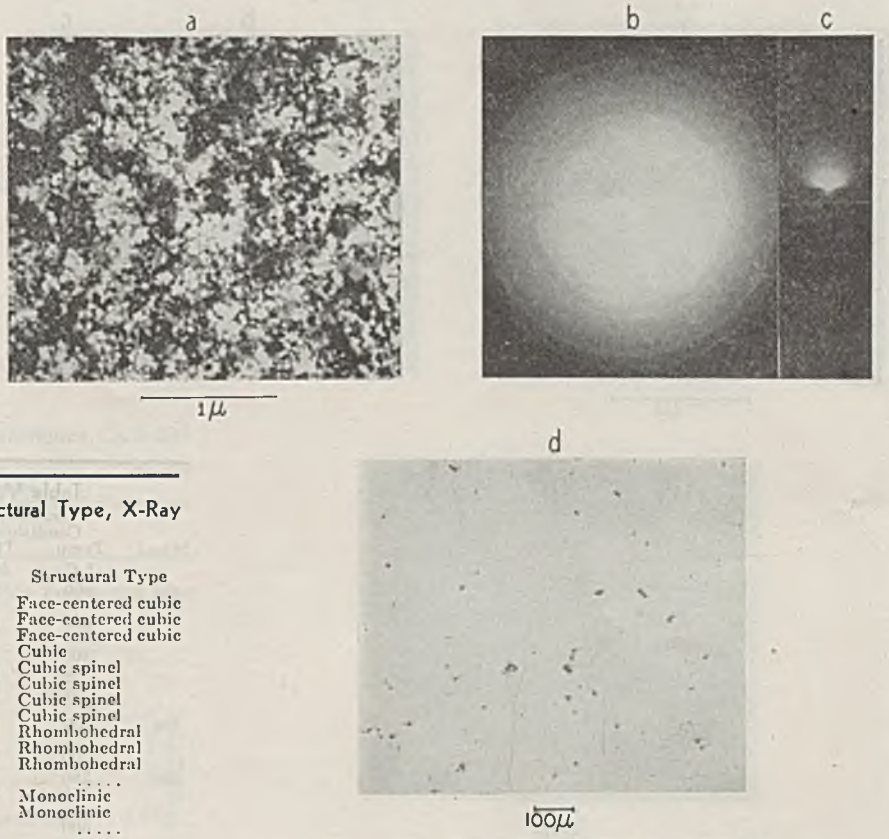

Figure 10. Oxide Film of Nickel, Ni 20–400

a. Electron micrograph stripped film
b. Electron diffraction transmission stripped film
c. Electron diffraction reflection film on metal
d. Light micrograph film on metal

Table IV. Oxide Lattice Parameters and Structural Type, X-Ray Data

Substance	Reference	Lattice Parameters *a*	*b*	*c*	*α*	Structural Type
FeO	*12*	4.28	..	..	...	Face-centered cubic
CoO	*12*	4.25	..	..	...	Face-centered cubic
NiO	*12*	4.17	..	..	...	Face-centered cubic
Cu_2O	*12*	4.24	..	..	...	Cubic
Fe_3O_4	*12*	8.40	..	..	...	Cubic spinel
γ-Fe_2O_3	*13*	8.32	..	..	...	Cubic spinel
Co_3O_4	*12*	8.11	..	..	...	Cubic spinel
γ-Al_2O_3	*13*	7.895	..	..	...	Cubic spinel
α-Fe_2O_3	*12*	5.42	..	..	55° 17′	Rhombohedral
Cr_2O_3	*12*	5.35	..	..	54° 58′	Rhombohedral
α-Al_2O_3	*12*	5.12	..	..	55° 17′	Rhombohedral
MoO_2	*12*	..	..	..	...	.....
CuO	*12*	4.66	3.40	5.09	...	Monoclinic
WO_3	*12*	7.28	7.48	3.82	...	Monoclinic
ChO	*7*	..	..	..	...	.....
Cb_2O_5	*7*	..	..	..	...	.....

Figure 9 (*Below*). Oxide Film of Molybdenum, Mo 5–450

a. Electron micrograph stripped film
b. Electron diffraction transmission stripped film
c. Electron diffraction reflection film on metal
d, e. Light micrograph film on metal

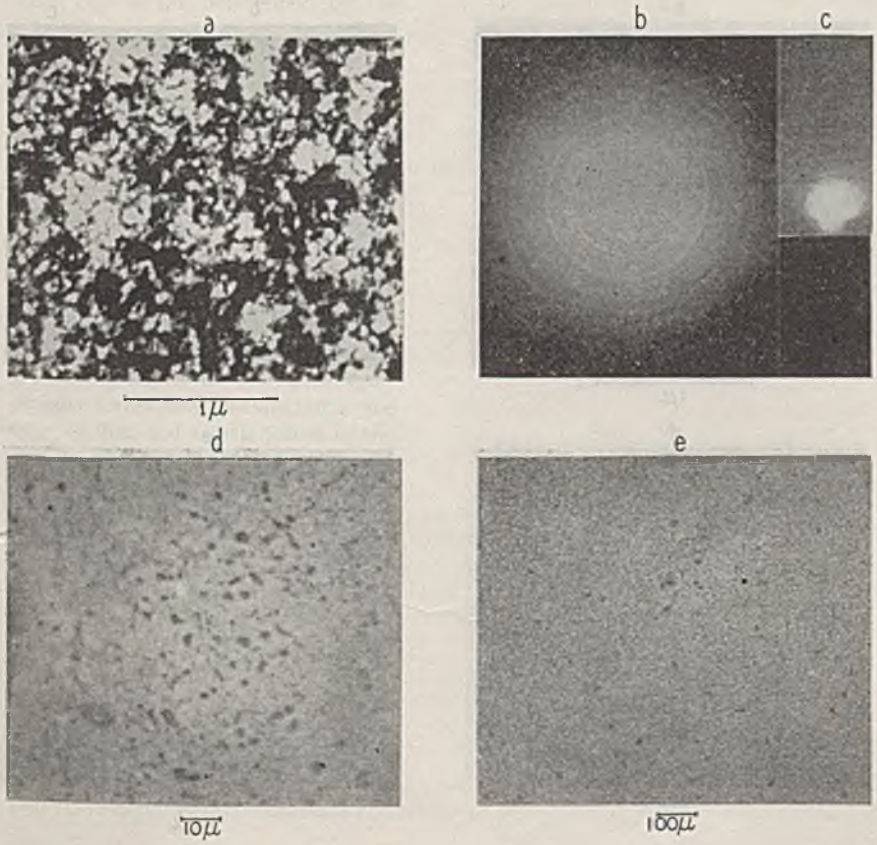

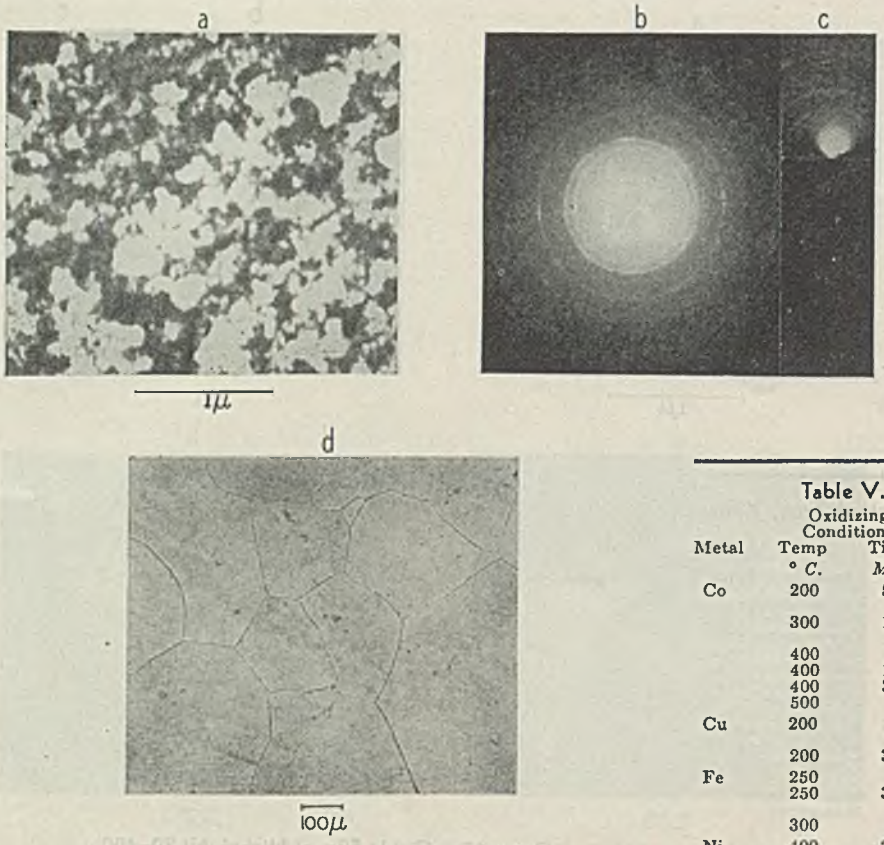

Figure 11. Oxide Film of Nickel, Ni 20–500

a. Electron micrograph stripped film
b. Electron diffraction transmission stripped film
c. Electron diffraction reflection film on metal
d. Light micrograph film on metal

If this effect is real, then the removal of the positive deviations in the stripped oxide film pattern is an interesting question. This may result from the electrochemical attack on the iron in solid solution in the oxide lattice or by removal of strains in the film after stripping from the metal. Support for the former hypothesis can be seen in the observations of Bernard (*2*) on the increase of the lattice parameter of FeO from 4.282 Å. to 4.298 Å. by the solid solution of iron in the lattice. This is of the same sign and magnitude as the positive deviations observed in Table VI.

The negative deviations are also of interest. They are greatest for Fe_3O_4 and Co_3O_4, where other oxides may be formed and go into solid solution, and are least for NiO and Cr_2O_3, where only one oxide is observed.

Electron Microscope. The size and shape characteristics of the crystals in an oxide film are determined by the rate of nucleation and the rate of growth of the oxide crystals. If the surface is limited in area and the rate of nucleation and growth sufficiently high, a two-dimensional mosaic structure will be formed. Further growth of a particular crystal must be at the expense of other crystals in the same plane or in a direction normal to the surface. The rates of nucleation and of growth are rate processes and are exponential functions of the free energy of activation and the temperature. These free energies of activation have unique values for each oxide and for each particular crystal

Table V. Lattice Parameters of Oxide Films

Metal	Oxidizing Conditions Temp ° C.	Time Min.	Composition and a By transmission	By reflection	X-ray Data
Co	200	50	Co_3O_4, 8.07; CoO, 4.24	CoO, 4.28	....
	300	10	Co_3O_4, 8.06; CoO, 4.25	Co_3O_4, 8.12	Co_3O_4, 8.11
	400	5	CoO, 4.24	CoO, 4.28	....
	400	10	CoO, 4.23	CoO, 4.22	CoO, 4.25
	400	30	CoO, 4.24	CoO, 4.28	....
	500	5	CoO, 4.25	CoO, 4.29	....
Cu	200	5	Cu_2O, 4.23	Cu_2O, 4.32; CuO	Cu_2O, 4.24
	200	30	Cu_2O, 4.24	Cu_2O, 4.33	....
Fe	250	5	Fe_3O_4, 8.35	Fe_3O_4, 8.49	Fe_3O_4, 8.40
	250	30	Fe_3O_4, 8.35; α-Fe_2O_3	Fe_3O_4, 8.44; α-Fe_2O_3	....
	300	5	Fe_3O_4, 8.37	Fe_3O_4, 8.43	γ-Fe_2O_3, 8.32
Ni	400	20	NiO, 4.17	NiO, 4.20	....
	450	5	NiO, 4.15	NiO, 4.20	NiO, 4.17
	500	5	NiO, 4.15	NiO, 4.20	....
	500	20	NiO, 4.15	NiO, 4.22	....
	500	60	NiO, 4.17		
	550	5	NiO, 4.19		

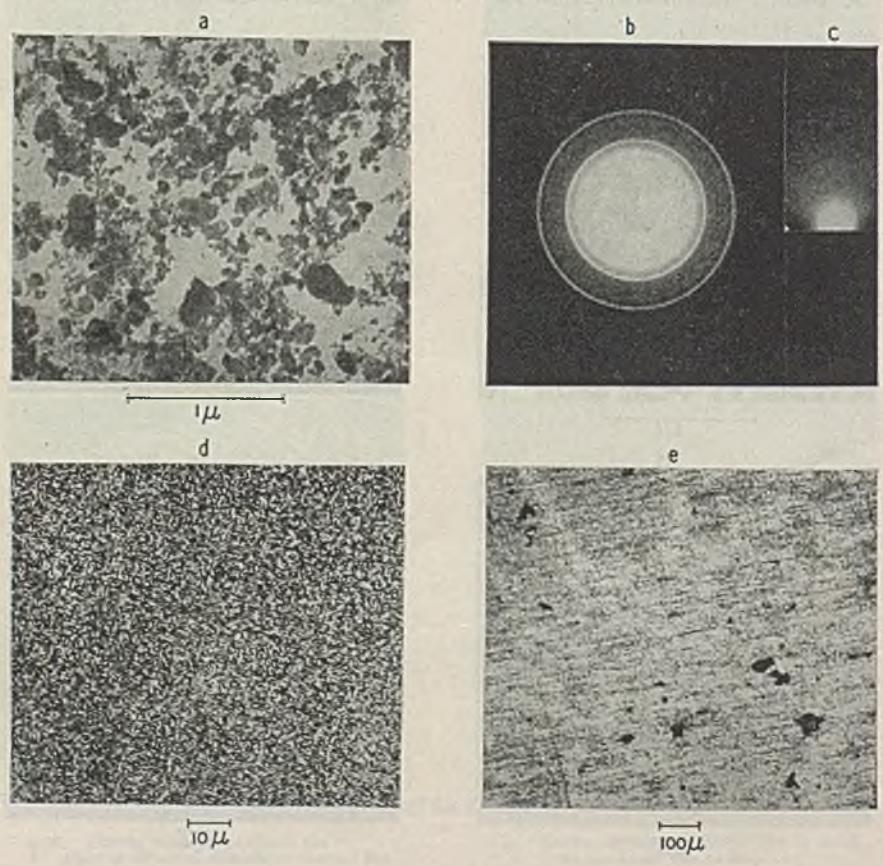

Figure 12. Oxide Film of Aluminum, Al 5–500

a. Electron micrograph stripped film
b. Electron diffraction transmission stripped film
c. Electron diffraction reflection film on metal
d. e. Light micrograph film on metal

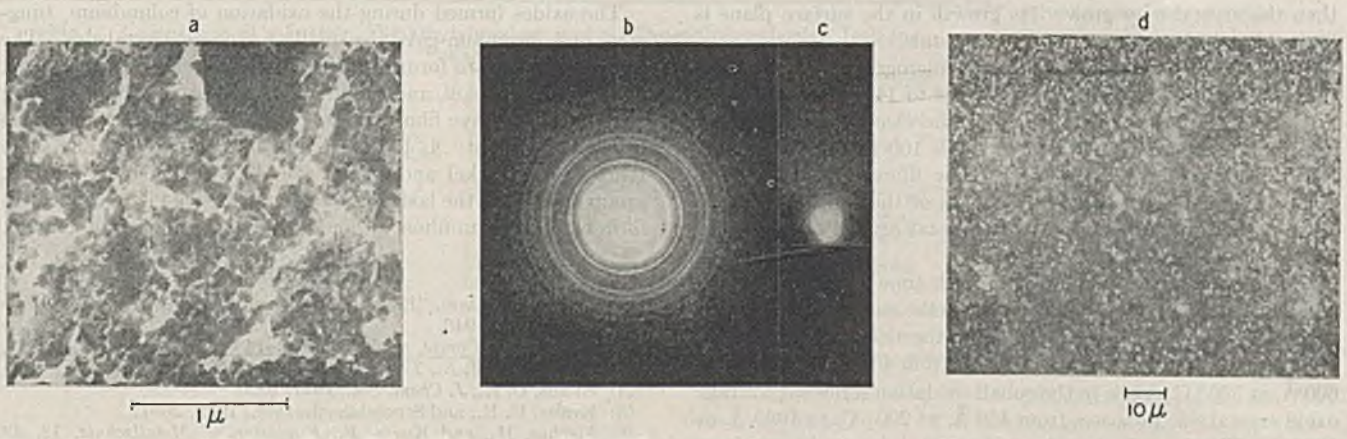

Figure 13 (*Above and Right*). Oxide Film of Columbium, Cb 5–400

a. Electron micrograph stripped film
b. Electron diffraction transmission stripped film
c. Electron diffraction reflection film on metal
d, e. Light micrograph film on metal

Table VI. Average Deviation of Oxide Lattice Parameters from X-Ray Values

	Transmission			Reflection		
Metal	No. of expts.	Composition	Deviation, %	No. of expts.	Composition	Deviation, %
Co	6	CoO	−0.20	5	CoO	+0.47
	2	Co_3O_4	−0.56	1	Co_3O_4	+0.12
Cu	2	Cu_2O	−0.12	2	Cu_2O	+2.0
Fe	3	Fe_3O_4	−0.55	3	Fe_3O_4	+0.63
Ni	6	NiO	−0.16	4	NiO	+0.84
Cr[a]	2	Cr_2O_3	+0.10	2	Cr_2O_3	+0.62
	Average deviation −0.20%			Average deviation +0.72%		

[a] Calculated from d_{hkl} values.

face. The number and size of the oxide crystals are therefore a function of the temperature. The shape, sharpness of the crystal boundaries, and other features of the oxide crystal are determined by the rate processes and the crystal structure of the oxide. Silica is known to be amorphous, while cuprous oxide is definitely crystalline.

Another point of view of the oxidation process which may be useful is a comparison of the volume ratio of the oxide to the metal. Metals which form oxides having a volume ratio greater than 1 are usually protective, while metals forming oxides with a volume ratio of less than 1 are usually nonprotective. If the crystals are to grow uniformly in all directions, compressive forces may be expected in one type of film and tensile forces in the other. This phenomenon has been used frequently to explain the porosity of some films and the cracking of others.

The process of formation of the first layer of crystals in the oxide film is interesting. The first stage of the reaction of a clean metal with oxygen has been shown to involve the formation of a uniform monomolecular layer of oxygen. A thin film of oxide has been found to grow rapidly after the initial layer has been formed (*9*). At some point crystal nucleation must start and

Figure 14 (*Below*). Oxide Film of Tungsten, W 5–400

a. Electron micrograph stripped film
b. Electron diffraction transmission stripped film
c. Electron diffraction reflection film on metal
d, e Light micrograph film on metal

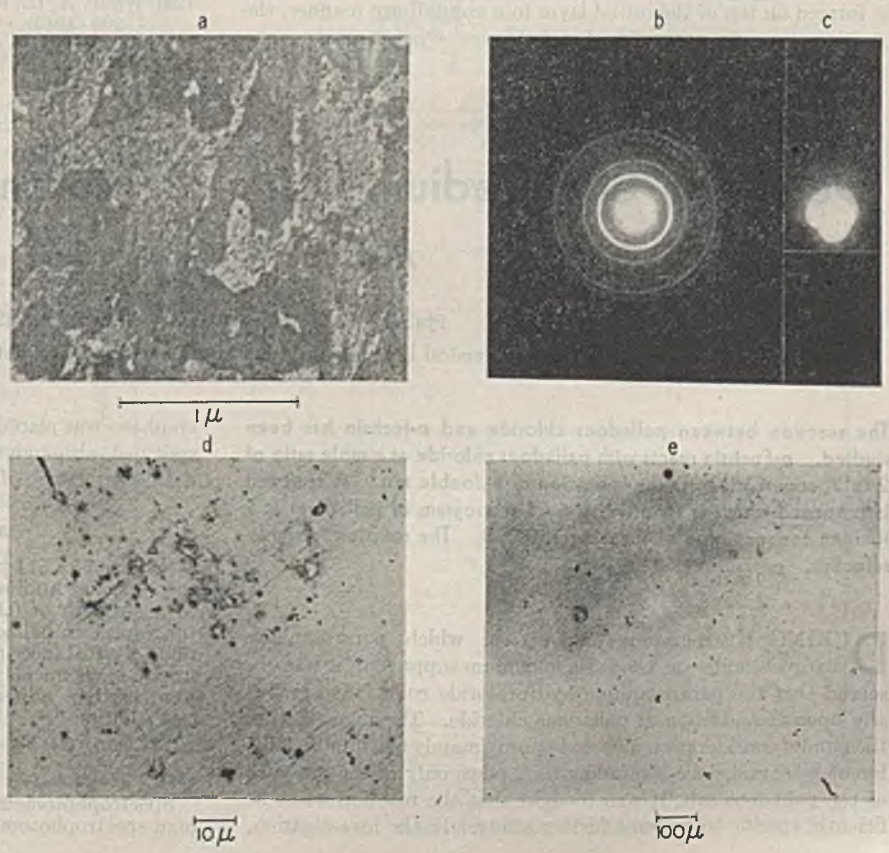

then the crystal may grow. Its growth in the surface plane is limited by the interference of other crystals.

The electron micrographs and light micrographs of the oxidation experiments are shown in Figures 4 to 14. Table III summarizes the information taken from the electron micrographs. The films consist of small oxide crystals 100 to 2500 Å. in size, largely of irregular shapes with a few films showing definite crystal shapes. The oxide crystals are of the order of 10^{-3} to 10^{-5} of the linear dimension of the metal crystal or grain and 10^{-6} to 10^{-10} of the area.

The crystal size is a function of both time and temperature. The effect of temperature can be shown in the series of oxidation experiments on cobalt and on nickel. For the nickel oxidation series the average oxide crystal size increases from 400 Å. at 400° C. to 600 Å. at 550° C., while in the cobalt oxidation series the average oxide crystal size increases from 450 Å. at 200° C. to 1000 Å. at 500° C. The time effect on the oxide crystal size can be seen from an analysis of the cobalt, copper, and iron experiments.

The oxide films are largely nonuniform, as they consist of thicker and thinner sections. This indicates a multilayer film of oxide crystals. Thus, nucleation occurs in contact not only with the initial thin oxide layer but with other oxide crystals. This multilayer nucleation process does not form oxide crystals in as regular a manner as in the first layer. Therefore, clustering of crystals in the outer layers is noticed and nonuniform films are formed. Local concentrations of impurities or a small void in the initial oxide layer may partially account for this phenomenon.

It is noticed from an analysis of the electron micrographs that frequently one crystal appears to overlap an adjacent one, causing a broad boundary zone to appear. This may be the result of (1) the physical overlap of two crystals, or (2) occurrence of the contact zone between crystals at an angle to the electron beam. Diffraction effects may give the same effect as physical overlapping of the crystals. This overlapping phenomenon is noticed in many of the films.

The irregular shape of the oxide crystals in the first layer of the oxide film is to be expected. If a second or third layer of crystals is formed on top of the initial layer in a nonuniform manner, the previous restraints are relaxed and the new crystals may assume a more normal growth (Figure 6).

The oxides formed during the oxidation of columbium, tungsten, and chromium gave the smallest average crystal size. The largest crystals are formed during the oxidation of copper, iron, molybdenum, nickel, and cobalt. The first group probably form the more protective films against oxidation under the conditions of the experiment. If the materials are compared at the same temperature, nickel and cobalt would be included in the first group and not in the last. The more protective metals appear to form more uniform films, although the correlation is not general.

LITERATURE CITED

(1) Ardenne, M. von, "Elektronon Ubermikroskope", Berlin, Julius Springer, 1940.
(2) Bernard, J., *Compt. rend.*, 205, 912–14 (1937).
(3) Darbyshire, J. A., *Trans. Faraday Soc.*, 27, 675 (1931).
(4) Evans, U. R., *J. Chem. Soc.*, 1927, 1020.
(5) Evans, U. R., and Stockdale, J., *Ibid.*, 1929, 2651.
(6) Fischer, H., and Kurtz, F., *Korrosion u. Metallschutz*, 18, 42 (1942).
(7) Grube, G., Kubaschewski, O., and Zwiauer, K., *Z. Elektrochem.*, 45, 885–8 (1939).
(8) Gulbransen, E. A., *J. Applied Phys.*, 16, 718–24 (1945).
(9) Gulbransen, E. A., *Trans. Electrochem. Soc.*, 81, 327–9 (1942).
(10) Gulbransen, E. A., and Hickman, J. W., unpublished manuscript.
(11) Hanawalt, J. D., Rinn, H. W., and Frevel, L. K., Ind. Eng. Chem., Anal. Ed., 10, 457 (1938).
(12) Haul, R., and Schoon, Th., *Z. physik. Chem.*, 44B, 216–26 (1939).
(13) Henneberg, W., *Stahl u. Eisen*, 61, 769 (1941).
(14) Hickman, J. W., and Gulbransen, E. A., unpublished manuscript.
(15) Iitaka, I., Miyake, S., and Iimori, T., *Nature*, 139, 156 (1937).
(16) Kutzelnigg, A., *Z. anorg. allgem. Chem.*, 202, 418 (1931).
(17) Mahl, H., *Korrosion u. Metallschutz*, 17, 1 (1941).
(18) Picard, R. G., *J. Applied Phys.*, 15, 678 (1944).
(19) Rooney, T. E., and Stapleton, A. G., *J. Iron Steel Inst.*, 131, 249 (1935).
(20) Smith, W., *J. Am. Chem. Soc.*, 58, 173 (1936).
(21) Steinheil, A., *Ann. Phys.*, 19, 465 (1934).
(22) Tammann, G., and Arntz, F., *Z. anorg. allgem. Chem.*, 192, 45 (1930).
(23) Vernon, W. H. J., Wormwell, F., and Nurse, T. J., *J. Chem. Soc.*, 1939, 621.
(24) Wernick, S., *J. Electrodepositors Tech. Soc.*, 9, 163 (1933–4).
(25) White, A. H., and Germer, L. H., *Trans. Electrochem. Soc.*, 81, 305 (1942).
(26) Withey, W. H., and Millar, H. E., *J. Soc. Chem. Ind.*, 45, 173T (1926).

Detection of Palladium Using Pararosaniline Hydrochloride

A Spot Test Procedure

PHILIP W. WEST AND EDWARD S. AMIS

Coates Chemical Laboratories, Louisiana State University, Baton Rouge, La.

The reaction between palladous chloride and *p*-fuchsin has been studied. *p*-Fuchsin reacts with palladous chloride at a mole ratio of 2 to 3, apparently with the formation of a double salt. A spot test is proposed which is sensitive to 0.01 microgram of palladium at a limiting concentration of 1 part in 750,000. The reaction is highly selective.

DURING polarographic analyses in which pararosaniline hydrochloride was used as a maximum suppressor, it was observed that the pararosaniline hydrochloride color faded gradually upon the addition of palladous chloride. The investigation then under consideration included approximately one hundred different ions, and since the fading took place only in the presence of the palladous salt, it was thought that the reaction was sufficiently specific to warrant further study. In the investigation, emphasis was placed on the adaptation of the reaction for use as a spot test, although considerable effort was directed toward elucidating the nature of the reaction.

REAGENTS AND CHEMICALS

Schultz No. 511 pararosaniline hydrochloride (*p*-fuchsin) from the National Aniline and Chemical Company, Inc., was made up to a strength of 0.01%, and c.p. palladium chloride to 0.01% (in respect to palladium) in distilled water. One per cent solutions of substances to be studied for interfering effects were made from c.p. chemicals; 2 *N* sodium hydroxide and 2 *N* acetic acids were used in adjusting the hydrogen-ion concentration of the test solutions.

APPARATUS

Spectrophotometric studies were made using a Model D Beckman spectrophotometer and 1.00-cm. cells.

Table I. Comparison of *p*-Fuchsin, Dimethylglyoxime, and *p*-Nitrosodiphenylamine Tests for Palladium

	p-Fuchsin[a]	Dimethylglyoxime	*p*-Nitrosodiphenylamine
Positive interferences	Au^{+++}, Hg^{+}, Pt^{++++}	Au^{+++}	Au^{+++}, Pt^{++++}
Negative interferences	Tl^{+}, Bi^{+++}, CN^{-}, $C_2O_4^{--}$, basic NH_4^{+}, F^{-}, CNS^{-}, formate, aniline, pyridine	Be^{++}, Ga^{+++}, basic NH_4^{+}, BO_2^{-}, S^{--}, $S_2O_3^{--}$, CN^{-}, $Fe(CN)_6^{----}$, CNS^{-}, $C_2O_4^{--}$	Basic NH_4^{+}, NO_2^{-}, CN^{-}, $Fe(CN)_6^{---}$, $Fe(CN)_6^{----}$, CNS^{-},
Masking interferences	Sn^{++}, V^{+++}, MoO_4^{--}, I^{-}, Ir^{+++}, hypophosphite	Ti^{+++}, hypophosphite, V^{+++}, CrO_4^{--}, I^{-}, Fe^{++}, Fe^{+++}, Rh^{+++}, Ir^{+++}	Ag^{+}, Ti^{+++}, Sn^{++}, hypophosphite, VO_3^{-}, S^{--}, Cr^{+++}, CrO_4^{--}, MoO_4^{--}, I^{-}, Co^{++}, Ru^{+++}, Ir^{++++}
Sensitivity	LI = 0.01 microgram LC = 1:750,000	LI = 0.18 microgram LC = 1:100,000	LI = 0.005 microgram LC = 1:750,000

[a] Positive interferences listed refer to reactions with *p*-fuchsin. Actual test based on use of this reagent, however, is free from positive interferences.

EXPERIMENTAL

Figure 1 shows the transmittancy curves for solutions of pararosaniline hydrochloride, palladous chloride, and a mixture of these two solutions. These transmittancy curves were determined using 0.005% solutions of pararosaniline hydrochloride and 0.0005% palladous chloride. The reference cell contained distilled water. The red color of the fuchsin solution fades on addition of the palladium salt. The maximum transmittancy difference occurs at a wave length of 380 mμ. Visual observation of this reaction discloses that dilute solutions of palladium cause a fading of the red fuchsin color, while large concentrations of palladium react with the fuchsin to form a finely dispersed brown precipitate.

The nature of the reaction involved was next investigated. The equivalent ratio of the two reactants was determined by means of a spectrophotometric titration. This procedure was based on the observation that the slopes of the transmittancy *vs.* molar concentration curves for the fuchsin and the palladous chloride solutions were quite different when determined at a wave length of 380 mμ. By adding known amounts of standard 0.000999 *M* palladium solution to fixed amounts (5.00 ml.) of 0.000247 *M* *p*-fuchsin, diluting the mixture to a total volume of 10.00 ml., determining the transmittancies, and plotting the log per cent transmittancy of each mixture, it was found that the equivalence point, as indicated by the intersection of the two curves, was at a mole ratio of *p*-fuchsin to palladous chloride of 2 to 3 (see Figure 2). As a check on this determination, analyses for carbon, hydrogen, and chlorine were run which confirmed that the composition of the reaction product was $2C_{19}H_{17}N_3HCl.3PdCl_2$. Analytical calculations for $2C_{19}H_{17}N_3HCl.3PdCl_2$: C, 38.71; H, 3.07; Cl, 24.06. Found: C, 38.73; H, 3.43; Cl, 24.36.

The nature of the fading action due to palladium was different from the fading brought about by acids or reducing agents. This was indicated by the transmittancy curves of acid-faded and sulfur dioxide–faded *p*-fuchsin as shown by Figure 3 when compared to Figure 1.

On the basis of the analytical data presented, the authors believe that the product of the palladous chloride–pararosaniline hydrochloride reaction is a double salt. The probability that the fading action was due to oxidation-reduction was ruled out on the basis of the transmittancy curves. The possibility that an inner-complex salt was formed was rejected because the functional groups of the pararosaniline were so far apart as to prohibit the formation of stable chelate rings. Normal salt formation was considered unlikely because the reaction occurred in slightly acidic medium. The belief that the reaction results in double salt formation is of interest, since this type of reaction has not previously been considered of analytical importance (*1, 8, 11*).

Because of the close similarity between members of the platinum group metals, special emphasis was placed on determining the possibility that other elements of this group might react with fuchsin in a manner similar to palladium. Transmittancy curves for mixtures of *p*-fuchsin and ions of ruthenium, rhodium, osmium, iridium, and platinum were run and it was found that the transmittancies of mixtures of the reagent with these ions were additive.

APPLICATIONS AS A SPOT TEST

There are several tests for palladium (*3–7, 9, 10, 12, 15*), the most sensitive of which is the *p*-nitrosodiphenylamine reaction (*15*). This test is sensitive to 0.005 microgram of palladium and there are few interfering substances. The method can also be used for quantitative determinations of the metal.

The authors have investigated *p*-fuchsin as a reagent for detecting palladium and have found it to be highly selective in its reaction. Most of the important interferences can be eliminated by simple means and since *p*-fuchsin is a common stable organic compound, and the test is so sensitive and easy to make, this method of testing for palladium should find considerable application in research and routine analytical laboratories.

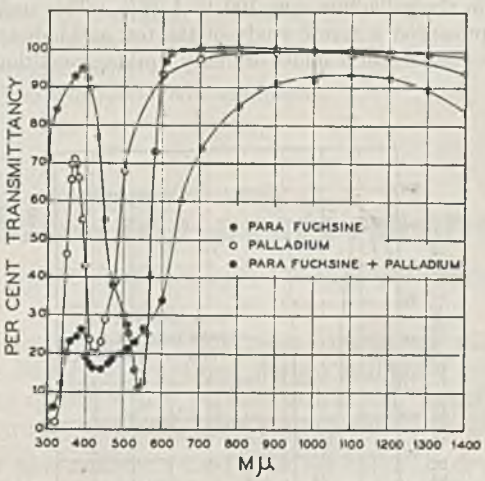

Figure 1. Transmittancy Curves

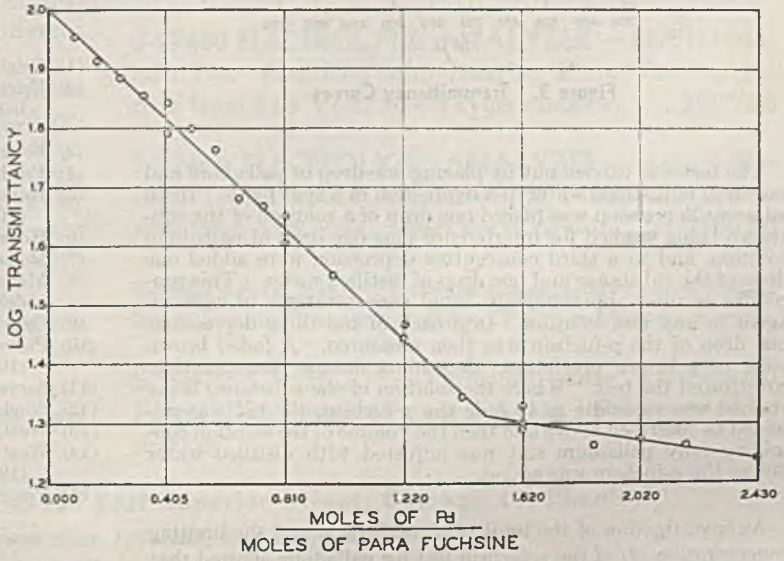

Figure 2. Equivalent Ratio of Reactants

SCOPE OF INVESTIGATION

The interference studies were made using 1% solutions of the ions and compounds listed below (the ions are listed in their most common forms, although it is realized that in many cases they are actually present as complexes):

Li^+, Na^+, K^+, Cu^{++}, Rb^+, Ag^+, Cs^+, Au^{+++}, Be^{++}, Mg^{++}, Ca^{++}, Zn^{++}, Sr^{++}, Cd^{++}, Ba^{++}, Hg^+, Hg^{++}, BO_2^-, $B_4O_7^{--}$, Al^{+++}, Ga^{+++}, Y^{+++}, In^{+++}, La^{+++}, Ce^{++++}, Tl^+, CO_3^{--}, SiO_3^{--}, Ti^{++++}, Sn^{++}, Sn^{++++}, Pb^{++}, Zr^{++++}, Th^{++++}, NH_4^+, NO_2^-, NO_3^-, $H_2PO_2^-$, $P_4O_{13}^{------}$ (tetraphosphate), $P_6O_{18}^{------}$ (hexametaphosphate), PO_3^-, HPO_4^{--}, $P_2O_7^{----}$, VO_3^-, AsO_2^-, $HAsO_4^{--}$, Sb^{+++}, Bi^{+++}, S^{--}, $S_2O_3^{--}$, SO_3^{--}, SO_4^{--}, Cr^{+++}, CrO_4^{--}, SeO_3^{--}, SeO_4^{--}, MoO_4^{--}, WO_4^{--}, TeO_3^{--}, UO_2^{++}, UO_4^{--}, F^-, Cl^-, ClO_3^-, Mn^{++}, MnO_4^-, Br^+, BrO_3^-, I^-, IO_3^-, ReO_4^-, Fe^{++}, Fe^{+++}, Co^{++}, Ni^{++}, Ru^{+++}, Rh^{+++}, OsO_5^{--}, Ir^{++++}, Pt^{++++}, CN^-, $Fe(CN)_6^{---}$, $Fe(CN)_6^{----}$, SCN^-, acetate, oxalate, malonate, formate, adipate, succinate, phthalate, tartrate, citrate, lactate, gluconate, isoinositol, *d*-sorbitol, mannitol, sucrose, dextrose, aniline, pyridine, resorcinol.

The pH of solutions made acidic by the addition of a drop of solution of such salts as Ti^{++++} and Sn^{++} was adjusted to a value of between 2 and 4, as indicated by universal indicator paper, by adding 2 to 3 drops of sodium hydroxide and then acetic acid until the desired pH was obtained. Usually 2 to 3 drops of acetic acid sufficed. The ratio of the substance being studied for interference to the palladium was 100 to 1 (*14*). This unfavorable ratio represented a severe study of the test and indicated what could be expected of it under ordinary working conditions.

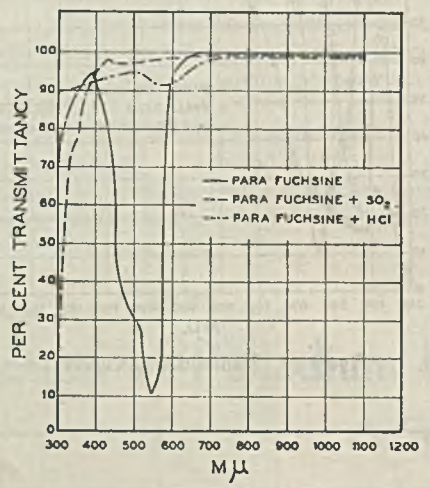

Figure 3. Transmittancy Curves

The test was carried out by placing one drop of palladium and one drop of distilled water in a depression of a spot plate. In an adjacent depression was placed one drop of a solution of the substance being studied for interference plus one drop of palladium solution, and to a third consecutive depression were added one drop of the substance and one drop of distilled water. This procedure ensured approximately equal concentrations of each reagent in any test solution. Into each of the three depressions one drop of the *p*-fuchsin was then measured. A faded brown color or a brown precipitate, depending on the concentration, constituted the test. Where the solution of the substance being studied was so acidic as to fade the *p*-fuchsin, the pH was adjusted as described above and then the volume of the solution containing only palladium salt was adjusted with distilled water before the *p*-fuchsin was added.

An investigation of the limit of identification and the limiting concentration (*2*) of the *p*-fuchsin test for palladium showed that the limit of identification was 0.01 microgram at a limiting concentration of 1 to 750,000. These limiting values were obtained using micro volumes of both the reagent and the palladium test solutions. The value for the limiting concentration does not include any volume increases due to the addition of reagents.

The interferences were classified in the manner described by West (*13*).

Positive interferences were given by auric gold, mercurous mercury, and large amounts of platinic platinum. These positive interferences can be obviated by making a confirmatory test with crystalline sodium hypophosphite. The hypophosphite reduces palladium in any solution with the formation, after a few seconds, of a black precipitate. Solutions containing gold or platinum alone are not visibly affected by hypophosphites, while solutions of mercurous mercury give a purple precipitate and this only upon standing. This confirmatory test should be run on solutions containing *p*-fuchsin, since otherwise mercurous mercury gives a black precipitate similar to that given by palladium. The reaction between platinum and *p*-fuchsin gives a visible effect only in solutions which contain over 5 mg. of platinum per ml.

Negative interferences were given by ammonium hydroxide, thallous thallium, nitrite, bismuth, cyanide, oxalate, and, upon standing (4 hours), fluoride, thiocyanate, formate, aniline, and pyridine. With the exception of bismuth, these negative interferences are due to competitive reactions which so reduce the effective concentration of palladium that it no longer gives its characteristic reaction with *p*-fuchsin. In the case of thallium, the reaction results in the formation of a precipitate, while in the case of the other ions, soluble complexes are formed. As a rule, these negative interferences would apply to any test for palladium.

Masking interferences were given by stannous tin, vanadous vanadium, hypophosphite, permanganate, iodide, and iridium. The tin, hypophosphite, and iodide react with palladium to give dark precipitates, while the other ions interfere, owing to the intense colors of their solutions. Of these interferences, the only one of practical significance is that of iridium; it can be eliminated by addition of thiosulfate until the color of the iridium just disappears. Excess thiosulfate should be avoided. Iridium in concentrations of less than 5 mg. per ml. does not mask the *p*-fuchsin test.

A comparison of the *p*-fuchsin test with the dimethylglyoxime and *p*-nitrosodiphenylamine tests for palladium is shown in Table I. All three tests were very satisfactory. Advantages claimed for the *p*-fuchsin test are that the positive interferences can be very easily obviated, and that no interferences of any type are given by other members of the platinum group of metals, provided that the initial concentration of the solution to be analyzed does not exceed 0.05%. Because of the nature of the test, it suffers least from masking interferences due to colored ions.

LITERATURE CITED

(1) Feigl, Ind. Eng. Chem., Anal. Ed., 8, 401 (1936).
(2) Feigl, "Specific and Special Reactions", pp. 5–17, Elsevier Publishing Co., distributed by Nordeman Publishing Co., New York, 1940.
(3) Feigl and Frankel, *Ber.*, 65B, 539 (1932).
(4) Feigl, Krumholz, and Rajmann, *Mikrochemie*, 9, 165 (1931).
(5) Hayes and Chandlee, Ind. Eng. Chem., Anal. Ed., 14, 491 (1942).
(6) Hoke, *Brass World*, 28, 159 (1932).
(7) Holzer, *Mikrochemie*, 8, 271 (1930).
(8) Mellan, "Organic Reagent in Inorganic Analysis", p. 1, Philadelphia, Blakiston Co., 1941.
(9) Overholser and Yoe, *J. Am. Chem. Soc.*, 63, 3224 (1941).
(10) Pierson, Ind. Eng. Chem., Anal. Ed., 6, 437 (1934); 11, 86 (1939).
(11) Sarver, *J. Chem. Education*, 13, 511 (1936).
(12) Singleton, *Ind. Chemist*, 3, 121 (1927).
(13) West, *J. Chem. Education*, 18, 528 (1941).
(14) West and Houtman, Ind. Eng. Chem., Anal. Ed., 14, 597 (1942).
(15) Yoe and Overholser, *J. Am. Chem. Soc.*, 61, 2058 (1939).

Presented before the Division of Analytical and Micro Chemistry at the 105th Meeting of the American Chemical Society, Detroit, Mich.

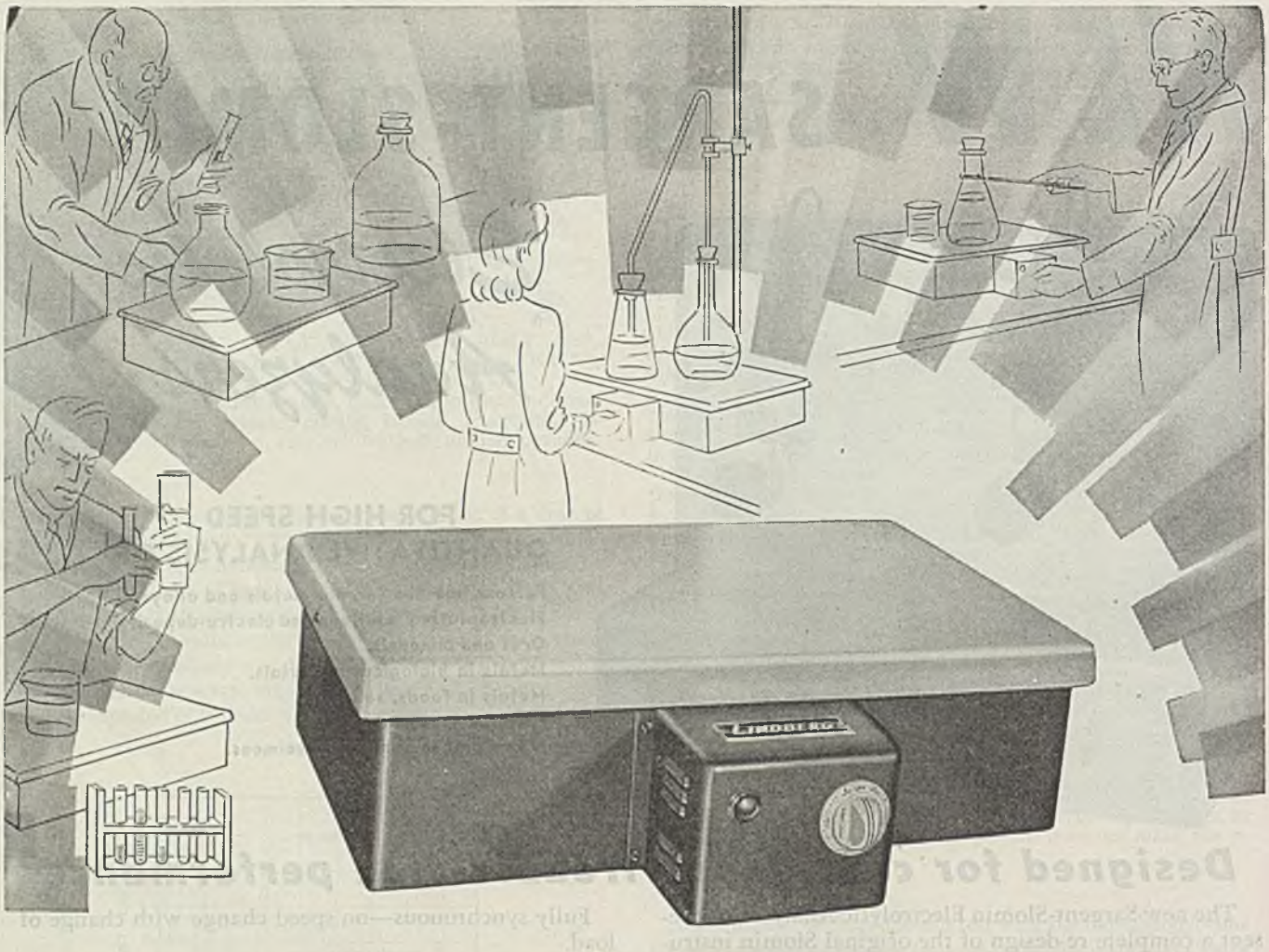

VYCOR brand 96% Silica Glass No. 790 possesses properties approaching fused quartz. A special glass of normal characteristics is treated by a new and patented process in which practically all the constituents other than silica are leached out. The silica residue, after being washed, is dried and finally fired at high temperatures. In its final form, it becomes a transparent vitreous glass with outstanding properties.

With such a low co-efficient of expansion, high softening point and exceptional chemical stability, Vycor Laboratory ware is particularly useful for high temperature work and rapid, accurate chemical analysis.

It is the perfect complement to the all-around "Pyrex" Laboratory ware —the two lines—Vycor and Pyrex Brand Ware—meeting practically any requirement involving glass apparatus which might arise in the laboratory.

Property	*Pyrex brand Chemical Glass No. 774*	*Vycor 96% Silica Glass No. 790*	*Vitreous Silica*
Softening point	820°C.	1500°C.	1650°C.
Annealing point	560°C.	900°C.	1150°C.
Strain point	510°C.	800°C.	1070°C.
Coefficient of expansion	$(32-33) \times 10^{-7}$	$(7.5-8.0) \times 10^{-7}$	$(5.5-5.8) \times 10^{-7}$
Density	2.23	2.18	2.20

TRADE MARK VYCOR REG. U.S. PAT. OFF.

"Vycor" and "Pyrex" are registered trade-marks and indicate manufacture by

CORNING GLASS WORKS • CORNING, NEW YORK

For High Temperature Reactions and Rapid Analysis

VYCOR LABORATORY GLASSWARE

Current Developments in INSTRUMENTATION IN ANALYSIS

Discussed by Ralph H. Müller

FROM Sweden comes interesting and stimulating news about a radical extension of the chromatographic technique. We were honored by receipt of a reprint, better described as a monograph, of 133 pages on "Studies on Adsorption and Adsorption Analysis with Special Reference to Homologous Series". Stig Claesson, who is working in the renowned Institute of Physical Chemistry at the University of Upsala, is the author, and the work appears in the *Arkiv för Kemi, Mineralogi och Geologi*, Bd. 23A, No. 1.

Flowing Chromatography

Claesson's work is an extension of the earlier investigations of Tiselius in which solutions were forced through a column and the successive effluents were examined by the Philpot-Svensson slit method. In the present method the concentration determinations are made in a very small cell and plotted against the volume or weight of solution which has passed through the column. The equipment permits the use of frontal analysis, elution analysis, or displacement development. Of these it is shown that frontal analysis and displacement development are the most useful.

In frontal analysis, the solution is poured into a reservoir from which it is forced through the column or filter. The effluent is continuously analyzed in a small cell. The curves, relating concentration to transpired volume, are steplike in shape. The first step contains component 1, the second step components 1 and 2, and so on. In displacement development a small amount of the solution is adsorbed on the top of the column, after which another solution containing a "developer" is forced through the column. The developer is characterized by a stronger adsorption affinity; consequently it drives the adsorbed components ahead of it. The resulting curves are also steplike, but in this case each step contains only one component. The height of the step is a characteristic constant for each component and the length of the step is proportional to the amount of that component.

Refractive index was chosen as the means for measuring concentration and two techniques were used. In the manual method, an interferometer is employed, permitting measurements on a volume of 0.13 ml. to an accuracy of 5×10^{-6} over a range of 6×10^{-3}. The interferometric method requires constant observation of the fringes and to eliminate the tedium a completely automatic instrument was devised. A differential photoelectric refractometer indicates the refraction increment. The galvanometer in this arrangement yields a deflection which is combined in a cross-mirror scheme with the deflection produced by a solution-weighing device. A photographic record may thus be obtained in which the ordinates represent the refraction increment and the abscissas, the weight of effluent. For dilute solutions the refraction increment is a very precise measure of concentration. The weighing device employs the deflection of a simple straight spring of steel, with oil damping, and a mirror attached to the free end. A choice of springs is available to accommodate a wide range of values—i.e., from 10 to 1000 grams.

Some of the advantages of this highly developed method of flowing chromatography are: (1) It is applicable to colorless substances; (2) colored adsorbents (carbon) can be used; (3) individual members of a homologous series can be identified with ease; (4) the same equipment can be used for analytical or preparative purposes.

An extended section deals with the theory of the method and shows how the identification is based on the constants in the Langmuir adsorption isotherm.

A self-recording apparatus for gases and vapors is also described in which nitrogen is used as "solvent". The gas is driven through the filter by a mechanism which also drives the recording drum. The concentration of the effluent gas is followed by measuring its thermal conductivity and the latter is automatically plotted against the volume of the gas.

We think this is a fine example of sound theory combined with first-class instrumentation—no great surprise coming, as it does, from an institute associated with the names of Svedberg, Tiselius, and Claesson. There are still some who will persist in calling this gadgeteering.

Pulsed Mass Spectrometer

A little nearer home, in the adjoining town of Cambridge, we attended the recent three-day meeting of the American Physical Society. While nuclear physics and microwave radar set the dominant note, there were several topics of interest for the analyst.

After our recent remarks in this column about mass spectrometers we were eager to hear the paper by W. E. Stevens of the University of Pennsylvania on a "Pulsed Mass Spectrometer with Time Dispersion". The new design proposes to accelerate ions out of a low-voltage ion source with microsecond pulses at millisecond intervals. In their passage down a long tube ions of different M/e acquire different velocities and therefore spread out into groups. The ions are caught in a Faraday cage. The amplified ion current is fed to the vertical plates of a cathode ray oscillograph. The horizontal linear sweep-circuit is synchronized with the pulses at the appropriate recurrence rate. The indication on the 'scope is continuous with mass numbers on the abscissas and intensities as ordinates, and, of course, is easily photographed. The advantages of this scheme are the elimination of magnets and stabilization equipment. Furthermore, the resolution is not limited by smallness of slits or alignment. The theory of operation and design features have been completed and a spectrometer of this type is under construction. The author indicated that mass discrimination of somewhat better than 1 unit in 50 is easily attained. This is sufficient for most organic systems. The suitability of this instrument for composition control, rapid analysis, and portable use was pointed out.

We take particular delight in this scheme. A radar man and a chemist could "cook up" some intriguing extensions and applications. For one thing, signaling the appearance of one or more species would be a simple matter of time interpolation, in which delay "gates" are generated electronically by the initial pulse. These serve to switch in the signaling amplifier at the desired time and keep it switched off at all other times. If the unmistakable identification of a molecule required the detection of three or four fragments of definite mass, suitably located "gates" would be set to trap each ion pulse. The gated pulses would then feed a slow recovery coincidence circuit. The latter would function, or say "yes", only if all the required species appeared. Similarly, the system could be monitored in a quantitative sense, for the one or more fragments required for certainty of identification, by subjecting each gated pulse to a discriminator circuit which rejects all signals unless they exceed a minimal value. We forego further speculation by pointing out that the particular advantage of the scheme resides in the fact that it can bring mass spectrometry into the class of time measurements for which the electronic techniques are particularly abundant.

Absorption of Microwaves by Gases

Another paper of great interest dealt with the absorption of microwaves by gases. J. E. Walter and W. D. Hershberger of the RCA Laboratories measured the absorption coefficients and dielectric constants of sixteen gases at the two wave lengths of 1.24 and 3.18 cm. Hydrogen sulfide, sulfur dioxide, carbonyl sulfide, methyl ether, ethylene oxide, ammonia, six halogenated methanes, and three amines were examined with improved waveguide technique, permitting the detection of absorption coeffi-

Instrumentation

cients as small as 0.2×10^{-4} cm.$^{-1}$ and measurement of larger coefficients with an accuracy of $\pm 5\%$. The theory permits the quantitative interpretation of the absorption coefficients from the spectra and molecular structure, and indicates that appreciable absorption in the microwave region should be shown by all heavy nonplanar molecules possessing a permanent dipole moment.

A second paper by Hershberger described means for detecting thermal and acoustic effects attending the absorption of microwaves by gases. If the gas is confined in a cavity resonator connected to a manometer, a temperature rise of about 0.5° per watt of average microwave power is observed. The rapid response to the field is easily demonstrated by liberating the gas in the field, or confining it in a rubber container exposed to the field. Audible and supersonic sound is generated in the absorbing gas, the quality of the sound depending upon the modulation frequency. By designing a gas-filled cavity which resonates electrically to the microwave frequency and acoustically to the modulation frequency, it is possible to detect 10 milliwatts of microwave power. A piezocrystal is coupled to the absorbing column as a detector.

We draw attention to these interesting contributions in the belief that they will soon command the attention of the analyst. There is much to be done in the way of pioneer work and the improvement of equipment before any extensive applications can be expected. On the other hand, these waves in the "super infrared" have properties which make them somewhat more tractable from the experimental standpoint. Although they are quasi-optical they are conveniently measured by direct electrical means. By comparison we may recall that infrared methods remained essentially impractical or too laborious for routine analytical work for many decades. Until suitable converters were developed, the cumbersome thermopile-galvanometer technique restricted the work in this field to the research laboratory.

Supersonics

A means for measuring the absorption and velocity of ultrasonic waves in liquids by pulse techniques was described by J. R. Pellam and J. K. Galt of the Radiation Laboratory of the Massachusetts Institute of Technology. The acoustical frequencies were 10 to 30 megacycles and were delivered to the liquid in 1-microsecond pulses or bursts. The transducer which generated the pulses also picked up the echoes returning from a plane reflector. The velocities were determined by measuring the distance the transducer had to be moved in order to delay the echoes by a specified amount. Absorption was determined by measuring the attenuation necessary to maintain a constant receiver signal as the transducer was moved. The attenuation could be measured with an accuracy of 5% and the sound velocity to 0.05%.

This is another field in which the techniques have been improved to a high degree, primarily by studies on sonar and radar, both of which are concerned with precise time measurements. The literature on supersonics is extensive and will undoubtedly increase rapidly.

Acoustical methods should be useful analytically, but, to the best of our knowledge, no applications exist. Strangely enough they were used in the early days of World War I. When the Germans first applied the Haber process for ammonia synthesis, the nitrogen-hydrogen mixtures were controlled by the so-called "whistling analyzer", in which the gas mixture was blown through a small organ pipe. The pitch is dependent not only on the length of the pipe but also on the gas density. The note was compared with a variable-speed siren. The method was abandoned in favor of more easily recorded data such as thermal conductance. The nuisance factor also may have contributed to its demise. The newer acoustical methods may well offer enough advantages to revive interest, particularly in the supersonic region.

For many years acoustics was the stepchild of physics, and although interest and progress in the field never languished in the communication industry, the advent of radio broadcasting unquestionably stimulated further inquiry and research. It is generally contended that new ideas and new problems create the need and demand for new and better instruments. We lean heavily on our personal bias, and keep insisting that new techniques and instruments are themselves a means for suggesting new problems.

The twin grating emission spectrograph is constructed so as to provide in a single exposure a spectrum reaching from 2000 A to 8000 A. This is accomplished without requiring the use of a very long film holder by mounting a 30 cm. long visual sensitive film above a similar length of film sensitized to ultra-violet radiation. Two gratings of the same radius of curvature (150 cm.) with 24,000 and 12,000 lines per inch, respectively, are mounted one above the other and placed in a Paschen mounting.

The light is transmitted to them via a beam splitter located immediately behind the slit. The mechanism of the beam splitter makes it possible to fill both gratings simultaneously or to confine all the radiation to either the ultra-violet or visual region. The average dispersion in the ultra-violet region is 7 A per mm., and in the visual it is 14 A per mm. The two spectra have the region from 3870 to 4060 A in common. Bulletin available upon request.

RAY CONTROL COMPANY

Pasadena 1, California

INDEX TO ADVERTISERS